THE UNIVERSITY
of EDINBURGH

Improving Sensor Performance by Characterising the Selectivity in Vapour Etching

Author:
Markus Rondé

Supervisors:
Dr. Jonathan G. Terry
Dr. Norbert Radacsi

A thesis submitted in fulfillment of the requirements for the degree of Doctor of Philosophy

in the

Institute for Integrated Micro and Nano Systems
School of Engineering
The University of Edinburgh

2021

Lay Summary of Thesis

THE UNIVERSITY of EDINBURGH

Name of student:	Markus Rondé	UUN	S1688517
University email:	Markus.ronde@ed.ac.uk		
Degree sought:	Doctor of Philosophy	No. of words in the main text of thesis:	35000
Title of thesis:	Improving the Sensor Performance by Characterising the Selectivity in Vapour Etching		

Insert the lay summary text here - the space will expand as you type.

Microsystem sensors have many applications and are essential in everyday life. For instance, they are used to trigger airbags in cars, pick up the sound of voice during a phone call, or measure the blood pressure during surgery. Typically, these sensors are on the micrometre scale and combine two components. A mechanical component that can physically move and an electric element that converts the sensation of the event it was designed to sense into an electric signal that can be processed in a computer. It is desirable to reduce these microsensors' size even further because it would improve their performance, enhance their sensitivity, and reduce the cost of many sensors.

Unfortunately, a critical process step called sacrificial layer etching makes it difficult to reduce their size further. Microsensors are fabricated using processes and techniques similar to making computer processors. Thin layers of conducting and insulating materials are stacked on a silicon wafer, interconnected and patterned into the required designs. The moveable component required for a microsensor is fabricated by removing the layer that is placed beneath the dynamic component. Traditionally, this was achieved by submerging the entire sample in a liquid etchant which would dissolve the sacrificial layer releasing a free-standing and moveable structure.

However, this etch process is not suitable for further miniaturisation because while the liquid dries, the structure that was created is pulled towards the underlying surface. Upon touch, the structure can stick to the underlying layer. This destroys the sensor. A technique to overcome this problem and the focus of this thesis is vapour etching. As the name suggests, liquids and the associated issues are avoided by removing the sacrificial layer in the vapour phase. However, compared to liquid etching, vapour etching has the disadvantage that besides the target material, other materials are attacked by the etchant as well. This property of an etchant to attack some material selectively to others is called the selectivity. This work aimed to improve the selectivity in xenon difluoride and hydrogen fluoride etch processes.

The etching under realistic conditions was studied using a newly developed method, and it was demonstrated that the selectivity in xenon difluoride etching could be improved by adding moderate amounts of hydrogen to the gas mixture during etching. Similarly, reducing the temperature and increasing the HF concentration improves the vapour etch selectivity in HF etching.

The results presented in this thesis suggest that it is now possible to develop and produce smaller sensors.

Document control

K:\AAPS\D-AcademicAdministration\02-CodesOfPractice,Guidelines&Regulations\24-MainReferencesCopiesPolicies\01-Current\Assessment BOE SCC & Feedback\Forms\ThesisLaySummary	
If you require this document in an alternative format please email Academic.Services@ed.ac.uk or telephone 0131 651 4990.	Date last revised: 20.06.19

Abstract

The vapour etching of sacrificial layers is often a critical process in the fabrication of micro/nano electromechanical systems (MEMS/NEMS) sensors. Compared to wet etch methods, it has several advantages. Smaller devices can be fabricated because stiction does not occur, sample cross-contamination can be avoided, and it is safer to operate. However, in contrast to wet etching, significantly lower etch selectivities are reported in the literature and observed by industry practitioners, limiting both this release method's and MEMS/NEMS sensors potential.

This work aims to improve the etch selectivity for the most commonly used vapour etch processes, the silicon etching with xenon difluoride (XeF_2) and hydrogen fluoride (HF) etching of silicon dioxide.

A novel test structure and measurement methodology that allows the accurate selectivity determination for a number of materials and resembles MEMS fabrication conditions was developed, fabricated and characterised.

The selectivity of XeF_2 vapour etch processes were characterised with this methodology. It was observed that materials such as silicon nitride, which are commonly inert to XeF_2 etched when located close to the sacrificial layer, and methods to improve the selectivity were evaluated. Firstly, it was observed that reducing the processing temperature from 25 to 10 °C increases the silicon (Si) to silicon nitride (SiN) selectivity by 68 %. Secondly, the Si: PECVD SiN selectivity improved by an order of magnitude and the Si: LPCVD SiN selectivity between 200 % and 600 % when moderate amounts of hydrogen were added to the processing gas mixture.

In contrast to xenon difluoride vapour etching, a catalyst (water or alcohol) and the

formation of a thin liquid layer on the sample is required to facilitate hydrogen fluoride vapour etching. To improve the limited process control resulting from the complex condensation phenomena, a novel model, which calculates the partial pressures of the individual gas components to establish vapour pressure within the gas phase, was developed and characterised.

It was observed that vapour HF etching behaves similar to wet HF etching under these controlled conditions. The silicon dioxide to silicon nitride selectivity was demonstrated to improve by 150 % when reducing the processing temperature from 20 to 5 °C and by 166 % when increasing the liquid film's HF concentration from 20 – 90 %.

The methods developed in this work substantially improve the vapour etch selectivity and enable the development of smaller, more sensitive and more robust micro and nanosensors.

Declaration of Authorship

I, Markus Rondé, declare that this thesis titled, "Improving Sensor Performance by Characterising the Selectivity in Vapour Etching" and the work presented in it are my own. I confirm that:

- This work was composed by myself.
- That neither this thesis nor parts of it have previously been submitted for a degree or any other qualification at this University or any other institution.
- Where I have consulted the published work of others, this is always clearly attributed.
- Where I have quoted from the work of others, the source is always given. With the exception of such quotations, this thesis is entirely my own work.
- I have acknowledged all main sources of help.
- That any included publications are my own work, except where indicated throughout the thesis and summarised and clearly identified on the declarations page of the thesis.

Signed:

Acknowledgements

My PhD was funded by CENSIS and the Engineering and Physical Sciences Research Council. I am grateful for this financial support and for Andy's, Ian's, Anthony's and Jon's support in securing the funding.

I could not have asked for a better team of supervisor. Thanks to Norbert for interviewing me in the first place, and despite me not having the background to do his project in question, for telling others that I would be an interesting PhD candidate. Thanks to Anthony for calling me and asking if I would be interested in doing this PhD project, presumably unknowing that 4 years later and freshly retired, he would spend countless hours reading, editing and improving my publication drafts and thesis chapters. Special thanks to Jon for guiding me through this project in a patient manner over the years, taking time for a discussion whenever needed and supporting my work wherever required.

The Scottish Microelectronics Center was a lovely environment to work in. Thanks to all of you, for the coffee morning and extended lunch breaks and especially to Camelia, Peter, Andreas, Stewart, Richard, Kevin, and Ewan, who continuously enabled and supported my work in the cleanroom. I would also like to thank the team of memsstar, in particular Tony, Dan and David for supporting my work. To my fellow CDT ISM and IMNS students for the comradeship, the funny discussions and the joyful hours spend at Christmas and post-conference parties.

I am grateful for Ulrike's and Murray's support in proof reading this thesis.

Finally, to my family who supported me throughout my journey even when it meant that I would spend many years away from home, my friends who always had an open ear and time for chat or a beer and to Carla for making every aspect of my live brighter.

Contents

List of Figures

List of Tables

List of Abbreviations

ACS	American Chemical Society
APC	Automatic Pressure Controller
BET	Brunauer-Emmett-Teller Theory
BPSG	Borophosphosilicate Glass
CMOS	Complementary Metal-Oxide-Semiconductor
CMUT	Capacitive Micromachined Ultrasonic Transducer
DRAM	Dynamic Random Access Memory
EDX	Energy dispersive X-Ray Spectroscopy
ER	Etch Rate
FIB	Focused Ion Beam
FTIR	Fourier-Transform-Infrared-Spectrometer
HF	Hydrogen Fluoride
IEEE	Institute of Electrical and Electronics Engineers
IOP	Institute of Physics (Publishing)
JLS	JLS Design Ltd (tool manufacturer, aquired by Plasma Therm in 2020)
LPCVD	Low Pressure Chemical Vapour Deposition
MEMS	Microelectromechanical Systems
MFC	Mass Flow Controller
ML	Mega Langmuir
NEMS	Nanoelectromechanical Systems
OPT	Oxford Plasma Technology (a tool manufacturer)
PECVD	Plasma Enhanced Chemical Vapour Deposition
RIE	Reactive Ion Etcher
SEM	Scattering Electron Microscope
UV	Ultra Violet (Light)

List of Symbols

ν	Poisson's Ratio
ρ	Density
R	Universal Gas Constant
T	Temperature
t	Time
f	Frequency
E	Young's Modulus
p	Pressure

Chapter 1

Introduction

1.1 MEMS Sensors

The term microelectromechanical systems (MEMS) sensors nowadays refers to a large group of sensors which share two common properties. Firstly, their dimensions typically range between 1 µm and 1 mm and secondly they integrate both electrical and non-electrical components. MEMS sensors are used in a great variety of devices across a broad range of sectors. For instance, they are used to trigger the airbags and measure the tyre pressure in modern cars, record sound in our smartphones or measure the intervascular blood pressure during surgery.

This work focuses on a subgroup of MEMS sensors which use free-standing structures as transducers to sense physical properties, such as for example sound [1][2], pressure [2], acceleration [2] and gas concentrations [2]. MEMS sensors are fabricated in batch processes [3]. The methods and tools used are similar to those used for integrated circuits [3]. The shared processing techniques are beneficial because often MEMS need to be combined with ICs in order to be integrated into larger electronic systems [4]. MEMS sensors are built by a device-specific process sequence which deposits layers of materials with different physical properties and patterns those layers to resemble the desired layout [3]. Over time, more and more fabrication processes have been developed which are specific to the manufacture of MEMS devices, such as bulk micromachining [5], wafer bonding [6] and deep reactive ion etching of silicon and glass [7]. Of particular interest to this work are etching techniques developed to remove sacrificial material or bulk silicon in order to release free-standing structures.

In many cases, the performance and cost advantages in MEMS sensing applications

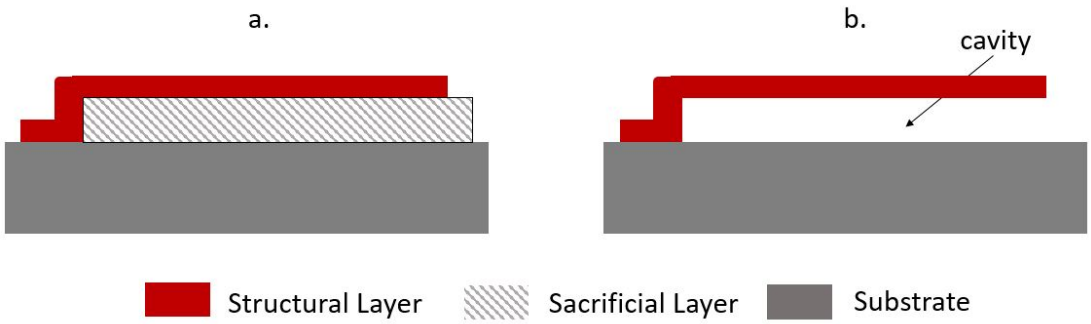

FIGURE 1.1: A schematic depiction of the release of free-standing structures by sacrificial layer etching on the example of a cantilever. (a) shows the cantilever being supported prior to etching. (b) shows the free-standing cantilever after the sacrificial layer has been removed.

derive from their small dimensions [8]. Therefore, it has been desirable to reduce the size of some MEMS sensors. This trend has continued in both research and industry, with dimensions being reduced into the nanoscale, to result in so called NEMS devices.

However, the translation of the MEMS fabrication methods towards NEMS is challenging because the large surface to volume ratios occurring at the nanoscale result in surface effects such as electrostatics, wetting and molecular adhesion which complicate fabrication steps such as the release etch of free-standing structures [8].

1.2 Sacrificial Layer Etching

A free-standing structure is formed by depositing the structural layer over a sacrificial layer, which is subsequently removed with an etch step. For easier understanding, a simple diagram is displayed in figure 1.1. It is a key process in the fabrication of microelectromechanical systems and highly critical for device functioning and production yields.

Silicon dioxide is a commonly used sacrificial layer and most commonly it is removed by wet etching the SiO_2 in hydrogen fluoride (HF) based solutions [9]. However, if required by the device-specific fabrication process, other sacrificial layer / wet etchant

combinations can be used. For instance, GaAs sacrificial layer can be etched by succinic acid ($(CH_2)_2(CO_2H)_2$) and germanium sacrificial layer can be etched by either $HNO_3/H_2O/HCl$ or $H_2O/H_2O_2/HCl$ solutions [10] [11]. It is even possible to use the bulk silicon as the sacrificial layer. Sugiyama et al. [12] released a free-standing membrane by anisotropically etching the bulk silicon of the wafer, for which they recommended the use of either potassium hydroxide (KOH) or tetramethylammonium hydroxide (TMAH). In general, the wet etch process is straightforward. The patterned wafers are submerged within a bath filled with the etchant, which reaches the sacrificial layer through specifically designed access holes or trenches and etches it.

While this method of releasing free-standing structures works remarkably well for MEMS devices with a design which results in moderate surface to volume ratios, an effect called stiction complicates the translation of this process into the NEMS scale, where these ratios increase substantially. Stiction is the term used for the adherence of a structural component of the electromechanical device to the underlying layer. Commonly, stiction occurs when the liquid which was used to rinse the etchant from the sample dries. Figure 1.2 displays the occurence of stiction on the basis of a drying cantilever. Usually, stiction causes failure of the device. The occurrence of it depends on the dimensions of the device, in particular the surface area to volume ratio [13]. The layers adhere to one another because the interfacial forces such as van der Waals, capillary, electrostatic forces and chemical bonding overcome the restoring forces [14][15]. In other words, the smaller the devices become, the more they are prone to stiction because the surface area to volume ratio increases by the power of three. Stiction can either occur during the fabrication of the MEMS or while using the MEMS device [14] [13]. While the former is primarily caused by the capillary forces during drying, the latter is caused by electrostatic or acceleration forces occuring while the MEMS is operating [14] [13] [15].

According to Tas et al. [14] capillary forces causing stiction can be illustrated by

$$F = \frac{2A\gamma cos\theta}{g} \tag{1.1}$$

where A is the wetted surface area, θ represents the contact angle between the liquid

and the solid, γ the surface tension at the liquid air interface and g the thickness of the liquid layer. In order to avoid stiction during drying, the capillary force needs to be balanced by the restoring force of the free standing structure. Tas et al. [14] provided an equation for the critical length l of a cantilever with a Young's Modulus E and a thickness t, which can be calculated by

$$l = \sqrt[4]{\frac{3Et^3g^2}{16\gamma cos\theta}} \tag{1.2}$$

Equation 1.2 shows, that the restoring force of a cantilever decreases with decreased thickness, while the capillary force increases with decreased gap height. Consequently, smaller MEMS are more prone to stiction during the fabrication of the device.

Stiction during the use of the MEMS sensor is prevented by one of the following three methods: by roughening the surface in order to reduce the contact area: by creating hydrophobic surfaces; or by self-assembled monolayer anti-stiction coatings [13] [16] [17] [18] [19].

However, as devices are scaled down, it becomes more and more difficult to prevent stiction during device manufacture. A number of methods have been used to overcome this. Critical point drying and vapour etching are particularly noteworthy. The process sequence of the former was comprehensively described by Jafri et al. [20]. After the etch of the sacrificial layer is completed, the samples are submerged in a solvent (often methanol) and then moved into a pressure chamber. Within the chamber, the liquid methanol is displaced by liquid carbon dioxide CO_2. Following the displacement, the temperature and pressure within the chamber are brought beyond the critical point, to a temperature of 31 °C and a pressure of 1071 psi (55386 Torr) where the phase boundary between the liquid and gas phase does not exist. Finally, the CO_2 and methanol are removed from the chamber, avoiding the liquid/gas phase transition. Capillary forces cannot occur under these conditions and therefore stiction is avoided [21] [20]. However, the wet etch plus critical point drying process has the disadvantage that any contamination of the etchant or the post-release solvent will be deposited on the samples [21].

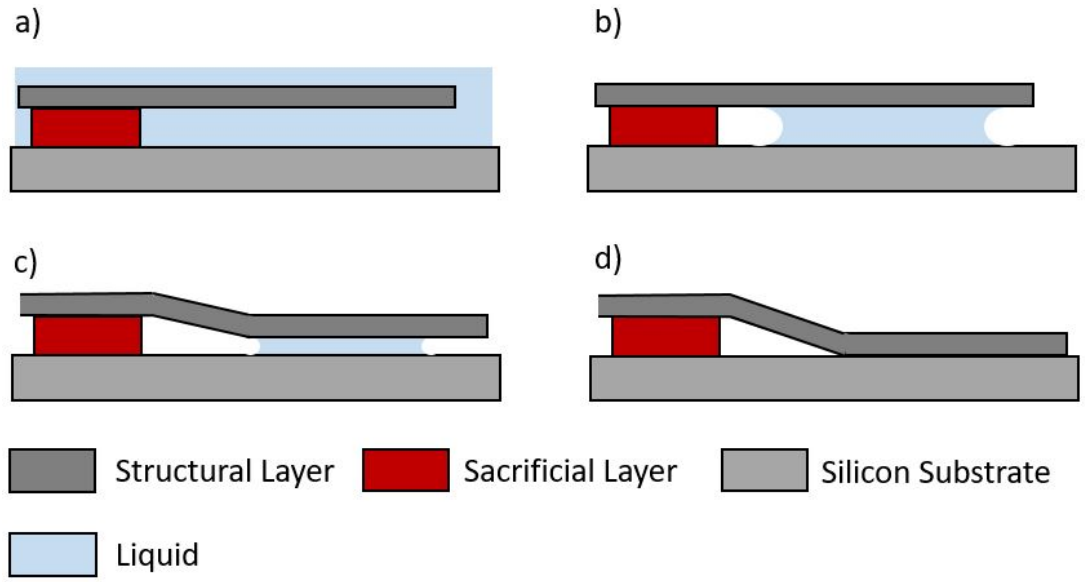

FIGURE 1.2: A schematic depiction showing how stiction can occur during the fabrication of a micro-cantilever. In a) the cantilever is submerged in the water that has been used to remove the etchant. The successive drying of the liquid displayed in b) and c) leads to a deflection of the cantilever until finally, in d) , the tip of the cantilever adheres to the substrate.

The other significant method for successfully releasing free-standing structures is vapour etching. In contrast to wet etching, vapour etching has various advantages. It is contamination-free and safer for the operator while the commercial etch systems available today enable accurate process control. Furthermore, this method eliminates the capillary action which can result in stiction, as the etchant and the etch product are in the vapour phase. Commercial systems are available, which use xenon difluoride (XeF_2) to etch silicon and vapour HF to etch silicon dioxide (SiO_2).

1.3 Selectivity and Sensor Performance

Vapour etching has potential disadvantages. Vapour etch rates have been observed to be significantly slower than in wet etching, thereby increasing production costs. Vapour etching selectivities can also differ from what would be expected from the literature, which mainly focuses on wet etching removal rates and selectivities. This makes it difficult for MEMS sensor designers and manufacturers to design reliable processes. In addition, it has been observed that layers which are inert to the etchant

when etched in isolation begin to etch if placed in close proximity to the by-products which result from the etching of the sacrificial layer [22]. This phenomenon, called the proximity effect, appears to be vapour etch specific and it can reduce the etch selectivities even further [22] [23]. For instance, silicon nitride was reported to etch 12 - 18 nm per minute in a XeF_2 atmosphere [24] and the author of this work observed polysilicon to silicon nitride selectivities as low as 5:4.

It is difficult to determine the overall impact which poor selectivities have on MEMS sensors because innumerable devices have been presented in (research) literature and have been commercialised. However, the consequences of unintended overetching on sensor performance can be clearly illustrated on the simplified example of a capacitive micromachined ultrasonic transducer (CMUT). A CMUT is a MEMS device which utilises a change in capacitance as a transducing mechanism for various sensing applications. They are also intensively researched at the moment and could become more sensitive when reduced in size. The impact of the etch selectivities on the sensors' resonance frequency and collapse voltage can be correlated. Hence they are ideal to illustrate how selectivities can impact sensor performance.

In broad terms, a CMUT consists of a top electrode, which is placed on top of a membrane which is separated from the bottom electrode by a cavity. When a bias voltage is applied, the vibration of the membrane will result in an alternating signal. For sensing applications, the integrity of the membrane is essential as various key properties of a CMUT, such as the collapse voltage and the resonance frequency, are affected by the thickness of the membrane. The effect of poor selectivities is theoretically examined based on a CMUT developed by Belgacem et al. [25].

The authors of the work paid close attention to the sacrificial layer selection to reduce etching of the membrane to a minimum and included sufficient data to enable calculating the impact that different selectivities would have on the sensor. The CMUT's membrane has a radius r of 25 μm and is made of 550 nm thick Si_3N_4, which has a Young's modulus E of 322 GPa, a Poisson's ratio ν of 0.26 and a density ρ that was calculated to be roughly 4412 kgm^{-3}. The cavity is 200 nm thick and is fabricated by

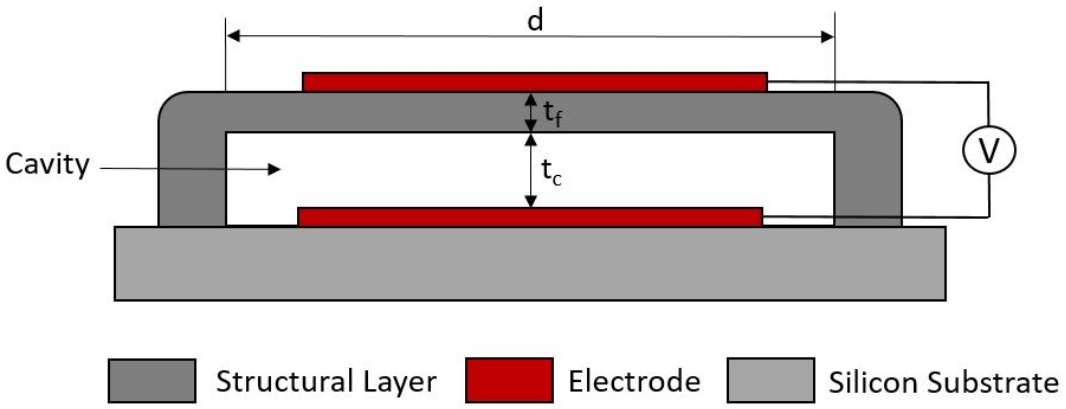

FIGURE 1.3: A schematic depiction of a CMUT showing the critical dimensions.

etching a SiO_2 sacrificial layer. The etch front propagates from the edge of the membrane towards the centre. The top electrode is made of aluminium and the bottom electrode is the silicon substrate. A schematic depiction of a CMUT is displayed in figure 1.3.

The resonance frequency f of a circular membrane can be calculated according to equation 1.3 which was also used by Belgacem et al. [25] and was obtained from [26].

$$f = \frac{10.33}{2\pi}\sqrt{\frac{E}{(1-v^2)\rho}}\frac{t_f}{r^2} \tag{1.3}$$

Where t_f represents the thickness of the membrane, which depends on the Si_3N_4 to SiO_2 etch selectivity. Using this equation, and calculating how the membrane thickness changes with different selectivities, the change in resonance frequency can be easily estimated. Thereby, the etch selectivity's impact on sensor performance can be quantified. The calculated frequencies for a range of Si_3N_4 to SiO_2 selectivities is displayed in table 1.1.

This example calculation suggests a linear correlation between the etch selectivity and the sensor performance. Assuming that the resonance frequency tolerance is 5

Si_3N_4 : SiO_2 Selectivity	∞	1: 1000	1: 100	1: 10	1: 2	1: 1
Membrane Thickness [nm]	550	549.8	548	530	450	350
Cavity Thickness [nm]	200	200.2	202	220	300	400
f [MHz]	12.80	12.79	12.75	12.3	10.5	8.15

TABLE 1.1: Simplified thought experiment showing how the resonant frequency of the CMUT membrane presented in [25] would change at different Si_3N_4 : SiO_2 etch selectivities.

percent, the device would be within the specifications up to a selectivity of 1: 10. Unfortunately, worse selectivities have been reported for vapour etching, in particular where the structural layer is in close proximity to the sacrificial layer, as it is the case for this CMUT [25] [27] [23][28].

This simple calculation clearly illustrates the importance of the etch selectivity with regard to sensor performance. However, in reality there is more to the process. During etching, the membrane's thickness is not uniformly reduced, as implied here, but instead more of the structural material would be removed at the edges of the membrane because it is exposed to the etchant for a longer time. The resulting membrane thickness gradient would reduce the mechanical robustness of the membrane. This is crucial because a biased CMUT experiences an electrostatic force which will deflect the membrane. If the membrane's mechanical robustness is insufficient, the collapse voltage decreases and device failure becomes more likely.

1.4 Problem Statement

As demonstrated in the CMUT example, insufficient understanding of vapour etch selectivities can result in limitations to successful scaling of MEMS. However, a better understanding of vapour etch selectivity under realistic MEMS fabrication conditions alongside improved selective etching methods development could give a significant push towards MEMS sensor miniaturisation.

In the author's opinion, there are two gaps of knowledge which need to be closed.

Firstly, the proximity etching effect demonstrates that the chemical processes underlying vapour etching are not fully understood. Secondly, there is very little information available on methods to control vapour etch selectivities.

1.5 Aim and Objectives

It is the aim of the work presented here to quantify and improve HF and XeF_2 vapour etch processes through a better understanding of etch chemistry and better control of etch selectivity. The following objectives and goals derive from this broad aim:

1. Design a test structure and an experiment for measuring the etch selectivities under realistic fabrication conditions.

2. Quantify the proximity effect and the effect of potential selectivity improving temperature changes and gas additions in XeF_2 vapour etching.

3. Quantify the effect of potential selectivity improving temperature changes, gas composition changes and gas additions in HF vapour etching.

1.6 Publications

The work presented here resulted in one conference and two journal publications. They are included in the appendix of this thesis.

M. Rondé, A. J. Walton, and J. G. Terry, "Test Structure for Measuring the Selectivity in Vapour Etch Processes," in IEEE 33rd International Conference on Microelectronic Test Structures (ICMTS), Edinburgh, United Kingdom, 2020, pp. 1–5.

M. Rondé, A. J. Walton, and J. G. Terry, "Manipulating Etch Selectivities in XeF_2 Vapour Etching," J. Microelectromachanical Syst., vol. 30, no. 1, pp. 156–164, 2021.

M. Ronde, A. J. Walton, and J. G. Terry, "Test Structure for Measuring the Selectivity in XeF_2 and HF Vapour Etch Processes," IEEE Trans. Semicond. Manuf., vol. Accepted, 2021.

The author of this thesis also created the Wikipedia page on vapor etching, and contributed most of the content.

https://en.wikipedia.org/wiki/vapor_etching

Chapter 2

Terms and Fundamental Chemistry

2.1 Introduction

This research project is interdisciplinary in nature since it investigates a primarily chemical process being used in an engineering context. Engineers might not be familiar with all of the terms used and concepts presented within this work. Therefore this section firstly defines the key terms commonly used in the context of vapour etching. Secondly, it elaborates on some fundamental physio-chemical and quantum chemical concepts on the basis of the literature, which are relevant to the body of this work.

2.2 Terms

2.2.1 Vapour Etching

In this work, vapour etching refers to isotropic chemical etch processes not involving plasmas, where the etchant is supplied to the reaction chamber in gaseous form. The etch reaction can take place in the gas state or in the liquid state if thin condensed films form.

2.2.2 Etch Rate

In many cases, the etch rate of a material is determined by etching chips or wafers which have been blanket coated with a thin film of a given thickness for a certain period of time [29] [30] [31] [32] [33]. The thickness of the film is measured with

an ellipsometer before and after the etch. The resulting etch rate β is the depth of material etched α divided by the etch time t.

$$\beta = \frac{\alpha}{t} \tag{2.1}$$

While the samples used can be easily fabricated and accurately measured, this method has two disadvantages. Firstly, it does not account for the lateral etch propagation in undercut etch applications. Secondly, it ignores time taken to initiate the etch reaction and the offset which results. To account for the former, the experimental section of this work will use the undercut etch rate. To overcome the latter, Van Barel et al. defined the steady-state etch rate to take the etch initiation and offset into account [34]. It is determined by repeating the etch at least three times for different etch durations. The steady-state etch rate can be determined from the graph when etch depth is plotted against the etch time. An example is displayed in figure 2.1, which displays the etch undercut of SiO_2 and SiN etched in vapour HF for etch times of 150, 180 and 210 seconds respectively. The etch rates of SiO_2 and SiN are 380 nm per second and 3.4 nm per second respectively. Furthermore, the figure suggests that the SiO_2 etch initiated after 40 seconds and the SiN etch initiated after 2 seconds. The delay in the SiO_2 etch initiation can be explained with the time that is required for the reactants to condense onto the surface.

2.2.3 Selectivity

The etch selectivity provides a comparison of the removal rates of two materials undergoing the same etch process. It is given as the etch rate of one material divided by the etch rate of another. The selectivity is usually reported as a ratio. For instance, a selectivity of 1:1 indicates that both materials etch at the same rate. The selectivity S can be expressed in a simple equation

$$S = \beta_1 : \beta_2 \tag{2.2}$$

where β_1 and β_2 are the etch rates of the two materials.

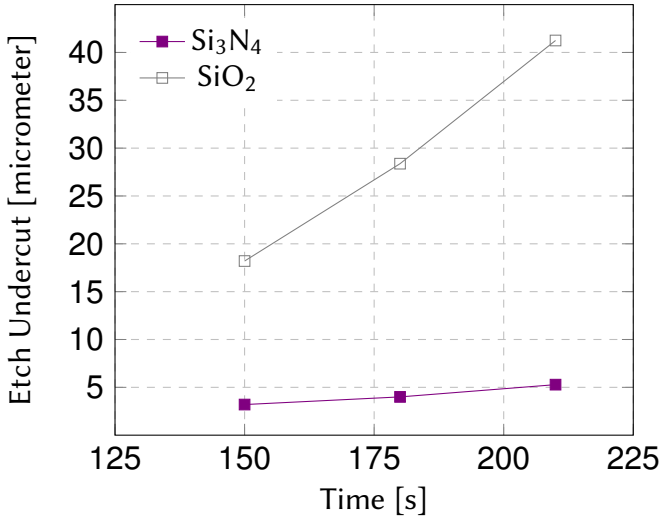

FIGURE 2.1: An example data set showing the steady state etch rate of SiO_2 and SiN etched in vapour HF. The raw data used to create this figure was also published in [28].

2.3 Fundamental Chemistry Underlying Vapour Etching

2.3.1 Arrhenius Equation

The temperature dependence of a chemical reaction rate k(T) can be described by the Arrhenius equation [35]

$$k(T) = Ae^{\frac{-E_a}{RT}} \tag{2.3}$$

where A is the rate constant, E_a is the activation energy for the reaction, R is the universal gas constant, and T is the absolute temperature. The equation displays why some molecules react under certain temperature conditions, while others do not. The underlying idea is that the molecule's specific activation energy has to be overcome to initiate the reaction, with the energy supplied in the form of heat [36]. From this, it follows that the fraction of molecules reacting increases with increasing temperature. The reader should keep this conclusion in mind because for HF vapour etching, the literature suggests that the opposite holds true.

2.3.2 Langmuir Adsorption and the Brunauer-Emmett-Teller Theory

In vapour etching, the interaction of gasses with solids is very important. The reactants can be brought to the surface either by condensation or by gas adsorption phenomena. Regarding the latter, two theories will be referred to in later elaborations and discussion. Firstly, the Langmuir adsorption model and secondly, its extension, the Brunauer-Emmett-Teller (BET) theory are considered. The underlying idea of the Langmuir adsorption model is that each surface has a number of active sites which a species can adsorb to or desorb from [37]. This can either be through chemisorption (high energy chemical bonding) or physisorption (weaker attraction by van der Waals forces). The adsorbed species occupies a certain fraction of the available sites and forms a monolayer. This fraction θ can be expressed as

$$\theta = \frac{v}{v_m} = \frac{K_a p_0}{1 + K_a p_0} \tag{2.4}$$

where v_m is the volume of the monolayer, p_0 the partial pressure of the adsorbent in the gaseous state and K_a represents the equilibrium constant of the adsorption or desorption reaction [38] [39]. The Langmuir model provides a good approximation of the surface coverage, but it has some shortcomings due to oversimplifications. For instance, it does not account for the surface roughness or the fact that adsorped species can form multilayers in reality. Therefore, some of the research previously conducted in vapour etch processes uses the Brunauer-Emmett-Teller theory (BET) [40]. In contrast to the Langmuir adsorption model, it assumes that the top adsorbed layer is in equilibrium with the vapour and that, as a result, stacks of adsorbed molecules can be formed. This gives an alternative expression for the fraction of occupied sites θ

$$\theta = \frac{v}{v_m} = \frac{cp}{(p_0 - p)[1 + (c+1)(p/p_0)]} \tag{2.5}$$

where p is the pressure at equilibrium and c is the BET constant, which is defined as

$$c = e^{\frac{E_1 - E_L}{RT}} \tag{2.6}$$

where E_1 is the heat adsorption of the first layer and E_L is the heat of liquefaction, R is the universal gas constant and T the temperature. The partial pressure p_0 and the BET constant c are temperature dependent. Rudakov [41] points out that with increasing temperature, the rate of adsorption on the surface decreases. This observation will become important when discussing the existing literature.

2.3.3 Hydrogen Fluoride Etching of Silicon Dioxide

Even though the reactants are supplied and removed from the sample in the gaseous state in HF vapour etching, the formation of a liquid thin film on the sample is required to initiate and maintain etching [42]. Knotter [43] presented a very comprehensive and detailed quantum mechanical investigation into the etch mechanisms of SiO_2 in HF based solutions. As a liquid film is required for etching, the etch mechanisms investigated in [43] should also be valid for vapour etch processes. The HF wet etch mechanism of SiO_2 is composed of two reactions. Firstly, the surface SiOH group is replaced with an SiF group by a reaction rate limiting elimination/addition reaction. After the first SiF group has been formed, the remaining Si-O bonds are substituted with Si-F bonds by a nucleophilic substitution reaction. Compared to the nucleophilic substitution reaction, the elimination/addition reaction proceeds 18-20 times slower.

The reaction scheme for the elimination/addition reaction is displayed in figure 2.2. Firstly, as displayed in C, an H^+ ion bonds to the surface O^- forming an OH group. The following reaction path depends on the pH value of the solution.

The pH value, is defined as the negative logarithm of the hydrogen ion concentration (also known as hydrogen ion activity) within a solution [44]. This definition can be expressed as

$$pH = -log_{10}([H^+]) \tag{2.7}$$

where $[H^+]$ is the concentration of positively charged hydrogen ions. From this follows, that a solution with a high concentration of hydrogen ions has a low pH value. Hydrogen ions are highly reactive and readily combine with other particles, because the removal or loss of the hydrogen atoms single electron only leaves the proton behind[45]. Consequently, hydrogen ions are also referred to as protons in chemistry[45].

If the pH value of the reaction displayed in figure 2.2 is lower than 1.5, which indicates a high concentration of H^+ ions within the solution, the reaction A to D takes place. Water is eliminated from the silicon oxide group, and either a $HF_2{}^-$ or H_2F_2 molecule donates the fluorine atom which bonds to the silicon dioxide as shown in reaction step D to E. If the pH value of the solution is larger than 1.5, the reaction follows the path B to D. An OH group is eliminated, and a fluorine atom is added to the SiO group as shown in D to E. Knotter points out that the H_2O elimination reaction is much faster than the OH elimination reaction.

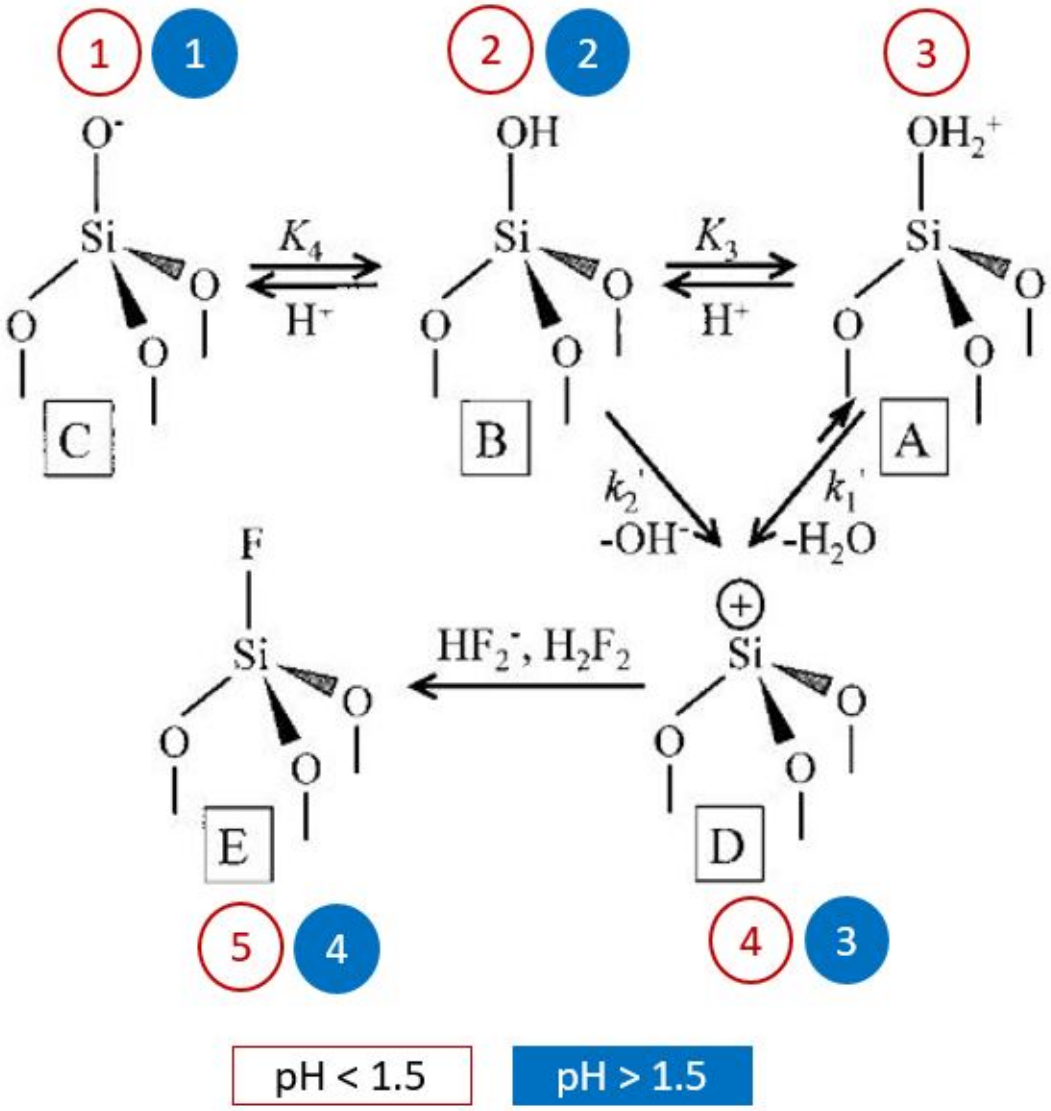

FIGURE 2.2: Proposed elimination/addition reaction, the etch rate limiting step, as proposed by Knotter [43]. Reproduced from [43] with permission from ACS. The numerical labels were added by the author of this thesis, to ease the understanding of the two pH dependent reaction paths.

The second part of the overall etch reaction, the three subsequent nucleophilic substitution reactions of the fluorine ions, which replace the remaining Si-O bonds to form SiF_4 proceeds 18-20 times faster than the preceding reaction because no high energetic intermediates need to be formed. The straightforward reaction pathway is displayed in 2.3.

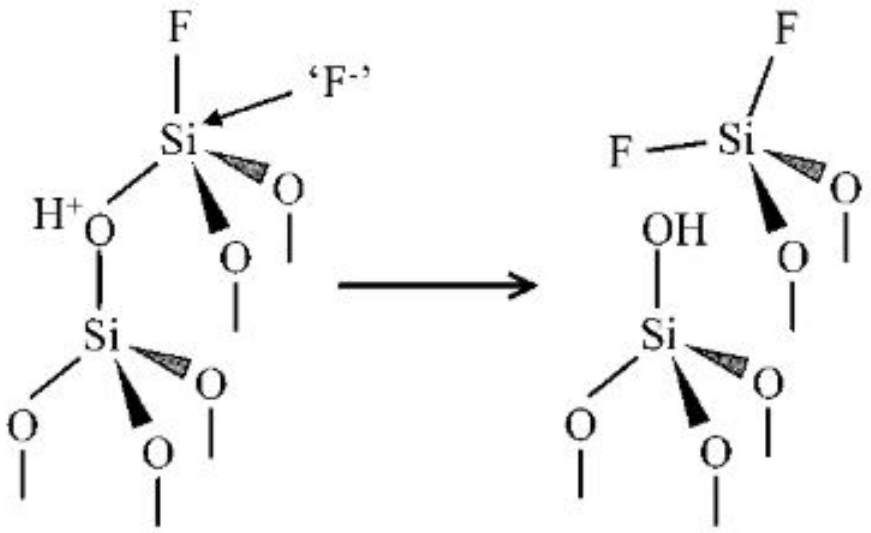

FIGURE 2.3: Nucleophilic substitution reaction as proposed by Knotter [43]. Reproduced from [43] with permission from ACS.

In a follow-up publication, Knotter [46] presented a figure which plots the different reaction pathways and their impact on the etch rate of SiO_2 over the pH value of the solution. This figure is reprinted in figure 2.4. It shows that the SiO_2 etch is driven by difluorides such as HF_2^- and H_2F_2. This is a very important discovery in the context of this work because Si_3N_4 is mainly etched by monofluorides. The silicon nitride etch mechanisms are elaborated on in Section 2.3.4 of this work and the manipulation of the fluoride composition within the solution is elaborated on in Section 3.5.

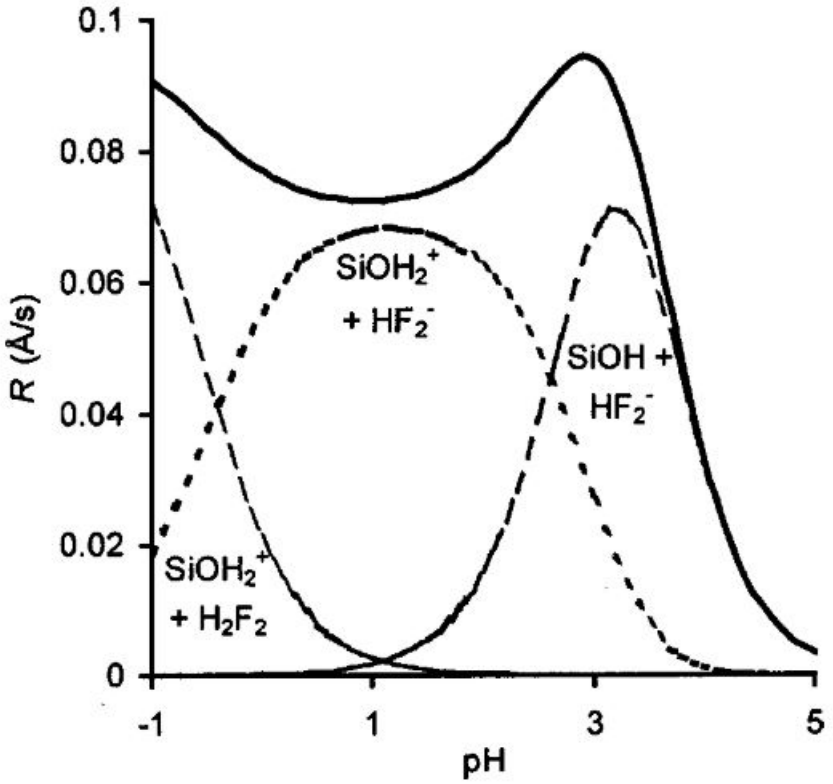

FIGURE 2.4: The suggested impact on different reactions on the SiO_2 etch rate as presented by Knotter et al. [46]. Reproduced from [46] with permission from IOP Publishing.

2.3.4 Hydrogen Fluoride Etching of Silicon Nitride

In HF vapour etching, the selectivities of SiO_2 towards SiN are important, because both materials are commonly used in close proximity to one another in MEMS fabrication processes. Knotter [46] also presented a comprehensive quantum chemical elaboration on the silicon nitride etch in HF based solutions. The etch reaction is very similar to the HF based etching of silicon dioxide. First, the NH_3 group is removed from the surface and replaced by a fluorine atom in an elimination/addition reaction. Figure 2.5 shows the scheme of the elimination/addition reaction. The reaction follows either of the three pathways. B to D to E shows the formation of $SiNH_2$, which is then removed and replaced by HF_2^-. The $SiNH_3$ shown in A is removed and the fluorine atom is substituted by either an HF molecule or a fluorine ion. The removal of the surface nitrogen atom is the rate-limiting step. The remaining nitride atoms

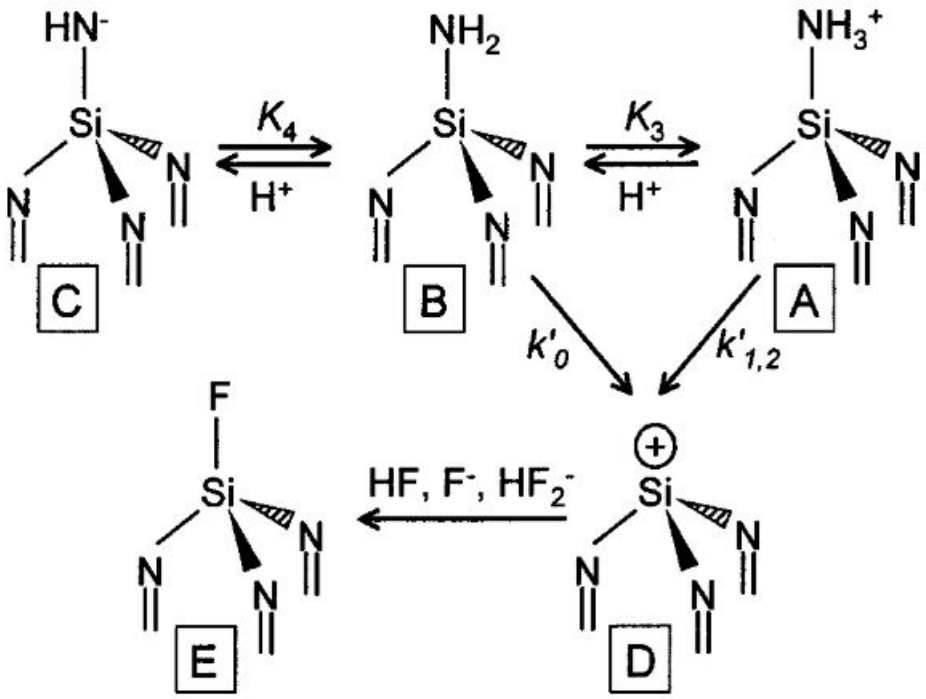

FIGURE 2.5: Proposed elimination/addition reaction removing the NH-group while etching silicon nitride in HF solutions as proposed by Knotter [46]. Reproduced from [46] with permission from IOP Publishing.

are successively replaced with fluorine by a low-energy nucleophile substitution reaction.

The dominant etch reaction path depends on the pH value of the solution. The distribution is displayed in figure 2.6. The highest etch rates are archieved at pH values of roughly 2.5, the lowest at high pH values of 4 or more. Knotter [46] points out, that the etch of silicon nitride in HF solutions is driven by monofluorides, as opposed to the etch of SiO_2 which is driven by difluorides. This is an essential observation for this study, and will be further elaborated on in Section 3.5 of this report.

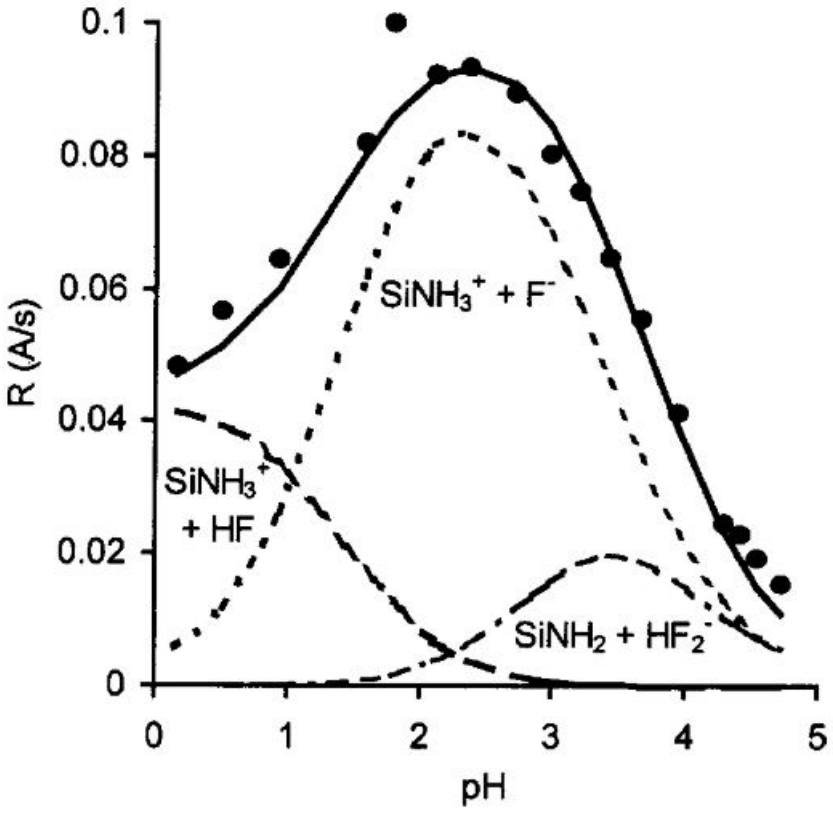

FIGURE 2.6: The suggested impact on different reactions on the SiN etch rate as presented by Knotter et al. [46]. Reproduced from [46] with permission from IOP Publishing.

2.3.5 Xenon Difluoride Etching of Silicon

The overall reaction of XeF_2 with silicon to form SiF_4 was established very early on by [47] and is displayed in reaction equation 2.8. The same investigation also found that SiO_2, Si_3N_4 and SiC were not etched in an XeF_2 atmosphere.

$$2\,XeF_2\,(g) + Si\,(s) \longrightarrow 2\,Xe\,(g) + SiF_4\,(g) \tag{2.8}$$

In 2002, researchers from the Ceyer Research Group at the Massachusetts Institute of Technology began investigating the quantum chemical processes involved in the XeF_2 etch process of silicon. The mechanisms presented in these high quality studies are relevant to this works Chapter 5 on XeF_2 etch selectivities [48] [49] [50]. In

their initial study [48], they used helium atom diffraction, beam-surface scattering and thermal desorption measurements to study the low energy interaction of XeF_2 with silicon and to compare an alternative silicon etchant, F_2. They found that both reactants fluorinate the silicon's dangling bonds. At a coverage of 1 ML (Megalangmuir), the saturation point - however, the F_2 ceases to react while the XeF_2 continues to fluorinate the dimer and lattice bonds. The investigation into this interesting phenomenon continued and in 2004 a Physical Review letter [49] suggested that the etching of silicon is the result of a double mechanism. Firstly, the XeF_2 abstracts a fluorine atom on the dangling bonds exposed on the silicon surface. The scattered XeF molecule absorbs a part of the 60 kcal/mol energy resulting from the reaction and is rovibrationally excited. It can now either abstract a second fluorine atom on another dangling bond or, if the excitation is greater than the bond energy (3 kcal/mol), dissociate into Xe and a fluorine radical [1]. The probability of the former mechanism occurring decreases as the fluorine coverage of the dangling bonds increases. Roughly 79% of the XeF formed dissociates to form Xe and F. In turn, 10% of these fluorine radicals are scattered towards the surface, where they either react with dangling, -lattice or -dimer bonds. Gradually, the Si-Si bonds are broken to form SiF_1, SiF_2, SiF_3 and SiF_4. The SiF_4 desorbs into the gas phase. The overall reaction is exothermic.

2.3.6 Proximity Effect

When considering selectivity, the formation and scattering of fluorine radicals as described in 2.3.5 is problematic because atomic fluorine is known to react with common microfabrication materials such as silicon dioxide and silicon nitride [51]. For instance, Arana et al. [52] were forced to develop a F_2 vapour etching process to release silicon nitride fuel processor tubes because the XeF_2 selectivity towards silicon nitride was insufficient to release the tubes in the initial fabrication process [53]. Most likely, the high silicon nitride etch rates which they observed were caused by fluorine radicals formed while etching the silicon surrounding the structures. Veyan et al. [22] investigated this effect in more detail and called it the proximity effect. In order to conduct their ground breaking study, they purpose-built an XeF_2 reactor which could be fitted into a Fourier-transform-infrared spectrometer (FTIR). It

[1] A radical is a molecule that has one unpaired electron, but in contrast to an ion does not carry a charge.

allowed them to measure the gas composition within the chamber during the etching of silicon as well as the silicon dioxide in direct proximity to it. In addition to that, they conducted complex quantum chemical calculations using the density function theory. They found that the silicon dioxide, which was previously considered to be inert to XeF_2 etched at a considerable rate and was eventually removed. Furthermore, the powerful combination of methodology and simulation tools used in this study allowed them to conclude that the SiO_2 was etched by the fluorine radicals formed during the etching of the XeF_2 as illustrated in figure 2.7. In 2.7 a), the XeF_2 etches the silicon with a reaction energy of -1.25eV, making this reaction energetically favourable. In contrast to that, the reaction with SiO_2 is positive, indicating the reaction is not energetically favourable. Figure 2.7 b) shows however, that the SiO_2 is etched by both the fluorine abstracted from XeF and the scattered fluorine radicals.

In realistic MEMS fabrication, it is very common that the sacrificial layer is placed in close proximity to functional, structural or isolating layers. Hence, the significantly reduced etch selectivities in proximity etching could cause a significant problem to industry practitioners and researchers. Therefore, the proximity effect is a focus point of this work and is highly relevant towards the chapters on test structure development and the improvement of XeF_2 etch selectivities.

2.4 Summary and Conclusion

In summary, key terms used through out the thesis, such as selectivity and etch rate were defined in this chapter. It further illustrated, that complex adsorption, desorption and condensation phenomena are required to bring the etchants to or remove them from the reaction site. Previous research into the chemical reactions leading to etching SiO_2 and SiN in vapour HF were presented, and the important observation was made, that silicon dioxide and silicon nitride are predominately etched by difluorides and monofluorides respectively. Finally, the xenon difluoride etch reaction with silicon was elaborated on and the latest research into the proximity effect, which could significantly reduce the selectivity in xenon difluoride vapour etching has been presented.

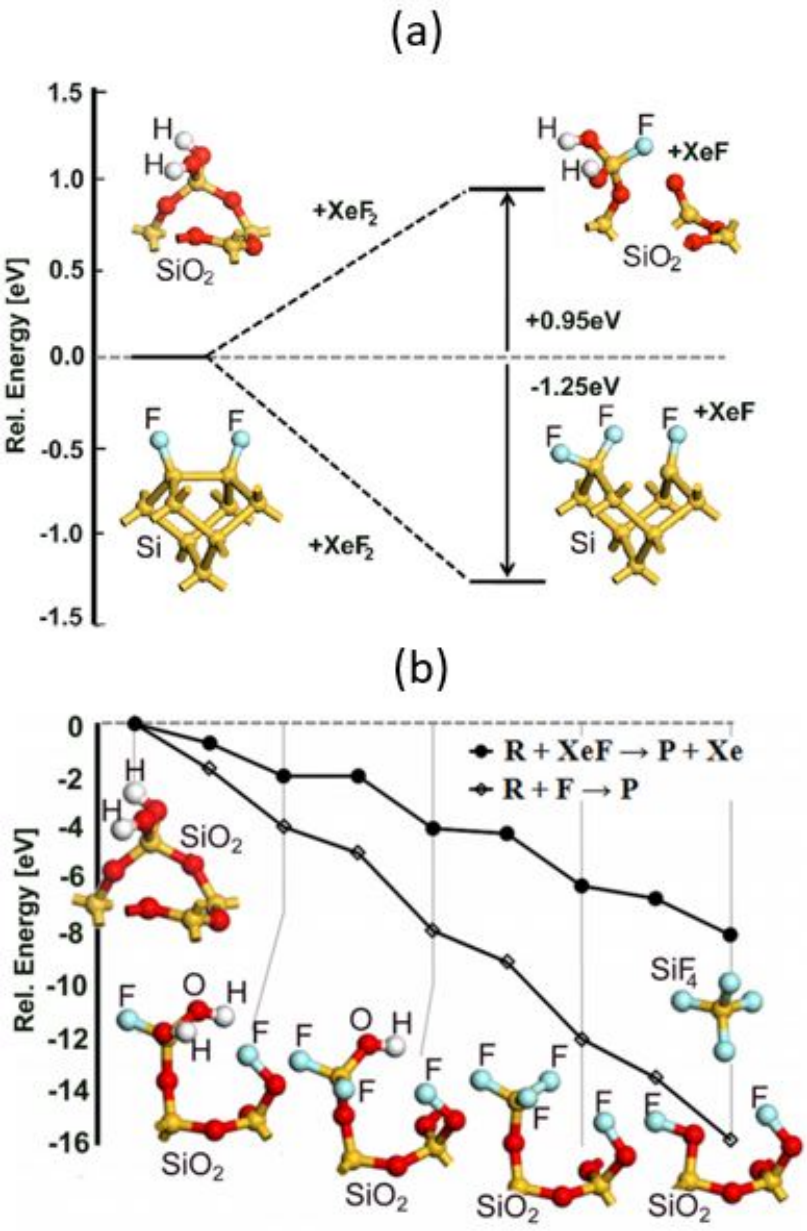

FIGURE 2.7: (a) illustrates the reaction energies calculated for single atom abstraction of XeF_2 while etching silicon (bottom) and SiO_2 (top). In (b) the relative energies calculated for the etching of SiO_2. Showing the successive fluorination from the XeF molecule (black markers) and secondly by the reaction with atomic fluorine (white marker). Reproduced from [22] with permission from AIP Publishing.

Chapter 3

Etch Selectivity Control

3.1 Introduction

In order to engineer the selectivity, it is necessary to utilise mechanisms which alter the etch rate of one material to a greater extent than that of the other. Only a few peer-reviewed works have focused on the selectivity in HF or XeF_2 etch processes. However, other gas etching techniques, in particular plasma etch processes are operated in systems similar to those for vapour etch processes. Furthermore, they utilise gasses, that are generally available in a clean room environment. From the broader literature, four predominant etch selectivity control methods can be extracted, namely surface modulation, reaction product neutralisation by gas addition, temperature dependent reaction rate and excitation.

The literature focusing on exploiting the temperature dependency and reactant neutralisation by gas addition methods were evaluated because they are straightforward to implement solution in existing vapour etch systems. The modulation of the surfaces as well as the excitation of reactant was evaluated because the author of this work presumed that these methods could significantly improve etch selectivities if they were successfully implemented.

3.2 Surface Modulation

Researchers from the Laboratoire d' électronique des technologies de l' information (CEA-Leti) in Grenoble have made significant progress in selectivity manipulation by surface modulation [54][55][56][57]. The need to develop highly selective etching methods for sub 10 nm CMOS fabrication drives this research. It introduced a new

method to etch Si_3N_4 with a very high selectivity towards silicon and SiGe, which utilises two mechanisms. Firstly [54], ion implantation of light ions into layers in order to replace stronger bonds with weaker ones and, secondly [57], the formation of new layers for surface passivation. The work in [54] can be summarised as follows. After the ion implantation, the implanted layer is etched selectively down to the untreated layer. Hydrogen, helium and argon were the initial ions of choice. Simulations showed that the maximum concentrations of argon, helium and hydrogen ions are to be expected at a depth of 2.5, 7 and 12 nm respectively. Furthermore, the plasma used to ionise the hydrogen does not etch the Si_3N_4. This is an advantage over helium and argon plasmas, as these etch silicon nitride at a slow rate of roughly 2 nm min^{-1}. They investigate the effect by comparing the etch rates of altered and pristine Si_3N_4 films. The altered films were modified by a 60-second exposure to a 100 W hydrogen plasma held at 50 mTorr. The samples were then etched in a 1 % HF solution. The resulting etch rates are of some interest and are displayed in figure 3.1. While the pristine film etched with a rate of roughly 1.2 nm min^{-1}, the modified film etched around 10 times more quickly. Following this initial success, the researchers tried to increase the thickness of the modified Si_3N_4 by tuning the bias power and the exposure time of the implant. The group found that the maximum thickness which can be modified by this process is roughly 19 nm thick.

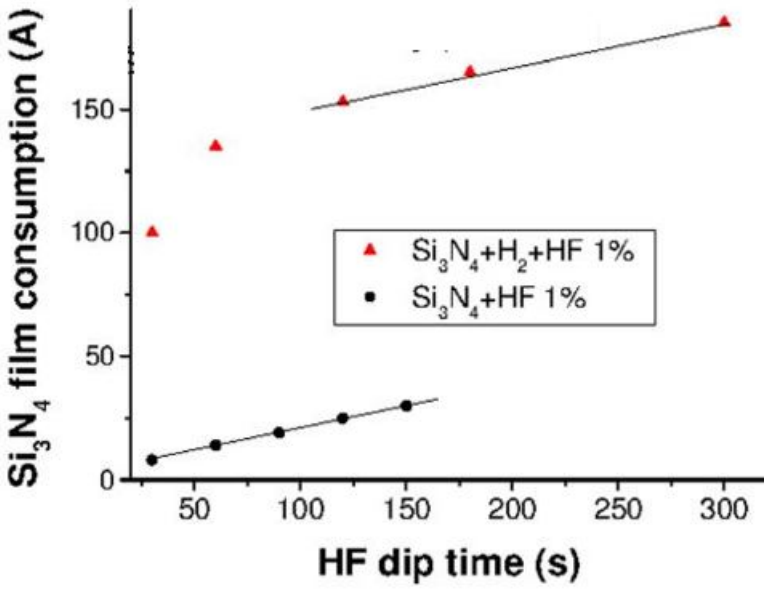

FIGURE 3.1: The Si_3N_4 film consumption as a function of etchant exposure time, with and without pre etch hydrogen plasma exposure. Reproduced from [54] with permission from AIP Publishing.

The HF solution used in this initial study [54] had the disadvantage that it also attacks SiO_2. Therefore, the follow-up publication [55] compared the etch selectivities of the modified ion implanted SiN, pristine SiN and SiO_2 when exposed to either an HF solution, gaseous HF and a nitrogen trifluoride (NF_3) nitrogen amonia (NH_3) remote plasma. HF vapour etching gave the best selectivities of modified SiN towards pristine SiN and SiO_2 with 31: 1 and 39:1 respectively. The remote plasma mixture etched the SiO_2 at the highest rate.

The vapour HF removal of the modified SiN layer was further investigated in [58]. They found that the enhanced etch rate of the modified SiN is caused by the breaking of the Si-N bonds. These are replaced by Si-H and N-H bonds which are more prone to etching. Finally, in [56] Posseme et al., modified and wet HF etched SiCO films. The ion implanting process successfully increased the etch rate of the modified SiCO by 100 times, demonstrating that the method is not limited to Si_3N_4. Hydrogen ion implantation into thin films seems to have great potential in sub 10 nm CMOS applications. However, its use in MEMS fabrication is limited for two reasons. Firstly, the maximum modification depth demonstrated in these studies was only 19 nm. Beyond

this, the etch properties of these materials resort to their typical values, making it unusable for sacrificial layer release processes. Furthermore, these studies focused on enhancing the etch rate of Si_3N_4. However, in MEMS fabrication it is more common to etch other materials while keeping silicon nitride films as stress moderators for other structural layers. Therefore, while the general concept is promising in CMOS fabrication, further advances are needed in either high energy ion implantation to achieve the necessary modulation depths or in MEMS miniaturisation to the extent that 19 nm layer release processes become relevant.

3.3 In-Situ Surface Modulation

Another method which has potential in MEMS etching is the passivation of surfaces that are not to be etched. Selectivity improvements caused by the formation of passivation layers were first reported by Loewenstein [59] in 1989. Si_3N_4 was etched in the discharge of CF_4 and SF_6 remote plasmas, which included H_2 and CH_4 in the processing gas mix, and the Si_3N_4 to Si and Si_3N_4 to SiO_2 selectivities improved significantly with increased flows of additional hydrogen or CH_4, as shown in tables 3.1 and 3.2. Two effects can explain the improvements. Firstly, consumption of atomic fluorine by the hydrogen, which will be elaborated on in section 3.4 and, secondly, the formation of a protective fluorocarbon layer on the Si and SiO_2 surface is enhanced when hydrogen is added to the mix. Loewenstein assumes that the fluorocarbon passivation layer is formed by the CF_2 (which is formed by the dissociation of the CF_4 in the plasma) reacting with the Si and SiO_2 surface as displayed below

$$CF_2\,(g) + Si\,(s) \longrightarrow Si(CF_2)(s) \tag{3.1}$$

$$Si(CF_2)_n\,(s) + CF_2\,(g) \longrightarrow Si(CF_2)_{n+1}\,(s) \tag{3.2}$$

	O sccm H_2	60 sccm H_2
Si_3N_4 : Si	15 : 100	3 :1
Si_3N_4 : SiO_2	15 : 8	30 : 2
Si : SiO_2	100 : 8	10 : 2

TABLE 3.1: A comparison of the etch selectivity of CF_4 etching of Si, SiO_2 and Si_3N_4 at H_2 flows of 0 and 60 sccm. Calculated from the data presented in [59].

	O sccm H_2	75 sccm H_2
Si_3N_4 : Si	1 : 10	12 : 1
Si_3N_4 : SiO_2	1.4 : 1	100 : 1
Si : SiO_2	80 : 1	2 : 1

TABLE 3.2: A comparison of the etch selectivity of SF_6 etching of Si, SiO_2 and Si_3N_4 at H_2 flows of 0 and 60 sccm. Calculated from the data presented in [59].

where n represents the quantity of these molecules. It was further assumed that this layer is removed from the surface by fluorine radicals forming volatile species. This could for example be according to

$$Si(CF_2)_{n+1}\,(s) + 6\,F\,(g) \longrightarrow SiF_4\,(g) + C_2F_6\,(g) \tag{3.3}$$

where both SiF_4 and C_2F_6 desorb from the surface easily [60].
The added hydrogen removes fluorine radicals by forming unreactive HF (Which will be explained in more detail in section 3.4). Thus it follows from equations 3.1, 3.2 and 3.3 that the addition of hydrogen supports the growth of the protective passivation layer on both the SiO_2 and the silicon. It is unclear why this layer is not formed on the silicon nitride and it also fails to explain, why the Si: SiO_2 selectivity in CF_4 etching decreases significantly from 12.5: 1 to 5: 1 after hydrogen is introduced in substantial quantities.

In 1999, Kastenmeier et al [61] successfully increased the selectivity of Si_3N_4 towards SiO_2 and Si by etching with a remote plasma O_2/N_2 discharge mixed with low flows of CF_4 and NF_3. CF_4 etch selectivities of Si_3N_4 : SiO_2 exceeding 500: 1 were presented,

compared to the 10: 1 selectivities reported in earlier works. Similarly, Si_3N_4 to Si selectivities were increased from 0.1-0.6: 1 reported in earlier works to 60: 1. In particular, the improvements in the relative silicon etch rates are impressive and were explained by three mechanisms. Firstly, the silicon etch rate correlates to the amount of fluorine supplied to the chamber. As this was reduced, the etch rate decreased in a similar manner. Secondly, the Si_3N_4 etch rate is enhanced by the NO that forms in the afterglow of the O_2/N_2 plasma. However, the third mechanism, namely, the rapid oxidation of the silicon surface was found to have the strongest effect on the selectivity. The surface is oxidised by the O_2 and O in the gas phase, reducing the etch rate of silicon to rates levels which are comparable to the etch rate of SiO_2.

More recently, in 2020, two more publications utilising the formation of passivation layers to improve etch selectivities were published by researchers at CEA-Leti. The first, by Posseme et al [57], observed a protective $SiO_x\,F_y\,Cl_z$ layer forming on silicon, which produce an increase in the Si_3N_4: Si selectivity. This was achieved by etching with a plasma composed of a CH_3F, O_2, He and $SiCl_4$ gas mixture. Finally, also in 2020, Rachidi et al [62] used a CF_4 / N_2 /O_2 downstream plasma to etch silicon selective to SiGe. They found that an 8 nm thick, highly selective SiO_xF_y layer is formed on the silicon, while a 2 nm thick passivation layer is formed on the SiGe, protecting it from etching. The passivation layer on the SiGe is a mixture of SiO_xF_y and GeO_xF_y. The measured etch rates were very low, with 20 nm min^{-1} for silicon and 1 nm min^{-1} for SiGe.

In summary, considerable selectivity improvements have been achieved with methods utilising in situ surface passivation. Due to the needs of integrated circuit development, most of the studies presented above focused on increasing the selectivity of silicon nitride towards silicon and silicon dioxide. This is the opposite of what is typically required in MEMS fabrications, where silicon and silicon dioxide are often used as sacrificial layers, and silicon nitride as a structural material. In general, these methods should not be disregarded because similar mechanisms could be utilised to passivate structural materials in MEMS manufacturing during vapour etching. However, both the primary focus materials of this study, silicon dioxide and silicon nitride, are often used to passivate silicon and no mechanism to alter them to achieve surface passivation has been found.

3.4 Gas Additions

The studies detailed in this section attempt to alter etch selectivities in reactive ion etching by the inclusion of additional gasses into the reaction chamber. In most cases, the aim is to neutralise atomic fluorine because, with activation energies of 3.55, 3.02 and 3.36 kcal/mol respectively [51], it is a potent silicon nitride, silicon and silicon dioxide etchant. The first study was conducted by Loewenstein [59], which observed the selectivity data displayed in tables 3.1 and 3.2 and explained them with two mechanisms. These were, firstly, the formation of a protective fluorocarbon layer on the Si and SiO_2, which was discussed in the previous section and, secondly, the removal of fluorine radicals from the gas phase according to

$$F + H_2 \longrightarrow HF + H \tag{3.4}$$

This mechanism is effective because the hydrogen neutralises the atomic fluorine by forming hydrogen fluoride, which does not etch SiO_2 or SiN in the absence of a catalyst. In another noteworthy publication by Zhang et al. [63] from 1998, the authors tried to increase the SiO_2 etch selectivities towards Si_3N_4, in order to fabricate self-aligning borderless contacts. Similarly to Loewenstein [59], they were trying to use hydrogen to neutralise fluorine radicals, while utilising fluorocarbon gasses (C_2F_4, C_2F_6, C_3F_6), with high carbon to fluorine ratios to passivate the surfaces.

In this straightforward experiment, high-density plasmas of various fluorocarbon gasses were generated within a commercial electron cyclotron resonance microwave plasma source. Wafers coated with thermally grown SiO_2 and LPCVD Si_3N_4 layers were placed on an electrostatic chuck which was held at a temperature of 5°C. The etch rate was monitored in situ with an ellipsometer. The fluorine neutralisation aspect of this work was not particularly successful because the SiO_2 to Si_3N_4 selectivities decreased with increased hydrogen additions, but the results are interesting for this study.

Figure 3.2 shows that the etch rate of both materials decreased when hydrogen was added to the process. In the case of etching with CF_4 , as the hydrogen flow was

increased from 0 to 50 %, the SiO_2 etch rate declined from 700 nm min^{-1} to 400 nm min^{-1} and the Si_3N_4 etch rate decreased from 400 nm min^{-1} to 300 nm min^{-1}. In both cases, the etch rate decrease is nearly linear. Similarly, in the case of etching with CHF_3, as the hydrogen addition increased from 0 to 40 %,the SiO_2 etch rate decreased from 450 nm min^{-1} to 250 nm min^{-1} and the Si_3N_4 etch rate decreased from 400 nm min^{-1} to 300 nm min^{-1}.

Based on extensive XPS analysis of the samples post etching, it was concluded that even though the hydrogen inhibited the formation of a protective fluorocarbon layer on both materials, the hydrogen addition also decreased the density of free fluorine and reduced the etch rate. The stronger decline of the SiO_2 etch rate compared to the Si_3N_4 etch rate was explained with the preferential etching of the Si_3N_4 as a result of the bombardment with energetic hydrogen. These findings are particularly interesting in the context of XeF_2 vapour etching, which aims to selectively etch silicon over both silicon dioxide and silicon nitride.

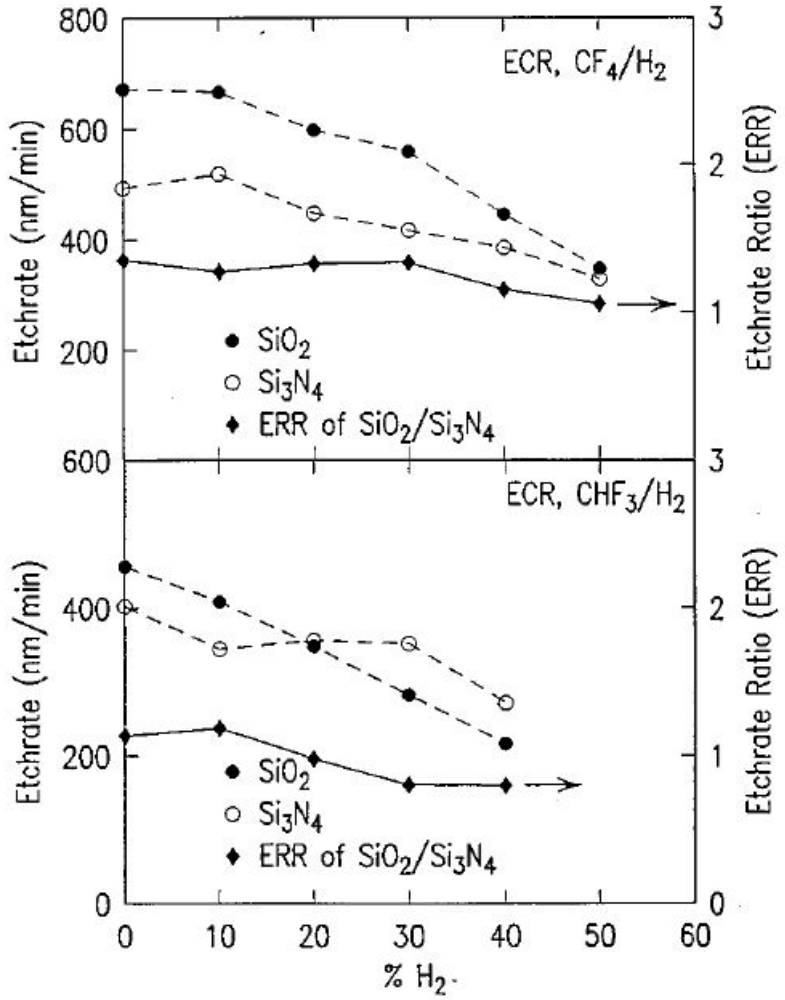

FIGURE 3.2: The silicon dioxide and silicon nitride etch rates and selectivity (called etchrate ratio) in etching with CF_4/H_2 (top) and CHF_3 (bottom) as a function of hydrogen flow. In this figure, ECR stands for electron cyclotron resonance and is the method that was used to generate the high density plasma. Reproduced from [63] with permission from AIP Publishing.

Hydrogen was also used to neutralise fluorine radicals in order to increase the selectivity of silicon over silicon dioxide in an experiment conducted by Nakazawa et al. [64] in 1998, in which silicon dioxide and silicon were etched with a mixture of remote plasma excited argon and anhydrous HF. The aim was to enhance the silicon dioxide etch rate while increasing the process control by avoiding moisture. Unfortunately, when adding the excited argon, the silicon etched at nearly the same rate as the silicon dioxide. This was found to be the result of the formation of fluorine radicals. To combat this, hydrogen was supplied into the chamber to suppress and neutralise the radicals. By adding the hydrogen, a silicon dioxide to silicon selectivity of 4: 1 was achieved with this process.

More recently, in 2020 two papers have been published which aim to improve selective isotropic plasma etching for MEMS [65][66]. There is evidence that Samsung Electronics Co., Ltd is driving the research because their research engineers Vladimir Volynets and Yuri Barsukov were involved in all the research activities, even though different academic institutions published them. These publications are highly relevant for this thesis because they focus on isotropic etch processes, use similar target materials and etch with fluorine radicals, rather than ions.

The publications by Volynets et al. [65] and Jung et al. [66] are a series and are presented in jointly in this review. The aim was to significantly increase the selectivity of Si_3N_4 over SiO_2 using a remote plasma etching process and investigated the underlying quantum chemistry in great detail. For the experiment, blanket coated Si_3N_4 and SiO_2 coupons (4 cm x 4 cm) were etched using an $NF_3/N_2/O_2/H_2$ gas mixture in a "damage free etcher", which appears to be a purpose built device, which generates fluorine radicals (rather than ions) using a remote plasma. In order to remove the $(NH_4)_2SiF_6$ which forms on the silicon nitride while etching with fluorine, a three-step etch, anneal, and cool process sequence was applied.

It was found that the selectivity strongly depends on the hydrogen flow. The data as presented in figure 3.3. (a) shows a gradual decrease of the Si_3N_4 etch rate, which seems to be nearly linearly proportional to the hydrogen flow rate. Figure 3.3 (b) shows that the SiO_2 etch rate is very low and follows a "V" shape, beginning at 0.03 nm min^{-1} for a rate of 24 sccm, decreasing further to less than 0.01 nm min^{-1} for

25 sccm and then rapidly increasing to 0.3 nm min^{-1}. Figure 3.3 (c) shows that the selectivity resulting from the data in parts (a) and (b)reaches a maximum of 380: 1 for a hydrogen flow of 25 sccm, representing a significant increase in the selectivity of silicon nitride over silicon dioxide.

Again, these findings are very interesting in the context of XeF_2 etch selectivities of silicon over silicon nitride and silicon dioxide because of the decline experienced in hydrogen flow-dependent silicon nitride etch rate. Unfortunately, the data is not very convincing, however, because only a small range of hydrogen flows is presented in these graphs. This is unexpected because other plots presented in the study show that the tool used could provide hydrogen flows from 0- 90 sccm. No explanation is given for this. Nonetheless, based on the results presented in figure 3.3, an interesting theory was put forward by the authors to explain the phenomena observed. This will be discussed in more detail in chapter 5 but, in summary here now, it is proposed that the fluorine radicals and the hydrogen form vibrationally excited HF, which reduces the activation energy of reactions of HF with Si_3N_4.

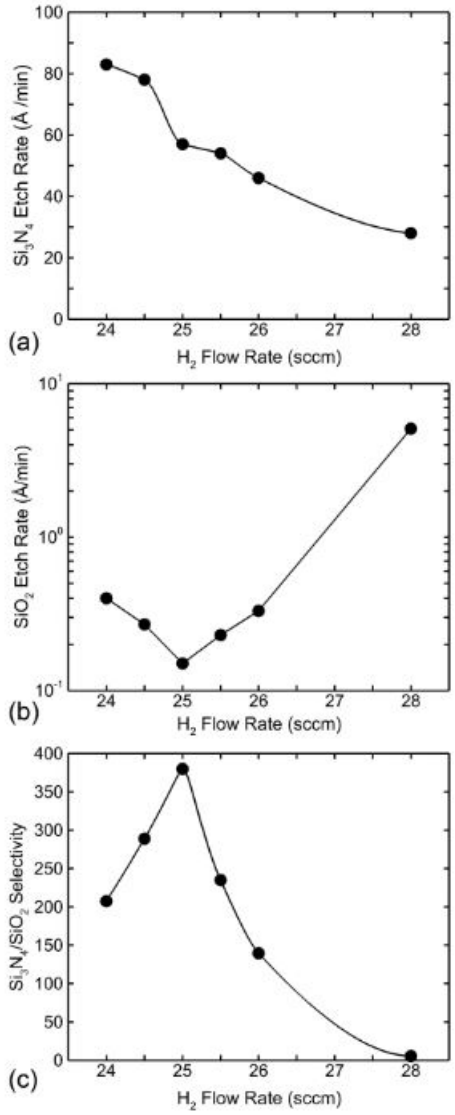

FIGURE 3.3: Hydrogen flow dependency of the etch rates and selectivity when etching Si_3N_4 and SiO_2 with an $NH_2/N_2/O_2/H_2$ remote plasma. Reprinted from [66] with permission from AIP Publishing.

A further dataset supporting the idea that H_2 additions reduce the SiN etch rate was presented by Pankratiev et al. [67]. The aim of the study was to enhance the etch rate of silicon nitride in the discharge of an SiF_6 plasma by adding helium. This resulted in roughly double the silicon nitride etch rate, while the SiO_2 etch rate remained constant. However, more interestingly for this thesis, the data showed a near-linear decrease of the silicon nitride etch rate from roughly 90 nm min^{-1} at a hydrogen flow of 0, to roughly 10 nm min^{-1} at a hydrogen flow of 20 sccm. This phenomenon was not elaborated on or discussed by the authors.

In summary, the addition of hydrogen appears to have the potential to reduce the etch rate of silicon nitride. The most likely underlying mechanism for this is the reaction of the free fluorine with the hydrogen. This forms HF, which does not etch silicon nitride in the absence of silicon dioxide. In industrial activities, it has been observed that the addition of hydrogen improves the etch selectivity. The vapour etch tool manufacturer memsstar [1], has patented the addition of hydrogen into the process gas stream [68]. However, to the author's knowledge, no evidence has been found of any study quantifying the effect of hydrogen additions or explaining the underlying reasons.

3.5 Temperature Adjustments

While the previous sections of the review were relevant for both HF and XeF_2 vapour etching, these methods need to be discussed separately when considering the impact of temperature because the condensation and evaporation of the reactants and the reaction products have a significant role in HF vapour etching.

The temperature reaction rate of XeF_2 with silicon is unexpected because the etch rate appears to increase with reduced temperature. Vugts et al. [69] conducted a molecular beam experiment in order to study the temperature dependency of the etch reaction of Si(100) when exposed to XeF_2. They observed the maximum etch rate at the minimum processing temperature of 150 K, below which XeF_2 condensates. As the temperature rises, the etch rate decreases until it reaches a minimum value at a

[1] A memsstar tool was used for the experimental work presented in this thesis and Dr. O'Hara kindly provided assistance in a consultant capacity.

temperature of roughly 400 K, where it stabilises. Between 600 - 900 K, the etch rate increases again. The findings of Vugts et al. [69] are supported by Ibbotson et al. [70], who observed a linear decline of the etch rate at temperatures below 360 K. The reaction activation energy of the reaction was reported to be -3.2 kcal mol^{-1} for temperatures below this benchmark. Negative reaction activation energies are uncommon and it was suggested that the formation of a surface layer might be the underlying reason. However, the detailed mechanisms causing this phenomenon have not been studied.

Nevertheless, these findings are promising, in particular when considering the proximity effect because there is evidence that the reaction rates of SiO_2 and SiN with fluorine radicals decreases as the temperature decreases. Loewenstein [51] investigated the temperature dependence when etching silicon nitride in atomic fluorine. This study also includes valuable benchmark data for polysilicon and silicon dioxide. The atomic fluorine was generated from F_2 in a remote plasma and helium was used as a carrier gas to transport the fluorine into the etch chamber. The polysilicon and silicon nitride were deposited onto wafers using high-temperature thermal vapour deposition. The SiO_2 was thermally oxidised. The raw temperature-dependent etch rates tabulated in the paper, are plotted in figure 3.4. It clearly shows that the etch rate increases with increasing temperature. Furthermore, positive reaction activation energies of 3.55 and 3.36 kcal/mol for Si_3N_4 and SiO_2 respectively have been calculated. In summary, these findings suggest that the selectivity of silicon over silicon nitride and silicon dioxide can be significantly increased when etching at reduced temperatures. So far, no systematic study has been undertaken to investigate the impact of the processing temperature on the etch selectivities in XeF_2 vapour etching.

The impact of the temperature on HF vapour etch selectivities is complicated because the condensation of the reactant and catalysts, the ion composition of the liquid reactive layer and the desorption of the reaction products all depend on the temperature. In 1966, Holmes and Snell [42] found that SiO_2 can be etched by HF vapour. Their rudimentary set up consisted of a temperature-controlled wafer, which was suspended above an HF bath. The temperature of the HF was controlled by heating or cooling Argon, which was pumped into the reactor and the experiment was

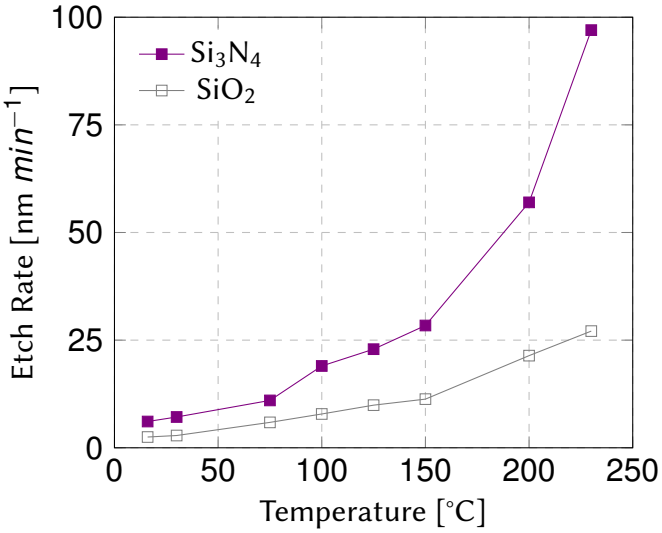

FIGURE 3.4: The silicon dioxide and silicon nitride etch rate when etched by fluorine radicals, plotted as a function of temperature. The data for this plot was obtained from Loewenstein [51].

conducted over a temperature range of 0 - 40 °C. The results displayed in figure 3.5 show that the etch rate reached a maximum at 23 °C, falling to roughly 40 % of this value at 5 °C. Above a temperature of 28 °C, the etch rate fell linearly to zero. During these experiments, the temperature dependent formation of liquid droplets on the surface was observed. Consequently, the lower etch rates at lower temperatures were explained to be a result of the dilution of the HF. At the higher temperatures, no droplets formed and no etch was observable. The temperature data should be viewed with caution because there was no control over the pressure conditions or the humidity in the reactor. However, the importance of the condensation and evaporation mechanism in HF vapour etching was correctly identified.

A poorly executed study into the temperature dependency of etching various oxides with vapour HF was conducted by Wong et al. [30]. They operated in a temperature regime of 25 - 50 °C. They found that the etch rate of doped oxides declined much slower than the etch rate of undoped oxides. This was explained with the drying of the wafer. It should be noted that the study has various flaws. For instance, the etch time in all cases was only 10 seconds. The incubation time to initiate the etch may be longer. Secondly, the total removal of various materials was only 0.01 - 0.8 nm, which

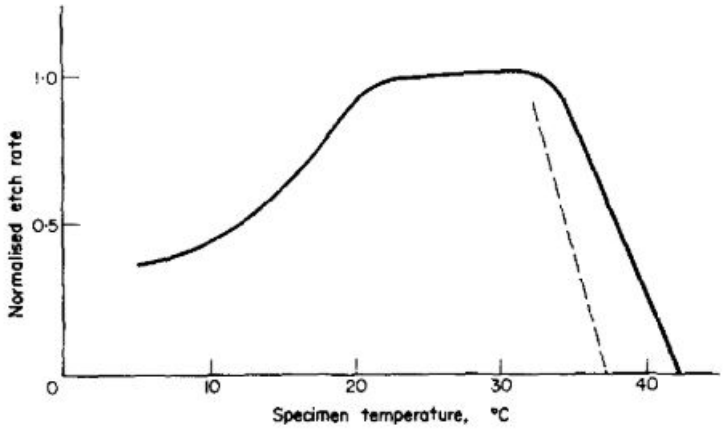

FIGURE 3.5: Etch rate of Silicon Dioxide plotted as a function of temperature. The data was normalised due to fluctuation with the daily humidity in the lab. Reprinted from [42] with permission from Elsevier.

is within the error range of most ellipsometers. Finally, the structure of the work, in particular, the introduction and the discussion are substandard.

Watanabe et al. [71] tried to improve the selectivity of borophosphosilicate glass (BPSG) towards SiO_2 in HF/H_2O solutions in order to reduce the size of the capacitors in dynamic random access memory (DRAM) devices. Experiments were conducted in a purpose built reactor at temperatures of 20, 45 and 65 °C and an increased selectivity of BPSG over SiO_2 at higher temperatures was observed. The reason postulated for this was the suppression of condensation of water at higher temperatures resulting in a decreased ionisation of the HF and a subsequent decrease in the SiO_2 etch rate. At the same time, even at 65 °C, a liquid layer of $H_3PO_4(H_2O)$ formed on the BPSG, which allowed the continuing ionisation of the HF and hence has a barely noticeable effect on the BPSG etch rate.

The previously described studies focused on managing the condensed liquid layer on the sample. However, more recent research shows that the temperature also changes the ionisation properties of HF within this liquid layer. Knotter suggests [46] that

at higher temperatures the HF equilibria shift from the difluorides to the monofluorides, and that SiO_2 is mainly etched by difluorides, while Si_3N_4 is mainly etched by monofluorides. This implies that Si_3N_4 etching accelerates as the temperature increases, while the SiO_2 etching decreases. On the other hand, it also means that a reduction of the temperature could result in a higher selectivity of SiO_2 over SiN, which is the aim of this research project. This effect has been observed and patented by memsstar [72]. However, the impact of this phenomena was not characterised.

In summary, a reduction of the temperature has the potential to increase the selectivity both in XeF_2 and HF vapour etching. While a temperature of 150 K might yield the highest selectivities in XeF_2 vapour etching, condensation mechanisms limit the minimum temperatures in achievable HF vapour etching. Nevertheless, both effects appear promising and are investigated for the first time, in this study.

3.6 Reactant Excitation

Schwentner et al. [73] [74] [75] [76] investigated the possibility of etching anisotropically with XeF_2. The underlying idea was to first suppress the spontaneous reaction of XeF_2 with silicon by diluting the XeF_2 with a selection of gasses, such as oxygen, argon and neon.

In most experiments, within those studies, the XeF_2 to dilutant ratio was 2: 100 and the etch pressure was roughly 7.5 Torr (1 mbar). Then, a nickel mesh was patterned onto the wafer. The wires of the mesh were 10 μm wide, and 100 μm apart. Finally, the samples were exposed to ultraviolet (UV) light at various wavelengths between 105 and 150 nm during the XeF_2 exposure. Using this approach, it was possible to create an array of anisotropic trenches. The best results were obtained at a wavelength of 120 nm because, at this wavelength, only the fluorosilicate layer forming on the surface is excited. The quantum efficiency was high, as 10 silicon atoms were removed per impacting photon. It was also found that the non-selective etching of shaded areas can occur at the absorption spectrum of gas-phase XeF_2, which has a broad maximum at a wavelength of 158 nm [74]. At this wavelength, the XeF_2 disintegrates into XeF and F [77]. Consequently, it was suggested that the shaded areas are etched by the fluorine radicals, a finding which is supported by another study,

published by Sugano et al. [78] in 2001.

It investigated wether SiO_2 and Si_3N_4 mask layers could be conveniently removed by UV light supported XeF_2 etching. A wagon wheel test structure was exposed to the XeF_2 and 0 - 3 W cm^{-1} of UV light, of unknown wavelength, to test if a change in the etch rate could be observed. It was found that the etch rates increased from 0.252 nm to 4.2 nm per pulse and from 2.73 nm to 40.3 nm per pulse for SiO_2 and Si_3N_4 respectively. This increase was nearly linear for both materials in the range of UV exposures of up to 1.5 W cm^{-1}. Beyond that point, the etch rate continued to increase, albeit at a slower rate. In contrast, the silicon etch rate seems to have remained constant, even though the findings do suggest, that fluorine radicals are formed during the UV light exposure.

In summary, it might be possible to enhance the selectivity of silicon over SiO_2 and Si_3N_4 with exposure to ultraviolet light. However, care must be taken that this happens at the optimum wavelength of 120 nm, otherwise the XeF_2 can disintegrate and forms free fluorine, which etches unselectively. Unfortunately, this method is not suitable for the release of free-standing structures because the 120 nm wavelength UV light needs to expose the surface in question, which can not be done when etching undercuts.

3.7 Summary and Conclusion

A number of different methods to increase the etch selectivity between two materials have been reviewed in this chapter. While surface modulation techniques are promising for the fabrication of integrated circuits, they are not particularly suitable for the fabrication of MEMS because the materials are only altered to a very small depth (19 nm) and because the etch rate of silicon nitride is enhanced, rather than reduced. Similarly, ultraviolet light exposure of the sample during etching seems unsuitable, because unless the wavelength is 120 nm, it leads to the disintegration of XeF_2 and the reduction of the selectivity. Furthermore, it is difficult to expose undercut areas to light in any form.

The addition of hydrogen to the gas mix has been shown to neutralise free fluorine

and therefore has a high potential to improve the selectivities in a MEMS fabrication context. Similarly, a reduction in the processing temperature has the potential to improve selectivities in both XeF_2 and HF vapour etching. In conclusion, temperature adjustments and hydrogen additions appear to be the most appropriate mechanisms for etch selectivity optimisation in vapour etching and it is these methods, which have been investigated further in this study.

Chapter 4

Methodology and Test Structure Design

4.1 Introduction

This chapter describes one of the primary research contributions of this project, namely the development of a test structure. As well as detailing the design of the test structure and the measurement based upon it, this chapter also includes insights obtained during their development.

4.1.1 Requirements

The aim of the test structure and associated metrology method was to measure etch selectivities of material combinations undergoing vapour etching. Prior to developing the test structure, the following requirements were defined.

- The test structure has to replicate realistic MEMS fabrication conditions.
- The test structure has to be able to measure the consequence of the proximity effect if it occurs.
- The measurement method has to be time efficient, to assure a high throughput. Ideally, the measurement should be automatable.
- The test structure has to be suitable for the investigation of a wide range of materials.
- The test structure has to cover a wide range of selectivities. Ideally, it should be adaptable for different etch rates and selectivities.

- It should be possible to integrate the test structure onto a production wafer.

4.2 Test Structures used in Vapour Etch Studies

The majority of vapour etch experiments are conducted on blanket layers, which are etched in increments, with the change in layer thickness being measured with an spectroscopic reflectometer . However, a number of more sophisticated test structures have been presented in the past. This section briefly elaborates on their functionality and compares them to the test structure requirements set out in section 4.1.1.

4.2.1 Aperture Test Structure

The post-etch surface roughness, loading [1], and etch rates have all been measured using aperture test structures [79][80] [81][82][52][83]. These consist of a mask layer, with circular or square openings of various dimensions, which are deposited on a sacrificial material. Post etching, a surface profiler is used to quantify the etched depth, the trench formation at the edges and the surface roughness. If the mask layer is transparent, the undercut can be measured under an optical microscope. This test structure is uncomplicated to fabricate, and accurate measurements can be obtained quickly. However, the aperture test structure does not fulfil the requirements specified in Section 4.1.1, because it can not be used to measure the selectivity, nor does it take the proximity effect into account. If analysing undercuts, only transparent mask layers can be used.

4.2.2 Waggon Wheel Test Structure

Sugano et al. [84] [85][78] used the waggon wheel test structure depicted in Figure 4.1 to measure the extent of etch undercuts. In this structure, the width of mask layer and the aperture continuously increases from the center outwards. Therefore, the underlying material closest to the center will be fully removed first. As the etch continues the etch front is pushed further outwards. Post etching, the distance, from the center to the tip of the triangular sacrificial layer is measured by optical microscopy. Even though this test structure measures undercuts, it does not comply with two of the requirements set out in Section 4.1.1 and therefore is not suitable for this study.

[1] The term loading describes the localised slowing of the etch rate due to reactant depletion.

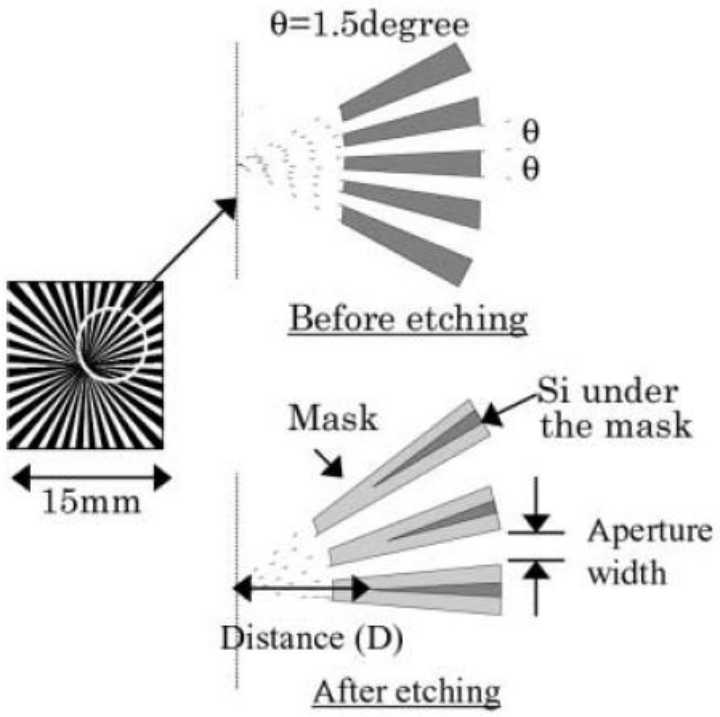

FIGURE 4.1: The waggon wheel test structure as used by Sugano et al. Reprinted from [84] with permission from Springer Nature.

Firstly, it requires a transparent mask layer, which excludes many materials of interest. Secondly, the measurement procedure is quite time consuming and difficult to automate.

4.2.3 Membranes and Cantilevers

Membranes have been used as test structures to demonstrate stiction free etching [86] [87]. Anguita's [86] hexagonal membranes had a surface area of 65 mm^2, and were released through 817 access holes with a diameter of 4 μm.

Initially, an improved version of the membrane like test structure presented in figure 4.2 was considered and tested for this work. The intention was to place the two target materials beside each other and to cover them with a polysilicon mask layer. Etch access holes of various diameters were placed above the interface. The layout and cross section of the test structure are presented in figures 4.3 (a) and (b) respectively.

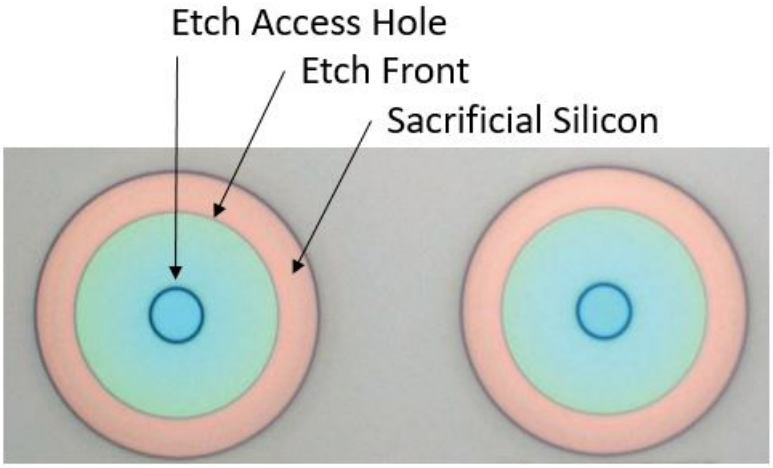

FIGURE 4.2: 190 μm diameter membrane test structure for evaluating the XeF_2 sacrificial etch. Published in [87] by courtesy of memsstar Ltd.

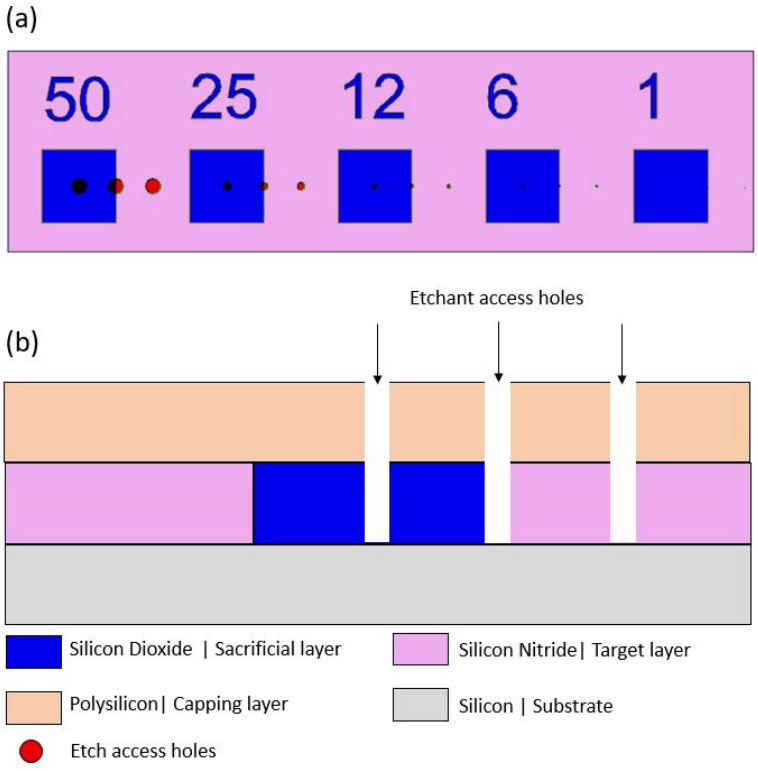

FIGURE 4.3: (a) presentes the layout of an initial attempt of a HF vapour etch selectivity test structure and (b) shows the cross section. The target and sacrificial layer were covered with a polysilicon capping layer. The labels above the squares indicate the diameter of the etch access holes.

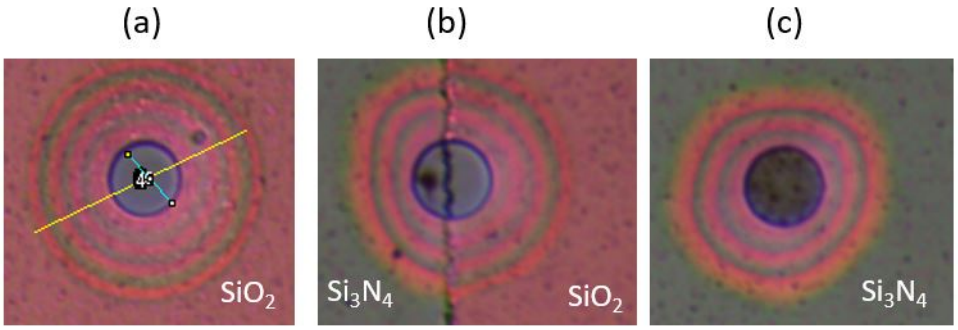

FIGURE 4.4: Optical images obtained from a preliminary HF vapour etch selectivity test structure. The diameter of the etchant access hole is $10\mu m$. The outermost ring indicates the extent of the undercut. (a) shows the undercut of the SiO_2, (b) shows the undercut of both Si_3N_4 and SiO_2 etched in proximity and (c) displays the undercut of the Si_3N_4.

The etch undercuts can be measured from images made using an optical microscope. Examples of such images are presented in figure 4.4. They were obtained from a preliminary sample that was fabricated using localised oxidation (LOCOS) process [2]. In this case the sacrificial and target layer were SiO_2 and Si_3N_4 respectively.

Eventhough the preliminary experiments with SiO_2 : Si_3N_4 samples were promising, it is very difficult to manufacture these test structures with PECVD SiO_2 and PECVD SiN, because chemical mechanical polishing (CMP) is required to planarise the surface after the deposition of the materials. In the case of PECVD SiN and PECVD SiO_2 special pads would have to be purchased in order to planarise both of these materials to one level. Another disadvantage of this method is, that only tranparent mask layers can be used. Therefore, this approach was not pursued and alternative methods were explored.

Cantilever test structures have been used to demonstrate stiction free etching [83] [88] and to demonstrate that certain etch processes are suitable for MEMS fabrication [89]. Van Barel et al. [34], [90] presented a very interesting concept for wet

[2]The locos process describes a fabrication method were Si_3N_4 is deposited on the substrate and patterned. SiO_2 is then grown in the open regions, while the remainder of the sample is protected by the Si_3N_4 mask.

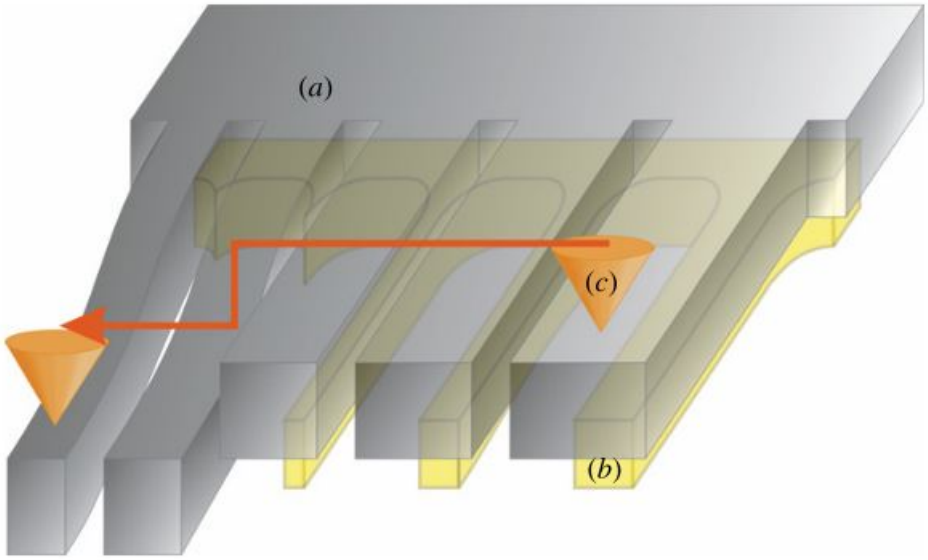

FIGURE 4.5: The surface profiler measurement of the cantilever test structures, developed by van Barel et al. [34]. The label (a) represents the mask layer (b) the sacrifical layer and (c) the profiler stylus tip. Reprinted from [34] with permission from IOP Publishing.

etch processes. Their test structure consists of an array of cantilevers with increasing width. After etching, a surface profiler scans the array. If suitable profiler setting are chosen, the released cantilevers deflect, while the cantilevers that have not been fully undercut remain at their original height. The undercut is equal to at least half of the width of the widest cantilever deflected. Figure 4.5 shows the operating principle. This measurement principal does not require a transparent mask layer, the surface profiler measurement can be easily automated and a wide range of etch rates can be measured. Furthermore, the release of free standing cantilevers is an excellent model for MEMS fabrication processes. Therefore, this design for an etch rate test structure was used as a starting point in the development of the selectivity test structure presented in this thesis.

4.3 Measurement Method

The metrology method developed in this work is based on releasing an array of free-standing bridges and measuring their displacement with a surface profiler stylus. The

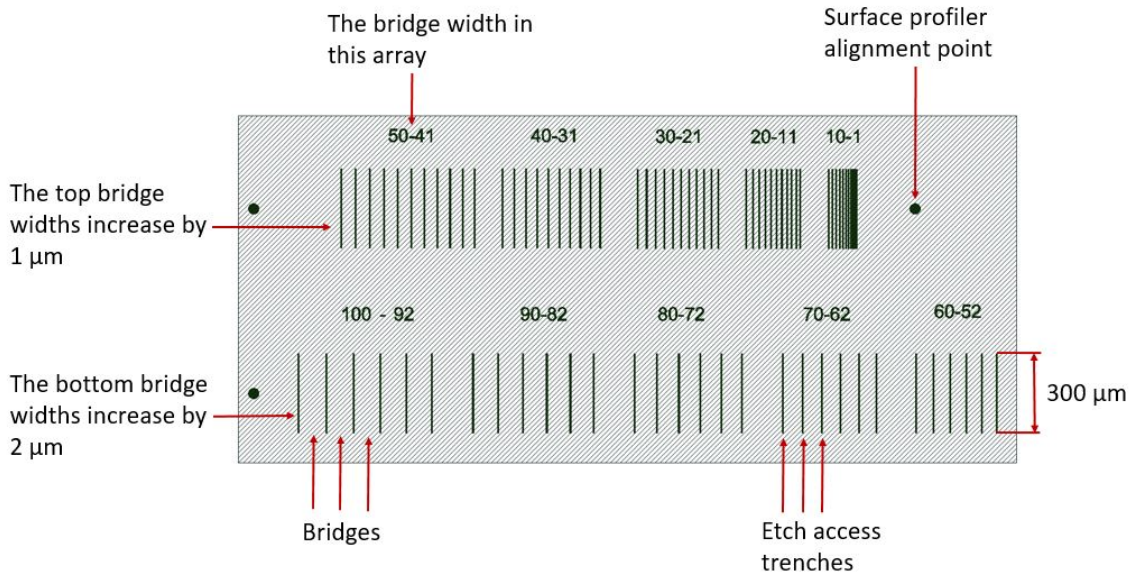

FIGURE 4.6: The annotated layout of the test structure bridge array. This figure has been in published in slightly different form in [23] and [28].

width of the bridges decreases incrementally, in a similar manner to the cantilevers presented by Van Barel et al. [34]. However, bridges are used in place of cantilevers, because they are more mechanically robust, they are less prone to stiction and give a more reliable indication of undercut by limiting the access of the etchant to two sides, rather than three. In this work, the release layer is underlain by a target layer (Compare figures 4.6 and 4.7 (a) for the layout and cross section respectively). The sacrificial layer can be made of any material, which is preferentially removed in the respective vapour etch process. For instance polysilicon in XeF_2 vapour etching and SiO_2 in HF vapour etching. The target layer, however, can be any material against which the etch selectivity needs to be known. The proximity effect is taken into account in this test structure due to the juxtaposition of the sacrificial layer and the target.

After both the sacrificial and the target layer have been exposed to the etchant for a predefined time, the bridge array is scanned by a surface profiler. If a bridge has been released, it can be vertically displaced by an amount equal to the thickness of the material which has been removed. The resulting surface profile clearly shows if

the bridge has been vertically displaced by the thickness of the sacrificial layer, or by the combined thickness of the sacrificial layer and the target layer. The undercut is half of the width of the widest bridge that can be fully displaced. The schematic cross section displayed in Figure 4.7 shows a bridge being etched and displaced by the surface profiler's stylus.

(a) shows the test structures cross-section prior to etching. It should be noted that both the sacrificial and the target layer are exposed to the etchant through the trench.

(b)-(d) show the gradual etch of both layers as more etch time passes.

(e) depicts the displacement of a bridge by the stylus profiler.

(f) shows a small hill of the target material and the surface profiler's stylus displaces the bridge vertically by the thickness of the sacrificial layer.

(g) shows that the etch has proceeded even further and both layers have been fully removed. In consequence, the profiler displaces the bridge by the combined width of both the sacrificial and the target layers.

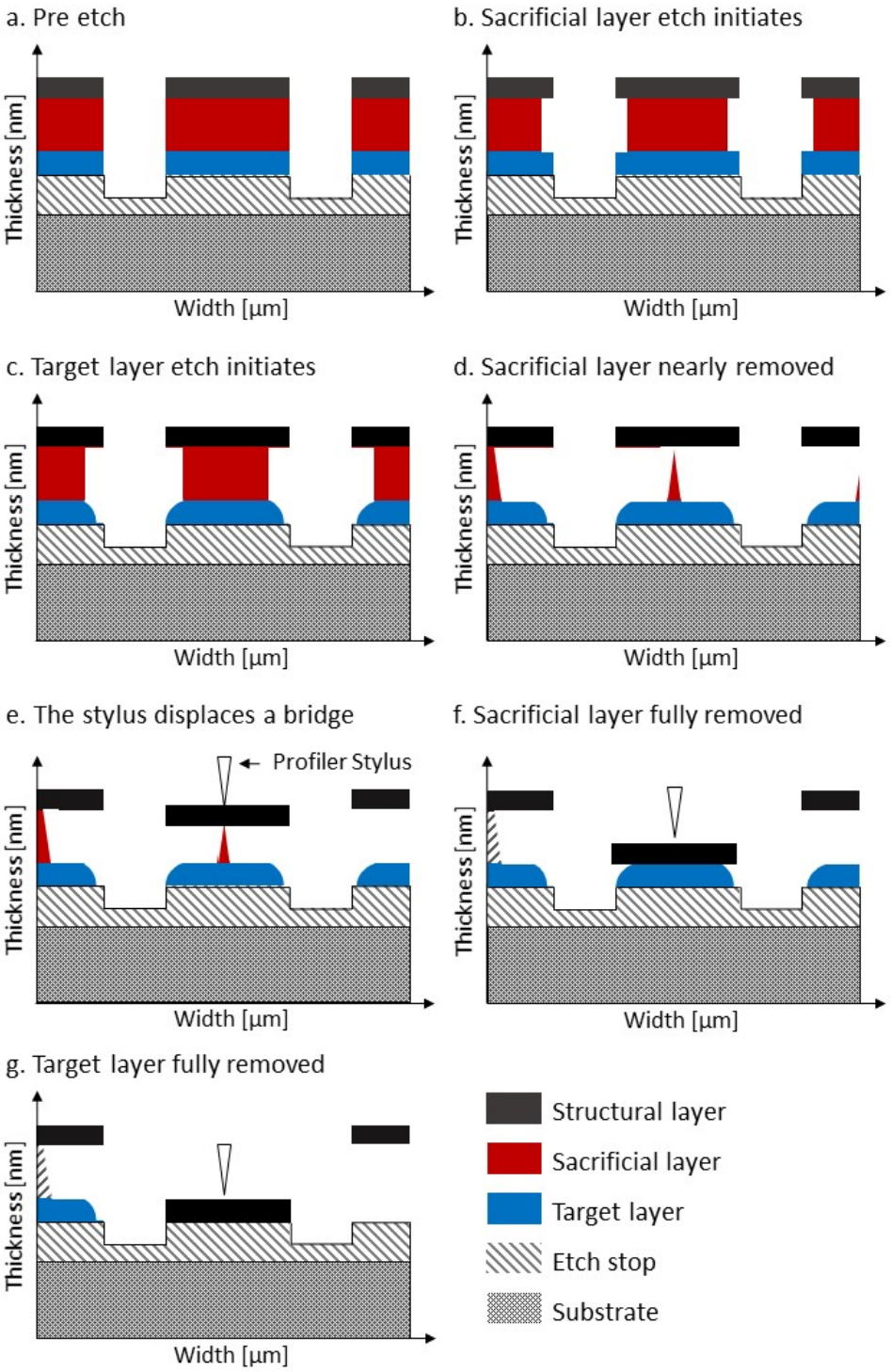

FIGURE 4.7: A generalised series of cross section showing the measurement methodology. The individual steps have been labelled within the figure. This figure has been in published in slightly different form in [23] and [28].

4.4 Materials, Layout and Design Considerations

A range of combinations of materials can be used as structural, sacrificial and target layers. When choosing the structural layer, the mechanical properties of the material need to be taken into account to ensure that the bridge does not collapse after the release or buckle extensively due to stresses within the layer. Furthermore, the material used should be inert to the etchant.

The sacrificial layer can be freely chosen in order to reflect realistic MEMS fabrication conditions. At this stage, it is crucial to accurately determine the thickness of the sacrificial layer because it is required as a benchmark for when the test structure is being measured with the surface profiler. In this study, blanket test wafers were processed under the same conditions as the sample wafer. They were then measured using a spectroscopic reflectometer. The desired sacrificial layer thickness was 500 nm because it enables a measurable displacement of the profiler whilst involving reasonably fast deposition times.

Similarly to the sacrificial layer, the target layer material can be chosen to reflect realistic MEMS fabrication conditions. Again, it is essential to determine the layer thickness accurately using a blanket test wafer. In this study, the target layer thickness of different samples varied between 200 and 450 nm. The etch rates for both layers appeared to be independent of the thickness of the layers. Even though it was not observed in this study, the etch rates may slow down if the layers are significantly thicker. This could either be due to the loading effect when the etchant is consumed faster than it is resupplied or due to gas flows within the undercut that prevent the reactants from flowing to the etch front. Similarly, stresses between the layers did not seem to cause any issues in the study into XeF_2 vapour etching. However, the test structures used in the HF vapour etch experiments required a 10 minute bake at 150 °C to release the stress in the copper capping layer. The etch stop layer is only required if the etchant is likely to attack the silicon substrate. This is the case for XeF_2, and 50 nm thick platinum layers were used as an etch stop. Using platinum has the advantage that it also acts as an etch stop for the reactive ion etching required to form the etch access trenches. However, platinum is expensive. Therefore, SiO_2 was used as a more cost-efficient etch stop layer where appropriate.

The layout of the test structure used in this study is displayed in Figure 4.6. The arrays on the top have bridge widths ranging from 2 to 50 μm and the width increases in increments of 1 μm. This results in an undercut measurement resolution of 500 nm. The widths of the bridges displayed in the arrays on the bottom of Figure 4.6 range from 50 μm to 100 μm. This results in an undercut measurement resolution of 1 μm. Those bridge widths were selected, because they allow to measure a selectivity range from 1: 1 to 50: 1, with an undercut resolution of 500 nm. If larger selectivity ranges need to be measured, a row of bridges with increased width can be added. When fabricating the test structure, it is important to control the bridge width during photolithography and anisotropic etching carefully because, in particular for the narrower bridges, width variations are one of the main error sources (More details are provided in the Section 4.7.1). In this study, multiple attempts were required to fine tune the photolithography process. Using the photoresist datasheet as a guideline, soft and hard baking temperatures and times between 90 and 115 °C and 70 to 90 s respectively were tested. In order to optimise the exposure dose, exposure times between 10 to 20 seconds were tested. The 300 μm long bridges were separated by 5 μm wide trenches as this allows the surface profiler's tip, which has a diameter of 2 μm, to measure the full depth of the trench. During the design and prototyping phase of this test structure, bridges arrays with 100 μm, 200 μm and 300 μm were fabricated and it was observed that the length did not have any effect on the etch rate. Therefore, the 300 μm long bridges were used in the final design. This bridge length is a trade-off between the required low spatial occupation of the test structure on a production wafer and the ease with which alignment of the test structure can be completed in preparation for the surface profiler measurement.

The test structures presented in this study were fabricated on 4 inch silicon wafers. Each wafer consisted of ninety chips with eight test structures and an identification label. The chips are bounded by 100 μm wide dicing channels.

4.5 Surface Profile Measurement and Interpretation

In the experiments presented, each sample is a chip which contained 8 test structures. Following etching, the chips were put on a custom-build chip holder with a capacity

for twelve chips. The chip holder was designed to be compatible with a Bruker Dektak XT, which can be programmed to operate automatically and to process and store the resulting data. It is essential to carefully fine-tune the surface profilers measurement parameters, in particular the downforce and the scan speed, to prevent measurement failure (modes described in Section 4.7). Each measurement results in a surface profile, an explanation of which is given using the example displayed in Figure 4.8. The test structure which produced this plot was used to measure the selectivity of polysilicon towards silicon nitride in a XeF_2 vapour etch process. It was etched at a pressure of 9 Torr at a temperature of 30 °C. The nitrogen carrier gas flow was 100 sccm and the etch time was 40 seconds. On the profile, five bridge arrays can be distinguished. The narrowest bridge is on the far right, the widest on the far left. The wider bridges in the two arrays on the left have not been displaced at all. In contrast to that, the narrower bridges of the two arrays on the right have been vertically displaced by more than 650 nm. In this example, the central array, within which the bridges are 21 μm to 30 μm wide, can be used to determine the etch rates. The widest bridge that has been displaced by 450 nm is 29 μm wide. This indicates that 14.5 μm of polysilicon have been undercut during the etch time. The 24 μm wide bridge is the widest one that has been displaced by more than 650 nm. Therefore, the silicon nitride has been undercut by 12 μm. The etch time was the same for both materials. Therefore, dividing both undercuts yields the selectivity. This example measurement results in a polysilicon to silicon nitride selectivity of 1.2:1.

4.6 Measurement Verification

Two methods were used to verify if the surface profile reliably represents the etch undercut. Firstly, five etched and measured samples from the process calibration were randomly selected. Then, the aluminium structural layer was removed by etching. Guided by the measured surface profile Energy-dispersive X-Ray spectroscopy (EDX)[3] was used to measure the chemical composition of the materials beneath the bridges.

[3]To conduct an EDX measurement an electron beam is focused on the sample. The beam's interaction with the specimen results in an element specific X-ray emission that allows to characterise the sample chemical composition [91].

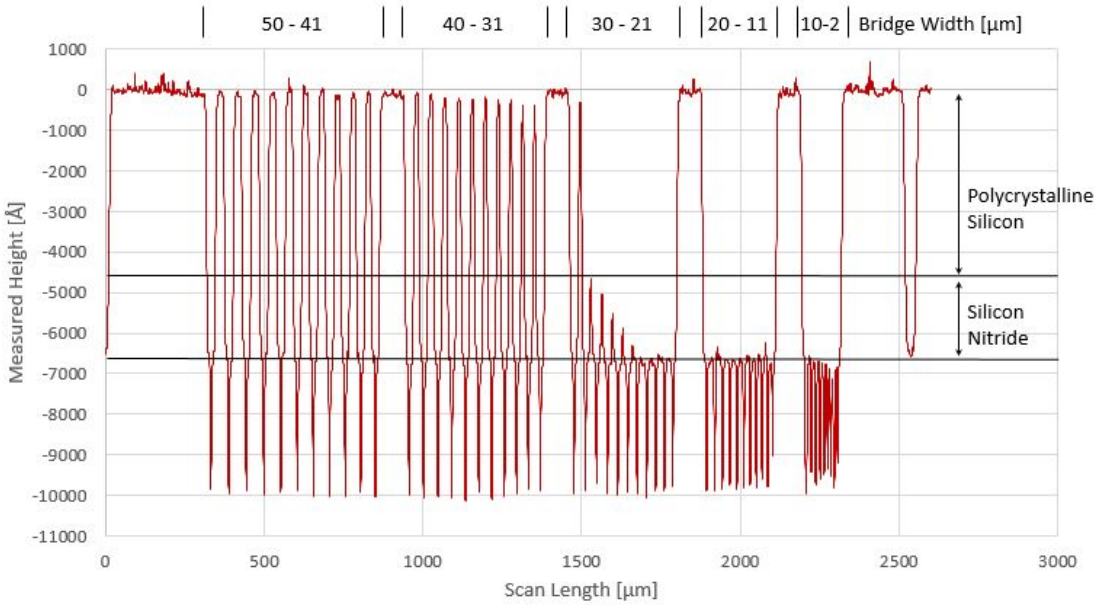

FIGURE 4.8: An example surface profile generated by the measurement of the test structure. The thickness of the polysilicon sacrificial layer and the silicon nitride target layer is indicated within the figure. Another measurement obtained from a different test structure on the same chip was published in [23].

An example surface profile with the corresponding EDX measurements is displayed in Figure 4.9. Each EDX measurement data point is the average of three measurements taken in the middle and at either end of the bridge structure along its centerline. The data shows that, with increasing bridge displacement, the nitrogen content decreases until no nitrogen is measured, thereby confirming the test structure, which had indicated the complete removal of the silicon nitride. Similarly, the oxygen content measured increases as layer thinning is indicated by the test structure. This indicates that silicon dioxide is becoming the dominant layer measured. The resulting material compositions from the EDX measurement agreed with the information obtained from the surface profiler measurements for all five samples. The vertical penetration of the electron beam can be upto 2 μm. This explains why oxygen was measured at locations that were covered by silicon nitride.

For the second verification method, cross-sections of the test structures were made using a focused ion beam (FIB). The cross-sections were then imaged using an SEM.

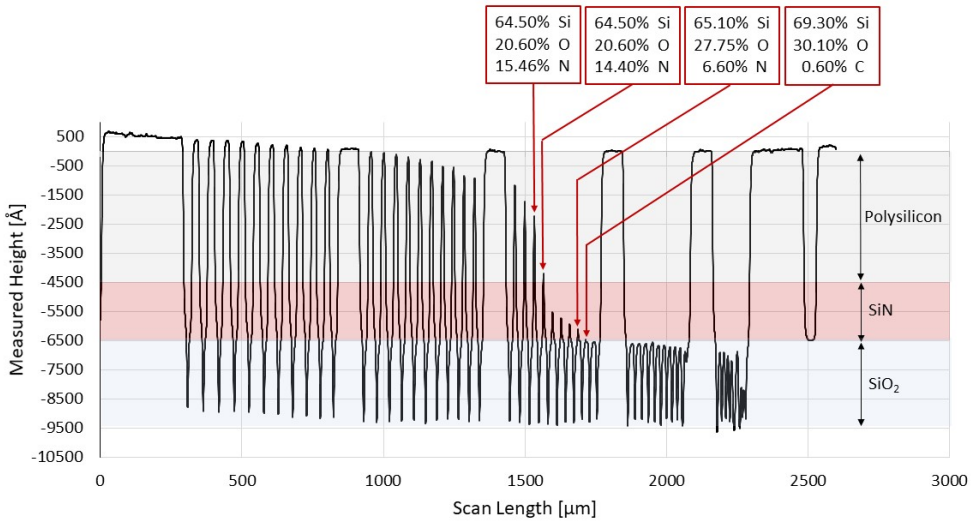

FIGURE 4.9: The surface profile of a test structure from the design phase with the respective EDX measurements displayed at the corresponding location. The test structure had an aluminium structural layer, a polysilicon sacrificial layer, a silicon nitride target layer and a silicon dioxide etch stop.

The example in Figure 4.10 shows a 31 μm wide bridge which is being supported by a narrow polysilicon pillar. The respective surface profile showed no bridge deflection. In contrast, Figure 4.11 shows that the polysilicon sacrificial layer has been fully removed from underneath the 28 μm wide bridge, while a small hill of the silicon nitride target material remains. The respective profile showed that this bridge had been deflected by the thickness of the polysilicon sacrificial layer. It also showed that the target layer had not yet been removed. Both figures were obtained from the same test structure. The information obtained from the SEM cross-sections are coherent and in agreement with the information obtained from the surface profiler measurements.

In summary, both measurement methods supported the conclusions drawn from the surface profiler measurement and confirm that the data obtained by this method is reliable and can be used for etch selectivity experiments.

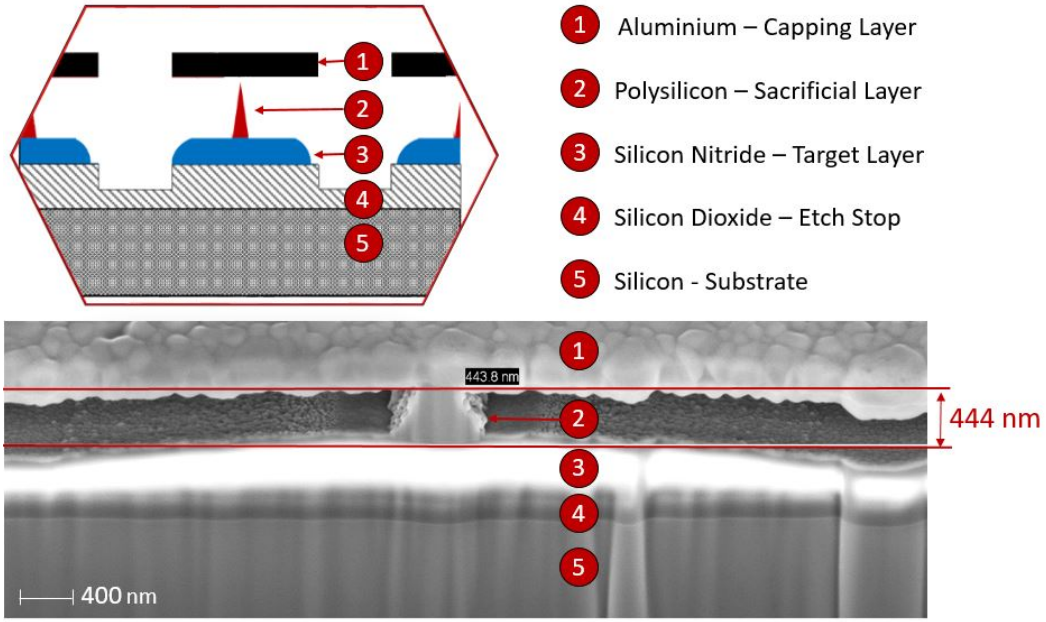

FIGURE 4.10: A cross section SEM image of a 31 μm wide bridge showing a narrow polysilicon pillar, supporting the aluminium bridge and preventing the deflection of the bridge during the surface profiler measurement. The SEM image component of the figure was also presented in [23] and [28].

4.7 Measurement Considerations

Some of the precautions which should be taken to ensure that the test structure delivers valid measurements are outlined in this section.

4.7.1 Photoresist Patterning

The bridge width has a substantial effect on measurement accuracy, in particular for the narrowest bridges. If, for example, the width of the 10 μm wide bridge deviated by 1 μm, the resulting measurement would give an error of 10 %. In order to minimize the width deviation, the photoresist patterning process was carefully developed in multiple iterations. The most accurate bridge widths were achieved with SPR-220 photoresist, spin-coated for 1 minute at 3000 rpm to give a 3 μm layer. The wafer was baked for 90 seconds at 115 °C and exposed in a mask aligner for 15 seconds (hard contact, power density $4 mW cm^{-2}$). The wafer was then post-exposure baked for 90 seconds at 115 °C and the resist was developed for 60 seconds in the resist developer

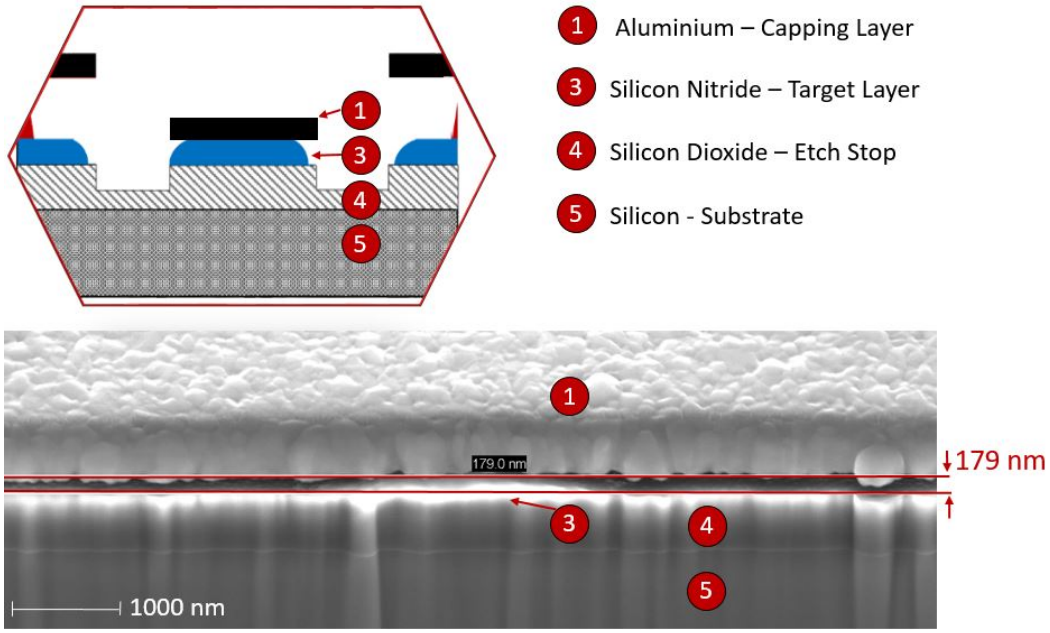

FIGURE 4.11: A cross section SEM image of a 28 μm wide bridge not showing any polysilicon. Instead, the aluminium bridge is supported by the 180 nm thick silicon nitride target layer. The SEM image component of the figure was also presented in [23] and [28].

MF-26. Furthermore, to assure the quality of each sample wafer fabricated, the width of five (between 11 -15 μm) bridges was measured under a microscope on five separate chips. One chip was located at the centre of the wafer, while the other four were those closest to the edges of the wafer (top, bottom, left and right). If the bridge width of the developed photoresist deviated by more than 5 % from the nominal width, the resist was removed and the resist deposition and patterning process was repeated.

4.7.2 Trench Etching

Compared to the photoresist patterning, the anisotropic etching of the layers to form trenches is more straightforward. However, care must be taken to prevent over or under etching. If XeF_2 is to be used in the subsequent vapour etch step, it is essential to keep the etch stop layer intact to prevent the etching of the underlying silicon substrate. The most secure method to achieve this is the use of an etch stop, which is inert to the reactive ion etch, such as platinum. If this is not possible and a transparent layer is used instead, the etch progress can be monitored by measuring the thickness

of the layer in the dicing channels with a spectroscopic reflectometer.

Similarly, the target layer would not be exposed to the etchant at the same time as the sacrificial layer if the sample was under etched. Therefore, the reactive ion etch progression was repeatedly measured using a surface profiler. The measured trench depth was compared with the layer thickness measured and recorded after the layer deposition. It should be noted that, for the reactive ion etcher used in this study, the etch rate in the centre of the wafer is slightly faster than the etch rate at the edges of the wafer. For the samples presented in this study where the etch stop layer was not inert to the reactive ion etch, the etch stop layer was slightly thinned at the centre of the wafer.

4.7.3 Duration of Etching

The first error source relates to over and under etching of the test structures during the vapour etch process. The narrowest bridge used in this study was 2 μm wide. Hence under etching occurs if the etched undercut is less than 1 μm. The under etch can be overcome by extending the etch time. If the etch time is fixed, and the technical means are available, the test structures can be fabricated with a reduced bridge width. The widest bridge used in this study is 100 μm wide. Hence, over-etching occurs when the etch undercut exceeds 50 μm. This can be overcome by reducing the etch time or by fabricating additional samples with wider bridges.

4.7.4 Mechanical Destruction of the Bridges

The bridges can be destroyed during the measurement if the wrong profiler settings are used. If the downforce is too high, or the scan speed is too fast, the bridges can be ripped from their anchors on either side. This can be prevented by using a lower downforce and by reducing the scan speed.

4.7.5 Bouncing Stylus

Care needs to be taken not too reduce the downforce to much, as this can results in the stylus bouncing off the bridges. This fault is easy to identify because the resulting

profile indicates a positive bridge displacement. A downforce of 2 - 3 mg avoided both the mechanical destruction of the bridges and prevented the bouncing of the stylus.

4.7.6 Bridge Deflection

It is suspected that too high a scan speed can result in the mechanical deflection of the bridge. In this case, the surface profiler signal shows one or more peaks of bridges within an array that has been otherwise released. This phenomenon can be easily overcome by reducing the scan speed.

4.8 Summary and Conclusion

Within this chapter, the requirements for the test structure and measurement methodology needed for this study were defined. These requirements, were compared with vapour etch test structures used in previous studies. It was found that the etch undercut can be conveniently and accurately measured with a surface profiler. Inspired by the literature, a bridge based test structure based on the release of bridge arrays with incrementally decreasing width has been designed and optimised, enabling the measurement of etch selectivities between pairs of materials.

This design reflects realistic MEMS fabrication conditions and where it occurs, it takes the proximity effect into account. Furthermore,the layout, design and lessons learned from practically designing and using the test structure and measurement method were presented. On the basis of the practical application of the test structure, error sources were identified and measures to prevent them from occurring were presented. Finally, advanced material characterisation methods were used to verify that the surface profile resulting from the test structure measurement reliably represents the etch front progression and material removal.

In conclusion the first test structure which can be used to characterise the vapour etch selectivity under realistic MEMS fabrication conditions has been presented. The layout can be adjusted to accommodate different selectivity ranges and, due to its small dimensions, can be easily placed on production wafers for industry applications. Furthermore, the measurement method allows the measurement of multiple

samples automatically, only requiring a tool operator for the initial alignment of the chip holder and to start the dedicated measurement programme. The resulting surface profiles can be analysed and the results read within a matter of seconds.

Chapter 5

Investigation of XeF_2 Selectivity

5.1 Introduction

This chapter focuses on XeF_2 vapour etch selectivity. The three aims of this study are the characterisation of (1) the proximity effect; (2) the effect of process temperature on the etch selectivity; and (3) the effect of supplying hydrogen and xenon difluoride into the etch chamber simultaneously on the etch selectivity.

5.2 Objectives of the Study

This chapter is focused on the efforts made to control XeF_2 vapour etch selectivities for material combinations commonly used in the MEMS and NEMS fabrication processes. The literature presented in chapter 2 and 3 suggests firstly that the proximity effect reduces the selectivity significantly and secondly that reducing the temperature and/or by flowing hydrogen into the chamber significantly increases selectivity. Based on the literature review, the above factors are examined in the following sections.

5.2.1 Characterisation of the Proximity Effect

The published knowledge regarding the proximity effect is minimal. Even though section 2.3.6 summarised the problem in MEMS fabrication caused by material proximity and suggested an explanation of the associated chemical reactions, the extent of the effect has not been fully characterised. To date, no methods to address the occurrence of low selectivities have been presented.

The following objectives were defined to facilitate an increased understanding of the proximity effect and thereby reduce its impact on MEMS and NEMS fabrication:

- Investigate, whether the proximity effect, previously only observed for silicon dioxide etching also occurs when etching silicon nitride.
- Measure the spatial extent of the proximity effect and determine the minimum layer separation required to prevent its occurrence.
- Quantify the selectivity of layers, etched subject to the proximity effect. In addition, etch and measure the selectivities of blanket layers processed under identical conditions to establish a benchmark. The resulting selectivities will then be compared with the data presented in the literature.
- Use the experimental data obtained to determine whether the data is in agreement with the theoretical description of the etch process suggested in the literature [49], [92] [22].

5.2.2 Characterisation of the Temperature Effect on the Selectivity

Section 3.5 presented research that suggested that the maximum etch rate of Si in XeF_2 occurs at the lowest possible temperature of 150 K. In the context of the proximity effect, it also presented evidence that the reaction rate of fluorine radicals with silicon dioxide or silicon nitride increases proportionally to the process temperature. Even though the theory suggests, that selectivity improvements could result from low temperature processing, this has not been confirmed experimentally, and the extent of these improvements is unknown. Hence the following objectives were defined:

- Investigate whether the reduced selectivity resulting from the proximity effect can be improved by reducing the processing temperature.
- Characterise the extent of possible improvements.
- Outline how these findings could be used to enhance the performance of vapour etch tools in the future.

5.2.3 Characterisation of the Effect of Adding Hydrogen as Processing Gas on Etch Selectivity

Publications presented in Section 3.4 suggest that flowing hydrogen into the processing chamber could result in a reaction with the fluorine radicals produced by the proximity effect, in order to create non-reactive hydrogen fluoride. It was also suggested that a protective fluorocarbon layer could form on the surface of SiO_2 films. To date, these phenomena have not been evaluated in the context of XeF_2 vapour etch selectivity. It is unclear if significant changes will be observed and hence the following objectives were defined:

- Investigate whether the reduced selectivity resulting from the proximity effect can be improved by supplying hydrogen into the reaction chamber during processing.
- Determine the relationship between the hydrogen concentration within the etch chamber and the selectivity.
- Outline how these findings could be employed to enhance the performance of vapour etch tools in the future.

5.3 XeF_2 Selectivity Experiment

5.3.1 Equipment

A schematic if the commercial memsstar Alpha Orbis XeF_2 etch tool that was used for this study is displayed in figure 5.1. In contrast to most of the previously published research on XeF_2 etching, the gas is continuously supplied to the reaction chamber of this tool rather than in pulses. Nitrogen is used as the carrier gas and the processing pressure is variable, adjustable to a maximum of 10 Torr in intervals of 0.1 Torr. The pedestal temperature can be varied and set at values between 5 and 45 °C in increments of 0.1 °C. Additional gasses, such as hydrogen can be flowed into the chamber during processing. The XeF_2 is stored in solid form in a bubbler and supplied to the reaction chamber by flowing controlled amounts of nitrogen through it. A limitation of this setup is, that the XeF_2 supplied to the chamber from the bubbler depends on the amount of solid XeF_2 within the bubbler. As the XeF_2 is depleted, the XeF_2 flow rate

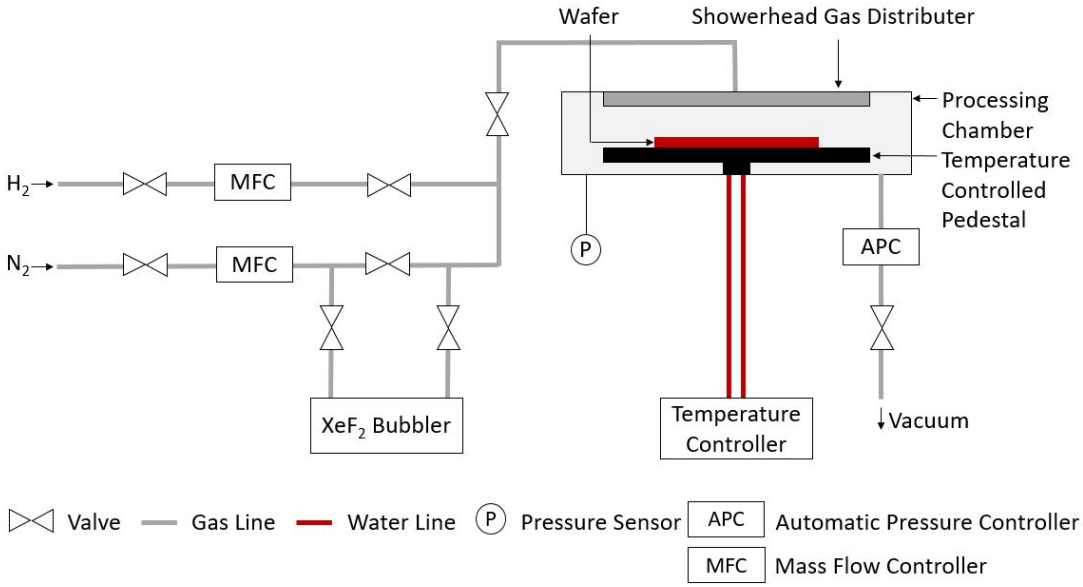

FIGURE 5.1: Schematic of the memsstar Alpha Orbis XeF_2 etch tool used in this study.

into the chamber decreases. In order to account for this, the XeF_2 flows were measured before and after every experimental session. The chamber pressure is automatically controlled by an automatic pressure controller. Compared to other commercial etch tools, the Alpha Orbis has two key advantages. Firstly, in pumped systems, the XeF_2 is consumed as the etch progresses and therefore, the etch rate gradually decreases during the etch process. In contrast to that, the continuous supply of the reactant allows the etch rate to be constant in this system. Secondly, the automatic pressure controller, mass flow and temperature controllers enable high process control.

5.3.2 Test Structures Fabrication

The test structure and measuring method described in chapter 4 was used for this experiment. Five different designs were fabricated, etched and measured. Those are identified by the material of their target layer as SiN-PECVD, SiN-LPCVD and SiO_2-PECVD. For those samples, the target material is placed below the sacrificial layer. Two of the designs labelled SiN-Reference and SiO_2 Reference are benchmark samples without a sacrificial polysilicon layer. In general, the fabrication process for all samples is the same, with only the layer composition being different. The general fabrication process of the test structures is presented in figure 5.2 (based on the sample

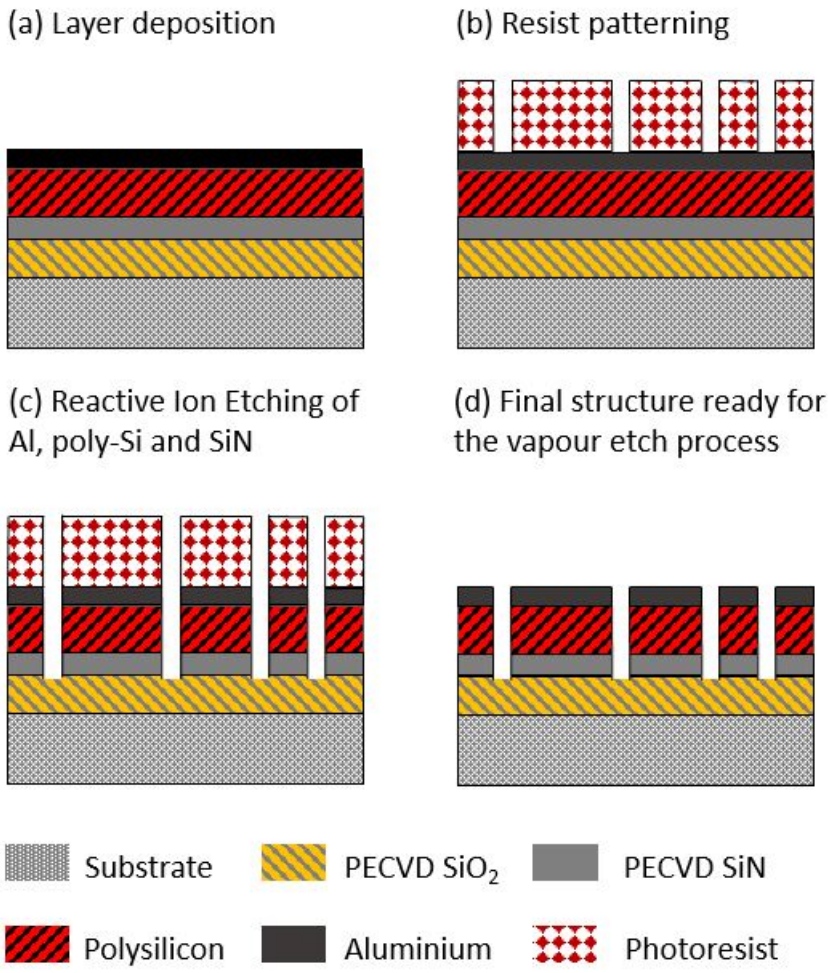

FIGURE 5.2: Schematic process flow of the fabrication process of the SiN-PECVD test structure. This figure has been published in [23].

with the SiN-PECVD target layer). Their layer composition and thicknesses are presented in table 5.1. The silicon nitride and silicon dioxide etch rates measured from the reference samples will be compared with the ones obtained from the other three samples in order to characterise the etch rate altering effect of proximity etching. The detailed layer composition of the samples with a target layer is presented in table 5.2. The deposition recipes and processing parameters for each sample are available in the run sheets, located in the appendix.

After deposition of the above layers the remaining fabrication process was identical for all samples. The photoresist was patterned using the method outlined in section

Layer Description	SiN-Reference	SiO_2-Reference
Capping Layer	350 nm Aluminium	350 nm Aluminium
Sacrificial Layer	-	-
Target Layer	450 nm PECVD SiN	500 nm PECVD SiO2
Etch Stop	50 nm Platnium	50 nm Platnium
Adhesion Layer	10 nm Ti	10 nm Ti
Wafer	Silicon	Silicon

TABLE 5.1: Layer configuration of the reference samples. This data has been published by the author of this study in [27].

4.7.1 and figure 5.2 (b) shows the design after photoresist patterning. The etchant access trenches were anisotropically etched into the aluminium capping layer and the polysilicon sacrificial layer with chlorine etch chemistry, using an STS Multiplex Reactive Ion Etcher (RIE). The trenches continued into the target silicon dioxide and silicon nitride layers through the use of fluorine etch chemistry with a Plasma Technology JLS RIE80. The detailed etch parameters for each sample are available in the run sheets. Finally, the resist was stripped and the wafers were diced into 11 mm long and 5 mm wide chips. Each chip consists of 8 test structure arrays and an alphanumerical identifier code.

Layer	SiN-PECVD	SiN-LPCVD	SiO2-PECVD
Capping Layer	350 nm Aluminium	350 nm Aluminium	350 nm Aluminium
Sacrificial Layer	500 nm LPCVD Polysilicon	500 nm Polysilicon	500 nm Polysilicon
Target Layer	450 nm PECVD SiN	500 nm LPCVD Si_3N_4	500 nm PECVD SiO2
Etch Stop	50 nm Platnium	500 nm SiO_2	50 nm Platnium
Adhesion Layer	10 nm Titanium	-	10 nm Titanium
Wafer	Silicon	Silicon	Silicon

TABLE 5.2: Layer configuration of the samples subject to the proximity effect. The data presented in this table has been published in [27].

5.3.3 Experimental Set-Up

In order to ensure that the Alpha Orbis process tool was running smoothly, a standard etch process was run on an empty chamber before every experimental session. The gas flows and pressure were monitored to verify the correct operation of the tool. Then, a tool-specific calibration run was performed to assure that all gas flowed as required and specified in the recipe. After the temperature of the pedestal was adjusted to the desired value, the chamber was vented and the sample loaded. At this point the etch recipe was programmed and the etch process started. The tool enables control of the pressure, carrier gas flow and etch time with reactants flowing into the reaction chamber continuously.

Preliminary experiments revealed that the chamber pressure and the carrier gas flow vary by less than 0.5 % during processing. However, the amount of XeF_2 carried into the chamber depends on the amount of solid XeF_2 within the bubbler. This gradually decreases over extended periods of tool usage. The quantity of gas carried into the chamber also decreases when running etch processes in rapid succession. Uniform process condition can be assured, if the tool is given a break of approximately one hour between every five etch runs. This must be taken into account when conducting more experiments that require more than five runs. The absolute amount of XeF_2 supplied to the chamber has a significant impact on the etch rate and is, therefore, the largest source of error.

An external cooling and heating unit controls the pedestal temperature. When operating within the range of roughly 10 – 35 °C the temperature displayed on the external unit is calibrated to the measured temperature of the pedestal. For values outside this range, an additional measurement of the pedestal temperature was made to assure that the pedestal had reached the required processing temperature.

5.4 Results: Proximity Effect Characterisation

5.4.1 Reference Samples

Multiple samples were etched under different process parameters. The pressure, XeF_2 flow and etch time ranged from 3 to 10 Torr, 15 to 35 sccm and 40 to 80 seconds respectively.

The first important observation was that if the target layers of the reference samples etched they did so with a rate of less than 250 nm min^{-1}. This was observed for any of the SiN-Reference and SiO_2-Reference samples (test structures without a target layer), during the entire experiment. The etch times varied between 60 and 120 seconds. Significantly longer etch rates were not conducted for three reasons:

Firstly, long runs are quite expensive due to the high cost of XeF_2. Secondly, long runs result in the depletion of XeF_2 that can lead to inconsistent gas flows over the duration of the experiment. Thirdly, the results observed were as the literature [93] suggests, with etch rates of PECVD silicon dioxide and stoichiometric silicon nitride in XeF_2 being "zero or very slow" and 12 nm min^{-1} respectively.

This observation is also in excellent agreement with blanket wafer etch experiments conducted by Drysdale [33]. He used the same deposition and etching equipment as used in this study and was unable to measure a change in the thickness of wafers that were blanket coated with PECVD SiO_2 and PECVD SiN layers after 4 minutes of etching.

5.4.2 PECVD Silicon Nitride

The apparent inertness of silicon nitride and silicon dioxide towards XeF_2 exhibited by the reference samples contrasts strongly with the data obtained from this work's test structures as presented in figures 5.3, 5.4, 5.5 and 5.6. These figures show rapid etching of silicon nitride and silicon dioxide target layers as a result of the proximity effect of the polysilicon sacrificial layer.

Figure 5.3 shows data obtained during preliminary experiments with a test structure similar to the *SiN-PECVD* sample described above (The only difference is the thickness of the target layer which was 210 nm in this case and 450 nm in the case of *SiN-PECVD*). Each data point presented was etched at a different carrier gas flow, processing pressure and etch time combination. Each measurement point is the average of 8 measurements taken on a single chip. The error bars show the standard deviation. Regardless of the different process settings, the selectivity of polysilicon to *PECVD SiN* is constant at approximately 1.25: 1.

This preliminary observation was further investigated later experiments. The data obtained from the sample *PECVD SiN* is presented in figure 5.4. (a) and shows that the ratio of the polysilicon and PECVD silicon nitride etch undercuts increases linearly over time. This suggests that the etch rate is constant over time. Furthermore, the polysilicon to silicon nitride selectivity lies between 1.2: 1 and 1.3: 1, which is in reasonable agreement to the 1.25: 1 selectivity measured in the preliminary experiment.

Figure 5.4 (b) plots the polysilicon and PECVD silicon nitride etch rates and their selectivity as a function of the XeF_2 flow. The etch rates decreases linearly with increasing XeF_2 flow, which can be explained by assuming an associated decrease in XeF_2 concentration. The effect is a result of the way in which the tool operates, whereby nitrogen is flowed through a bubbler filled with XeF_2 in order to supply the gaseous etchant to the process chamber. For instance, if 25 sccm of N_2 is used as the carrier gas, roughly 16 sccm XeF_2 is transported to the chamber. This corresponds to a ratio of 3 to 2. However, if 100 sccm of N_2 was used as the carrier gas, roughly 36 sccm of XeF_2 flows into the chamber, corresponding to a ratio of 3 to 1. This shows that the XeF_2 partial pressure decreases with increasing carrier gas flow. The XeF_2 flows were obtained through tool inherent flow calculation measurements. For these measurements a predefined volume of nitrogen is flown through the bubbler and a mass flow meter measures the volume of gas leaving the bubbler. The difference between the two values is the volume of XeF_2 supplied into the chamber. For XeF_2 flows of 16 and 25 sccm, the polysilicon to PECVD silicon nitride selectivity is roughly 1.25: 1 and in good agreement with the previous observations of PECVD SiN being subject to the proximity effect. At the highest XeF_2 flow rate the selectivity increases slightly to

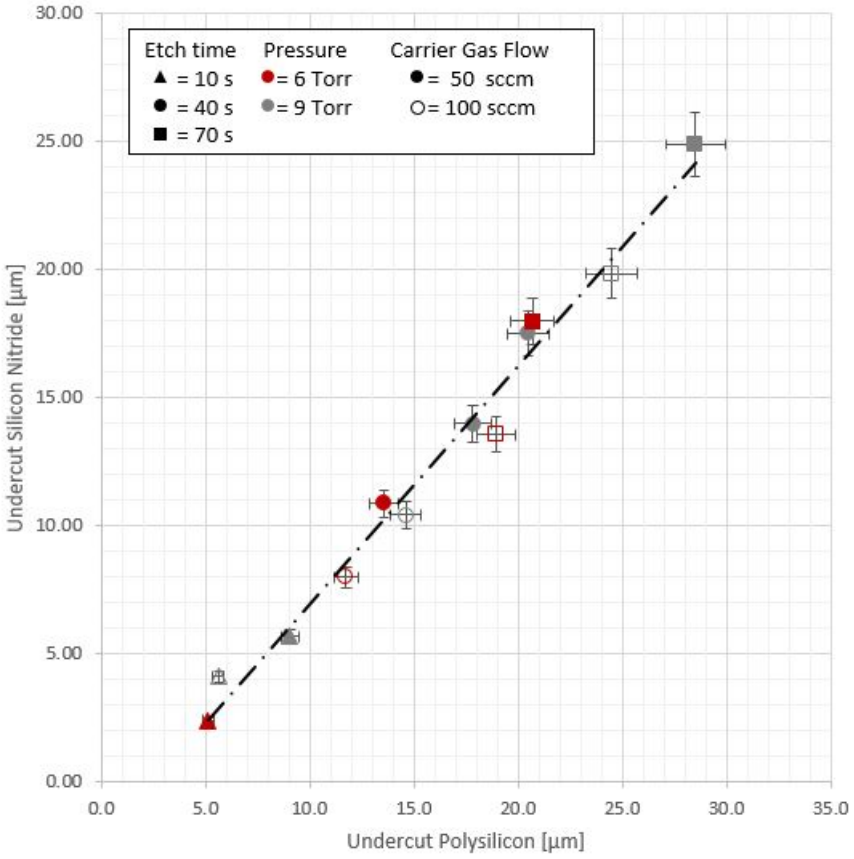

FIGURE 5.3: Dataset from preliminary experiments, comparing the undercuts of polysilicon to that of PECVD SiN. Obtained at various gas flow, chamber pressure and etch time parameters at a constant temperature of 25 °Celsius. The data suggests a parameter independent selectivity of 5: 4. The figure was obtained from [23] and [28].

1.6: 1. This may suggest a concentration dependence of the proximity effect, however more measurement data is required to confirm this.

The data presented in figure 5.4 (c) is different from the previous figures. Firstly, as would be expected, the etch rate increases with increasing chamber pressure up to 9 Torr. However, the etch rate then reaches a plateau between 9 and 10 Torr. Unfortunately, 10 Torr is the upper pressure limit and therefore, this trend could not be further investigated. With regard, to the selectivity, the impact of the chamber pressure is even more interesting. At lower pressures, a selectivity of 2.5: 1 was measured, which is significantly higher than the 1.25: 1 selectivity measured at a pressure of 9

Torr. This is in contrast to the preliminary data presented in figure 5.3, where no pressure-related change of the selectivity was observed.

5.4.3 LPCVD Silicon Nitride

Figure 5.5 is structured as the previous one, showing the undercuts and selectivity of polysilicon and LPCVD SiN as a function of time in (a), the XeF_2 flow in (b) and the processing pressure in (c), respectively. The first observation that can be made is that the LPCVD silicon nitride etch rates are slower than the ones observed for PECVD SiN, but still much higher than the 12 nm per minute suggested by the literature. The dataset clearly shows that the proximity effect also affects LPCVD silicon nitride.

The polysilicon etch rate behaves in a similar manner to that of the PECVD SiN sample. It increases linearly proportional to the etch time and processing pressure and decreases in a near linear manner with the XeF_2 flow. In contrast to that, the etch behaviour of the LPCVD SiN appears to be different from that of the PECVD SiN. Over time, the etched undercut appears to be constant at roughly 2 μm. This suggests that the LPCVD SiN ceases to etch at some point in time. Presumably, the SiN etch reaction ceases once the polysilicon in proximity has been etched away.

This observation is further supported by figure 5.5 (c). At low pressures, when the polysilicon is etched more slowly and remains in the vicinity of the LPCVD Si_3N_4 for a longer time, the silicon nitride etches longer, and therefore, the observed etch rate is comparatively higher. This is probably caused by the molecular movement. The fluorine radicals disperse as they scatter away from their point of origin. A critical concentration of fluorine is required to sustain the etch reaction of LPCVD Si_3N_4 and SiO_2. The reaction will therefore stop once the sacrificial layer etch front has travelled beyond its close "proximity". For the LPCVD Si_3N_4 datasets presented here, this distance appears to be 2-3 μm.

The polysilicon to LPCVD SiN selectivity is higher and more volatile than the ones observed for the PECVD SiN. They range between 4: 1 and 17: 1 and do not appear to follow any obvious pattern. Probably this is because the LPCVD SiN etch reaction

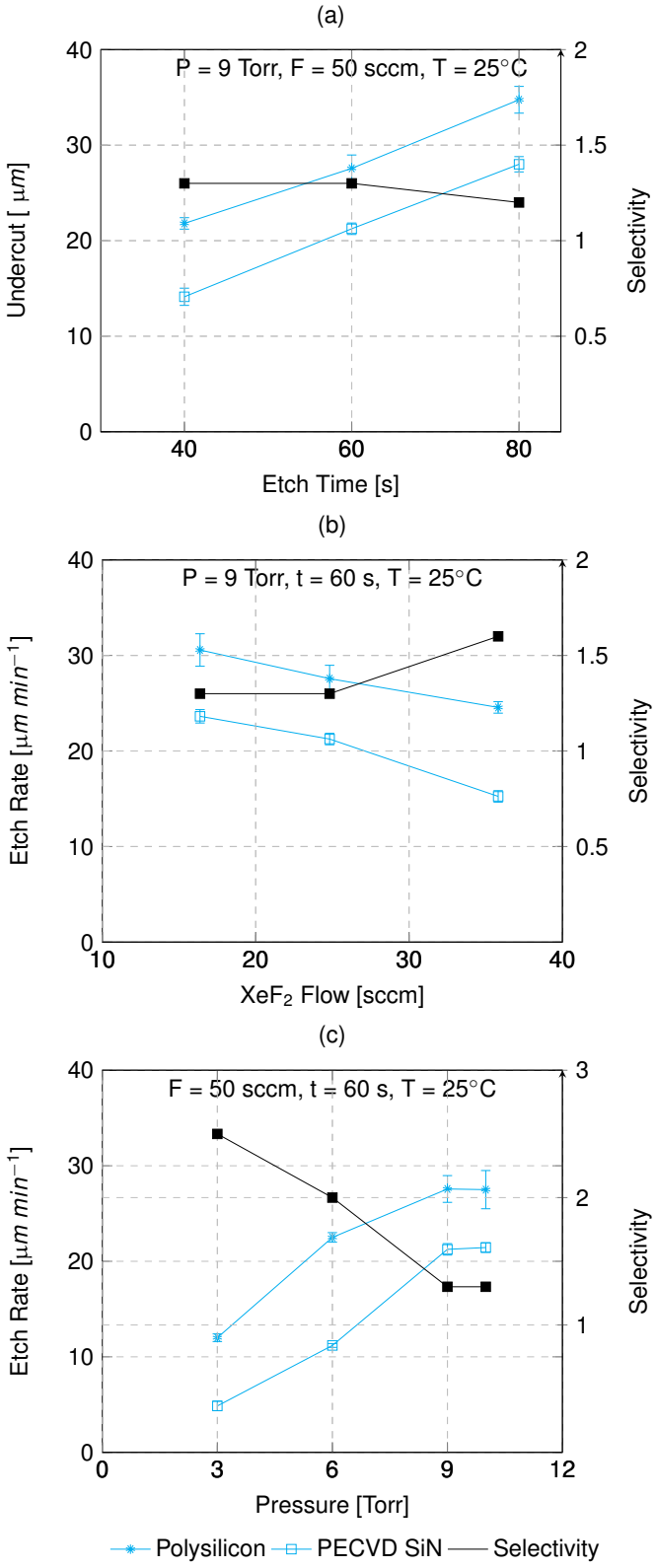

FIGURE 5.4: The etch rates of polysilicon and PECVD SiN when etching in proximity as a function of in (a) time, in (b) the XeF_2 gas flow and in (c) the processing pressure. The figures were previously published in slightly different form in [27]. Each datapoint is the average of eight measurements taken from different test structures located on the same chip. The error bars indicate the standard deviation of the measurements.

stops once the polysilicon has etched beyond the 2 - 3 μm distance required to maintain the proximity effect.

5.4.4 PECVD SiO_2

Figure 5.6 shows how the undercuts and selectivity vary with time, XeF_2 flow and process chamber pressure for adjacent layers of polysilicon and PECVD SiO_2. Again, as expected, the polysilicon follows the same trends as earlier samples. The silicon dioxide etched more slowly than both silicon nitride samples, but still at a significant rate. In direct contradiction to the literature suggesting that SiO_2 is inert to XeF_2 [93], this dataset is further evidence of the existence of the proximity effect, confirming Veyan et al.[22].

Similar to the observation for LPCVD SiN, the PECVD SiO_2 etch rate appears to remain constant at around 0.5 - 1 μm per minute, but decreases with increasing pressure. Both observations suggest that once the polysilicon sacrificial layer's etch front has exceeded beyond the vicinity of the SiO_2, the SiO_2 ceases to etch.

The measured selectivities between polysilicon and SiO_2 ranged from a minimum at 5: 1 at a pressure of 3 Torr, to a maximum of 30: 1 at a pressure of 10 Torr. As shown in figure 5.6 (c), the selectivity increases with increased pressure. The data clearly shows that etching at high process chamber pressure is beneficial for the polysilicon to PECVD silicon dioxide selectivity. This is the case because, at higher pressures, the polysilicon etch rate increases and "out-runs" the proximity effect sooner.

5.5 Discussion of the Proximity Effect

5.5.1 Comparing the Measurement with Proposed Theoretical Mechanism

Veyan [22] suggested that fluorine radicals, which are formed during the etching of polysilicon, can attack other materials (Compare section 2.3.6). Two observations

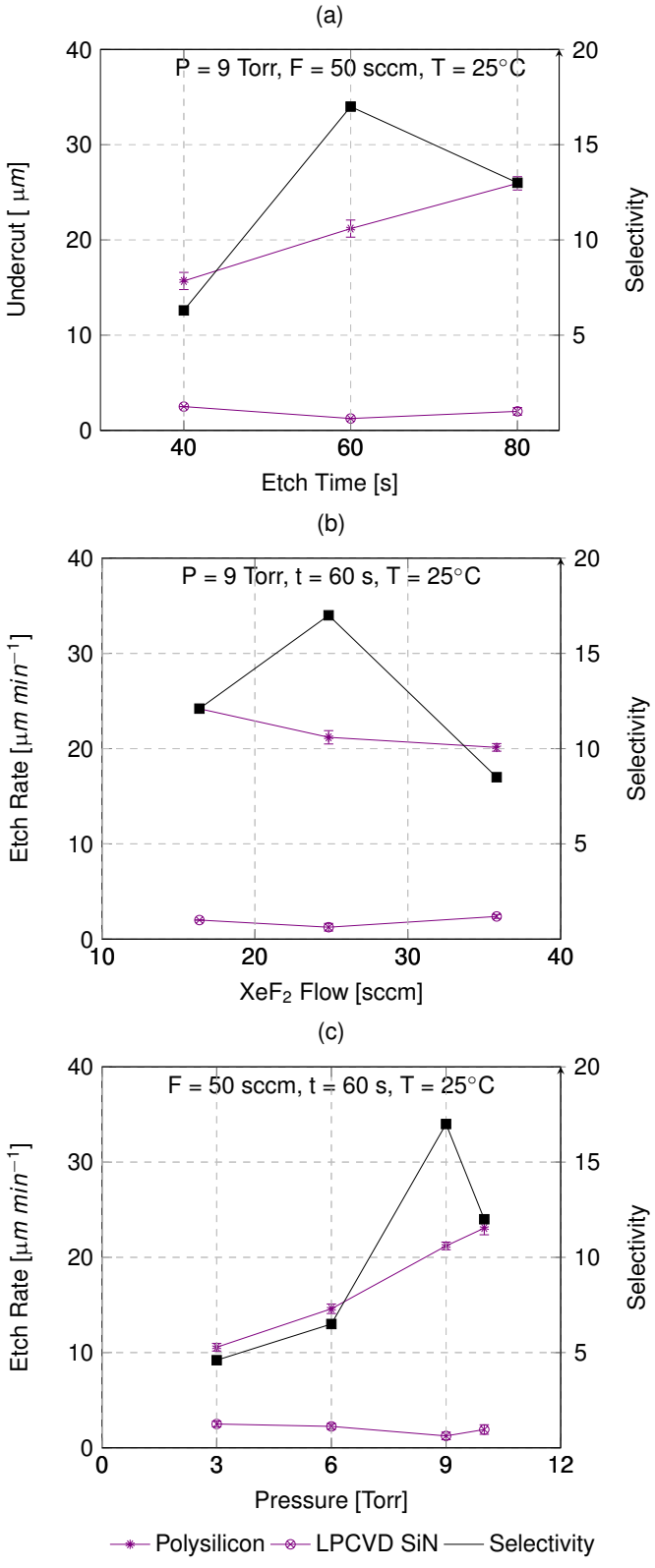

FIGURE 5.5: The etch rate of polysilicon and LPCVD SiN when etching in proximity as a function of (a) time, in (b) the XeF_2 gas flow and in (c) the processing pressure. The figures were previously published in slightly different form in [27]. Each datapoint is the average of eight measurements taken from different test structures located on the same chip. The error bars indicate the standard deviation of the measurements.

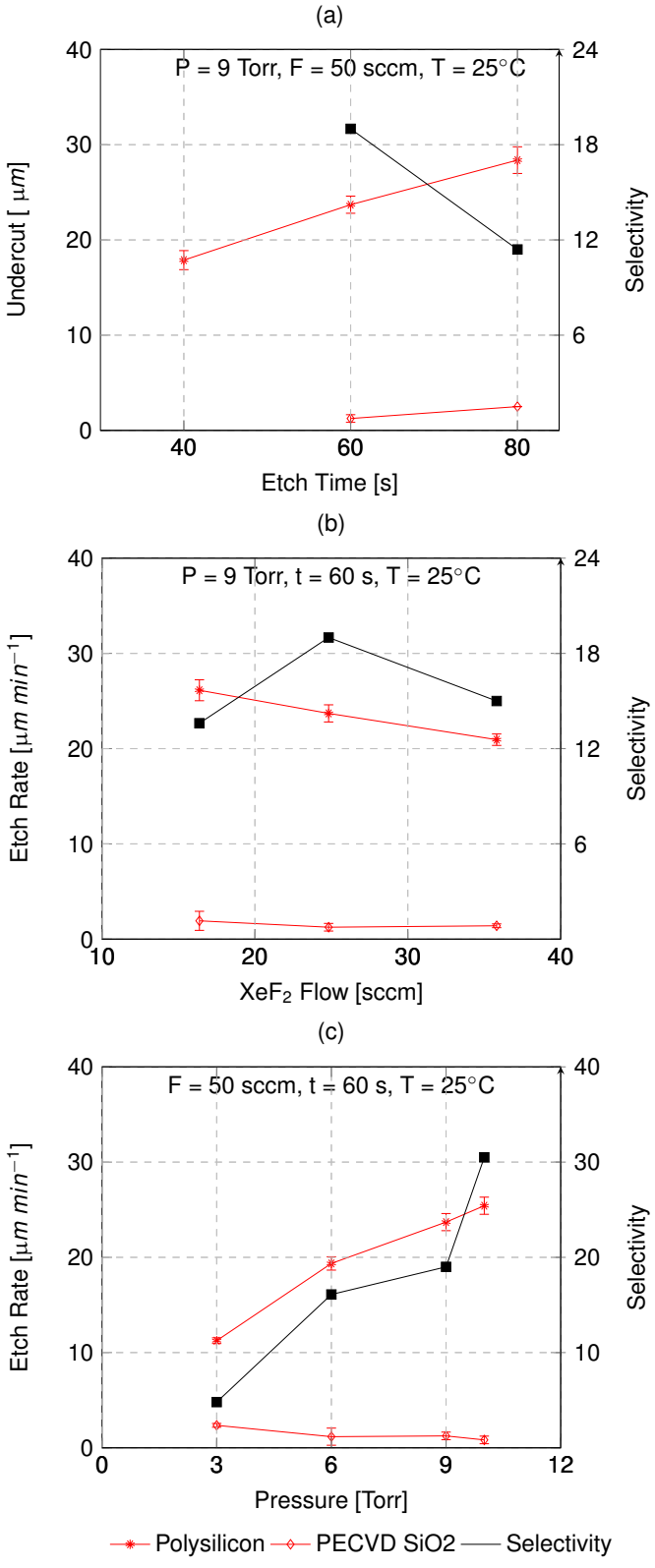

FIGURE 5.6: The etch rate of polysilicon and PECVD SiO_2 when etching in proximity. As a function of (a) time, (b) XeF_2 gas flow and (c) the processing pressure. The figures were previously published in slightly different form in [27]. Each datapoint is the average of eight measurements taken from different test structures located on the same chip. The error bars indicate the standard deviation of the measurements.

have been made in this experiment which provide supporting evidence towards that hypothesis. Firstly, no etch could be measured for the reference samples where no polysilicon layer was etched. In contrast to that, all three materials were etched at a measurable rate when placed in the proximity of a sacrificial polysilicon layer.

This suggests that LPCVD Si_3N_4 and SiO_2 are inert to XeF_2. However, they appear to be etched by the fluorine that is formed as a reaction by-product during the etching of the polysilicon. Secondly, as can be observed in figure 5.4, the linear increase of both the polysilicon and PECVD SiN undercuts over time suggests that they reach a steady state and etch at a constant rate. In contrast to that, the SiO_2 and LPCVD Si_3N_4 cease to etch once a $2-3\ \mu m$ undercut has been reached. Therefore, the data indicates that the source of the fluorine radicals needs to be in close proximity to the target layer in order to facilitate this etching effect.

The extensive research into the XeF_2 etch mechanics conducted by Hefty et al. [50], [92] can explain both phenomena. The reaction path they suggested is summarised here, however more details were presented in section 2.3.5. The XeF_2 abstracts [1] a fluorine atom at a dangling bond of the silicon, and the remaining XeF molecule is scattered into the gas phase. It can follow one of two reaction paths. It can either abstract the second fluorine atom on another dangling bond or dissociate and scatter the xenon atom and fluorine radicals. Some of the fluorine radicals are backscattered onto the silicon. There, they break Si-Si lattice bonds and gradually fluorinate the polysilicon, thereby forming SiF, SiF_2 and SiF_3. Once all the Si-Si bonds are broken, the resulting SiF_4 desorbs into the gas phase.

It was further observed [50] [92] that the XeF_2 etch rate of silicon is an order of magnitude higher than that of F_2. It has been suggested that the fluorine radicals originating from the XeF_2 backscatter on the silicon surfaces and thereby enhance the etch rate. Most likely, these backscattered fluorine atoms react with the silicon dioxide or silicon nitride, causing the proximity effect. Relative energy calculations conducted by Veyan et al. [22] of the reaction between SiO_2 and fluorine that has been abstracted from XeF_2 provided strong evidence that this reaction path is energetically favourable. It releases 15.9 eV of energy exothermically.

[1] The term abstraction describes the removal of an atom by a radical

It was also observed that the PECVD SiN etched significantly faster than the LPCVD Si_3N_4. The main difference between these materials is the hydrogen content. While the atomic hydrogen content of LPCVD Si_3N_4 is 4 -5 %, the hydrogen concentration within the PECVD SiN thin film is process condition dependent and values between 13 -39 % have been reported [94]. Unfortunately, it was not possible to measure the hydrogen concentration of the PECVD SiN films used in this study. Furthermore, Chow et al. [94] found a correlation between the hydrogen content of the PECVD SiN layers and their respective etch rates when etching the samples in a 13: 2 NH_4F: HF solution. Knotter [46], observed something similar when etching PECVD SiN in HF. He reported that the etch rate of PECVD SiN in HF increased as a function of etch time and attributed this observation to the larger amounts of hydrogen incooperated within the film's lower layers. Neither of the publications, however, proposed a chemical mechanism explaining these findings. However, in the context of the proximity effect the intermolecular bonds of the hydrogen-rich PECVD SiN are likely weaker than those of the LPCVD Si_3N_4. Consequently, the fluorine radicals can etch the hydrogen-rich PECVD SiN quicker.

5.5.2 Comparing the Results with Previous Experimental Data from the Literature

The selectivities reported in this study are not only in excellent agreement with the theory of the etch reaction discussed above; they also agree very well with fluorine etch data previously reported:

Loewenstein's [51] investigation of the temperature-dependent etch rates of thermal SiO_2, LPCVD Si_3N_4 and polysilicon in the remote plasma generated fluorine, resulted in etch rates very similar to the ones observed in this study. The material properties of the polysilicon and the LPCVD Si_3N_4 layers were very similar across both studies. From the published data, polysilicon to LPCVD Si_3N_4 selectivities of 7.1:1 and 11.4:1 can be determined for 16 °C and 30 °C respectively. It is more problematic to equate

the thermal SiO_2 used in the published study with the PECVD SiO_2 used here. Therefore, those figures have not been directly compared.

In addition to that, Van de Ven et al. [95] reported a a-Si: Si_3N_4 selectivity of 8:1 when etching with fluorine. Both reference values are in good agreement with the polysilicon to LPCVD Si_3N_4 selectivity range of 8.5:1 to 12:1 reported in this study.

Unfortunately, no numerical fluorine etch selectivities were found in the literature for polysilicon towards PECVD SiN. However, it was suggested that "plasma nitride" (most likely PECVD SiN) etched at a similar rate to Si in CF_4/O_2 plasmas in [95], [96], and [97]. If the "plasma nitride" is indeed PECVD SiN, their findings are in excellent agreement with the 1.25: 1 polysilicon to silicon nitride selectivities observed here.

There is only a minimal amount of data available on fluorine etching of SiO_2, and therefore no polysilicon to SiO_2 reference selectivities were found. However, Flamm et al. [98] etched SiO_2 in gaseous fluorine and measured etch rates of 60 and 600 Å per minute at processing temperatures of 250 K and 370 K respectively. These etch rates are about an order of magnitude lower than the ones observed during SiO_2 proximity etching in this study. This disparity could possibly be explained by the lower chamber pressures of 0.5 Torr used in Flamm's experiment.

5.5.3 Deduction and Hypothesis

The experimental results are in excellent agreement with both the theoretical suggestion that fluorine forms during the XeF_2 etch of polysilicon, and the experimental data obtained in previous studies for fluorine etching of silicon nitride and silicon dioxide.

Generally speaking, these findings indicate that all materials etched by fluorine are likely to be subject to the proximity effect. Table 5.3 shows a list of materials used in MEMS technology, the reaction product with fluorine and the respective boiling point of the fluorine-containing compound. If this boiling point temperature is lower than the processing temperature, the respective material will likely be etched by the fluorine as a result of the proximity effect. This data would appear to be in agreement with the hypothesis that common MEMS materials such as gallium, germanium and

Element	Fluoride Compound	BP [°C]
B	BF_3	-100
Al	AlF_3	1297
Ga	GaF_3	1000
P	PF_3	-101
	PF_5	-75
As	AsF_3	-63
	AsF_5	-53
Sb	SbF_3	376
	SbF_5	141
Si	SiF_4	-86
c	Si_2F_6	-19.1
Ge	GeF_4	-37
Ti	TiF_4	184
Ta	TaF_5	230
W	WF_6	17
Se	SeF_6	-47
	SeF_4	102
Te	TeF_4	19
	TeF_6	-39

TABLE 5.3: MEMS materials, the compounds resulting from atomic fluorine exposure and the respective boiling point temperatures. The data presented here was selected from a more comprehensive table presented in [99].

tungsten will etch if subject to the proximity effect.

5.6 Summary of Proximity Effect Characterisation

The characterisation of the proximity effect study gave a number of results so far unseen in the scientific literature, or reaffirming hypothesis developed by other researchers.

1. The data experimentally proved that both silicon dioxide and silicon nitride layers can be affected by the proximity effect.

2. The proximity effect appears to be limited to a distance of 2 - 3 μm.

3. The study confirmed that silicon dioxide and silicon nitride are inert to XeF_2 when exposed in isolation.

5.7 Results: Process Temperature Dependence

5.7.1 Polysilicon

The figures presented in this section of the thesis plot the etch rates of polysilicon, PECVD SiN, LPCVD SiN and PECVD SiO_2 as a function the processing temperature. In all cases, the data clearly shows a temperature dependency of the polysilicon etch rate; it decreases with increased temperature. This observation was expected. It has been reported before by Chang et al. [82], and Ibbotson et al. [70] and is in agreement with theories developed by Flamm et al. [100] and Vugts et al. [69]. The details of those studies were presented in section 3.5.

5.7.2 PECVD Silicon Nitride

This section includes three datasets investigating the temperature dependency of the PECVD silicon nitride's etch rate and selectivity towards polysilicon. The data shows a mixed picture. Figure 5.7 is the result of preliminary experiments. The data was excluded from publication [27] because the XeF_2 storage of the bubbler was very low during execution, which resulted in an inconsistent gas flow into the chamber that in turn gave variable etch rates.

Nevertheless, this dataset is comprehensive and should not be completely disregarded. Figures 5.7 (a) and (b) show that for etch times of both 40 and 70 seconds respectively, the PECVD SiN etch rate decreases with increased temperature. It should be noted that the data presented at 6.5 °C displayed in the figure, was measured roughly a month after the others and that the reduced etch rates are most likely a result of XeF_2 depletion rather than the processing temperature. With regards to the selectivity, the data is ambivalent. In figure 5.7, the 6.5 °C data point represents a polysilicon to PECVD SiN selectivity of roughly 2: 1, while the remaining data points represent selectivites of roughly 1.2: 1. In figure 5.7 (b), the selectivity is nearly constant at 1.2:

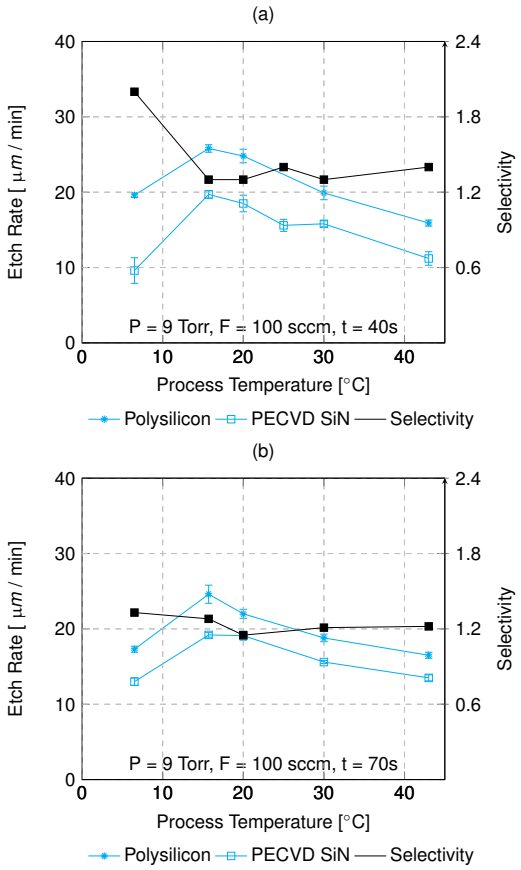

FIGURE 5.7: The polysilicon and PECVD SiN etch rates and selectivity obtained from preliminary experiments as a function of temperature. (a) with an etch time of 40 seconds and (b) with an etch time of 70 seconds. Note: The data points at 6.5 °C have lower etch rates than the others because they were etched sometime later and the XeF_2 in the bubbler had depleted significantly resulting in lower etch rates.

1 over the entire temperature range.

In contrast to the preliminary experiment, figure 5.8 shows data obtained with a recently refilled bubbler and therefore constant XeF_2 flows. In this case, the PECVD silicon nitride etch rate appears to increases with the process temperature up to a temperature of 25 °C, after which it stabilises. The polysilicon to PECVD SiN selectivity shows a similar relationship. It reaches nearly 2: 1 at a temperature of 10 °C and then drops to 1.25: 1 at temperatures exceeding 25 °C.

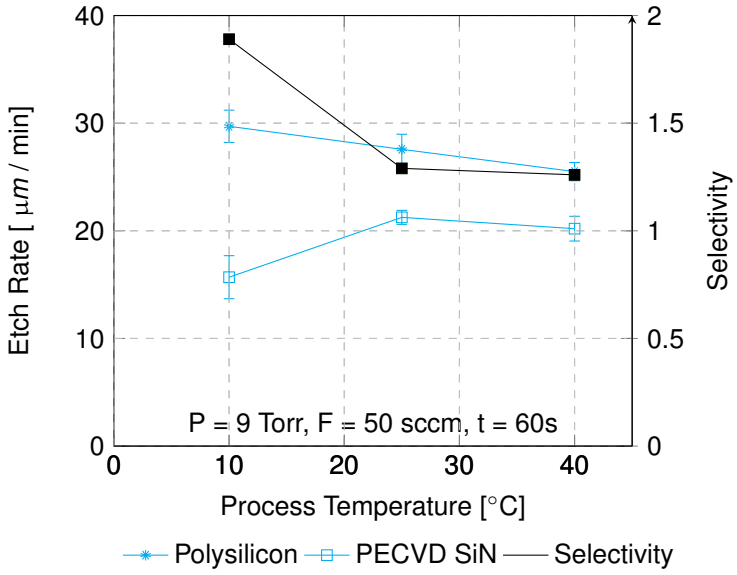

FIGURE 5.8: The etch rates and selectivity as a function of the processing temperature - Polysilicon: PECVD SiN. Compared to figure 5.7 the gas flows were stable, because the XeF_2 bubbler was freshly filled. The figure was previously published in slightly different form in [27]. Each datapoint is the average of eight measurements taken from different test structures located on the same chip. The error bars indicate the standard deviation of the measurements.

5.7.3 LPCVD Silicon Nitride

The etch rate of the LPCVD silicon nitride does not appear to have any dependency on the process temperature. The selectivity data for those samples is presented in figure 5.9. The measured etch rates of the silicon nitride were very slow. Small variations in the silicon nitrides etch rate have had a tremendous impact on the selectivity. Therefore, the quality of the selectivity data is low and does not allow for a conclusion to be drawn.

5.7.4 PECVD Silicon Dioxide

The data presented in figure 5.10 suggests that the SiO_2 etch rate is unaffected by the change in temperature. The data for those samples does not allow to draw a conclusion on the temperature dependency on the selectivity, because small variations in the silicon dioxides etch rate have a considerable impact on the selectivity.

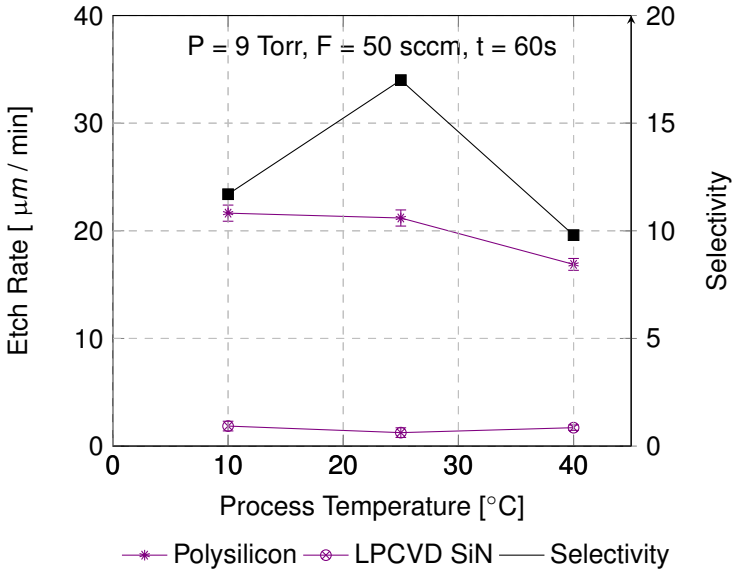

FIGURE 5.9: The etch rates and selectivity as a function of the processing temperature - Polysilicon: LPCVD SiN. The figures was previously published in slightly different form in [27]. Each datapoint is the average of eight measurements taken from different test structures located on the same chip. The error bars indicate the standard deviation of the measurements.

In contrast to the data presented in figure 5.10, a preliminary dataset that was obtained using test structures from the same wafer, suggested that the SiO_2 etch stops at temperatures below 15 °C. The data is displayed in table 5.4. However, this data is less reliable because the experiment was conducted when the XeF_2 levels in the bubbler were deficient, and therefore the amounts of gaseous XeF_2 supplied to the chamber was variable. As a result, the enhanced selectivities at lower temperatures cannot be confidently attributed to temperature effects alone.

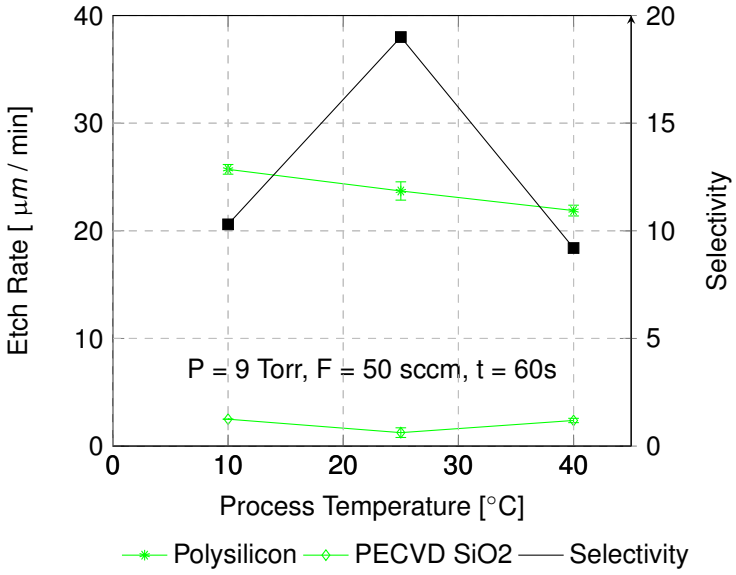

FIGURE 5.10: The etch rates and selectivity as a function of the process temperature- Polysilicon: PECVD SiO_2. The figure was previously published in slightly different form in [27]. Each datapoint is the average of eight measurements taken from different test structures located on the same chip. The error bars indicate the standard deviation of the measurements.

5.8 Discussion of Process Temperature Dependence

5.8.1 Comparing the Results with Theoretical Mechanisms

Considering the Arrhenius equation that was presented in more detail in section 2.3.1,

$$k = Ae^{\frac{-E_a}{RT}} \tag{5.1}$$

one would expect that the etch rate (k) increases when the temperature (T) rises because the gas constant (R) and the pre-exponential factor (A) are constants and most commonly the activation energy (E_a) is positive. This temperature-dependent increase in the etch rate has been observed for the fluorine etching of polysilicon, SiO_2 and thermally grown Si_3N_4 [51]. This contrasts strongly with the temperature dependency of the polysilicon observed in this work, where the decreasing etch rate with

T [°C]	Polysilicon ER[µm min^{-1}]	SiO_2 ER [µm min^{-1}]	Selectivity
8	14.8	0.0	>29.6
15	14.8	0.0	>29.6
25	14.6	1.3	11.3
46	11.05	1.15	9.8

TABLE 5.4: Polysilicon and SiO_2 etch rates (ER) and selectivities resulting from preliminary experiments. Conditions: N_2 flow = 100 sccm, P = 9 Torr, t = 120 s

increasing temperature suggests a negative activation energy, which was calculated to be -3746 J mol^{-1} (0.9 kcal mol^{-1}).

5.8.2 Comparison with Published Experimental Data

Even though negative activation energies are uncommon, similar observations have been made before. Vugts et al. [69] observed the highest XeF_2 etch rates of silicon (100) at 150 K. As the temperatures increased, the reaction rate decreased, reaching a minimum reaction probability of roughly 20 percent at around 400 K. The reaction rates began to rise again in the temperature range of 600 K to 900 K. Similarly, Ibbotson et al. [70] observed an inverse proportional relationship between the etch rate and the temperatures below 360 K. They calculated a reaction activation energy for this temperature spectrum of - $3.2 kcal mol^{-1}$ $(-13.4 kJ mol^{-1})$ which is roughly 300 % lower than the activation energy calculated in this study. This could either be caused by the different materials used in those studies, crystalline Si (100) instead of the polycrystalline silicon used in this study, or the lower pressures used by Ibbotson et al. [70] (0.05 - 2 Torr).

Nevertheless, all three studies observed a negative reaction energy for XeF_2 etching of silicon at temperatures below 360 K. It is unclear why it is negative, but it has been suggested that the XeF_2 forms a bound surface layer prior to etching [70]. However, this hypothesis does not agree with the etch mechanisms described by Hefty et al. [49], [50] which have been in excellent agreement with the previous findings of this study.

No unambiguous trend can be derived for the PECVD SiN, LPCVD SiN and PECVD SiO_2 datasets. Figure 5.8 suggests that the PECVD SiN etch rate might increase with increased temperature, but the data for LPCVD Si_3N_4 and PECVD SiO_2 shows no temperature correlation. However, this observation does not rule out a temperature effect entirely, because the SiO_2 and LPCVD Si_3N_4 etch reactions could have stopped once the sacrificial layer had etched beyond the proximity etch distance as discussed earlier.

In contrast to the observations made here, the literature suggests that the SiO_2 and LPCVD Si_3N_4 reaction rate with fluorine is in fact temperature dependant. Loewenstein [51] reported positive activation energies of $14853 Jmol^{-1}$ ($3.55 kcal mol^{-1}$) and $14058 Jmol^{-1}$ ($3.36 kcal mol^{-1}$) for LPCVD Si_3N_4 and SiO_2, respectively. This data suggests that the reaction rate will increase as the temperature increases.

5.8.3 Deductions and Hypothesis

With regards to the temperature dependency of the polysilicon etch rate, the following novel hypothesis is suggested. The Brunauer-Emmett-Teller (BET) theory [40] [41] states that the rate of molecular adsorption increases with decreased temperature. This increased adsorption could lead to an increased rate of fluorine abstraction, thereby enhancing the etch rate. This hypothesis is in agreement with both the theory of the etch reaction developed by Hefty et al. [49], [50], as well as the observations of the experiments conducted here and by others [70] [69].

With regards to the hypothesis that the selectivity can be improved at lower temperatures, the data presented in this study clearly shows that the polysilicon etch rate increases with lower temperatures. However, for the other materials studied the data is inconclusive. No clear trends could be observed for the temperature dependence of the silicon nitride or silicon dioxide etch rates.

Nevertheless, the author presumes that investigations at low sub-zero degree Celsius temperatures might yield greater selectivity improvements. Assuming it is the case that the etch rate of the target materials remained constant regardless of the temperature, the polysilicon etch rate increases at very low temperatures could result in

selectivity improvements. Unfortunately, to date there are no available tools with this capability on the market.

5.9 Summary of Process Temperature Dependence

The previous sections have evaluated the hypothesis that temperature adjustments can be used to mitigate the proximity effect, and restore better selectivities. This has resulted in a number of findings new to the engineering community, and a re-evaluation of hypotheses developed by other researchers. To summarise:

1. The data in this work has experimentally confirmed data from the literature that the polysilicon etch rate shows a significant response to process temperature change, increasing with decreasing temperatures over the range of measurements taken.

2. Contrary to theory and the literature, no unambiguous temperature response was observed for PECVD SiN, LPCVD SiN and PECVD SiO_2.

3. Selectivity improvements could be achieved from the temperature dependence of the polysilicon etch rate if the process temperature could be reduced to sub-zero degree Celsius temperatures.

5.10 Results: Dependence on Hydrogen Addition to the Process Chamber

Figures 5.11 and 5.12 show the etch rates of polysilicon and PECVD SiN and polysilicon and LPCVD Si_3N_4 as a function of the hydrogen flowrate respectively.

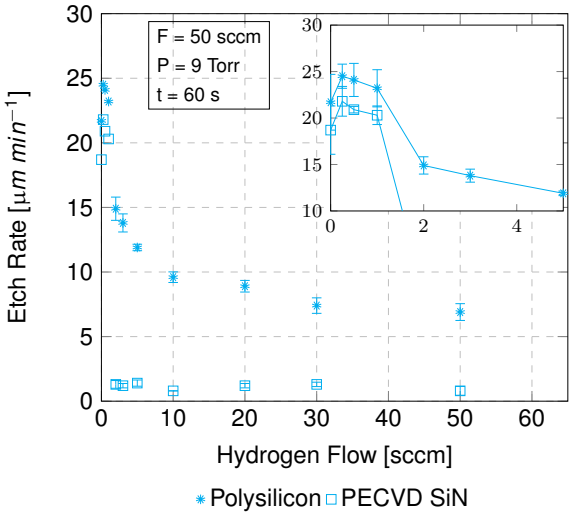

FIGURE 5.11: The etch rates of polysilicon, and PECVD SiN plotted as a function of the hydrogen flow into the chamber. The inset shows the magnified plot between H_2 flows of 0-4 sccm. The process temperature was constant at 25 °C. The figure was published in [27]. Each datapoint is the average of eight measurements taken from different test structures located on the same chip. The error bars indicate the standard deviation of the measurements.

5.10.1 Polycrystaline Silicon

Figures 5.11 and 5.12 show that flowing hydrogen into the processing chamber during etching has a strong impact on the etch rate of polysilicon. At flow rates up to 2 sccm, the etch rate increases by roughly 9 %, but as the hydrogen flow rates are increased to 10 sccm, the etch rate is seen to decrease rapidly. The etch rate decrease slows significantly at hydrogen flows above 10 sccm and the etch rate appears to stabilise at 20 - 35 % of etch rate without hydrogen addition after the flows exceed 30 sccm.

5.10.2 PECVD SiN

The effect of adding hydrogen to the gas mixture is even more pronounced for the etching of PECVD SiN. Figure 5.11 shows that the etch rate drops from a maximum of 20 μm min^{-1} at a flow of 1 sccm hydrogen to 1 μm min^{-1} for a flow of 2 sccm hydrogen. The data shows that a further increase in the hydrogen flow does not yield a further reduction of the etch rate.

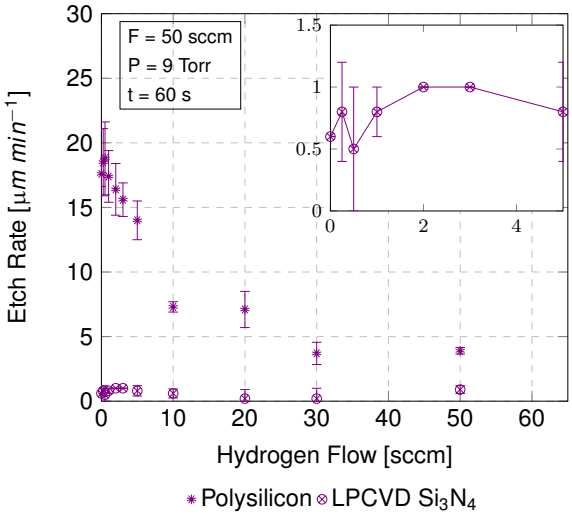

FIGURE 5.12: The etch rates of polysilicon and LPCVD Si_3N_4 plotted as a function of the flow rate of hydrogen continuously added into the chamber. The inset shows the magnified plot between H_2 flows of 0-4 sccm. The process temperature was constant at 25 °C. The figure was published in [27]. Each datapoint is the average of eight measurements taken from different test structures located on the same chip. The error bars indicate the standard deviation of the measurements.

5.10.3 LPCVD SiN

Supplying hydrogen also results in a decrease in the LPCVD Si_3N_4 etch rate. Figure 5.12 shows that it dropped from roughly 1 μm min^{-1} at hydrogen flows of up to 10 sccm to 200 nm min^{-1} at hydrogen flows beyond 20 sccm. During the experiment, the XeF_2 flows fluctuated by up to 1.3 sccm because the XeF_2 supply bubbler was nearly empty. Therefore five samples were etched after the bubbler was refilled at a constant XeF_2 flow rate of 24.85 sccm. The data suggested a linear etch rate decrease of 160 nm min^{-1} per sccm of hydrogen supplied into the chamber for the hydrogen flow range of 0 - 20 sccm.

5.10.4 PECVD SiO_2

In contrast to the polysilicon and the silicon nitrides, adding hydrogen did not appear to have an effect on the etch rates of the SiO_2. Four samples were etched for 5 minutes each. Gas mixtures with 0, 1, 3 and 10 sccm of added hydrogen were investigated. The resulting silicon dioxide undercuts were between 2.1 and 2.6 μm min^{-1}. Then,

the experiment was repeated with a reduced etch time of 2 minutes. This time the measured undercuts were 2.3 to 2.6 μm min^{-1} and appeared to be independent of the hydrogen flows. The very similar undercuts measured for both experiments could indicate that the SiO_2 etch stopped after the polysilicon within its proximity had been fully etched.

5.10.5 Selectivity Dependence of Hydrogen Addition

The selectivity of polysilicon towards PECVD silicon nitride improved by an order of magnitude from 1.2: 1 to 12.8: 1 when the hydrogen flow was increased from a flow of 0 to 10 sccm. A further increase of the hydrogen flow decreases the selectivity because, beyond that point, the polysilicon etch rate decreases faster than that of the PECVD silicon nitride.

The selectivity of polysilicon to LPCVD silicon nitride also improved strongly from 15.8: 1 at a hydrogen flow of 0 sccm to a maximum of 38: 1 at a hydrogen flow of 0.5 sccm. Hydrogen flows between 0.5 and 10 sccm also yield significant improvements, compared with no hydrogen flowing into the chamber. However, in the case of hydrogen flows beyond 20 sccm, the selectivity drops below that with no added hydrogen because the polysilicon's etch rate decreases more quickly than that of the LPCVD silicon nitride.

As mentioned earlier, the data obtained for the SiO_2 was insufficient to attribute any observation to the supply of hydrogen, and therefore no conclusion can be drawn.

5.11 Discussion of Supplying Hydrogen

5.11.1 Comparison of the Results with Theoretical Mechanisms

The reduced etch rates of the polysilicon and silicon nitride suggest that hydrogen neutralises the reactive species formed by the proximity effect. If, as suggested by the research, fluorine radicals are the product of the proximity effect, they could react with the hydrogen to form hydrogen fluoride (HF).

$$H_2 + F \longrightarrow HF + H \tag{5.2}$$

HF is a commonly used etchant for SiO_2 and etches silicon nitride to some extent as well [46]. However, for such an etch to proceed it requires water or alcohol as a catalyst. Neither of these is present in the etch process and therefore it is assumed that the HF formed by this reaction will not etch the silicon nitride. The fluorine radicals also attack and etch silicon, and so the decrease in the polysilicon etch rate with increased hydrogen flows is in good agreement with this hypothesis. However, the reaction of the PECVD and LPCVD silicon nitride was not completely halted, which limits the effectiveness of this method.

5.11.2 Comparison with Published Experimental Data

The broader literature presents two possible explanations for this apparent limit to the effectiveness of the method. Firstly, the hydrogen radicals that form as a by-product of the neutralisation reaction, described by equation 5.2, could etch the silicon nitride. When studying plasma etching with hydrogen radicals, Chang et al. [101] observed etch rates of 1.5 nm min^{-1} for SiO_2 and 25 -50 nm min^{-1} for LPCVD Si_3N_4. These etch rates are roughly 10 % of the values reported in this work. However, it is difficult to compare the two datasets, because the processing parameters used by Chang et al. [101], particularly the pressures, were not reported.

The alternative explanation is that the formation of hydrogen fluoride in an excited state could result in etching of the silicon nitride. Volynet et al.[65], and Jung et al. [66] discovered, that excited hydrogen fluoride can transport additional energy to a reaction site. They demonstrated the effect by selectively etching LPCVD Si_3N_4 over SiO_2. Interestingly, they observed that the maximum etch rates were measured after hydrogen was added to the gas mix. The same observation can be made for the data presented in this study.

5.11.3 Deduction and Hypothesis

Even though both explanations elaborated on in the previous section could explain why the supply of hydrogen did not entirely halt the etch of the SiN and SiO_2, there is also a third possible mechanism that could explain the limitation of this specific method.

Assuming that the proximity effect produces fluorine radicals and these react with the added hydrogen to produce HF, there is still a requirement that the two collide in order to initiate the reaction. The average distance a molecule travels before colliding with another one is called its mean free path and can be calculated with

$$\lambda = \frac{RT}{\sqrt{2}d^2 N_a P} \tag{5.3}$$

where λ represents the mean free path in meters, T the temperature, P the pressure, d the effective diameter of the gas, R the universal gas constant and N_a Avogadro's number [102]. Even though the mean free path of the gas mixture is unknown, the mean free paths of hydrogen and fluorine under the conditions used in this experiment were calculated using equation 5.3 to be 13.4 nm and 8.9 nm respectively.

Hefty et al. [50] found that the XeF dissociation occurs within a 2 Å [2] distance from the abstraction reaction site at the polysilicon surface. In consequence, the path distance of the roughly 50 % of fluorine radicals scattered is very short. (The proportion of fluorine radicals scattered towards the silicon surface.) If for instance a fluorine radical was scattered towards the polysilicon with a horizontal and vertical angle of 85 °, the path length would only be 46 Å. The formation of neutral HF is quite unlikely in the affected regions, because a collision event has a low chance of occurring. The reason for that is that the path distance of a significant proportion of the formed fluorine radicals is much smaller than the mean free path of the hydrogen.

This low likelihood of a hydrogen/fluorine radical collision events would explain the observation that the increased amount of hydrogen in the gas mixtures does not yield further polysilicon to silicon nitride selectivity improvements. However, it falls short of explaining why small hydrogen flows result in an increased etch rate. Furthermore, the mean free path length is pressure-dependent and therefore processing at higher pressures might make the method of flowing hydrogen into the chamber more significant. Unfortunately, this experiment was conducted at the maximum processing pressure of the tool, and therefore it could not be confirmed that higher pressures result in better selectivities.

[2] Angstrom (Å) is a length unit commonly used in chemistry. 1 Å = 10^{-10} m = 0.1 nm

Nevertheless, a recommendation of this work is the building of a test reactor to investigate if flowing hydrogen into the chamber at higher pressures improves the selectivity.

5.12 Summary of Dependence on Hydrogen Addition to the Process Chamber

The hypothesis that the supply of hydrogen into the reaction chamber improves the etch selectivity and mitigates the proximity effect has been evaluated. The following findings were made:

1. The supply of hydrogen improves the selectivity of polysilicon over silicon nitride. The data showed an increase from 1.2: 1 to 12.8: 1 for PECVD SiN and from 15.8: 1 to 38: 1 for LPCVD SiN. No change was observed for the etch rate of SiO_2.

2. The selectivity improvement does not linearly correlate with the hydrogen flow. Instead, the etch rates appear to stabilise after the hydrogen flow supplied into the chamber exceeds a critical flow rate. Consequently, the highest selectivities were measured at comparatively low flow rates of up to 10 sccm for PECVD SiN and at 0.5 sccm for LPCVD SiN.

3. The selectivity increases appear to result from the reaction of fluorine radicals with the hydrogen. The HF formed by this reaction does not etch the silicon nitride or silicon dioxide in the absence of a catalyst such as water or alcohol.

4. There appears to be an inherent limit to the potential of this method. Three potential reasons for this were presented, the attack of the silicon nitride by hydrogen radicals, the attack of the silicon nitride by HF in an excited state and a reaction limitation resulting from the difference of the fluorine radicals travel distance and the mean free path of the hydrogen molecules. The validity of this third reason could be checked with a capability of processing at pressures higher than achievable in this work.

5.13 Conclusion

This chapter presented the work investigating how the etch selectivities of common MEMS materials are adversely affected by etching them in close proximity of one another, and how this can be prevented. It was observed that a proximity effect resulted in preferential etching of both silicon dioxide and silicon nitride films. From this, it was proposed that a similar effect would occur with all materials that are etched by fluorine radicals. The spatial extent of the proximity effect appears to be 2 - 3 μm in the materials tested. This might be tolerated in larger MEMS devices. However, the effect needs to be carefully considered when designing NEMS devices. Two methods to mitigate the effect have been characterised: reducing the process temperature and adding hydrogen to the process gas mixture. The first method showed that the polysilicon etch rate increases with decreasing temperature. However, for the other materials tested in this study, the results were not so clear, and therefore the possibility to improve the selectivity by reduced process temperature remains unconfirmed. However, because the temperature range investigated was limited by the capability of the equipment used, it would be beneficial to conduct similar experiments, should this situation change. The second method yielded an increased selectivity of polysilicon over silicon nitride. It is proposed that this improvement results from the formation of HF by a reaction of fluorine radicals and the added hydrogen. Possibly, those improvements can be enhanced by operating at higher processing pressure. This was also beyond the capabilities of the equipment used, however, future researchers are encouraged to conduct these experiments.

Chapter 6

HF Etch Selectivity

6.1 Introduction

Vapour hydrogen fluoride (HF) etching is becoming a common release method for silicon dioxide sacrificial layers used to fabricate micro and nanoelectromechanical systems (MEMS and NEMS). Key benefits of the process are the avoidance of stiction and cross-contamination which can occur during free-standing structure release in wet etch solutions. In contrast to XeF_2 vapour etching, the available knowledge relating to HF etch selectivities is much greater, as wet HF etching is a long-established and thoroughly characterised process. However, compared to XeF_2 vapour etching, controlling the HF etch process is more complicated due to the complex condensation and evaporation dynamics that are involved.

6.1.1 Objectives of the Study

This chapter investigates three promising approaches to increase the etch selectivity between silicon dioxide and silicon nitride (two commonly used MEMS materials):

1. The addition of hydrogen to the process gas mix in order to reduce the etch rate of the silicon nitride by neutralising free fluorine radicals in a similar manner to that observed for the etching with XeF_2.

2. Changing the HF to H_2O concentrations within the liquid layer in order to change the etch selectivity.

3. Manipulation of the etch rates of silicon dioxide and silicon nitride by operating at lower temperatures. According to theoretical studies [46][43], the equilibrium of reactants should shift from monofluorides towards difluorides at lower temperatures which predominantly etch silicon dioxide.

6.2 Equipment and Sample Fabrication

6.2.1 Equipment

Two commercially available tools were used during this study. A memsstar Alpha Orbis HF etch tool is commonly used for research and the commercial fabrication system memsstar Xeric. Both systems operate in a continuous flow regime over a temperature range of 5 to 45 °C. Besides the HF etchant, an H_2O catalyst, N_2 carrier gas, and H_2 additive gas can be supplied into the chamber. Compared to the Xeric system, the Alpha Orbis has particular advantages for research [1]. The gas flows can be set with a 0.1 sccm accuracy and the pedestal temperature can be measured with an external thermometer. In addition, the chamber can be ramped to processing pressure with nitrogen alone, which ensures there is no early etching of the samples before the desired processing conditions have formed within the tool. However, a considerable disadvantage is that the maximum stable processing pressure is limited to around 30 Torr, beyond which the tool does not maintain a constant pressure. This complicates experiments at higher temperatures (>30 °C) where higher pressures are required to condense the reactants on the sample.

6.2.2 Test Structure Fabrication

The test structure layout and measuring method used during this work was described in Chapter 4. There are two differences compared to the XeF_2 test structures used in Chapter 5. Firstly, the layer configurations were altered, with SiO_2 being used as the sacrificial layer in HF etching. Secondly, copper was used as the capping layer because HF would attack the aluminium used for the XeF_2 test structures. A cross section of the fabrication process is presented in figure 6.1.

[1] Some of the experiments were conducted on the Xeric System because the Alpha Orbis became unavailable before the experiments were completed

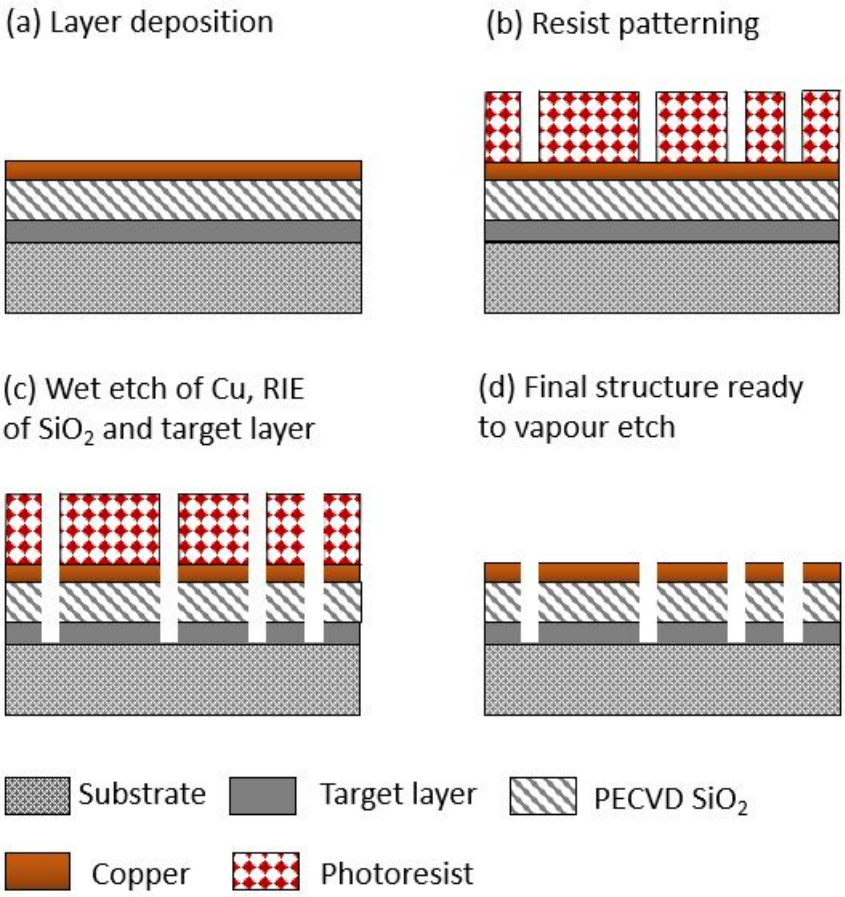

FIGURE 6.1: Schematic of the HF test structure fabrication process. Reproduced from [28].

Four different designs were fabricated and the layer configurations are presented in table 6.1. Two of the designs labelled *SiO_2-Reference* and *SiN-Reference* are patterned benchmark samples (similar to the benchmarks used for XeF_2 experiments). These were used to determine the SiO_2 and the PECVD SiN undercut etch rates in isolation. The second set of samples were used to measure the etch selectivities of *PECVD SiO_2: PECVD SiN* and *PECVD SiO_2: LPCVD Si_3N_4* and take the proximity effect into account.

After the layers were deposited and the pattern was transferred into the SPR-230-3.0 photoresist using a Karl Suss mask aligner, the trenches were created by wet etching the copper layer with a wet copper etchant (MSDS: Copper Etch 300). Then the trenches were reactive ion etching into the silicon dioxide and silicon nitride, after which the resist was removed by submerging the samples in 1165 resist remover. The

Layer	SiO_2: PECVD SiN	SiO_2: LPCVD Si_3N_4	SiO_2-Reference	PECVD SiN-Reference
Capping Layer	500 nm Copper	500 nm Copper	500 nm Copper	500 nm Copper
Sacrificial Layer	500 nm PECVD SiO_2	500 nm PECVD SiO_2	500 nm PECVD SiO_2	-
Target Layer	260 nm PECVD SiN	215 nm LPCVD Si_3N_4	-	260 nm PECVD SiN
Wafer	Silicon	Silicon	Silicon	Silicon

Table 6.1: Layer configuration of the samples used in this study.

runsheets and fabrication recipes are documented in appendix D.

6.3 Proximity Effect in HF Vapour Etching

While the proximity effect significantly affects XeF_2 vapour etching, it has not been reported in the context of HF vapour etching. However, it is important to evaluate it as close proximity of certain material combinations could significantly alter the observed selectivity.

6.3.1 Experiment

For this evaluation, the four test structures previously presented were HF vapour etched on the memsstar Xeric etch tool for 100 seconds at a temperature of 25 °C. A temperature specific standard recipe was used with HF, N_2 and H_2O gas flows of 200 sccm, 100 sccm and 60 sccm, respectively. The gas was continuously supplied to the chamber while it ramped up to a pressure of 20 Torr. All four samples were etched simultaneously and were baked for 10 minutes after etching at 150 °C to stress relieve the copper film. The data presented in figure 6.11 shows how post etch annealing improves the quality of the measurement. Three test structures from each chip were characterised using a surface profiler, and the data point is the average undercut determined from the measurements.

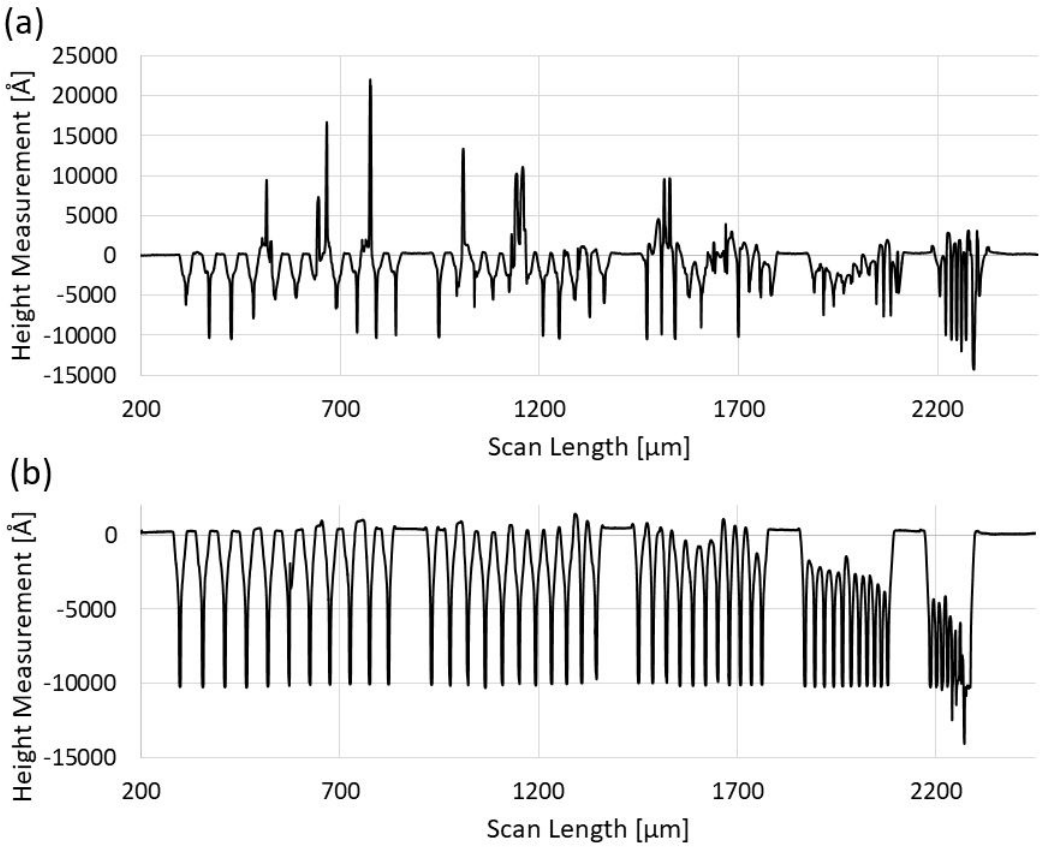

FIGURE 6.2: A comparison of the test structure's post etch surface profiles. In (a) without heat treatment, and in (b) after annealing the etched test structure on a hotplate set to 170 °C for 60 seconds. This figure was published before in [28].

6.3.2 Result

The etch rates presented in this section are summarised in table 6.2. For both the *SiO_2-Reference* and *SiN-Reference* samples a horizontal undercut etch rate of 2.5 μm min^{-1} was measured. In contrast to that, a SiO_2 etch rate of 20.5 μm min^{-1} was observed when it was etched in close proximity to PECVD SiN, for which an etch rate of 3.1 μm min^{-1} was measured. Compared to etching in isolation, the SiO_2 etch rate is eight times higher when PECVD SiN was etched in close proximity, resulting in a SiO_2: PECVD SiN selectivity of 6.5: 1. Similarly, when PECVD SiO_2 was etched in close proximity to the Si_3N_4, the oxide etched at a rate of 29 μm min^{-1}, while the Si_3N_4 etch rate was 2 μm min^{-1}. In this case, the SiO_2 etch rate is 11 times higher than the rate observed on the reference sample, resulting in the PECVD SiO_2: Si_3N_4

Sample	Measured etch rate $[\mu m/min]$		
	PECVD SiO_2	PECVD SiN	Si_3N_4
PECVD SiO_2 Ref	2.5	-	-
PECVD SiN Ref	-	2.5	-
PECVD SiO_2: PECVD SiN	20.5	3.1	-
PECVD SiO_2: Si_3N_4	29	-	2

TABLE 6.2: Etch rates measured from the different samples during the proximity effect experiment.

selectivity being 15: 1.

Unfortunately, no specific reference etch rates for the vapour etching of PECVD SiO_2 under those processing conditions were found available in the literature. Similarly, it was not possible to obtain reference data for the HF vapour etching of PECVD SiN. The only benchmark is an etch rate of 1.68 μm min^{-1} which was obtained by Witvrouw et al. [29] in a 49 % HF/H_2O solution at a temperature of 21 °C.

Both the PECVD SiO_2 and PECVD SiN etch rates are also substantially higher than the etch rates which were observed on blanket chips that were vapour etched under similar conditions as the conditions used here in preliminary experiments (Blanket chips are different to the reference samples used in this study, as the entire surface of the chip is etched and not an undercut).

6.3.3 Discussion

Two phenomena were observed in this study that have not been reported before in the literature. Firstly, the SiO_2 etch rates measured on the test structure were higher than they would be on blanket chips and secondly, the SiO_2 etch rate increases significantly when etched in proximity to silicon nitride.

The fact that the etch rates on the reference samples presented here are higher than observed for blanket chips could result from the geometry of the test structure. Compared to blanket wafers or chips it has a much smaller etch front (etchable surface

exposed to the etchant) and the trapping of the reactants and reaction products below the capping layer.

Considering that difluorides mainly etch SiO_2 (See Section 2.3.3 for details), the trapping of the reactants could accelerate the reaction if the fast-reacting difluoride species (HF_2^- and H_2F_2) that form within the HF/H_2O mixture are available at a larger concentration close to the reaction site.

While these mechanisms could explain the observed faster etch rates, it remains unclear what causes them. Neither mechanism has been reported in the literature before. An experimental investigation of the underlying chemistry would be beyond the scope of this work.

Similarly, it is unclear why the PECVD SiO_2 that was stacked onto the PECVD and thermal silicon nitride etched 8 and 12 times faster respectively, compared to the PECVD SiO_2 on the reference sample. Possibly, difluorides formed during the silicon nitrides' etch reaction increased the concentration of difluoride species close to the reaction site.

An alternative explanation could be the formation of ammonia as a reaction by product. The reaction path presented in figure 2.5 suggests, that ammonia (NH_3^+) can form during the elimination and addition reaction that removes the surface nitrogen atom during the etching of Si_3N_4 in HF solutions. If this ammonia came into contact with the liquid film formed during the HF etch of the silicon dioxide, it could possibly form ammonium hydroxide (NH_4OH), which has been shown to etch silicon dioxide at rates of 0.18 nm/min at a temperature of 50 °C [103]. Unfortunately, the etch rates that were reported by Lee et al. [103] are very slow, and therefore unlikely to have caused the phenomena observed here.

However, further research into the chemistry of silicon nitride etching in HF must be undertaken to confirm the hypothesis that reaction byproducts increase the etch rate of silicon dioxide.

6.3.4 Summary

While the SiO_2 etch rates increased 8 to 12 times when etched in proximity to PECVD SiN and Si_3N_4, the silicon nitride's etch rate only increased very slightly by roughly 20 %. This clearly indicates that some form of proximity effect is present. Possibly, difluorides form at the silicon nitrides etch front, which subsequently increases the SiO_2 etch rate. However, as the theoretical understanding of silicon nitride etching in HF is very limited, other so far undiscovered mechanisms could cause this observation.

6.4 The Impact of Supplying Hydrogen on the HF Etch Selectivities

As detailed in Section 3.4 of this thesis, hydrogen can neutralise atomic fluorine to form HF. Knotter [46] found that silicon nitride is mainly etched by monofluorides, while SiO_2 is mainly etched by difluorides. Figure 2.6 shows, that F^- contributes significantly to the etching of silicon nitride. Therefore, the supply of hydrogen to the processing chamber and the resulting removal of the fluorine could potentially reduce the silicon nitride's etch rate and improve the etch selectivity significantly.

6.4.1 Experiment

For this experiment, the *SiO_2: PECVD SiN*, *SiO_2: LPCVD Si_3N_4* and both the reference test samples were etched on the memsstar Xeric system at a constant temperature of 25 °C. The processing pressure was 23 Torr during those experiments and the gas flows were set to 200 sccm, 100sccm, and 60 sccm for HF, N_2 and H_2O, respectively. Four etch runs were conducted. The tool was ramped to processing pressure and the etch was maintained for 100 seconds. The hydrogen flows were set to be 0, 20, 50 and 80 sccm (The tool's hydrogen flow is limited at 80 sccm). The etch parameters are summarised in the run order in table 6.3. Post etching, the samples were baked for 10 minutes at 150 °C to relieve the copper film's stress. Three test structure arrays from each chip were measured on a surface profiler and the average undercut was calculated.

T [°C]	HF [sccm]	N_2 [sccm]	H_2O [sccm]	P [Torr]	t [s]	H_2 [sccm]
25	200	100	60	23	100	0
25	200	100	60	23	100	20
25	200	100	60	23	100	50
25	200	100	60	23	100	80

Table 6.3: The experimental parameters used for the hydrogen addition experiment.

6.4.2 Results

Figure 6.3 shows the hydrogen flow-dependent etch rates that were obtained from the *SiO_2 and SiN reference* samples. The SiO_2 etch rate displayed in figure 6.3 (a) appears to increase slightly from 2.5 to 3.5 μm min^{-1} between hydrogen flows of 0 and 50 sccm, beyond which it drops to the original level. In contrast to that, the etch rate of the PECVD SiN displayed in figure 6.3 (b) does not appear to be affected by the hydrogen flow. The increase of the SiO_2 etch rate with increasing hydrogen flow could be explained by the hydrogen bonding to fluorine atoms to form a difluoride species. The reason for the decrease measured at a hydrogen flow of 80 sccm is unclear.

The measured silicon nitride etch rates were unexpected. Considering the chemical etch theory of silicon nitride in HF developed by Knotter [46], and that the substantial amount of hydrogen supplied into the chamber should reduce the number of fluorine atoms available to etch the silicon nitride a decrease of the the etch rate was expected.

Finally, it can be observed that the etch rates of SiO_2 and PECVD SiN are very similar. Considering the short etch time of 100 seconds, that is to be expected. In contrast to silicon dioxide, silicon nitride does not require a liquid layer formation to initiate etching. Consequently, it begins to etch while the tool is ramping up to processing pressure, earlier than the SiO_2. Those issues could be overcome on the Alpha Orbis tool by supplying the HF into the chamber after the processing pressure had been reached. Unfortunately, due to the much larger etch chamber, this was not possible with the Xeric system used in this study.

Figure 6.4 shows the etch rates and selectivities that were measured for the *SiO_2:*

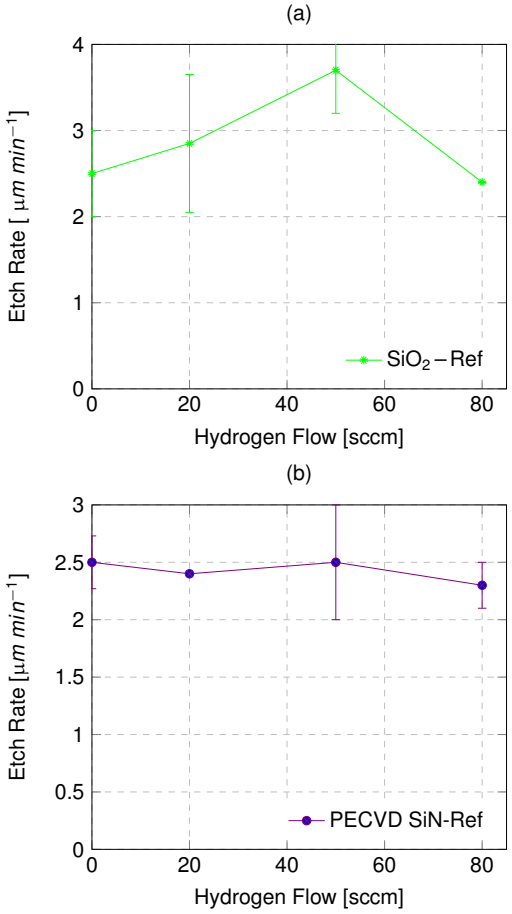

FIGURE 6.3: The etch rates of (a) PECVD SiO_2 and (b) PECVD SiN as a function of the hydrogen flow rate when etched in isolation. The data was obtained from the reference samples. Each data point is the average of 3 measurements.

PECVD SiN sample. When 20 sccm of hydrogen are added, the SiO_2 etch rate decreases slightly from 20 to 16.5 μm min^{-1}. It appears to stabilise at this value as the hydrogen flow is increased. Compared to the *SiO_2-Reference* sample (Figure 6.3 (a)), the etch rates of the PECVD SiO_2 etched in proximity are 5 to 8 times higher, which is consistent with the observation made in the context of the proximity effect (Section 6.3). Furthermore, the trend observed in the SiO_2 etch rate of *SiO_2: PECVD SiN* sample is noticeably different from the *SiO_2-Reference* sample.

The SiN etch rate of the *SiO_2:PECVD SiN* sample also differs from that of the *SiN-reference* sample. Low hydrogen flow rates of up to 20 sccm do not appear to affect

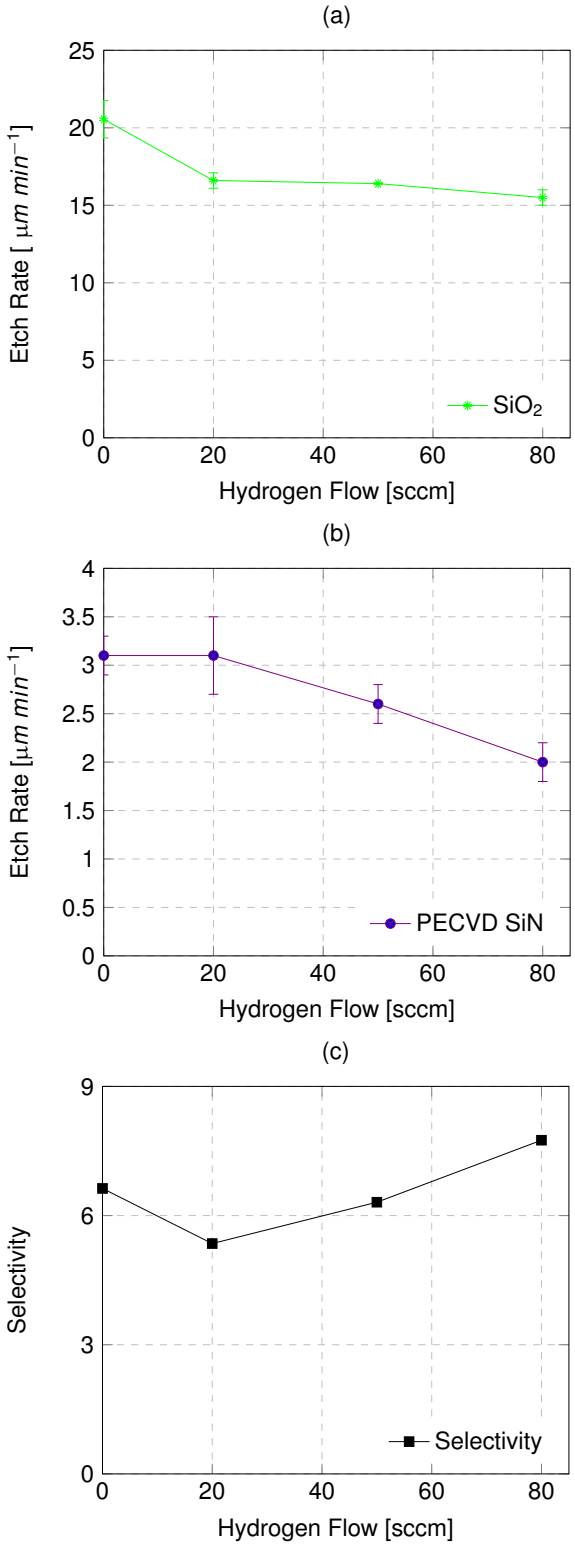

FIGURE 6.4: The hydrogen flow dependent etch rate of (a) SiO_2 and (b) PECVD SiN, determined from measurement of SiO_2:PECVD SiN samples. Plot (c) shows the selectivity between the two layers. Each data point is the average of three measurements.

the etch rate, which is consistent with the *SiN-reference* sample (Figure 6.3 (b)). However, more extensive hydrogen flow rates appear to result in a linear decline of the etch rate, reaching a minimum of 2 μm min^{-1} at a hydrogen flow rate of 80 sccm.

Figure 6.4 shows that adding hydrogen to the process gas mixture does not substantially change the SiO_2: PECVD SiN selectivity. Without the supply of hydrogen, the selectivity is roughly 6.5: 1. It decreases to a minimum of 5.3: 1 at a hydrogen flow of 20 sccm and then linearly increases to reach a maximum of 7.75: 1 at a hydrogen flow of 80 sccm.

Figure 6.5 shows that the etch rate of the SiO_2 etched in proximity to the LPCVD Si_3N_4 target layer displays the same behaviour as the SiO_2 which was etched in proximity to the PECVD SiN. The only notable difference is that the etch rate is roughly 10 μm min^{-1} higher when no hydrogen is supplied to the chamber. When hydrogen is supplied to the chamber, the SiO_2 etch rates are identical in both cases, which suggests that the same mechanism reduces the SiO_2 etch rate.

The LPCVD Si_3N_4 etch rates, displayed in figure 6.5 appear to be unaffected by the supply of hydrogen. Similar to the PECVD SiN, this is unexpected because the theory suggests that the hydrogen addition would reduce the concentration of fluorine atoms close to the reaction site and that, consequently, the etch rate would decrease.

As a result of the reduced SiO_2 etch rate, the PECVD SiO_2: LPCVD Si_3N_4 selectivity decreases from 15: 1 to 8: 1 when hydrogen is increased to 20 sccm, after which it stabilises.

6.4.3 Discussion

The results presented in the previous section differ significantly from the expectation predicted by the theory of the etch mechanism [46][43]. The hydrogen addition was expected to cause a significant decrease of the silicon nitride's etch rate, but this was only observed for the *SiO_2: PECVD SiN* sample. In the case of the SiO_2, no change or a slight increase in the etch rate was expected. However, the addition of a moderate amount of hydrogen caused a significant drop of the etch rate, which then stabilised

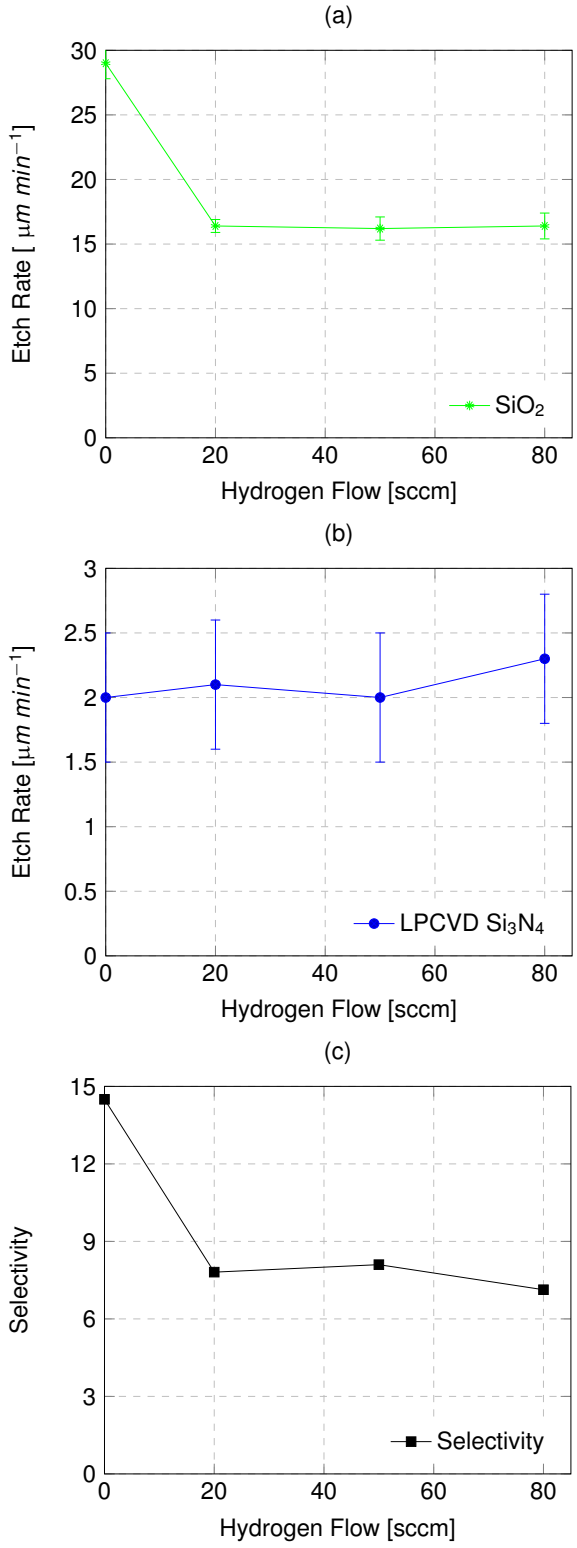

FIGURE 6.5: The hydrogen flow dependent etch rate of (a)SiO_2 and (b) LPCVD Si_3N_4, determined from measurement of SiO_2:LPCVD SiN samples. Plot (c) shows the selectivity between the two layers. Each data point is the average of 3 measurements.

when the hydrogen flow increased further. Consequently, the hydrogen addition resulted in an unexpected reduction of the etch selectivity.

The reduction in the SiO_2 etch rate when proximity etching could be a result of the formation of a protective layer as described by Loewenstein [59] for etching with CF_4 remote plasmas. However, no reference to the surface passivation of SiO_2 by H_2 was found in the literature. It is also unclear why the SiO_2 etch rate would not be affected by such a hypothetical passivation mechanism if etched in isolation.

A further literature review was undertaken to identify a possible explanation for the observed silicon nitride etch rate behaviour, but unfortunately this also failed to yield a feasible explanation.

The inability to explain the experimental observation based on the available literature suggests the existence of so far undiscovered etch mechanisms. This is not surprising, as the body of research for the fundamental etch chemistry of HF vapour etching is small. Further research is required to determine a sensible explanation for the experimental observations.

6.4.4 Summary

The hypothesis that adding hydrogen into the HF vapour gas mixture improves the etch selectivity of SiO_2 to PECVD SiN and LPCVD Si_3N_4 was evaluated. It was noted that despite the theory suggesting otherwise, no significant improvements resulted from the addition of hydrogen. It is unclear why the silicon nitrides etch rate was not reduced significantly, and it is suggested that more research into the fundamental etch chemistry is required to develop a robust hypothesis.

6.5 Condensation Controlled HF Etch Process Control

This section describes a model that has been developed to determine the temperature and concentration-dependent processing parameters necessary to maintain the condensed layer's composition over a range of temperatures and reactant concentrations.

T [°C]	P [Torr]	t [s]	ER PECVD SiO_2 $[\mu m/min]$	ER LPCVD Si_3N_4 $[\mu m/min]$
5	9	100	22.2	2.2
15	18	80	15.28	3.75
25	23	100	25.29	2
35	30	90	16.66	3.33

TABLE 6.4: The processing parameters used for the dataset presented in figure 6.6. ER stands for etch rate.

The need for such a model arises from the complex condensation and evaporation phenomena involved in HF vapour etching which can inhibit an accurate and comparable study of the effects on the etch selectivity caused by process temperatures and reactant concentrations.

This process control problem is illustrated in figure 6.6, which shows a dataset of SiO_2: LPCVD Si_3N_4 selectivity samples which were etched at temperatures of 5, 15, 25 and 30 °C, using the Xeric system. The gas flows were 200 sccm, 100 sccm and 60 sccm for HF, N_2 and H_2O, respectively. Each temperature was paired with a processing pressure that resulted in a SiO_2 etch rate within the same order of magnitude to the rest of the group. The etch times were adjusted to allow the silicon dioxide and silicon nitride undercuts to be measured within the same test structure. The processing parameters used are displayed in table 6.4.

The temperature-dependent etch rates and selectivities displayed in figure 6.6 show a great variation and cannot be used to study the impact of the etch selectivity's temperature. The variable data is a result of the complex evaporation and condensation phenomena, which were deliberately not considered in this experiment to illustrate the problem. In particular, the following needs to be taken into account in the experimental design:

- A thin liquid layer is required to initiate the SiO_2 etch reaction. However, the flux of HF into the liquid layer becomes too large and the H_2O formed as a reaction product floods the sample, leading to stiction.

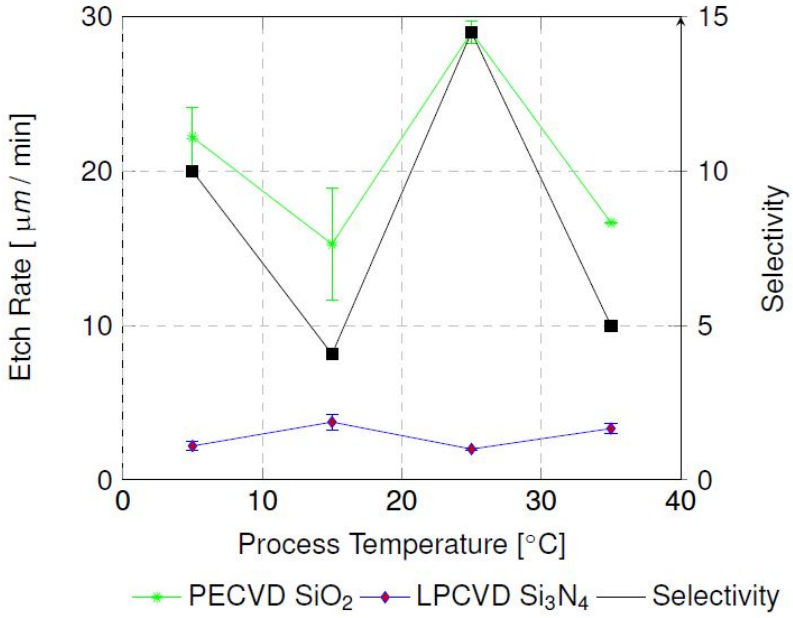

FIGURE 6.6: The temperature depended etch rates of SiO_2 and LPCVD Si_3N_4 and selectivity, as measured in a benchmark experiment. Each data point is the average of 3 measurements.

- The pressure needs to be carefully controlled so that the flux of reactants onto the surface is moderated and the reaction products can evaporate from the surface.
- The etch rate depends on the HF concentration within the liquid film which is not identical to the gas concentrations of the reactants.

These issues have been identified before and an initial attempt to model HF vapour etching has been made by Helms and Deal [104]. However, due to the limited computing power in 1992, their model is only applicable to 5 specific temperatures. Hence, it is challenging to use it in practice.

However, this thesis revisits their work, and a tool has been developed that models the molecular flows into and out of the condensed liquid layer. With this model, tool input parameters can be calculated for a broad range of process temperatures which ensure that the etch takes place at equilibrium vapour pressure [2].

[2]According to the encyclopedia Britanica [105] the vapour pressure is defined as "the pressure exerted by a vapour when the vapour is in equilibrium with the liquid or solid form, or both, of the same substance i.e., when conditions are such that the substance can exist in both or in all three phases."

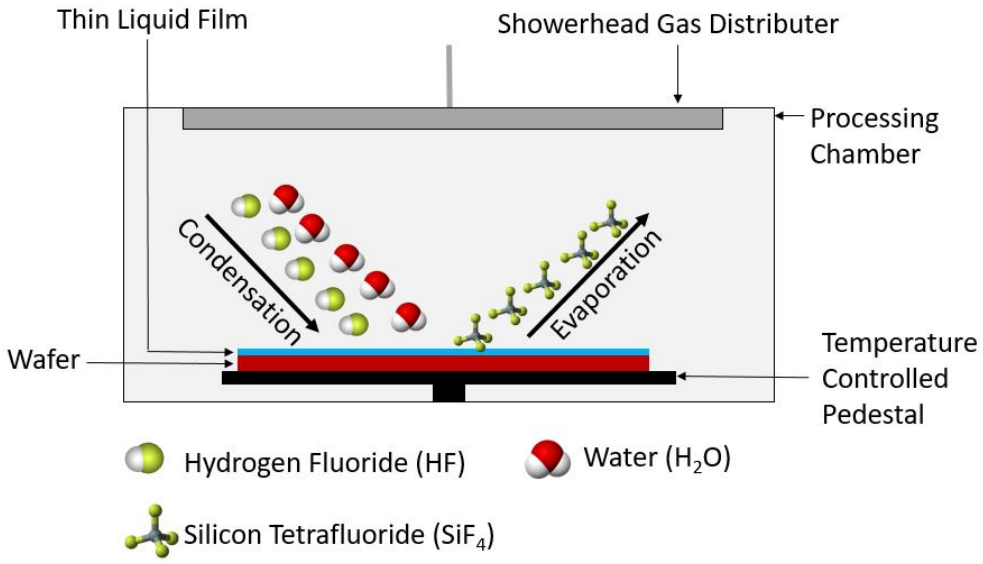

FIGURE 6.7: The evaporation and condensation of reactants and reaction products in HF vapour etching.

At equilibrium vapour pressure, the condensation and evaporation of the reactants form an equilibrium, resulting in the creation of a stable thin condensed layer of water and HF that allows effective etching while avoiding stiction. Furthermore, the reactant concentration within the layer is known and can be controlled.

6.5.1 Model Development

The model was developed based on empirical data published in previous studies [106][104]. To verify that the condensation and evaporation effects have been successfully separated from the performance parameters, the impact of the reactant concentration and the temperature on the etch rate of SiO_2 are measured and compared to results obtained with wet etching.

The condensation and evaporation of mixtures form a thermodynamic equilibrium at vapour pressure. If the partial pressure exceeds the vapour pressure, a stable condensed layer forms [104] as shown in figure 6.7. The vapour pressure of a gas in a

gas mixture depends on the process temperature and partial pressures of other components within the mixture. Due to these complex interdependencies, empirical data is required to determine the vapour pressure. The most comprehensive dataset available for HF/H_2O systems was published by Munter et al. [106] in 1949. They provided the vapour pressures for a temperature range of 0.1 – 70 ° C and a liquid HF weight percentages range of 10 to 70 %. From this limited data, the authors were able to determine a table of constants for the vapour pressure equation which takes the form

$$LogP = B - \frac{A}{t} \tag{6.1}$$

where P represents the pressure in Torr, B and A are liquid HF weight percentage dependent variables and T is the temperature. Based on this equation, Munter's data was computationally extrapolated to create equation 6.2, which enables the calculation of the corresponding H_2O partial pressure p_{H2O} leading to the vapour pressure as a function of the HF partial pressure p_{HF}

$$p_{H2O} = cln(p_{HF}) + d \tag{6.2}$$

The parameters c and d are functions of temperature that were found empirically to be

$$c = -0.1464(T + 0.049) \tag{6.3}$$

and

$$d = 0.635(T - 2.442) \tag{6.4}$$

From this set of equations, equilibrium conditions can be calculated for any set of HF partial pressure/processing temperature combinations. Once the partial pressures required have been determined, the corresponding tool parameters, particularly the gas

flows and pressure, can be calculated easily.

The partial pressure can thus be controlled in two ways, either by adjusting the processing pressure or adding a third inert buffer gas into the mix to effectively adjust the chamber volume. In this experiment, the second method proved more controllable and nitrogen was used as the buffer gas.

6.5.2 Experimental Verification

The experiments presented to verify the model were conducted on the memsstar Alpha Orbis vapour etch tool. The concentration of the etch by-product SiFx above the sample is continuously measured with a nondispersive infrared gas sensor, and the data plotted over time. This plot clearly shows the onset and offset of the etch reaction, and from it, the effective etch time can be obtained.

Experiments were conducted using two sets of samples. Both were 15 x 15 mm chips, one coated with a 1000 nm thick layer of PECVD SiO_2 and the other with a 1300 nm thick layer of PECVD SiN. On each sample, the layer thickness before and after etching was measured with a Nanospec reflectometer. In order to maintain stable gas concentrations and avoid premature etching of the silicon nitride, N_2 was supplied into the chamber until the processing pressure was reached, at which point the HF and H_2O were supplied into the reaction chamber.

The first test of this new model was to determine whether the effect of the gaseous HF concentration on the SiO_2 etch rate can be measured. Knotter [46][43], found that SiO_2 is mainly etched by difluorides which prevail in less diluted HF/H_2O mixtures. Therefore, one would expect the SiO_2 etch rate to increase with an increased HF concentration within the liquid layer. Table 6.5 displays the partial pressures which were calculated from the model and the corresponding input parameters used during this experiment. The resulting etch rates are plotted as a function of the HF gas concentration in figure 6.8. The lowest and highest HF gas concentrations within this experiment were 17.4 % and 91 %, respectively, and the relationship between etch rate and concentration appears to resemble a sigmoid function.

Partial Pressures [Torr]			Gas Flows [sccm]		
P_{HF}	P_{H2O}	P_{N_2}	HF	H_2O	N_2
1.2	6.6	12.2	3.6	19.7	36.7
2.1	5.3	12.5	6	16	38
3	4.6	12.4	9	14	37
4	4.0	12.0	12	12	36
7.4	2.7	9.9	22	8	29
9	2.3	8.7	27	7	26
14	1.3	4.7	42	4	14
19.3	0.7	0.04	58	2	0

TABLE 6.5: The calculated partial pressures and gas flows for the concentration experiment. The process chamber temperature at 15 °C, the etch time was 80 s and the sum of the partial pressures was kept constant at 20 Torr.

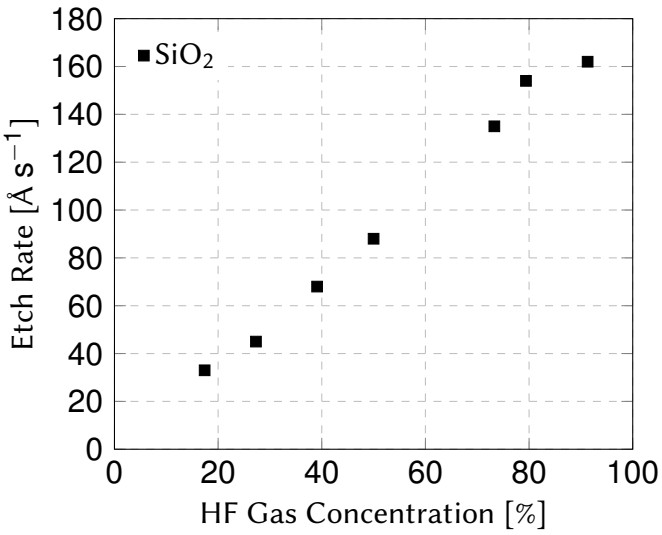

FIGURE 6.8: The silicon dioxide etch rate dependency on the gaseous HF concentration. The etch parameters are available in table 6.5. The process chamber temperature was 15 °C. The etch was not subject to the proximity effect. Each data point represents a single measurement.

The lowest etch rate of 33 Å s^{-1} (Angstroms [3] per second) was measured at a concentration of 17.4 % HF, increasing to 154 Å s^{-1} at a concentration of 80 % HF. Beyond that point, the plot flattens and only marginal increases in the etch rate can be obtained by further increasing the HF concentration. Unsurprisingly, increased HF concentration resulted in increased etch rates. This has been observed before [107] and is in good agreement with theoretical expectations [43][46]. At concentrations below roughly 50 % HF, the plot's trend is in good agreement with wet HF etch data presented elsewhere [108] [109]. The etch rates presented here are less than those reported for wet etching, which may be due in part to the lower processing temperature used in this work. Unfortunately, for the higher HF concentrations, no reference data could be sourced, probably because it is very uncommon in practice to wet etch in HF solutions with concentrations higher than 49 %. Nevertheless, the data presented here is in good agreement with the low concentration data presented within the literature. This suggests that the model used in this study enables concentration effects to be measured independent of condensation phenomena.

The second test of the method was to determine whether the processing temperature on the etch rate can be studied independently of condensation phenomena. The Arrhenius equation suggests that the reaction rate increases with increased temperature. Therefore one might presume that the SiO_2 etch rate similarly increases with increased temperature. This SiO_2 etch rate increase has been observed for wet HF etching [109], however, previous publications [30], [42], [29] suggest that the etch rate decreases with increased temperature in HF vapour etch processes. The consensus was that this decrease results from fewer reactants condensing onto the surface being etched.

The data presented in figure 6.9, shows an increase in the SiO_2 etch rate with increasing temperature, under the condition that the partial pressures are adjusted to a level that allows operation at vapour pressure (the tool parameters used are displayed in table 6.6). For this experiment, the temperature range was relatively small (5 - 20 °C) because the processing pressure required to establish equilibrium at higher temperatures was beyond the tool's capability. However, within this range the etch

[3] Angstrom (Å) is a length unit commonly used to describe the distance component in slow etch rates. 1 Å = 10^{-10} m = 0.1 nm

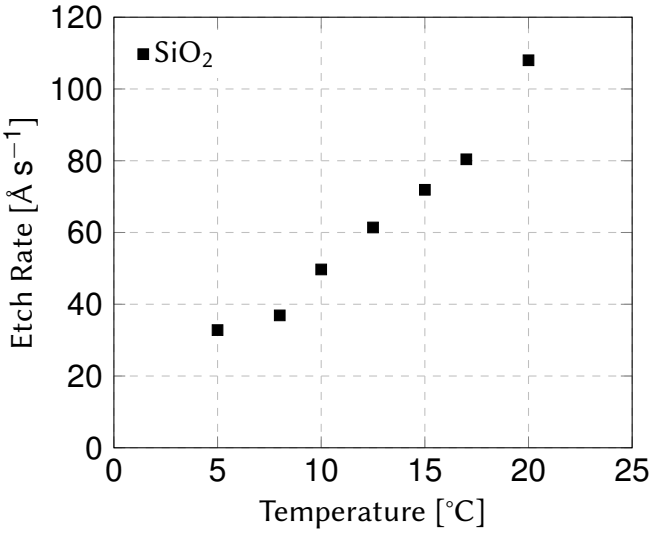

FIGURE 6.9: The etch rate dependency on the temperature. The gaseous HF concentration was 40 +/-2 %. The etch was not subject to the proximity effect. Each data point represents a single measurement.

rate increased significantly from 33 Å s^{-1} at 5 °C to 108 Å s^{-1} at 20 °C. Furthermore, the best fit to the data suggests an exponential increase in the reaction rate. This observation is in excellent agreement with the expectation derived from the Arrhenius equation.

While there is much wet etch benchmark data for temperatures above 25 °C, only one reference could be found for operation at lower temperatures. Mai [109] provides an etch rate over temperature plot for etching thermally deposited SiO_2 in a 12 % HF solution over a temperature range from 0 -50 °C. The plot's general trend looks similar to the one displayed in figure 6.9. The etch rates reported here are roughly an order of magnitude higher, which could be explained by the higher HF concentration used in this experiment (40 ± 2 %) and the fact that PECVD SiO_2 was etched, rather than the denser and more etch-resistant thermal SiO_2 used in [109].

T [°C]	Partial Pressures [Torr]			Gas Flows [sccm]		
	P_{HF}	P_{H2O}	P_{N2}	HF	H_2O	N_2
20	4.1	6.3	9.6	12	19	29
17	3.4	5.2	11.4	10	16	34
15	3.0	4.6	12.4	9	14	37
12.5	2.6	3.9	13.5	8	12	40
10	2.2	3.4	14.5	7	10	43
8	1.9	2.9	15.2	6	9	45
5	1.5	2.4	16.1	5	7	48

TABLE 6.6: The calculated partial pressures and gas flows for the temperature experiment. The etch time was constant at 80 s and the sum of the partial pressures was constant at 20 Torr.

6.5.3 Evaluation of the Model

The data presented suggests that the model enables the determination of the required partial pressures for H_2O and HF, which are required to establish equilibrium vapour pressure for any given HF concentration or processing temperature. From these vapour pressures, the required etch parameters were derived. The results of the verification experiments strongly suggest that this method enables the exclusion of condensation effects from HF vapour etching.

The resulting process control is akin to HF wet etch processes. Furthermore, the experimental data showed that the SiO_2 etch rates behaved identically to wet etch processes.

The results of the temperature experiments conducted here contradict the vapour HF etch literature, which suggests that the etch rate decreases with increased temperature. The dataset presented in figure 6.9 clearly shows that the HF vapour etch rates' behaviour is identical to wet etch processes when the extent of the thin liquid film is carefully controlled.

There are, however, limitations to the thin liquid film control method. Firstly, the gas flows need to be supplied with an accuracy of 0.1 sccm and the gas flows need to remain stable during processing. Secondly, the processing temperature deviations

should be accurate at roughly $\pm$ 1 °C. Thirdly, a broad range of processing pressures (5-50 Torr) is required to establish vapour pressure at a temperature range from 5 to 45 °C. While the Alpha Orbis tool performed well with the temperature and gas flow accuracy, it was limited by the maximum processing pressure. The alternative, Xeric system which was developed for commercial applications, is not suitable for the thin film modulation method because the processing gas flows have a relatively limited flow rate range and cannot be set to the required accuracy.

6.6 HF Concentrations Effect on the Etch Selectivity

Knotter [46] suggested that in wet HF etching, the etch selectivity of SiO_2 over SiN is a function of the HF concentration because difluorides prevail over monofluorides in less diluted HF solutions.

6.6.1 Experimental Design

The etch parameters presented in table 6.5 were used to etch blanket PECVD SiN chips in the Alpha Orbis tool. The processing temperature was 15 °C. The film thickness was measured before and after etching using a Nanospec reflectometer.

6.6.2 Results and Discussion

The concentration-dependent PECVD SiN etch rates are displayed in figure 6.10.

The lowest etch rate of 5 Å s^{-1} was measured at an HF concentration of 17.4 %, while the maximum etch rate of 12.5 Å s^{-1} was measured at an HF concentration of 91.3 %. Similar to the data presented for the SiO_2 etch rates in figure 6.8, the plot appears to resemble a sigmoid function. Unfortunately, the author of this work could not find comprehensible concentration dependent silicon nitride etch rates for either wet or vapour HF etching in the literature. However, Van Witvrouw et al. [29] reported a PECVD SiN etch rate of roughly 16 Å s^{-1} in a 49 % HF/H_2O solution, which is roughly double the etch rate reported at 50 % gaseous HF concentration here. Unfortunately, the temperature of their solution was not reported. Assuming their solution was at room temperature, the difference in etch rate might be explainable by the lower temperatures of 15 °C used in this study.

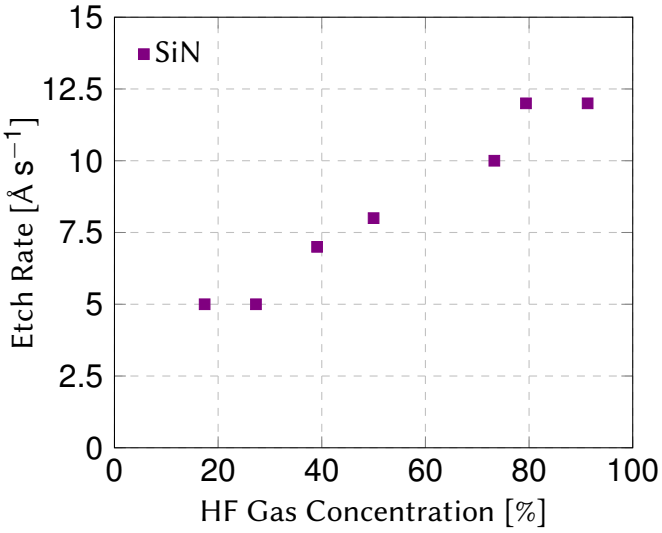

FIGURE 6.10: The silicon nitride etch rate dependency on the gaseous HF concentration. The etch parameters are available in table 6.5. The process chamber temperature was 15 °C. The etch was not subject to the proximity effect. Each data point represents a single measurement.

Figure 6.11 shows the etch SiO_2: PECVD SiN selectivity as a function of HF concentration. In excellent agreement with Knotter [46], the lowest selectivity of 7: 1 is observed at a concentration of 17.4 %. It then increases, reaching a maximum of 13.2: 1 at an HF concentration of 91.3 %. The good agreement between the vapour etch selectivities reported here and the theoretical expressions developed by Knotter for wet HF etching suggests that the extent of the thin etchant film was controlled successfully and that the etch reactions taking place within the film are similar to wet etching.

Furthermore, the observation that the etch selectivity almost doubled clearly demonstrates that the method of thin-film modulation has the potential to improve HF vapour etch process control.

6.6.3 Summary

The data presented in this section clearly showed that the SiO_2: SiN selectivity depends on HF's concentration. It was found that the etch selectivity improved from

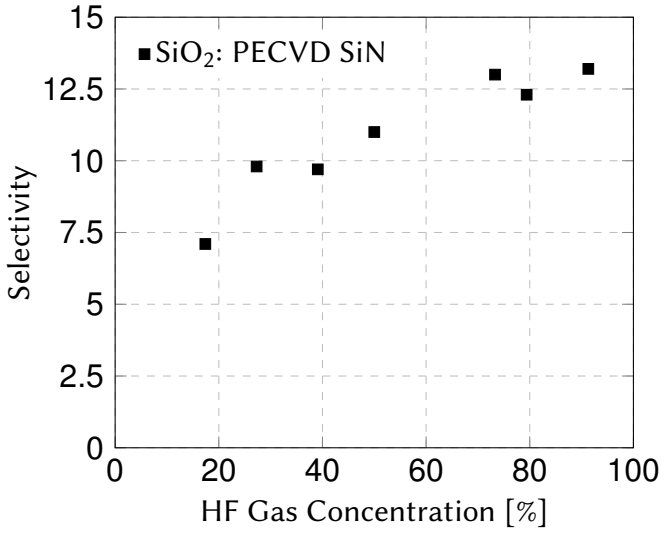

FIGURE 6.11: The silicon dioxide to silicon nitride etch selectivity as a function of the HF concentration within the HF/H_2O gas mixture. The etch parameters are available in table 6.5. The temperature was 15 °C. The etch was not subject to the proximity effect.

7.5: 1 to 12.6: 1 when the HF concentration was increased significantly from 20 % to 91 %.

6.7 The Effect of Cooling on the Selectivity

Knotter [46] [43] also suggested that in wet HF etching the etch selectivity of SiO_2 over SiN is a function of the temperature, because difluorides prevail over monofluorides at lower temperatures.

6.7.1 Experimental Design

The etch parameters presented in table 6.6 were used to etch blanket PECVD SiN chips in the Alpha Orbis tool for 80 seconds. The processing HF concentration was constant at 40 +/-2 %. The film thickness was measured before and after etching, using a Nanospec reflectometer.

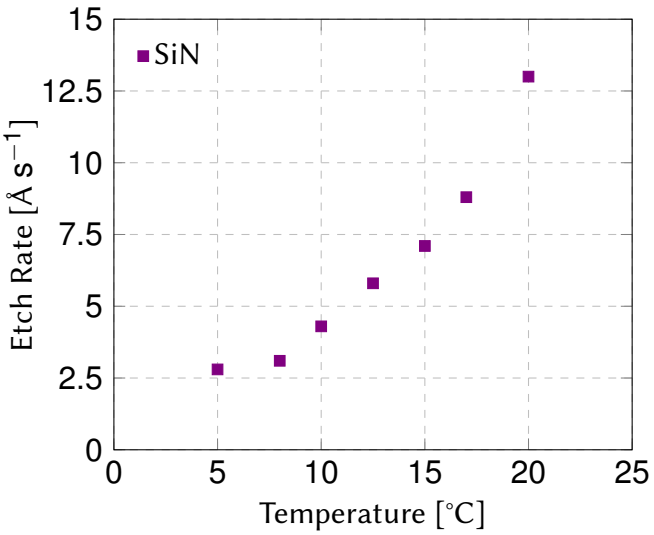

FIGURE 6.12: The PECVD SiN etch rate as a function of the processing temperature. The etch parameters are available in table 6.6. The HF/H_2O concentration was constant at 40 % ± 2 %. The etch was not subject to the proximity effect. Each data point represents a single measurement.

6.7.2 Results and Discussion

Figure 6.12 shows the PECVD SiN etch rate as a function of temperature. It can be seen that when the extent of the thin etchant film is controlled, the PECVD SiN etch rate increases in an exponential manner as the processing temperature is increased. The lowest etch rate of 2.5 Å s^{-1} was observed at a temperature of 5 °C, while the maximum of 12.6 Å s^{-1} was measured at a temperature of 20 °C. Even though no reference etch rates were available in the literature, the data is in excellent agreement with the theoretical expectation.

Figure 6.13 shows the SiO_2: PECVD SiN selectivity as a function of temperature. It can be seen that the reduction of the processing temperature by 15 °C results in a significant selectivity increase from 8: 1 to 12: 1, once again in agreement with the expectation derived from theory. However, the selectivity appears to stop increasing when cooling below a temperature of 8 °C. The reason for this is unclear, but as this is the tool's absolute cooling limit, the actual processing temperature may not be accurately known. If that is the case, etching may not have proceeded at equilibrium and in consequence, the reactants flux towards the surface would have been lower.

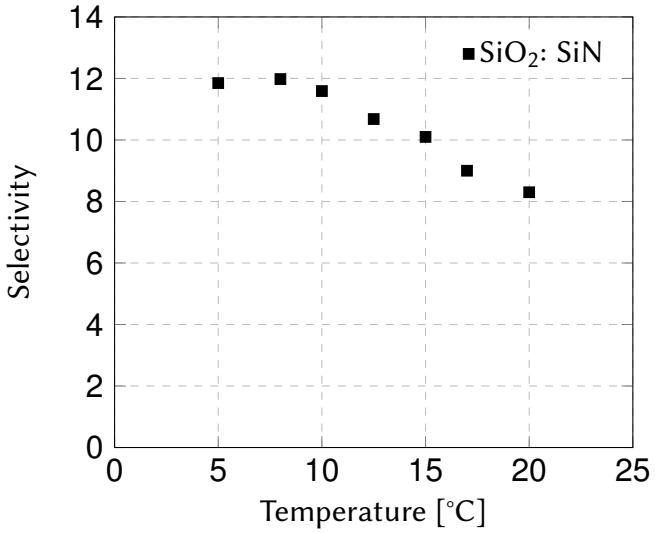

FIGURE 6.13: The silicon dioxide to silicon nitride etch selectivity as a function of the processing temperature. The etch parameters are available in table 6.6. The HF/H_2O concentration was constant at 40 $\pm$ 2 %. The etch was not subject to the proximity effect.

6.7.3 Summary

The data presented in this section clearly showed that selectivity improvements result from etching at reduced temperature. Compared to etching at 20 °C, the selectivity of SiO_2: PECVD SiN increased by 1.5 times as the temperature was lowered to 8 °C.

6.8 Summary and Conclusion

This chapter investigated whether the HF vapour etch selectivity of SiO_2: PECVD SiN can be improved. It was found that even though a proximity effect exists in HF vapour etching, it does not reduce the etch selectivity. Instead, the effect causes an increase in the SiO_2 etch rate while having little or no impact on the SiN etch rate. As a result, the selectivity between the two materials increases. Furthermore, it was confirmed that the supply of hydrogen into the processing chamber does not improve the selectivity.

A model that was developed to control the extent of the thin condensed layer required for HF etching has yielded exciting results. It was found that the etch rates behaviour is comparable to that of wet etching when the vapour etch process is carefully controlled. More importantly, however, it was also found that the etch selectivity can be increased by 200 % and 150 % by etching at high HF concentrations and low temperatures, respectively. Combining both effects would likely improve the etch selectivity even further.

However, the potential of this method is currently limited by the technical capabilities of commercially available processing equipment. The following is recommended in order to improve the next generation of vapour etch tools:

- Mass flow control capable of regulating the gas flow to an accuracy of 0.1 sccm.
- The maximum processing pressure should be increased to 60 Torr. If selective etching of SiN over SiO_2 is desired, higher pressures limits are required.
- Finally, it might be possible to increase the selectivity even further if the process chamber temperature can be reduced further. This would require a system with sub-zero temperature capabilities.

Chapter 7

Conclusion and Future Work

7.1 Conclusion

The release of free standing structures is a critical process in MEMS fabrication. Stiction, a process limitation that is inherent to wet etching and inhibits the miniaturisation of MEMS devices, can be overcome by vapour etching processes, provided that the etch selectivity is reasonably high.

The aim of the work reported in this thesis was to develop a better understanding of the mechanisms that determine material removal in two standard vapour etch processes used for the removal of sacrificial layers in MEMS fabrication processes. In this way it was hoped to achieve better selectivity control to optimise the release of structures such as membranes, bridges and cantilevers which are key elements of MEMS sensors. This was made possible by the development of a test measurement protocol, which takes important process characteristics such as the etch selectivity and proximity effect into account.

The two processes characterised in this thesis were the etching of silicon and silicon dioxide with xenon difluoride and hydrogen fluoride respectively. While both processes are used to release the free standing component of MEMS devices, there are notable differences in the chemical and physical mechanisms underlying XeF_2 and HF vapour etching.

Firstly, the XeF_2 vapour etch of silicon remains in the vapour phase throughout the entire process, whereas a condensed layer is required to form on the sample to facilitate the HF etching of silicon nitride. Secondly, HF requires a catalyst such as water or alcohol to initiate the etch reaction while XeF_2 does not.

Unsurprisingly, different selectivity issues have been reported for both processes. The generally high selectivity observed in XeF_2 etching decreases when two materials are etched in close proximity to one another. In contrast, the HF vapour etch selectivity is generally lower than those of HF wet etching, but no further decrease has been reported for etching in the proximity of other materials.

However, both processes share a number of key features. They were developed to deliver a stiction free etch of sacrificial layers. They both use fluorine-based molecules as the etchant, have similar hardware requirements and are evaluated using identical performance parameters.

The first significant contribution to the understanding of vapour etch processes presented in this thesis has been made possible by the successful development of a test structure and measurement protocol which can be used to characterise vapour etch processes. The delivery of this capability makes it possible to study and compare process selectivity for a wide range of materials under realistic MEMS fabrication conditions. Furthermore, the metrology has been successfully automated, allowing for quick and convenient measurements. With these advantages and its small size, the test structure is well suited for both etch process research in academia or quality control in industry.

By employing test structure measurement, this study has significantly improved the understanding of the proximity effect in XeF_2 vapour etching. It was previously only measured for silicon dioxide, but this study observed that it also significantly reduces the etch selectivity of polysilicon towards silicon nitride. The underlying mechanisms that were identified in this study suggest that a broad range of other MEMS materials is also likely to be affected.

Investigations to mitigate the proximity effect revealed that the supply of moderate amounts of hydrogen to the reaction chamber during XeF_2 vapour etching improves the selectivity of polysilicon towards silicon nitride significantly. Thereby this method solves some of the selectivity issues associated with XeF_2 vapour etching.

The proximity effect was also observed and characterised for HF vapour etching. However, in contrast to XeF_2 vapour etching, it improved the etch selectivity between silicon dioxide and silicon nitride. This interesting observation has not been previously reported in the literature.

Alongside this, a process control method has been developed and characterised for HF vapour etching. It was demonstrated that the etch selectivity between silicon dioxide and silicon nitride improved significantly when etched at low temperatures or with high HF concentrations. The methodology can enable vapour etch processes to be run with the same control as those of wet HF etching methods.

7.2 Impact on Sensor Performance

The vapour etch characterisation undertaken in this study has showed that many of the etch selectivities measured would not be suitable to fabricate MEMS sensors under realistic MEMS fabrication conditions. For instance, the CMUT example sensor presented in section 1.3 requires a sacrificial layer to structural layer selectivity of at least 10: 1 to be within the specification. In this work, however, polysilicon to silicon nitride selectivity as low as 5: 4 and silicon dioxide to silicon nitride selectivity of only 6:1 were measured when vapour etching with XeF_2 and HF respectively. Consequently, to fabricate the devices with the above process, would require additional process design and development.

Fortunately, several methods to improve the etch selectivity in both vapour HF and XeF_2 etching have been demonstrated in this thesis. By adding hydrogen to the reaction chamber, the XeF_2 vapour etch selectivity has been improved to 13: 1, which would enable the fabrication of the CMUT example sensor with a resonance frequency within the specified range.

Similarly, by controlling the composition of the thin liquid film to reduce the processing temperature and/or to increase the HF concentration in vapour HF etching, the selectivity can be doubled. Again, the resulting improvement of the selectivity enables this example sensor to be fabricated.

Wet etch release of structures is a commonly employed process in MEMS technology. However, it requires devices to be submerged in a liquid etchant and so stiction is a potential issue. The ability to vapour etch devices leads to stiction free structural layer release. It helps to facilitate the drive to towards smaller dimensions. The size reduction can enable novel sensor applications, increase the sensitivity of existing concepts, and reduce device unit costs.

The selectivity improvements which can be achieved with an increased understanding of the proximity effect, and the implementation of the process improvements presented in this thesis, could help to mitigate a potential drawbacks of vapour etching.

7.3 Impact of the Pandemic

Some measurements could not be taken due to the restrictions that were put in place to control the coronavirus disease 19 (COVID-19) pandemic of 2020 and 2021. More specifically, it was planned to determine the composition of the thin films used before and after etching using secondary ion mass spectroscopy (SIMS) measurements. Those measurements would have allowed determination of how much hydrogen was embedded in the thin films, if the embedded hydrogen changes the etch characteristics and if the composition of the films was altered after etching. However, access to the measurement equipment was revoked due to the pandemic.

In addition to that, the cleanroom access limitation during the pandemic reduced the time that could be spent in the laboratory significantly. Therefore, the number of data points collected for each HF etch measurement had to be reduced. Furthermore, the model could not be tested with the test structure.

7.4 Future Directions

While the work reported in this thesis has made significant progress in understanding vapour etch selectivity, the equipment capability has been a limiting factor.

More specifically, it was planned to determine the composition of the thin films used before and after etching using secondary ion mass spectroscopy (SIMS) measurements. Those measurements would have allowed determination of how much hydrogen was embedded in the thin films, if the the embedded hydrogen changes the etch characteristics and if the composition of the films was altered after etching. Unfortuntaley, access to the measurement equipment was revoked due to the pandemic. Consequently, the suggested future work requires the boundaries of the hardware provision to be expanded.

XeF_2 etching at subzero temperatures could further improve etch selectivity, as the polysilicon etch rate has been observed to increase as the processing temperature decreases. Reducing the temperature to -20 °C or even -70 °C has the potential to yield substantial improvements. However, a novel cooling concept would need to be developed and implemented, as currently available systems are limited to temperatures above 5 °C.

High pressure XeF_2 etching while supplying hydrogen to the chamber could improve this study's selectivity enhancement even further. Current equipment is limited to a maximum pressure of 10 Torr, but changing the pressure control system to allow for higher processing pressures could be a straightforward tool modification.

Increasing the range of controllable processing parameters in HF etching also has the potential to increase the selectivity. The results from the experiments to control the liquid thin film, developed and presented in this study, suggest that this method should improve HF vapour etch selectivity significantly. However, to achieve this, hardware modifications would be required, specifically to enable a greater range of gas flows to be supplied to the chamber. In parallel, mass flow controllers would need to supply gas flows with a fluctuation of less than 0.1 sccm, with a processing pressure range of at least 3 to 70 Torr. It would be interesting to repeat the experiments presented in this work on such an improved tool, with the test structures developed here.

References

[1] S. A. Zawawi, A. A. Hamzah, B. Y. Majlis, and F. Mohd-Yasin, "A review of MEMS capacitive microphones," *Micromachines*, vol. 11, no. 5, pp. 1–26, 2020, ISSN: 2072666X. DOI: 10.3390/MI11050484.

[2] R. Bogue, "Recent developments in MEMS sensors: A review of applications, markets and technologies," *Sensor Review*, vol. 33, no. 4, pp. 300–304, 2013, ISSN: 02602288. DOI: 10.1108/SR-05-2013-678.

[3] J. W. Judy, "Biomedical applications of MEMS," *Technical Digest - International Electron Devices Meeting*, pp. 239–242, 1996, ISSN: 01631918. DOI: 10.1109/iedm.1996.553575.

[4] A. C. Fischer, F. Forsberg, M. Lapisa, S. J. Bleiker, G. Stemme, N. Roxhed, and F. Niklaus, "Integrating MEMS and ICs," *Microsystems and Nanoengineering*, vol. 1, no. March, pp. 1–16, 2015, ISSN: 20557434. DOI: 10.1038/micronano.2015.5.

[5] P. J. French and P. M. Sarro, "Surface versus bulk micromachining: The contest for suitable applications," *Journal of Micromechanics and Microengineering*, vol. 8, no. 2, pp. 45–53, 1998, ISSN: 09601317. DOI: 10.1088/0960-1317/8/2/002.

[6] F. Niklaus, G. Stemme, J. Q. Lu, and R. J. Gutmann, "Adhesive wafer bonding," *Journal of Applied Physics*, vol. 99, no. 3, 2006, ISSN: 00218979. DOI: 10.1063/1.2168512.

[7] B. Wu, A. Kumar, and S. Pamarthy, "High aspect ratio silicon etch: A review," *Journal of Applied Physics*, vol. 108, no. 5, pp. 8–11, 2010, ISSN: 00218979. DOI: 10.1063/1.3474652.

[8] T. Gotszalk, "From MEMS to NEMS," *Lecture Notes in Electrical Engineering*, vol. 573, pp. 115–141, 2020, ISSN: 18761119. DOI: 10.1007/978-3-030-21496-8_12.

[9] J. Bühler, F. P. Steiner, and H. Baltes, "Silicon dioxide sacrificial layer etching in surface micromachining," *Journal of Micromechanics and Microengineering*, vol. 7, no. 1, 1997, ISSN: 09601317. DOI: 10.1088/0960-1317/7/1/001.

[10] K. Hjort, "Sacrificial etching of III-V compounds for micromechanical devices," *Journal of Micromechanics and Microengineering*, vol. 6, no. 4, pp. 370–375, 1996, ISSN: 09601317. DOI: 10.1088/0960-1317/6/4/003.

[11] B. Li, B. Xiong, L. Jiang, Y. Zohar, and M. Wong, "Germanium as a versatile material for low-temperature micromachining," *Journal of Microelectromechanical Systems*, vol. 8, no. 4, pp. 366–372, 1999, ISSN: 10577157. DOI: 10.1109/84.809050.

[12] O. Tabata, K. Shimaoka, R. Asahi, and S. Sugiyama, "Micromachined sensors using polysilicon sacrificial layer etching technology," *Sensors and Materials*, vol. 8, no. 1, pp. 057–067, 1996, ISSN: 09144935. DOI: 10.1109/iedm.1994.383448.

[13] Y. P. Zhao, L. S. Wang, and T. X. Yu, "Mechanics of adhesion in MEMS—a review," *Journal of Adhesion Science and Technology*, vol. 17, no. 4, pp. 519–546, 2003. DOI: 10.1163/15685610360554393. [Online]. Available: https://doi.org/10.1163/15685610360554393.

[14] N. Tas, T. Sonnenberg, H. Jansen, R. Legtenberg, and M. Elwenspoek, "Stiction in surface micromachining," *J. Micromech. Microeng*, vol. 6, pp. 385–397, 1996. [Online]. Available: http://iopscience.iop.org/0960-1317/6/4/005.

[15] R. Maboudian and R. T. Howe, "Critical Review: Adhesion in surface micromechanical structures," *Journal of Vacuum Science Technology B: Microelectronics and Nanometer Structures*, vol. 15, no. 1, p. 1, 1997, ISSN: 0734211X. DOI: 10.1116/1.589247.

[16] R. Maboudian, W Ashurst, and C Carraro, "Self-assembled monolayers as anti-stiction coatings for MEMS: Characteristics and recent developments," *Sensors and Actuators A: Physical*, vol. 82, pp. 219–223, 2000. DOI: 10.1016/S0924-4247(99)00337-4.

[17] I. Penskiy, A. P. Gerratt, and S. Bergbreiter, "Friction , adhesion and wear properties of PDMS coatings in MEMS devices," *2011 IEEE 24th International Conference on Micro Electro Mechanical Systems*, pp. 440–444, 2011. DOI: 10.1109/MEMSYS.2011.5734456.

[18] T. Yamashita, T. Itoh, and T. Suga, "Sensors and Actuators A : Physical Investigation of anti-stiction coating for ohmic contact MEMS switches with thiophenol and 2-naphthalenethiol self-assembled monolayer," *Sensors Actuators: A. Physical*, vol. 172, no. 2, pp. 455–461, 2011, ISSN: 0924-4247. DOI: 10.1016/j.sna.2011.09.034. [Online]. Available: http://dx.doi.org/10.1016/j.sna.2011.09.034.

[19] J. Li, T. Mattila, and V. Vuorinen, *MEMS Reliability*. Elsevier Inc., 2015, pp. 744–764, ISBN: 9780323299657. DOI: 10.1016/B978-0-323-29965-7.00041-5. [Online]. Available: http://dx.doi.org/10.1016/B978-0-323-29965-7.00041-5.

[20] I. H. Jafri, H. Busta, and S. T. Walsh, "Critical point drying and cleaning for MEMS technology," *MEMS Reliability for Critical and Space Applications*, vol. 3880, no. August 1999, pp. 51–58, 1999, ISSN: 0277786X. DOI: 10.1117/12.359371.

[21] P. J. Resnick and P. J. Clews, "Whole wafer critical point drying of MEMS devices," *Reliability, Testing, and Characterization of MEMS/MOEMS*, vol. 4558, no. October 2001, pp. 189–196, 2001, ISSN: 0277786X. DOI: 10.1117/12.443011.

[22] J. F. Veyan, M. D. Halls, S. Rangan, D. Aureau, X. M. Yan, and Y. J. Chabal, "XEF_2-INDUCED REMOVAL OF SIO_2 NEAR SI SURFACES AT 300 K: AN UNEXPECTED PROXIMITY EFFECT.," *Journal of Applied Physics*, vol. 108, no. 11, pp. 1–9, 2010, ISSN: 00218979. DOI: 10.1063/1.3517148.

[23] M. Rondé, A. J. Walton, and J. G. Terry, "Test Structure for Measuring the Selectivity in Vapour Etch Processes," in *IEEE 33rd International Conference on Microelectronic Test Structures (ICMTS), Edinburgh, United Kingdom*, 2020, pp. 1–5, ISBN: 9781728140087. DOI: 10.1109/ICMTS48187.2020.9107934.

[24] K. R. Williams and R. S. Muller, "Etch Rates for Micromachining Processing," *Journal of Microelectromachanical Systems*, p. 256, 1996. DOI: 10.1109/84.546406.

[25] B. Belgacem, D. Alquier, P. Muralt, J. Baborowski, S. Lucas, and R. Jerisian, "Optimization of the fabrication of sealed capacitive transducers using surface micromachining," *Journal of Micromechanics and Microengineering*, vol. 14, no. 2, pp. 299–304, 2004, ISSN: 09601317. DOI: 10.1088/0960-1317/14/2/019. arXiv: 08992363-8-2-303 [10.1215].

[26] W Waver, P. S. Timoshenko, and D. H. Young, "Vibration Problems in Engineering," in *Vibration Problems in Engineering*, 5th ed., New York: Wiley, 1990, p. 503, ISBN: 978-0-471-63228-3.

[27] M. Rondé, A. J. Walton, and J. G. Terry, "Manipulating Etch Selectivities in XeF_2 Vapour Etching," *Journal of Microelectromachanical Systems*, vol. 30, no. 1, pp. 156–164, 2021. DOI: 10.1109/JMEMS.2020.3044688.

[28] M. Ronde, A. J. Walton, and J. G. Terry, "Test Structure for Measuring the Selectivity in XeF_2 and HF Vapour Etch Processes," *IEEE Transactions on Semiconductor Manufacturing (Early Access)*, pp. 1–7, 2021. DOI: 10.1109/ICMTS48187.2020.9107934.

[29] A. Witvrouw, B. Du Bois, P. De Moor, A. Verbist, C. A. Van Hoof, H. Bender, and C. Baert, "Comparison between wet HF etching and vapor HF etching for sacrificial oxide removal," vol. 4174, pp. 130–141, 2000, ISSN: 0277786X. DOI: 10.1117/12.396423. [Online]. Available: http://proceedings.spiedigitallibrary.org/proceeding.aspx?articleid=924496.

[30] M. Wong, M. Moslehi, and R. Bowling, "Wafer Temperature Dependence of the Vapor Phase HF Oxide Etch," *Journal of The Electrochemical Society*, vol. 140, no. 1, pp. 205–208, 1993, ISSN: 00134651. DOI: 10.1149/1.2056088. [Online]. Available: http://jes.ecsdl.org/content/140/1/205.short.

[31] D Drysdale, T. O. Hara, and C. H. Wang, "Characterisation and comparison of water and alcohol as catalysts in vapour phase HF etching of silicon oxide films," *Design, Test, Integration and Packaging of MEMS/MOEMS (DTIP), 2011 Symposium on*, pp. 35–40, 2011.

[32] M Wong and R. A. Bowling, "Silicon Etch Using Vapor Phase HF/H_2O and O_3," *Electrochemical Society Active Member*, vol. 140, no. 2, 1993.

[33] D. Drysdale, "Vapour Phase HF and XeF_2 Etching Methods with Improved Selectivity for MEMS Manufacturing," Ph.D. dissertation, Heriot-Watt University, 2015. DOI: 10399/3232.

[34] A. W. Van Barel, Bert du Bois, Rita Van Hoof, Jef De Wachter, Ward De Ceuninck, "Apparent and steady-state etch rates in thin film etching and underetching of microstructures: II. Characterisation," *Journal of Micromechanics and Microengineering*, vol. 20, no. 5, 2010, ISSN: 09601317. DOI: 10.1088/0960-1317/20/5/055033.

[35] S. Arrhenius, "Über die Dissociationswärme und den Einfluss der Temperatur auf den Dissociationsgrad der Elektrolyte," *Zeitschrift für Physikalische Chemie*, vol. 4U, no. 1, 2017, ISSN: 0942-9352. DOI: 10.1515/zpch-1889-0408.

[36] D. Camuffo, "Consequences of the Maxwell–Boltzmann Distribution," in *Microclimate for Cultural Heritage, Second Edition*, Elsevier B.V., 2014, ch. 9, pp. 347–366, ISBN: 9780444632968. DOI: 10.1016/b978-0-444-63296-8.00010-x.

[37] I. Langmuir, "The adsorption of gases on plane surfaces of glass, mica and platinum," *Journal of the American Chemical Society*, vol. 40, no. 1, pp. 1361–1402, 1918, ISSN: 15205126. DOI: 10.1021/ja01340a008.

[38] D. Ballantrine, R. M. White, S. J. Martin, J. Ricco, E. T. Zeller, G. F. C, H Wohltjen, M Levy, and R Stern, *Acoustic Wave Sensors: Theory, Design and Physico-Chemical Applications - Chapter 5: Chemical and Biological Sensors*. 1997, ISBN: 0120774607. DOI: 10.1016/B978-0-12-077460-9.50005-8.

[39] T. Zuyi and C. Taiwei, "On the Applicability of the Langmuir Equation to Estimation of Adsorption Equilibrium Constants on a Powdered Solid from Aqueous Solution," *Journal of Colloid and Interface Science*, vol. 12, no. 231, pp. 8–12, 2000. DOI: 10.1006/jcis.2000.7057.

[40] B. S. Brunauer and P. H. Emmett, "Adsorption of Gases in Multimolecular Layers," *Journal of American Chemical Society*, vol. 60, no. 2, pp. 309–319, 1938. DOI: 10.1021/ja01269a023.

[41] G. A. Rudakov, "Gas-Phase Etching of SiO_2 Layers in an HF / C_2H_5OH Mixture," *Russian Microelectronics*, vol. 46, no. 2, pp. 114–117, 2017. DOI: 10.1134/S1063739717010097.

[42] P. Holmes and J. E. Snell, "A vapour etching technique for the photolithography of silicon dioxide," *Microelectronics and Reliability Pergamon Press*, vol. 5, no. 1, pp. 337–341, 1966. DOI: 10.1016/0026-2714(66)90162-4.

[43] D. M. Knotter, "Etching mechanism of vitreous silicon dioxide in HF-based solutions," *Journal of the American Chemical Society*, vol. 122, no. 18, pp. 4345–4351, 2000, ISSN: 00027863. DOI: 10.1021/ja993803z.

[44] R. D. A.K Convington, R.G Bates, "Definition of pH Scales, Standard Reference Values, Measurement of pH and related terminology.," *Pure Appl. Chemistry*, vol. 57, no. 3, pp. 531–542, 1985, ISSN: 00399450.

[45] The Editors of the Encyclopedia Britanica, *Hydrogen ion*. [Online]. Available: https://www.britannica.com/science/hydrogen-ion (visited on 05/26/2021).

[46] D. Martin Knotter and T. J. J. (Dee) Denteneer, "Etching Mechanism of Silicon Nitride in HF-Based Solutions," *Journal of The Electrochemical Society*, vol. 148, no. 3, F43, 2001, ISSN: 00134651. DOI: 10.1149/1.1348262. [Online]. Available: http://jes.ecsdl.org/cgi/doi/10.1149/1.1348262.

[47] H. F. Winters and J. W. Coburn, "The etching of silicon with XeF2 vapor," *Applied Physics Letters*, vol. 34, no. 1, pp. 70–73, 1979, ISSN: 00036951. DOI: 10.1063/1.90562.

[48] J. R. Holt, R. C. Hefty, M. R. Tate, and S. T. Ceyer, "Comparison of the interactions of XeF_2 and F_2 with Si(100)(2 × 1)," *Journal of Physical Chemistry B*, vol. 106, no. 33, pp. 8399–8406, 2002, ISSN: 10895647. DOI: 10.1021/jp020936p.

[49] R. C. Hefty, J. R. Holt, M. R. Tate, D. B. Gosalvez, M. F. Bertino, and S. T. Ceyer, "Dissociation of a product of a surface reaction in the gas phase: XeF_2 reaction with Si," *Physical Review Letters*, vol. 92, no. 18, pp. 18–21, 2004, ISSN: 00319007. DOI: 10.1103/PhysRevLett.92.188302.

[50] R. C. Hefty, J. R. Holt, M. R. Tate, and S. T. Ceyer, "Atom abstraction and gas phase dissociation in the interaction of XeF_2 with Si(100)," *Journal of Chemical Physics*, vol. 129, no. 21, 2008, ISSN: 00219606. DOI: 10.1063/1.3025901.

[51] L. M. Loewenstein, "Temperature dependence of silicon nitride etching by atomic fluorine," *Journal of Applied Physics*, vol. 65, no. 1, pp. 386–387, 1989, ISSN: 00218979. DOI: 10.1063/1.342555.

[52] L. R. Arana, N. D. Mas, and R. Schmidt, "Isotropic etching of silicon in fluorine gas for MEMS micromachining," 2007. DOI: 10.1088/0960-1317/17/2/026.

[53] L. R. Arana, S. B. Schaevitz, A. J. Franz, M. A. Schmidt, S. Member, and K. F. Jensen, "A Microfabricated Suspended-Tube Chemical Reactor for Thermally Efficient Fuel Processing," *Journal of Microelectromachanical Systems*, vol. 12, no. 5, pp. 600–612, 2003. DOI: 10.1109/JMEMS.2003.817897.

[54] N Posseme, O Pollet, and S Barnola, "Alternative process for thin layer etching : Application to nitride spacer etching stopping on silicon germanium," *Applied Physics Letters*, vol. 105, no. July 2014, pp. 1–5, 2017. DOI: 10.1063/1.4892543. [Online]. Available: http://dx.doi.org/10.1063/1.4892543.

[55] O. Pollet, N. Posseme, V. Ah-leung, and M. G. Barros, "Thin Layer Etching of Silicon Nitride : Comparison of Downstream Plasma , Liquid HF and Gaseous HF Processes for Selective Removal After Light Ion Implantation," vol. 255, p. 69 610 440, 2016. DOI: 10.4028/www.scientific.net/SSP.255.69.

[56] N. Posseme, M. Garcia-barros, F. Leverd, D. Benoit, O. Pollet, G. Audoit, C. Guedj, A. Jannaud, S Barnola, N. Posseme, M. Garcia-barros, F. Leverd, and D. Benoit, "Thin layer etching of low-k SiCO spacer using hydrogen ion implantation followed by hydrofluoric acid," *Journal of Vacuum Science Technology B: Microelectronics and Nanometer Structures*, vol. 052201, no. July, 2018. DOI: 10.1116/1.5038617. [Online]. Available: http://dx.doi.org/10.1116/1.5038617.

[57] N. Posseme, M. Garcia-Barros, C. Arvet, O. Pollet, F. Leverd, and S. Barnola, "Silicon nitride spacer etching selectively to silicon using CH_3F / O_2 / He / $SiCl_4$ plasma Silicon nitride spacer etching selectively to silicon using CH_3F / O_2 / He / $SiCl_4$ plasma," *Journal of vacuum science technology*, vol. 38, p. 03 304, 2020. DOI: 10.1116/1.5145158.

[58] V. Ah-leung, O. Pollet, N. Possémé, M. G. Barros, N. Rochat, C. Guedj, G. Audoit, and S. Barnola, "Understanding of a new approach for silicon nitride spacer etching using gaseous hydrofluoric acid after hydrogen ion implantation," vol. 021408, 2017. DOI: 10.1116/1.4977077. [Online]. Available: http://dx.doi.org/10.1116/1.4977077.

[59] L. M. Loewenstein, "Selective etching of silicon nitride using remote plasmas of CF_4 and SF_6," *Journal of Vacuum Science Technology A*, vol. 7, no. September 1988, p. 686, 1988. DOI: 10.1116/1.575866.

[60] D. Edelson and D. L. Flamm, "Computer simulation of a CF4 plasma etching silicon," *Journal of Applied Physics*, vol. 56, no. 5, pp. 1522–1531, 1984, ISSN: 00218979. DOI: 10.1063/1.334108.

[61] B. E. E. Kastenmeier, P. J. Matsuo, and G. S. Oehrlein, "Highly selective etching of silicon nitride over silicon and silicon dioxide," *Journal of Vacuum Science Technology A: Vacuum, Surfaces, and Films*, vol. 17, no. 6, pp. 3179–3184, 1999, ISSN: 0734-2101. DOI: 10.1116/1.582097.

[62] S. Rachidi, A. Campo, V. Loup, C. Vizioz, J.-M. Hartmann, S. Barnola, and N. Posseme, " Isotropic dry etching of Si selectively to Si 0.7 Ge 0.3 for CMOS sub-10 nm applications," *Journal of Vacuum Science Technology A*, vol. 38, no. 3, p. 033 002, 2020, ISSN: 0734-2101. DOI: 10.1116/1.5143118.

[63] Y. Zhang, G. S. Oehrlein, and F. H. Bell, "Fluorocarbon high density plasmas . VII . Investigation of selective SiO_2 -to- Si_3N_4 high density plasma etch processes," *Journal of vacuum science technology*, vol. 2127, no. July 1995, 1998. DOI: https://doi.org/10.1116/1.580091.

[64] Y. Nakazawa and Y. Saito, "Selective Etching of Silicon Native Oxide with Remote-Plasma-Excited Anhydrous Hydrogen Fluoride," *Japanese Journal of Applied Physics*, pp. 35–38, 1998.

[65] V. Volynets, Y. Barsukov, G. Kim, J.-E. Jung, S. K. Nam, K. Han, S. Huang, and M. J. Kushner, "Highly selective Si_3N_4 / SiO_2 etching using an NF_3 / N_2/ O_2 /H_2 remote plasma. I. Plasma source and critical fluxes," *Journal of Vacuum Science Technology A*, vol. 38, no. 2, p. 023 007, 2020, ISSN: 0734-2101. DOI: 10.1116/1.5125568. [Online]. Available: https://doi.org/10.1116/1.5125568.

[66] J.-E. Jung, Y. Barsukov, V. Volynets, G. Kim, S. K. Nam, K. Han, S. Huang, and M. J. Kushner, "Highly selective Si_3N_4 /SiO_2 etching using an NF_3 /N_2 /O_2 /H_2 remote plasma. II. Surface reaction mechanism," *Journal of Vacuum Science Technology A*, vol. 38, no. 2, p. 023 008, 2020, ISSN: 0734-2101. DOI: 10.1116/1.5125569. [Online]. Available: https://doi.org/10.1116/1.5125569.

[67] P Pankratiev, Y. Barsukov, A Vinogradov, V Volynets, and A Kobelev, "Selective SiN / SiO_2 etching by SF_6 / H_2 / Ar / He plasma," in *AIP Conference Proceedings*, vol. 2179, 0200, 2020, pp. 6–10, ISBN: 9780735419261.

[68] T. O'Hara, *Selectivity in a Xenon Difluoride Etch Process, US2018029883A1*, 2018.

[69] M. J. M. Vugts, G. L. J. Verschueren, M. F. A. Eurlings, L. J. F. Hermans, and H. C. W. Beijerinck, "Si/XeF_2 etching: Temperature dependence," *Journal of Vacuum Science Technology A: Vacuum, Surfaces, and Films*, vol. 14, no. 5, pp. 2766–2774, 1996, ISSN: 0734-2101. DOI: 10.1116/1.580198.

[70] D. E. Ibbotson, D. L. Flamm, J. A. Mucha, and V. M. Donnelly, "Comparison of XeF_2 and F-atom reactions with Si and SiO_2," *Applied Physics Letters*, vol. 44, no. 12, pp. 1129–1131, 1984, ISSN: 00036951. DOI: 10.1063/1.94665.

[71] H. Watanabe, H. Kitajima, I. Honma, H. Ona, R. Wilhem, and A. J. L. Sophie, "Influence of Water Adsorption/Desorption Processes on the Selectivity of Vapor HF Etching," *J. Electrochem. Soc. J. Appl. Phys.*, vol. 142, no. 30, pp. 1583–3615, 1995.

[72] T. O'Hara, *Vapour Etch of Silicon Dioxide with enhanced Selectivity, US2014017901A1*, 2014.

[73] B. Li, U. Streller, H.-P. Krause, I. Twesten, and N. Schwentner, "Efficient dry etching of Si with vacuum ultraviolet light and XeF_2 in a buffer gas," *Journal of Applied Physics*, vol. 350, no. 77, 1995. DOI: 10.1063/1.359329.

[74] U. Streller, A. Krabbe, and N. Schwentner, "Selectivity in dry etching of si(100) with XeF_2 and VUV light," *Applied Surface Science*, vol. 106, pp. 341–346, 1996, ISSN: 01694332. DOI: 10.1016/S0169-4332(96)00396-0.

[75] U. Streller, A. Krabbe, and N. Schwentner, "High efficiency in dry etching of Si for wavelengths around 120 nm," *Applied Physics Letters*, vol. 3004, no. June 1998, pp. 15–18, 1996. DOI: 10.1063/1.116820.

[76] U Streller, A Krabbe, H Raaf, and N Schwentner, "Microstructuring of Si (100) by light induced dry etching in the VUV," *Superlattices and Microstructures*, vol. 23, no. 2, 1998. DOI: 10.1006/spmi.1996.0356.

[77] G. Black, R. Sharpless, D. Lorents, D. Huestis, R. Gutcheck, T. Bonifield, D. Helms, and G. Walters, "XEF_2 PHOTODISSOCIATION STUDIES . I . QUANTUM YIELDS AND KINETICS OF XEF (B) AND XEF (C)," *Journal of Chemical Information and Modeling*, vol. 75, p. 4840, 1981. DOI: 10.1063/1.441920.

[78] K. Sugano and O. Tabata, "Etching Rate control of mask material for XeF_2 etching using uv exposure," *Micromachining and Microfabrication Process Technology VII*, vol. 4557, no. September 2001, pp. 18–23, 2001. DOI: 10.1117/12.442931.

[79] D. Ibbotson, D. L. Flamm, J. A. Mucha, and V. M. Donnelly, "Comparison of XeF_2 and F-atom reactions with Si and SiO_2," *Applied Physics Letters*, vol. 44, pp. 1129–1131, 1984.

[80] P. B. Chu, J. T. Chen, R. Yeht, G. Lin, J. C. P. Huang, E. A. Warneket, and K. S. J. Pister, "Controlled Pulse-Etching with Xenon Difluoride," *Tranducers '97 - 1997 International Conferecne on Solid-State Sensors and Actuators Chicago June 16-19*, pp. 664–668, 1997.

[81] B. Bahreyni and C Shafai, "Deep etching of silicon with XeF_2 gas," in *Canadian Conference on Electrical and Computer Engineering (CCECE)*, 2002, pp. 460–464, ISBN: 0780375149.

[82] F. I. Chang, R. Yeh, G. Lin, P. B. Chu, E. G. Hoffman, E. J. Kruglick, K. S. J. Pister, and M. H. Hecht, "Gas-phase silicon micromachining with xenon difluoride,"

Microelectronic Structures and Microelectromechanical Devices for Optical Processing and Multimedia Applications, vol. 2641, no. September 1995, p. 117, 1995. DOI: 10.1117/12.220933.

[83] K. Shimaoka and J. Sakata, "A New Full-Dry Processing Method for MEMS," *R&D Review of Toyota CRDL*, vol. 37, no. 3, pp. 59–66, 2002. [Online]. Available: http://teabeetitrep.59.to/english/review/rev373epdf/e373_059shimaoka.pdf.

[84] K. Sugano and O. Tabata, "Effects of aperture size and pressure on XeF_2 etching of silicon," *Microsystem Technologies*, vol. 9, no. 1-2, pp. 11–16, 2003, ISSN: 09467076. DOI: 10.1007/s00542-002-0195-5.

[85] K. Sugano and O. Tabata, "Reduction in surface roughness and aperture size effect for XeF_2 etching of Si," *Proc. SPIE 4979 ,Micromaching and Microfabrication Process Technology VIII*, no. January 2003, 2003. DOI: 10.1117/12.473376.

[86] J Anguita and F Briones, "HF/H_2O vapor etching of SiO_2 sacrificial layer for large-area surface-micromachined membranes," *Sensors and Actuators A*, vol. 64, pp. 247–251, 1998.

[87] G Schiavone, S Smith, J Murray, J. G. Terry, M. P. Y. Desmulliez, and A. J. Walton, "Micromechanical test structures for the characterisation of electroplated NiFe cantilevers and their viability for use in MEMS switching devices," in *2013 IEEE Int. Conf. Microelectronic Test Structures*, IEEE, 2013, pp. 13–18, ISBN: 9781467348485. DOI: 10.1109/ICMTS.2013.6528138.

[88] J. H. Lee, W. I. Jang, C. S. Lee, Y. I. Lee, C. A. Choi, J. T. Baek, and H. J. Yoo, "Characterization of anhydrous HF gas-phase etching with CH_3OH for sacrificial oxide removal," *Sensors and Actuators, A: Physical*, vol. 64, no. 1, pp. 27–32, 1998, ISSN: 09244247. DOI: 10.1016/S0924-4247(98)80054-X.

[89] W. I. Jang, C. A. Choi, M. L. Lee, C. H. Jun, and Y. T. Kim, "Fabrication of MEMS devices by using anhydrous HF gas-phase etching with alcoholic vapor," *IEEE Journal of Microelectromechanical Systems*, vol. 12, pp. 297–306, 2002. DOI: 10.1088/0960-1317/12/3/316.

[90] G. Van Barel, L. Mertens, W. De Ceuninck, and A. Witvrouw, "Apparent and steady-state etch rates in thin film etching and under-etching of microstructures: I. Modelling," *Journal of Micromechanics and Microengineering*, vol. 20, no. 5, 2010, ISSN: 09601317. DOI: 10.1088/0960-1317/20/5/055033.

[91] J. I. Goldstein, D. E. Newbury, J. R. Michael, N. W. M. Ritchie, J. H. J. Scott, and D. C. Joy, *Scanning Electron Microscopy and X-Ray Microanalysis*, 4th Editio. Springer Science and Business Media, 2018, pp. 209–234, ISBN: 9781493966745. DOI: 10.1007/978-1-4684-2046-3_11.

[92] R. C. Hefty, J. R. Holt, M. R. Tate, and S. T. Ceyer, "Mechanism and dynamics of the reaction of XeF_2 with fluorinated Si(100): Possible role of gas phase dissociation of a surface reaction product in plasmaless etching," *Journal of Chemical Physics*, vol. 130, no. 16, 2009, ISSN: 00219606. DOI: 10.1063/1.3118629.

[93] K. R. Williams, K. Gupta, and M. Wasilik, "Etch rates for micromachining processing - Part II," *Journal of Microelectromechanical Systems*, 2003, ISSN: 10577157. DOI: 10.1109/JMEMS.2003.820936. arXiv: arXiv:1011.1669v3.

[94] R. Chow, W. A. Lanford, W. Ke-Ming, and R. S. Rosler, "Hydrogen content of a variety of plasma-deposited silicon nitrides," *Journal of Applied Physics*, vol. 53, no. 8, pp. 5630–5633, 1982, ISSN: 00218979. DOI: 10.1063/1.331445.

[95] E Van de Ven, T. Shankoff, and R. Heinecke, "Gas etching of dielectrics and metals," Std. Telecom Lab. ltD, Harlow, Essex, Tech. Rep., 1973.

[96] R. Maddox, "Applications of reactive plasma practical microelectronic processing systems," *Solid State Technology*, vol. 21, no. 4, p. 107, 1978.

[97] A. Jacob, "The Versatile Technique of RF Plasma Etching Part III: Mechanistic Consideration for Selective Etching," *Solid State Technology*, vol. 21, no. 4, pp. 95–98, 1978.

[98] D. L. Flamm, C. J. Mogab, and E. R. Sklaver, "Reaction of fluorine atoms with SiO2," *Journal of Applied Physics*, vol. 50, no. 10, pp. 6211–6213, 1979, ISSN: 00218979. DOI: 10.1063/1.325755.

[99] C. Cardinaud, "Fluorine-based plasmas: Main features and application in micro- and nanotechnology and in surface treatment," *Comptes Rendus Chimie*, vol. 21, no. 8, pp. 723–739, 2018, ISSN: 16310748. DOI: 10.1016/j.crci.2018.01.009. [Online]. Available: https://doi.org/10.1016/j.crci.2018.01.009.

[100] D. L. Flamm and V. M. Donnelly, "The design of plasma etchants," *Plasma Chemistry and Plasma Processing*, vol. 1, no. 4, pp. 317–363, 1981, ISSN: 02724324. DOI: 10.1007/BF00565992.

[101] R. P. Chang, C. C. Chang, and S. Darack, "Hydrogen Plasma Etching of Semiconductors and Their Oxides.," *Journal of vacuum science technology*, vol. 20, no. 1, pp. 45–50, 1982, ISSN: 00225355. DOI: 10.1116/1.571307.

[102] W. A. Alexander, *Chapter 8 - Particle Beam Scattering From the Vacuumn-dash;Liquid Interface*. Elsevier Inc., 2018, pp. 195–243, ISBN: 9780128136416. DOI: 10.1016/B978-0-12-813641-6.00008-X. [Online]. Available: http://dx.doi.org/10.1016/B978-0-12-813641-6.00008-X.

[103] K. T. Lee and S. Raghavan, "Etch Rate of Silicon and Silicon Dioxide in Ammonia-Peroxide Solutions Measured by Quartz Crystal Microbalance Technique," *Electrochemical and Solid-State Letters*, vol. 2, no. 2-4, pp. 172–174, 1999, ISSN: 10990062. DOI: 10.1149/1.1390773.

[104] C. R. Helms and B. E. Deal, "Mechanisms of the HF / H_2O vapor phase etching of SiO_2," *Journal of Vacuum Science Technology A*, vol. 806, no. 1992, 2014. DOI: 10.1116/1.577676.

[105] The editors of the encyclopedia Britanica, *Vapour Pressure*, 2020. [Online]. Available: https://www.britannica.com/science/vapor-pressure (visited on 03/31/2021).

[106] P. A. Munter, O. T. Aepli, and R. A. Kossarz, "Partial Pressure Measurements on the System Hydrogen Fluoride–Water," *Industrial Engineering Chemistry*, vol. 41, no. 7, pp. 1504–1508, 1949, ISSN: 0019-7866. DOI: 10.1021/ie50475a051.

[107] J. Liu, Y. C. Tai, J. Lee, K. C. Pong, Y. Zohar, and C. M. Ho, "In situ monitoring and universal modelling of sacrificial PSG etching using hydrofluoric acid," *IEEE Micro Electro Mechanical Systems*, pp. 71–76, 1993. DOI: 10.1109/memsys.1993.296954.

[108] G. Spierings, "Review Wet chemical etching of silicate glasses in hydrofluoric acid based solutions," *Journal of Material Science*, vol. 28, pp. 6261–6273, 1993. DOI: 10.1007/BF01352182.

[109] C. C. Mai, "Thermal Growth and Chemical Etching of Silicon Dioxide Films," Ph.D. dissertation, 1964, ISBN: 5358210000330.

Appendix A: Conference Publication

Conference: 33th International Conference on Microelectronic Test Structures
Year: 2020
Title: Test Structure for Measuring the Selectivity in Vapour Etch Processes **Authors**: Markus Rondé, Anthony J. Walton, Jonathan G. Terry
Declaration: The test structure design and development, as well as the characterisation experiments presented in this publication were conducted by Markus Rondé. The text and figures were prepared by Markus Rondé. Jonathan Terry supervised the project and both he and Anthony Walton reviewed the manuscript and provided suggestions to improve it.

2020 INTERNATIONAL CONFERENCE ON MICROELECTRONIC TEST STRUCTURES, April 6-9, EDINBURGH, UNITED KINGDOM 6.4

Test Structure for Measuring the Selectivity in Vapour Etch Processes

Markus Rondé, Anthony J. Walton, Jonathan G. Terry
School of Engineering, Institute for Integrated Micro and Nano Systems,
The University of Edinburgh, EH9 3FF, UK
Email: markus ronde@ed ac uk

Abstract— **Etch selectivity between layers is critical in the fabrication of microelectronics and microsystems. This is particularly true in the case of isotropic gas/vapour etching methods used to release free standing structures through the selective etching of sacrificial layers. Commonly used structural materials have been reported to be largely inert when exposed to a given vapour etchant, indicating high selectivity when measured against typical sacrificial layers. However, there is growing evidence that these structural layers are actually etched at an enhanced rate if they are located in the proximity of the sacrificial layer being removed. Hence, removal rates given in the literature that have resulted from measurements of layers that have been etched in isolation can no longer be trusted to characterize critical etch processes in device fabrication. In this paper, a test structure is reported that enables a far more accurate determination of the etch selectivity between sacrificial and structural materials. The method is demonstrated by a XeF_2 vapour etch of a polysilicon sacrificial layer located above a silicon nitride structural layer. A dataset is presented for the polysilicon and silicon nitride layers, which shows a selectivity of 5:4.**

I INTRODUCTION

Etching sacrificial layers to release free standing structures is a critical process step in the fabrication of micro and nano-electromechanical systems (MEMS/NEMS) Historically, sacrificial layers such as silicon (Si) or silicon dioxide (SiO_2) were removed using wet etch processes However, the commercial advantages and novel scientific possibilities inherent with smaller sensors and actuators has fueled a trend towards miniaturization In the micro and nanoscale, the high surface to volume ratios may cause stiction resulting in the adherence of the released structures to the surface underlying the sacrificial layer Stiction results from surface tension during the drying of the liquid etchant [1] and can be avoided by the use of a gas/vapour phase etchant Vapour etching of silicon dioxide and silicon by hydrogen fluoride (HF) and xenon difluoride (XeF_2) respectively are now commonly used release processes in industry In most applications of sacrificial vapour phase etch processes, the structural layers of a device being fabricated are in close proximity to the sacrificial materials being removed It has been observed, that a structural material, which is not significantly affected when introduced to the vapour etch in isolation, can be severely attacked when in the proximity of a sacrificial material [2][3] In this situation, determining the etch selectivity between the materials is non-trivial and requires a measurement method that can quantify the undercut etch rates of two materials on a single die when isotropically etched in close proximity to one another This paper presents a test structure that has been developed for this purpose, as well as the results of experiments to determine the etch selectivity between a structural plasma enhanced chemical vapour deposited (PECVD) silicon nitride layer and a low pressure chemical vapour deposited (LPCVD) sacrificial polysilicon layer being processed in a xenon difluoride vapour etch tool The following sections briefly explain the measurement method, elaborating on the layout and the design The interpretation of the resulting surface profile is then discussed with the presentation of

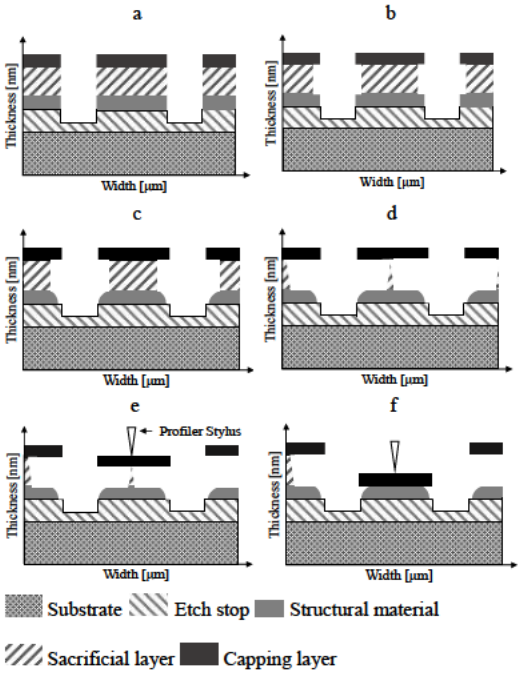

Fig 1 Schematic of the bridge array methodology a shows the test structure before etching b-c show the etch initiation on the sacrificial and structural material respectively d - f show the test structure with increasing etch times

978-1-7281-4008-7/20/$31 00 ©2020 IEEE

evidence verifying the method Finally a review of the test structures performance in practical use is given based on a dataset obtained during experiments

II MEASUREMENT METHOD

The test procedure measures the mechanical displacement of an array of etch-released free-standing bridge structures The width of the bridge structures in the array is incrementally increased in a similar manner to [3] and [4], which uses cantilevers to measure etch rates Following an etch release process, a profilometer is scanned across the array of bridges and, if release has been achieved, the down force of the stylus vertically displaces the bridges, with the vertical displacement set by the thickness of etched material The width of the widest bridge structure that has been displaced by the thickness of the sacrificial layer is equal to twice the undercut distance This undercut distance and the etch time can then be used to determine the apparent etch rate The structural material is the layer below the sacrificial material and the etch rate of this second material can be obtained in a similar manner, from the widest bridge that is displaced by the height of both the sacrificial and the structural layers Figure 1 shows a schematic cross-section of one of the bridges being gradually etched and the stylus displacing the bridge during the measurement

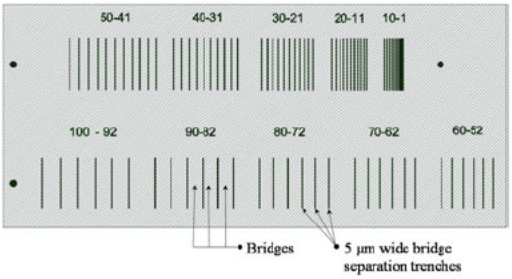

Fig 2 Design layout of the test structure showing the 5 x 300 µm trenches Each section is labelled with the bridge width The trenches are the dark lines and the separation gradually decrease by 1 µm at the top row and 2 µm at the bottom array

III TEST STRUCTURE DESIGN

A. Layout

The test structure is formed of a stack of deposited thin films, comprising a structural layer, a sacrificial layer and finally a capping layer The example structure reported here uses a PECVD silicon nitride structural layer in combination with a LPCVD polysilicon sacrificial layer These are capped by a layer of aluminium that is unaffected by the vapour etch Trenches are etched in the layer stack using a reactive ion etch, which defines the bridge structures and exposes the layer edges to the vapour etch process As part of the design the bridge width is incrementally reduced and the layout is shown in figure 2 For measurements of large undercuts the bridge width decreases from 100 to 52 µm in increments of 2 µm Narrower bridges are defined with widths from 50 to 2 µm in increments of 1 µm

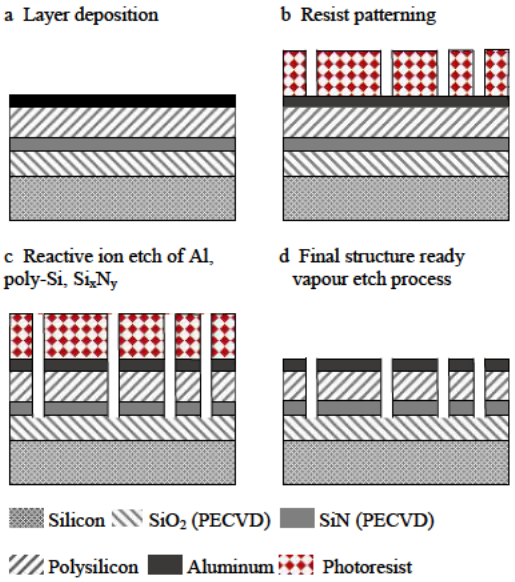

Fig 3 Schematic process flow of the fabrication of the vapour etch selectivity test structure

The bridge structure has a number of advantages over alternative architectures It is less prone to stiction issues during testing, it enables a 1D etch front propagation and it gives less noisy deflection measurements compared with other designs such as the cantilever structures of [3] The maximum bridge length of 300 µm reduces the wafer real estate required by the test structure, while the layer thicknesses between 200-500 nm can withstand the vertical and horizontal displacement during measurement For the initial investigation bridges with lengths of 100 µm, 200 µm and 300 µm were employed The measured etch undercuts and selectivities were found to be independent of the bridge length However, the alignment of the shorter test structures for the automated profilometer measurement of multiple test structures becomes very time-consuming The 5 µm trench width enables the tip of the profilometer stylus to measure the full depth of the trenches and simplifies the photolithography

B. Layer Configuration

The test structure can be used to measure the selectivity of various materials in close proximity For example, figure 3 shows the fabrication process flow for a test structure used to determine the etch selectivity of polycrystalline silicon versus silicon nitride in XeF_2 vapour etching The structural layer is placed below the sacrificial layer, which allows the etch rates of the two materials to be determined with a single surface profilometry measurement In this example, the 500 nm thick silicon dioxide etch stop layer and the 210 nm thick silicon

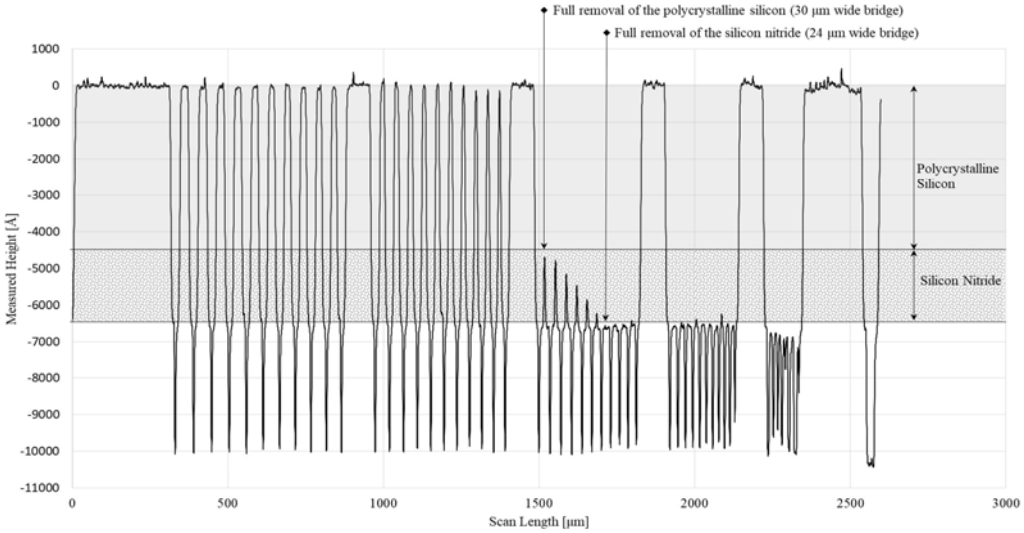

Fig 4 Surface profile retrieved after vapour etching the test structure The thicknesses of the polycrystalline silicon and silicon nitride layers are represented by the different underlyings of the graph

nitride structural layer were deposited using plasma enhanced chemical vapour deposition (PECVD) at low and high frequencies respectively Silicon dioxide was selected as an etch stop because it is largely unaffected by the XeF_2 vapour etch process while remaining stable at high temperatures If the etchant used attacks silicon dioxide, a 50 nm thick platinum layer can be used as an alternative etch stop The 450 nm thick sacrificial layer of polycrystalline silicon and 350 nm thick capping layer of aluminum were deposited using LPCVD and sputter deposition respectively Aluminum was employed as the capping layer, because it is not attacked by the XeF_2 vapour process, can be sputter deposited and reactive ion etched while its mechanical properties prevent fracture of the bridges during the profilometer measurement Aluminum is not recommended as first choice capping layer for hydrogen fluoride vapour etching, because it fluorinates and the resulting particulates on the sample create noise during the measurement A contact mask aligner was used to transfer the pattern from a chromium photomask into a 3 µm thick layer of photoresist (SPR 220 – 3 0) which was subsequently developed for 1 minute in MF-26 The trenches in the aluminum, polycrystalline silicon, and the silicon nitride layer stacks were anisotropically etched by reactive ion etching After the resist was removed, the organic residues were cleaned from the wafer in an oxygen plasma and the wafer was diced into 90 chips with an edge length of 11 x 5 5 mm

IV INTERPRETING THE SURFACE PROFILE

After the test structures have been scanned by the profilometer the resulting surface profile is used to obtain the undercut for the sacrificial and the structural layer The measurement reading procedure is explained on the basis of test structures that were exposed to a xenon difluoride vapour for 40 seconds at a process pressure of 9 Torr, with a nitrogen carrier gas flow of 100 sccm, at a temperature of 30°C

The resulting surface profile is displayed in figure 4 For these particular process parameters, the 30 µm wide bridge was the widest one that has been vertically deflected by more than 450 nm (the thickness of the polysilicon) indicating the sacrificial material has been fully etched The resulting undercut is 15 µm with an apparent etch rate of 375 nm s^{-1} The 24 µm wide bridge has deflected by 650 nm (the combined thickness of the polysilicon and silicon nitride layers), indicating the structural layer of silicon nitride has also been fully etched with an apparent etch rate of 300 nm s^{-1} This suggests an etch selectivity between the polysilicon and silicon nitride layers of 5:4 Depending on the output format of the profilometer used, programming can be used to automatically extract the undercut data from the surface profile

V MEASUREMENT VERFICIATION

The test structure measurements were verified using two different methods Firstly, five samples from a larger pool of chips, that were etched and measured during the process calibration, were randomly selected and the capping aluminum layer removed Energy-dispersive X-Ray spectroscopy (EDX) was used to determine if the silicon nitride was removed at the bridge width indicated by the surface profilometry In all cases, the EDX measurement agreed with the results of the surface profile Secondly, cross sectional SEM images of etched structures confirmed that the polycrystalline silicon and silicon nitride were removed at the bridge, indicated by the test structure Figure 5a shows the 31 µm wide bridge being supported by a thin pillar of sacrificial polysilicon Figure 5b

shows the 28 µm wide bridge of the same test structure, the sacrificial layer has been fully removed and the aluminum bridge is suspended above the silicon nitride layer

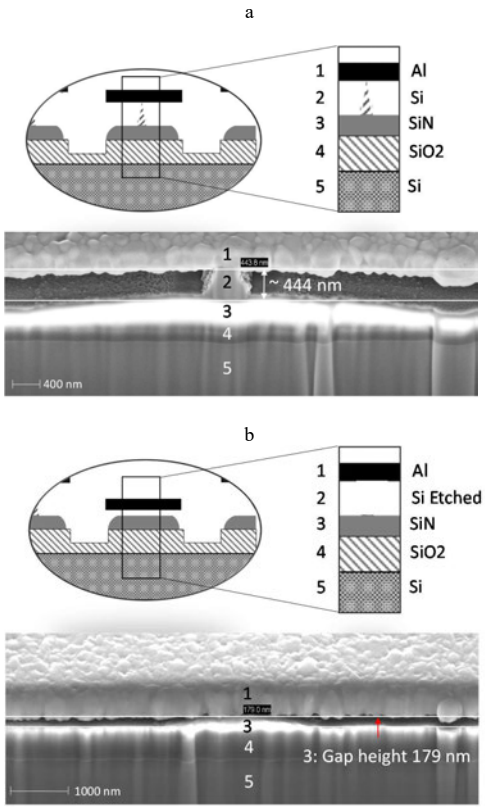

Fig 5 Scattering electron microscope (SEM) images of focus ion beam (FIB) cut crossesctions of a the centre of the 31 µm wide bridge The polycrystalline silicon pillar has not been fully removed yet and prevents deflection of the bridge during profiling b The polycrystalline silicon layer of the 28 µm wide bridge has been fully etched The bridge has deflected and is supported by the remaining silicon nitride

VI Result and Discussion

A. Experimental Result

A series of etch experiments was undertaken on a XeF_2 vapour etch tool, to characterize the performance of the test structures The tool operates in a continuous flow configuration, constantly supplying the xenon difluoride to the etch chamber It has the capability to change the processing pressure, chamber temperature and allows additional supply gasses to be introduced into the etch chamber The nitrogen carrier gas flows through a bubbler, introducing the xenon difluoride into the chamber The xenon difluoride concentration within the etch chamber is inversed proportional to the carrier gas flow An excerpt of a larger dataset is displayed in figure 6, with each of the 12 data points representing a sample They were etched at different process pressures, carrier gas flows and etch times at a constant temperature of 25°C Eight test structures were measured on each sample The average measurement and the etch parameters used are presented in figure 6 and the error bars indicate the standard deviation of each dataset The data is consistent and shows a polycrystalline silicon to silicon nitride selectivity of 5:4 Furthermore, it shows that the selectivity is independent of the processing pressure, xenon difluoride concentration and etch time The reasons for this and methods to significantly improve the selectivity are currently being researched by the authors

B. Performance

A total of 56 chips with 8 test structures per chip, were vapour etched in a XeF_2 atmosphere at different conditions to characterize the resulting variance in the etch undercuts of the structures on each sample The maximum polysilicon and silicon nitride undercut standard deviations were 1 96 µm (mean 27 86 µm) and 2 2 µm (mean 28 5 µm) respectively The population standard deviations and the yield of successful measurements are displayed in table 1 The performance can be significantly improved, by adopting the design and measurement considerations presented in the next section into account

TABLE I Performance of tests structure

	Polysilicon	**SiN**
Number of attempted measurement	448	448
Number of successful measurements	426	350
Successful measurement in [%]	95	75
Population Standard Deviation σ [µm]	0 4	0 37

C. Test Structure Measurement Consideration

The authors observed five modes that can cause a faulty or incomplete measurement Firstly, it is important to carefully define the etch time to prevent both over and under etching In this example, over etching would occur once the 100 µm wide (widest) bridge is released, because in that case the maximum undercut cannot be determined Similarly, no measurement can be obtained, if twice the undercut is less than the width of the narrowest bridge If a fixed etch time is required, this problem can be overcome by adjusting the test structure design

The three remaining measurement issues are caused by suboptimal surface profiler settings Firstly, mechanical destruction of the bridges can occur if the downforce of the surface profiler's stylus is too high In consequence, the bridges are ripped from their anchoring, adhere to the stylus and contaminate the tool Secondly, the stylus bounces off the bridges if the downward force is too low This leads to a perturbed signal that resembles a positive bridge deflection up to 10 micrometers A down force of 2 – 3 mg yielded the best results for the samples presented in this study

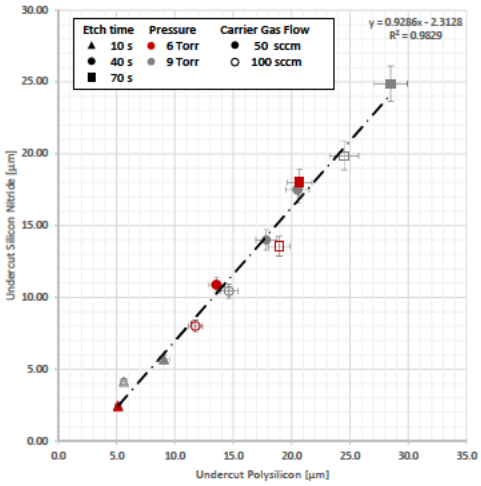

Fig 6 This example dataset presents the selectivity between polysilicon and PECVD silicon nitride It is based on 12 samples with the layer configuration and design presented in section III The etch parametes can be derived from the indivdual markers design

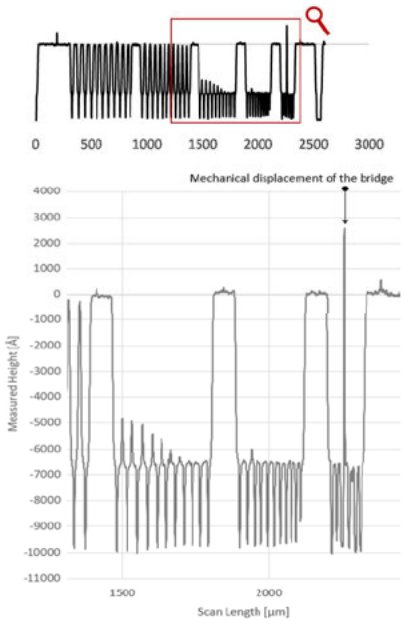

Fig 7 This surface profile was obtained from the same sample as figure 4's The signal is imprecise due to a horizontal displacement of a 8 µm wide bridge caused by a too high scan speed

The final issue is identified in figure 7, resulting from a mechanical deflection of a narrow bridge caused by too high a scan speed The exact origin of this fault is unclear It was only observed on bridges that were narrower than 10 µm at scan speeds higher than 40 µm s^{-1} Hence it can be easily avoided by reducing the scan speeds for samples were the accurate measurement of this segment of the test structure is essential

VII CONCLUSIONS

This paper has reported for the first time a bridge based test structure that can characterize the isotropic etch selectivity between two materials under realistic MEMS fabrication conditions The test structure is designed to be used in vapour etch processes but can also be adapted for wet etch release processes It can be employed to characterize a wide range of materials with the fabrication of the test structure being quick and straightforward

The measurement methodology has been demonstrated using an example stack of layer materials, which may not be those that would be used in a commercial process, but that provide an experimental dataset that clearly shows that these test structures deliver coherent measurement information The design can be employed in industrial MEMS fabrication processes, with the area required being small enough to be placed on production wafers The test structure can be easily adapted to accommodate different dimensional requirements Individual test structure arrays can be measured within 15 seconds and the measurement process can be easily automated

ACKNOWLEGEMENT

Markus Rondé's work was supported by the EPSRC CDT in Intelligent Sensing and Measurement Grant Number EP/L016753/1 and the CENSIS Studentship Award programme

DATASHARE

The data presented in this work is available online at https://doi org/10 7488/ds/2763

REFERENCES

[1] N Tas, T Sonnenberg, H Jansen, R Legtenberg, and M Elwenspoek, "Stiction in surface micromachining," *J. Micromech. Microeng*, vol 6, pp 385–397, 1996

[2] J F Veyan, M D Halls, S Rangan, D Aureau, X M Yan, and Y J Chabal, "XeF2-induced removal of SiO2near Si surfaces at 300 K: An unexpected proximity effect ," *J. Appl. Phys.*, vol 108, no 11, 2010

[3] G Van Barel, Bert du Bois, Rita Van Hoof, Jef De Wachter, Ward De Ceuninck, and A Witvrouw "Apparent and steady-state etch rates in thin film etching and under-etching of microstructures: II Characterisation," *J. Micromechanics Microengineering*, vol 20, no 5, 2010

[4] G Van Barel, L Mertens, W De Ceuninck, and A Witvrouw, "Apparent and steady-state etch rates in thin film etching and under-etching of microstructures: I Modelling," *J. Micromechanics Microengineering*, vol 20, no 5, 2010

Appendix B: First Peer Reviewed Journal Publication

Journal: JOURNAL OF MICROELECTROMECHANICAL SYSTEMS, VOL. 30, NO. 1
Year: 2021
Title: Manipulating Etch Selectivities in XeF_2 Vapour Etching
Authors: Markus Rondé, Anthony J. Walton, Jonathan G. Terry
Declaration: The study presented in this publication was designed, conducted and analysed by Markus Rondé. The text and figures were prepared by Markus Rondé. Jonathan Terry supervised the project and both he and Anthony Walton reviewed the manuscript and provided suggestions to improve it.

156 JOURNAL OF MICROELECTROMECHANICAL SYSTEMS, VOL. 30, NO. 1, FEBRUARY 2021

Manipulating Etch Selectivities in XeF_2 Vapour Etching

Markus Rondé, *Member, IEEE*, Anthony J. Walton, *Senior Member, IEEE*, and Jonathan G. Terry, *Senior Member, IEEE*

***Abstract*— The vapour etching of silicon sacrificial layers is often a critical process in the fabrication of micro/nanosystems. This method has a number of attractive features, in particular, high etch rates of sacrificial silicon layers and good selectivities associated with photoresist, SiO_2, stoichiometric Si_3N_4 and a number of regularly used metal films. However, materials that are commonly inert to XeF_2 are etched when located in the proximity of a silicon sacrificial layer. This proximity is a common situation in the fabrication of such systems and can become a critical issue affecting process control and device reliability. This work uses test structures that have been designed to be very sensitive, thereby delivering much lower selectivities then are typically reported in the literature. This sensitive quantification of the proximity effect is used to evaluate methods designed to improve the selectivity. This work suggests that a reduction in the processing temperature from 25°C to 10°C increases the Si: PECVD SiN selectivity by 68%. However, a more easily implemented modification is to flow hydrogen into the reaction chamber. This method improves the Si: PECVD SiN selectivity by an order of magnitude and the Si: LPCVD SiN selectivity between 200% and 600%. [2020-0346]**

***Index Terms*— Vapour etching, XeF_2, selectivity, proximity effect.**

I. Introduction

THE etching of sacrificial silicon with XeF_2 vapour in order to release free-standing structures in micro- and nanosystems has a number of benefits. High undercut etch rates of up to 40 μm/min have been achieved [1]. Stiction [2] [3] does not occur during processing, and high selectivities towards photoresist, silicon dioxide (SiO_2), stoichiometric, low pressure chemical vapour deposited silicon nitride (LPCVD Si_3N_4), silicon carbide (SiC), aluminum and plasma enhance chemical vapour deposited silicon nitride (PECVD Si:N:H) have been reported [4]–[8]. However, there is a growing body of evidence that some of these selectivities are significantly reduced if these layers are positioned in the proximity of the sacrificial silicon layer [9] [10], [11] (referred to as the 'proximity effect'). This issue can complicate the fabrication and design process of MEMS significantly, inhibiting the development of devices and reducing yields and process reliability. The following work investigates the impact of the proximity effect on the etch rates of a range of commonly used materials, and investigates methods than can be applied to improve their selectivity.

Veyan *et al.* [9] were the first to observe the rapid proximity etching of SiO_2. The authors of this current work reported silicon to PECVD silicon nitride selectivities as low as 5:4 [10]. Research conducted by Hefty *et al.* [12]–[14], suggests that a fluorine radical of the XeF_2 molecule is removed at a dangling bond of the silicon surface. The remaining XeF molecule remains in the gas phase. It can either lose the remaining fluorine on another dangling bond or disintegrate forming both a xenon and a fluorine radical. This highly reactive fluorine radical might collide with either the silicon or a material in its vicinity. During sacrificial etching, the probability of collision with the other material increases, because the reactive fluorine radicals are trapped underneath the structural layer. The conclusion is that any material that can be etched by fluorine radicals is prone to attack when in proximity to the silicon sacrificial layer. This hypothesis is evaluated in this work by proximity etching a number of materials commonly used in MEMS devices, which are known to be etched by fluorine. PECVD SiO_2, LPCVD Si_3N_4 and PECVD SiN (Si:N:H) were selected because the fluorine etch mechanisms involved have been extensively researched in the context of plasma etching.

To investigate improvements in the etch selectivity, four general mechanisms known to change etch selectivities have been identified from the broader literature:

1) The Arrhenius equations suggest that adjusting the temperature may have a greater effect on the reaction rate of one material than that of another [15]–[17], [18]. In the case of XeF_2 etching of Si, it has been observed that the etch rate dependence on temperature follows a "U-curve". The highest reaction rate occurs at 150 K, below which the XeF_2 condenses on the surface. The rate gradually decreases to 20% of the maximum etch rate as the temperatures rise from 150 to 400 K. Beyond this low point at 400 K, the reaction rate increases again with rising temperature. The experiment was conducted at a pressure of 10^{-8} Torr [19].

2) In some cases, the addition of gases can passivate the surface of otherwise reactive materials, making them inert to the etchant [20] [21].

3) In other cases, the addition of gases can alter the products of the etch. For example, hydrogen additions have

Manuscript received October 12, 2020; revised December 1, 2020; accepted December 5, 2020. Date of publication December 21, 2020; date of current version January 15, 2021. This work was supported in part by Engineering and Physics Research Council (UK) (EPSRC) Center of Doctoral Training (CDT) in Sensing and Measurement under Grant EP/L016753/1 and in part by CENSIS Studentship Award Programme. Subject Editor R. T. Howe. *(Corresponding author: Markus Rondé.)*

The authors are with the Institute of Integrated Micro and Nano Systems, School of Engineering, University of Edinburg, Edinburgh EH9 3FF, U.K. (e-mail: markus.ronde@ed.ac.uk).

Color versions of one or more figures in this article are available at https://doi.org/10.1109/JMEMS.2020.3044688.

Digital Object Identifier 10.1109/JMEMS.2020.3044688

been reported to significantly improve the selectivity of fluorine-based etch processes [22], [23].

(4) Sugano *et al.* [24] observed that the selectivity of Si: Si_3N_4 and Si: SiO_2 decreases from 488:1 to 29:1 and from 5287:1 to 281:1 respectively if the samples are exposed to 3 Wcm^{-2} of UV light at a wavelength of 310 – 340 nm. Another study by Streller *et al.* [25] suggested that XeF_2 dissociates into XeF and F if excited by ultraviolet light with short wavelength (<150 nm).

This paper focuses on the first and the third of these four mechanisms, the adjustment of the processing temperature and the addition of gases. Firstly, the equipment, test structures and measurement method used during this experiment are detailed, after which the results from the XeF_2 vapour etching proximity effect characterization are presented and discussed. Various samples with SiO_2, LPCVD Si_3N_4 and PECVD SiN structural (target) layers were etched at pressures of 3 – 9 Torr, XeF_2 gas flows of 15 – 35 sccm and temperatures 5°C - 45°C. The impact on the selectivities, when adding hydrogen to the gas mix, is also presented.

II. Equipment, Test Structure and Method

A commercial memsstar Alpha Orbis XeF_2 etch tool was used in this work. In contrast to most of the previously published research on XeF_2 etching, the memsstar tool continuously supplies XeF_2 to the reaction chamber (rather than in pulses), In addition the processing pressures are comparatively high (up to 10 Torr). The chamber temperature is controllable and can be adjusted to values between 3°C and 45 °C in increments of 0.1°C. Nitrogen is used as a carrier gas to transport the XeF_2 into the reaction chamber, and additional gases can be added to the mix.

A customized test structure and measurement method were developed for this experiment. A detailed description of the design, fabrication procedure and measurement method, as well as a thorough characterization, have been previously presented [10]. The test structures were designed to measure the selectivity between a target layer and a sacrificial layer. It should be stressed that the selectivities measured are specific to the layout and architecture of the test structures, which have been specifically designed to ensure very close proximity of the materials being evaluated. As a result, the selectivity values measured using the test structures may be significantly poorer than those quoted elsewhere.

The test structure consists of an array of aluminum bridges that are suspended above the sacrificial layer, which in turn sits above the target layer. In these experiments, the target layer was either silicon nitride or silicon dioxide. In this case, the width of the bridges increases in increments of 1 μm in the width range between 2 μm and 50 μm and in increments of 2 μm for the 50 μm to 100 μm wide bridges. These values are sufficient to measure etch selectivties at a range from 1.5:1 to 50: 1 with an undercut resolution of 500 nm.. All bridges are 300 μm long. In a previous study, the selectivities were found to be independent of the bridge length. The 300 μm long bridges are a trade-off between the requirement to minimize the real estate required by the test

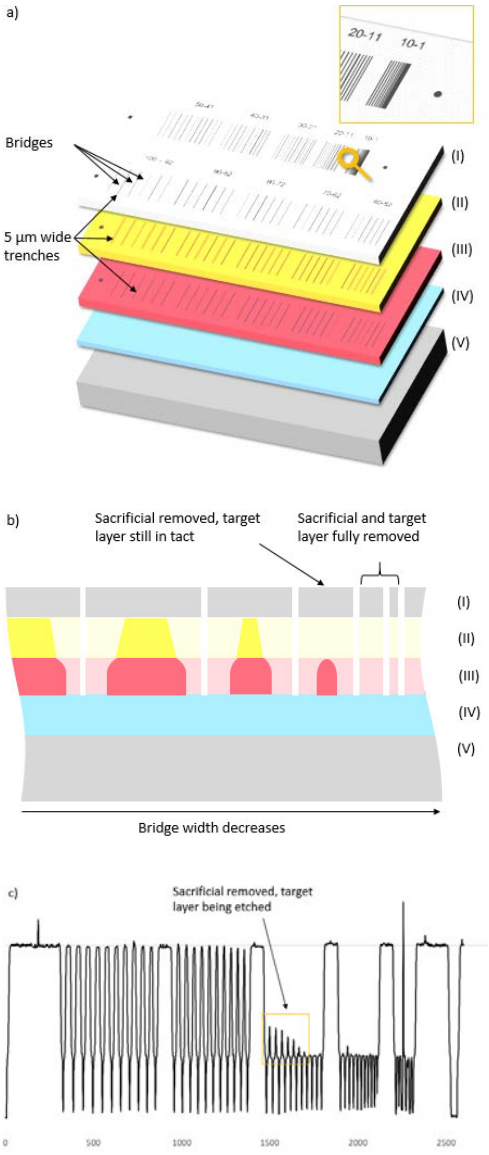

Fig. 1. Graphic depiction of the functionality of the test structure. Showing the layout in a) and a cross-section of a partially etched structure in b); where (I) is the capping, (II) the sacrificial, (III) the target, and (IV) the etch stop layer; (V) represents the substrate. c) Shows an example surface profiler from an etched array.

structure on a production wafer and the requirement to align the samples on a surface profiler for the measurement [10]. For reference, the layout and the cross section of a partially etched test structure are displayed in Fig. 1 a). and b). The wafer

TABLE I
LAYER CONFIGURATION OF THE SAMPLES USED

Layer Description	SiN-Reference	SiN-PECVD	SiN-LPCVD	SiO_2-Reference	SiO_2-PECVD
Capping Layer	350 nm Aluminium	350 nm Aluminium	350 nm Aluminium	350 nm Aluminium	350 nm Aluminium
Sacrificial Layer	-	500 nm Polysilicon	500 nm Polysilicon	-	500 nm Polysilicon
Target Layer	450 nm PECVD SiN	450 nm PECVD SiN	500 nm LPCVD Si_3N_4	500 nm PECVD SiO_2	500 nm PECVD SiO_2
Etch Stop	50 nm Platnium	50 nm Platnium	500 nm SiO_2	50 nm Platnium	50 nm Platnium
Adhesion Layer	10 nm Ti	10 nm Ti	-	10 nm Ti	10 nm Ti
Wafer	Silicon	Silicon	Silicon	Silicon	Silicon

with the test structures was diced into chips 11 mm long and 5 mm wide. Each chip contained 8 test structure arrays. The sacrificial layer was etched using varying process parameters for each chip. After the release, the bridge array was scanned by a surface profiler. During the measurement, the bridges where the sacrificial layer has been etched were deflected by the height of the sacrificial layer. If the target layer (SiO_2 or SiN) has also been removed, the total deflection of the bridge is the height of the sacrificial and the target layer. If the bridge has not been fully released, the extent of etching is still revealed by the deflection of the bridge. The etch undercut of the sacrificial layer is equal to half of the width of the widest bridge deflected by the height of the sacrificial layer. The etch undercut of the target layer is obtained similarly. It is half of the widest bridge deflected by the height of both the target and the sacrificial layer. An example of the resulting surface profile is presented in Fig. 1 c), it shows the signal that would result from the partially etched structure depicted in the cross-section of Fig. 1 b). The accuracy of this measurement was previously verified by imaging the cross sections of five randomly selected samples [10]. In all cases, the cross sectional images were in full agreement with the surface profile.

In total, five 100 mm diameter wafers were prepared with different layer configurations of materials available to the authors, diced into chips and used for this experiment. For reference, the layer compositions are detailed in table I. For example, two samples were prepared for silicon dioxide measurements. The first was a reference sample, with a 500 nm thick layer of PECVD silicon dioxide and no sacrificial layer, denoted *SiO_2-Reference*. The second sample also has a 500 nm thick PECVD SiO_2 layer, this time covered by a 500 nm thick polysilicon sacrificial layer, denoted *SiO_2-PECVD*. A 50 nm thick platinum layer with a 10 nm thick titanium adhesion layer was used as an etch stop for both samples.

A 350 nm thick aluminium layer was sputter deposited on to all the samples. After photolithographic patterning of the layout displayed in Fig. 1 a), the aluminium and the polysilicon sacrificial layer were reactive ion etched (RIE). The exposed SiN and SiO_2 were also patterned using RIE in order to provide the vapour etch access to the layered stack to be etched. After resist removal, the wafers were cleaned in an oxygen plasma and diced.

III. EXPERIMENT

Before starting an experimental session, the vapour etch tool chamber was vented, and a standard etch process was run on an empty chamber. Then, another tool-specific calibration run was performed to determine the gas flows. After the temperature of the pedestal was adjusted to the desired value, the chamber was vented, and the sample loaded. At this point the etch recipe was programmed, and the etch process started. The tool enables control of the pressure, carrier gas flow and etch time with reactants flowing into the reaction chamber continuously.

The chamber pressure and the carrier gas flow vary by less than 0.5 % during processing. The amount of XeF_2 carried into the chamber, however, depends on the amount of solid XeF_2 within the bubbler. It slowly decreases over the long term (10 – 20 of hours of etch time). It also decreases when running etch processes in rapid succession. It then recovers again after a break of roughly one hour. This must be taken into account when conducting more extensive experiments. The level of XeF_2 supplied to the chamber has a significant impact on the etch rate and is, therefore, the largest source of error. An external cooling and heating unit controls the pedestal temperature. When operating within the range of roughly 10 – 35 °C the temperature displayed on the external unit is equal to the measured temperature of the pedestal. For values outside this range, an additional measurement of the pedestal temperature was made for assurance. Undercut etching at the edges of the diced chips can be expected. While no silicon loading was observed in this experiment, it can occur if larger samples are processed, or if the XeF_2 concentration within the reaction chamber is lower. In that case, the loading effect can be reduced by covering the edges of the sample.

IV. RESULTS

Three variable process parameters typically define the vapour etch process, the chamber pressure, the etch time and the XeF_2 gas flow into the chamber. In this experiment, two additional parameters are considered, the chamber temperature and the flow of additional gases, specifically hydrogen. The experiment was conducted on chips from the five samples described above. The *SiN-Reference* and *SiO_2-Reference* samples could not be measured using the test structure because the etch rates were below the limit of detection. This observation is critical, as these benchmark samples suggest very high selectivities of SiO_2 and SiN towards XeF_2. However, the SiO_2, PECVD SiN and LPCVD Si_3N_4 layers etched when placed in proximity to the sacrificial layer. The following section describes the results of this proximity etching in more detail, and the observations are summarized in Table II.

A. Impact of the Etch Parameters on the Etch Rates

Fig. 2 shows that the removal of sacrificial polysilicon is linear over time with etch rates between 392 nm/s and 545 nm/s

TABLE II
THE EFFECT OF ADJUSTING THE ETCH PARAMETERS XeF_2 FLOW, PRESSURE AND TEMPERATURE ON THE ETCH RATE

Sample ID	*Material*	*Flow XeF_2*† [μm min^{-1} $sccm^{-1}$]	*Pressure* [μm min^{-1} $Torr^{-1}$]	*Temperature* [μm min^{-1} K^{-1}]
SiN-PECVD	Polysilicon	- 0.31	2.24	- 0.14
	PECVD SiN	- 0.44	2.56	0.15
SiN-LPCVD	Polysilicon	- 0.2	1.8	-0.156
	Si_3N_4	Constant	-0.13	Constant
SiO_2-PECVD	Polysilicon	- 2.6	1.97	-0.128
	SiO_2	Constant	-0.19	Constant

†pressure constant at 9 Torr

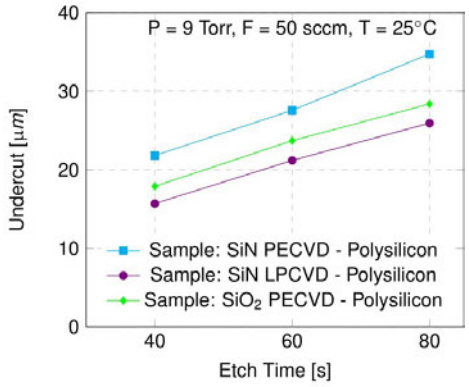

Fig. 2. Polysilicon etch undercut over time.

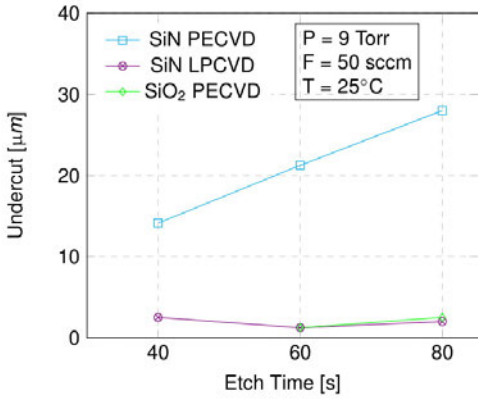

Fig. 3. The etch of the target materials as a function ot time.

being measured. The spread of the etch rates suggests that different etch by-products can affect the rate of polysilicon removal. It is possible that the proximity effect does not only affect the target material but also increases the etch rate of the sacrificial layer. From Fig. 3, it can be observed that the PECVD silicon nitride is etched at a rate of 347 nm/s, and follows the same linear trend.

In contrast, the undercuts for the LPCVD SiN and the PECVD SiO_2 appear to be independent of time. This can be explained by the etch halting once the fluorine radical generating materials in its proximity have been fully removed. The PECVD SiO_2 sample that was etched for 40 seconds could not be adequately measured and therefore, does not have a data point. Fig 4. presents three graphs, which show that the etch rate linearly decreases with increased XeF_2 flow. This seems counter-intuitive, but there are two possible explanations. Firstly, the XeF_2 is supplied through a bubbler, and the flow increase is achieved by increasing the carrier gas flow. The decline in the etch rate with increased XeF_2 flow, as displayed in Fig. 4, can be explained by the larger carrier gas flows required to supply the reactant. For instance, if 25 sccm of N_2 is used as the carrier gas, roughly 16 sccm XeF_2 are transported to the chamber. This corresponds to a ratio of around 3 to 2. However, if 100 sccm of N_2 was used as the carrier gas, roughly 36 sccm of XeF_2 flows into the chamber, corresponding to a ratio of around 3 to 1. This suggests that the XeF_2 partial pressure decreases with increasing carrier gas flow.

Secondly, the carrier gas flow determines the time it takes for the chamber to ramp up to the processing pressure, with lower flows resulting in longer ramp times. With XeF_2 etchant being supplied to the chamber during the ramp time, the effective etch time increases with lower gas flows. As this is not taken into account when calculating the etch rate, the apparent etch rate appears to be higher. The tool's in-built etch monitor measures the amount of silicon fluorine bonds in the reaction chamber and gave a response of 1491, 1072 and 790 counts for XeF_2 gas flows of 16.4 sccm, 24.8 sccm and 35.8 sccm respectively. This indicates a higher level of SiF_4 within the reaction chamber at lower XeF_2 flows. The PECVD silicon nitride and polysilicon etch rates also appear to be similarly affected by the gas flows. However, the LPCVD silicon nitride and the PECVD silicon dioxide etch rates are not observed to correlate in the same way.

The data presented in Fig. 5 show the effect that the processing pressure has on the removal of polysilicon and the respective target materials. The data indicates that there is a correlation between the processing pressure and etch rate. For polysilicon, it indicates, that increased processing pressure increases the etch rate. The same effect takes place with the PECVD silicon nitride. In contrast, the etch rate varies very

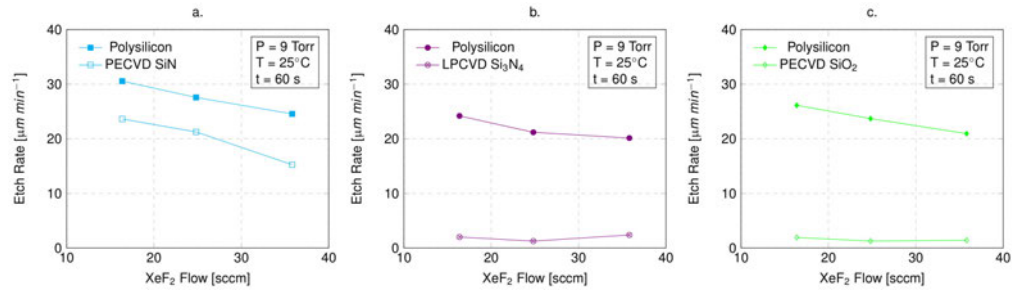

Fig. 4. The XeF_2 flow dependency of the etch rate at a pressure of 9 Torr, 25°C and an etch time of 60 seconds. a) polysilicon towards PECVD SiN b) Polysilicon towards LPCVD Si_3N_4 and c) polysilicon towards PECVD SiO_2.

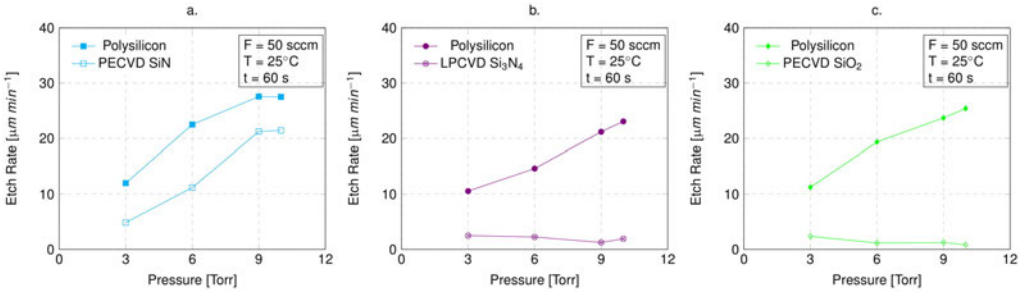

Fig. 5. The pressure dependency of the etch rate a) Polysilicon towards PECVD SiN b) Polysilicon towards LPCVD Si_3N_4 c) Polysilion towards PECVD SiO_2.

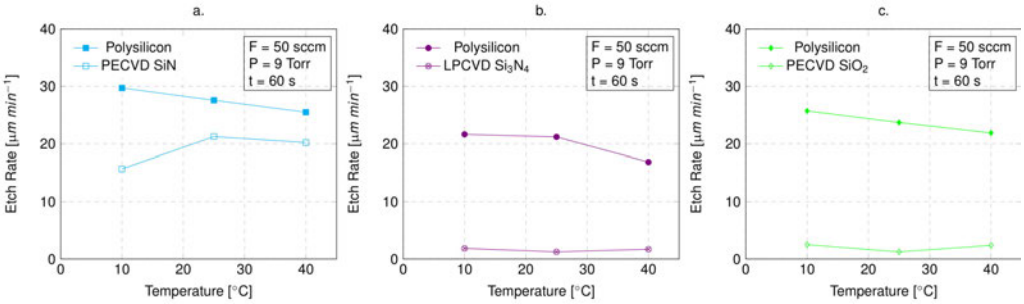

Fig. 6. The temperature dependency of the etch rate a) Polysilicon towards PECVD SiN b) Polysilicon towards LPCVD Si_3N_4 c) Polysilion towards PECVD SiO_2.

little with increased pressure for the LPCVD silicon nitride and the PECVD silicon dioxide.

The data presented in Fig. 6 indicates a temperature dependency of the etch rate of the polysilicon and the target PECVD SiN. The polysilicon etch rate linearly decreases with increasing temperature at a rate between 128-159 nm/min/°C. This temperature-dependent etch rate decrease was expected, as it has been reported before by Chang *et al.* [5] and Ibbotson *et al.* [18] and is coherent with theories developed by Flamm *et al.* [15] and Vugts *et al.* [19]. In contrast, the PECVD silicon nitride etch rate increases with increasing temperature with a rate of roughly 150 nm/min/°C. The etch rate of the LPCVD silicon nitride, and the PECVD silicon dioxide appears to be unaffected by the change in temperature.

The data presented in Fig. 6 indicates a temperature dependency of the etch rate of the polysilicon and the target PECVD SiN. The polysilicon etch rate linearly decreases with increasing temperature at a rate between 128-159 nm/min/°C.

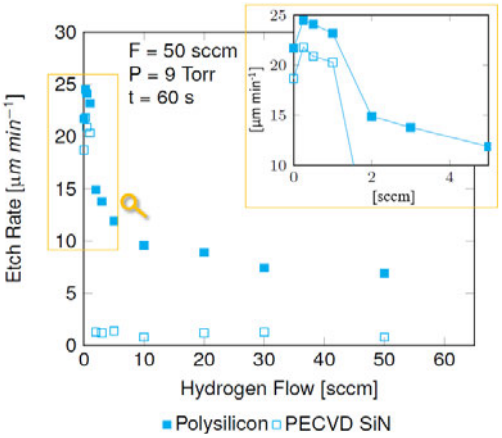

Fig. 7. Polysilicon and PECVD SiN etch rates of sample PECVD SiN relative to the amount of hydrogen supplied to the etch chamber. The inset magnifies the data for the hydrogen flows of 0 to 4 sccm.

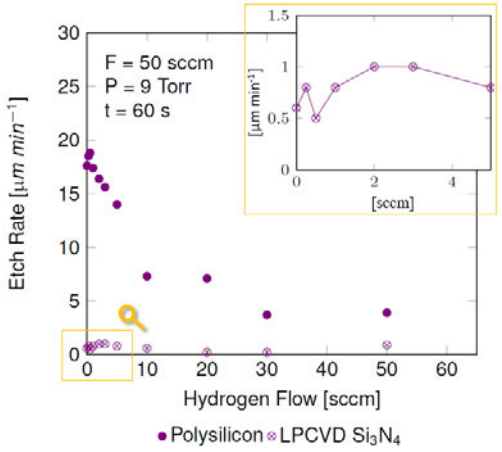

Fig. 8. Polysilicon and thermally grown Si3N4 of sample LPCVD SiN relative to the amount of silicon supplied to the chamber. The inset magnifies the data for the hydrogen flows of 0 to 4 sccm.

This temperature-dependent etch rate decrease was expected, as it has been reported before by Chang *et al.* [5] and Ibbotson *et al.* [18] and is coherent with theories developed by Flamm *et al.* [15] and Vugts *et al.* [19]. In contrast, the PECVD silicon nitride etch rate increases with increasing temperature with a rate of roughly 150 nm/min/°C. The etch rate of the LPCVD silicon nitride, and the PECVD silicon dioxide appears to be unaffected by the change in temperature.

The addition of hydrogen has a significant effect on the etch rates of polysilicon and both PECVD and LPCVD silicon nitride. Both Fig. 7 and 8 show that the polysilicon etch rate

TABLE III

THE XeF_2 VAPOUR ETCH SELECITIVITIES AND THE RESPECTIVE ETCH CONDITIONS THEY WERE OBSERVED

Material Combination	*Selectivity*	*Condition*††	*Source*
Si: PECVD SiN	5: 4	Proximity Effect	Fig. 2 & 3
Si: PECVD SiN	1.9: 1	Low T (10°C)	Fig. 6. a
Si: PECVD SiN	12: 1	2 sccm H_2 added	Fig. 7
Si: LPCVD Si_3N_4	6.3: 1 – 17: 1	Proximity Effect	Fig. 2 & 3
Si: LPCVD Si_3N_4	12: 1	Low T (10°C)	Fig. 6 b
Si: LPCVD Si_3N_4	38: 1	0.5 sccm H_2 added	Fig. 8
Si: PECVD SiO_2	11.4: 1 – 19: 1	Proximity Effect	Fig. 2 & 3
Si: PECVD SiO_2	10.3: 1	Low T (10°C)	Fig. 2 & 3

††T: Temperature

increases by roughly 9% as the hydrogen flow is increased to 0.5 sccm. A further increase of the hydrogen flow leads to a sharp reduction of polysilicon etch rate. For example, the etch rate drops from 25 μm/min for a hydrogen flow of 0.5 sccm to 10 μm/min at a flow of 10 sccm. After this sharp decrease, the etch rate stabilizes and decreases slowly as the hydrogen flow is increased. For the *PECVD SiN*, the effect is even more pronounced. The etch rate sharply drops from 20 μm/min at a hydrogen flow of 1 sccm to 1 μm/min for a flow of 2 sccm. Beyond that point, additional hydrogen does not seem to reduce the etch rate any further. The general etch rates of the LPCVD silicon nitride are very low, which makes accurate measurements difficult. Fig. 8 shows a slight decrease in the etch rate from 1 μm/min without hydrogen to 0.2 μm/min with the addition of 30 sccm hydrogen. During this experiment, the XeF_2 flow fluctuated by roughly 1.3 sccm. Five samples were etched at a constant XeF_2 flow of 24.85 sccm. For these, a linear decrease of roughly 160 nm/min per sccm of hydrogen was observed between hydrogen flows of 0 and 20 sccm. At 30 sccm, no further decrease was observed.

A similar experiment was conducted for the *PECVD-SiO_2* samples. The hydrogen addition did not change the etch rate of the SiO_2. Four samples were etched for 300 seconds, with 0, 1, 3 and 10 sccm hydrogen additions. The silicon dioxide undercuts varied between 2.1 and 2.6 μm, indicating an etch rate of 0.42 to 0.52 μm/min. The standard deviation of the undercuts lay between 0.2 and 0.6 μm. Similarly, four more samples were etched for 120 seconds using the same conditions and hydrogen flows as for the previous samples. Again, the etch undercuts were between 2.3 and 2.6 μm and showed no correlation with the hydrogen flow into the chamber. The very similar undercuts measured on the samples etched for 120 seconds and 300 seconds indicate that the SiO_2 etch stops once the polysilicon in the proximity of it has been entirely removed.

B. Impact of the Etch Parameters on the Selectivity

The selectivities that can be calculated from the data presented in figs 2 to 8, and the conditions under which they were obtained are summarized in table III.

While the PECVD silicon nitride selectivity does not appear to correlate with the XeF_2 flow, the selectivity of polysilicon towards silicon dioxide and the LPCVD silicon nitride does slightly increase at a flow rate of 25 sccm XeF_2. The change

of the pressure does not have a significant impact on the selectivity in any of the presented material combinations. The temperature, however, does have an impact with the polysilicon etch rate decreasing with rising temperatures, while the etch rates of the LPCVD silicon nitride and the PECVD silicon dioxide remain constant. This causes a decrease in selectivity with increasing temperatures. This effect is even more pronounced for polysilicon and PECVD silicon nitride.

The addition of hydrogen has a significant impact on the polysilicon to PECVD silicon nitride selectivity. It rapidly improves from roughly 1.2:1 to 12.8:1 when the hydrogen flow is increased from 0 to 10 sccm. However, the 10 times increased selectivity is at the expense of decreasing polysilicon etch rate (from 22.4 to 9.6 μm/min). Increasing hydrogen additions leads to a decrease in selectivity because the polysilicon etch rate decreases faster than the silicon nitride etch rate beyond this threshold. The polysilicon to LPCVD silicon nitride selectivity also strongly improved with the addition of hydrogen. The maximum selectivity was measured at 38:1 for a 0.5 sccm hydrogen flow to the chamber. The lowest selectivity is reached at 10 sccm, with 12.3:1. The addition of hydrogen did not appear to have any impact on the SiO_2 etch rate. Unexpectedly, the polysilicon and PECVD silicon nitride etch rates are higher at 0.5 and 1 sccm hydrogen flows, than they are without any hydrogen addition. It should be noted that the XeF_2 partial pressure within the reaction chamber decreases as the amount of hydrogen supplied increases.

V. Discussion

A. Proximity Effect

The first hypothesis presented in this work was that fluorine radicals are formed during the etching of polysilicon that can attack other materials. Two observations have been made that provide supporting evidence. Firstly, no etch could be measured for the reference samples where no polysilicon is present. However, all three materials were etched at a measurable rate when placed in proximity of the sacrificial polysilicon. This suggests that LPCVD Si_3N_4 and SiO_2 are inert to XeF_2 but are etched by the reaction product (fluorine) that is formed during the etching of the polysilicon. Secondly, as can be observed in Fig. 2 and Fig. 3, the linear increase of the polysilicon and PECVD SiN undercut over time suggests that they reach a steady-state and etch at a constant rate. In contrast to that, the SiO_2 and LPCVD Si_3N_4 begin to etch but seem to stop etching, once 2 – 3 μm have been undercut.

Both phenomena can be explained by the results of extensive research into the XeF_2 etch mechanics conducted by Hefty *et al.* [12], [14]. They concluded that the XeF_2 abstracts[1] a fluorine atom at a dangling bond of the silicon. The remaining XeF molecule is scattered into the gas phase and can follow either of two reaction paths. It can abstract the second fluorine atom on another dangling bond or dissociate and scatter the Xe and fluorine atom. The fluorine radicals that are scattered onto the silicon break Si-Si lattice bonds and gradually fluorinate the polysilicon forming SiF, SiF_2 and SiF_3. Finally, all Si-Si bonds are broken, and SiF_4 desorbs into the gas phase. They also suggested that the backscattering of fluorine radicals onto the silicon surface explains why the Si etch rate with XeF_2 is an order of magnitude larger than the reaction rate with F_2. It is highly likely that these backscattered fluorine atoms can react with the silicon dioxide or silicon nitride. Relative energy calculations conducted by Veyan *et al.* [9] for the reaction of XeF_2 abstraction generated fluorine with SiO_2 suggest that it is energetically favourable, releasing 15.9 eV exothermally.

Furthermore, Loewenstein [16] investigated the temperature-dependent etch rates of SiO_2, LPCVD Si_3N_4 and polysilicon in remote plasma-generated fluorine. The SiO_2 used was LPCVD and is not directly comparable with the PECVD SiO_2 used in this study. However, the polysilicon and the LPCVD Si_3N_4 used are very similar to the layers described here. From the data, polysilicon to LPCVD Si_3N_4 selectivities of 7.1:1 and 11.4:1 can be calculated for 16°C and 30°C respectively. Van de Ven *et al.* [26] reported a-Si: Si_3N_4 selectivity of 8:1 when etching with fluorine [15]. Both reference values are in good agreement with the polysilicon to LPCVD Si_3N_4 selectivity range of 8.5:1 to 12:1 reported here. The PECVD SiN etched at a very high rate, and the selectivities in proximity etching are very low. Apparently, it has been observed, that "plasma nitride" (PECVD SiN) etches at a similar rate or even more rapidly than Si in CF_4/O_2 plasmas [15], [26]–[28]. Assuming that they refer to PECVD SiN and that fluorine is the reactive species in the CF_4/O_2 plasma etching process, their observations are in excellent agreement with those presented here.

In the case of the reference samples, no fluorine was generated as no sacrificial polysilicon was available for fluorine abstraction. Therefore the reactant to etch silicon nitride and silicon dioxide was not available.

Regarding the etch rate to pressure plots displayed in Fig. 5, these indicate, that the etch reaction of the LPCVD Si_3N_4, and the SiO_2 ceases once the polysilicon in proximity has been etched away. At low pressures, when the polysilicon is etched more slowly and remains in the vicinity of the LPCVD Si_3N_4 and SiO_2 for a longer time, the structures etch for longer, and the etch rate is higher. Most likely, this is caused by the dynamics of molecular movement. The fluorine radicals have a limited mean free path and disperse as they scatter away from their point of origin. A critical concentration of fluorine is required to sustain the etch reaction of LPCVD Si_3N_4 and SiO_2. The reaction will therefore stop once the sacrificial layer etch front has travelled beyond its proximity. For the LPCVD Si_3N_4 and SiO_2 datasets presented here, this distance appears to be 2-3 μm.

In conclusion, the discussion above suggests that fluorine radicals are formed and scattered during the reaction of XeF_2 with silicon. Hence, it is highly likely that the proximity effect affects all materials that are etched by fluorine.

B. Effect of Temperature on Selectivity

Having established that the formation of fluorine radicals causes the proximity effect, this work considered methods

[1]Abstraction describes the removal of an atom by a radical.

to improve the selectivity. The temperature dependence of the etch rate of silicon using XeF_2 is the first promising mechanism that was investigated.

Considering the Arrhenius equation:

$$E.R. = \mathrm{A}e^{-\left(\frac{E_a}{RT}\right)} \tag{1}$$

One would expect that the etch rate (E.R.) increases when the temperature (T) rises because the gas constant (R) and the pre-exponential factor (A) are constants and the activation energy (E_a) is positive. This behaviour has been observed for the etching of polysilicon, SiO_2 and high-temperature chemical vapour deposited Si_3N_4 with fluorine [16]. In contrast, Vugts *et al.* [19] observed the highest XeF_2 etch rates of silicon at 150 K. As the temperatures increases, the reaction rate decreases, reaching a minimum reaction probability of roughly 20% at around 400 K. The reaction rates then rise again in the temperature range of 600 K to 900 K. Ibbotson *et al.* [18] observed that the reaction rate to temperature plot behaves linearly at temperatures below 360 K and calculated a reaction activation energy for this temperature spectrum of −13.4 kJ/mol (−3.2 kcal/mol).

The data in Fig. 6 shows the same trend over a limited temperature range. The calculated reaction energies are significantly lower at −3.75kJ/mol (−0.9 kcal/mol). It is unclear why the activation energy is negative in this case. Ibbotson suggested that the XeF_2 forms a bound surface layer prior to etching [18]. This hypothesis does not fully agree with the etch mechanism described by Hefty *et al.* [12], [13]. However, the Brunauer-Emmett-Teller (BET) theory [29] suggests that the rate of molecular adsorption increases with decreased temperature. Possibly, the abstraction of the fluorine on the silicon dangling bonds increases at lower temperatures. This would be consistent with previous research that found that the reaction layer grows at an accelerated rate between 200 K and 250 K [19].

Fig. 6 a. suggests that the etch rate of PECVD silicon nitride increases with increasing temperature. From the graph, the activation energy was calculated to be 6.221 kJ/mol (1.48 kcal/mol). Unfortunately, no reference value for the PECVD SiN fluorine etch activation energy could be obtained from the literature, but the value presented here appears reasonable. The data does not show a temperature correlation for the LPCVD Si_3N_4 and the SiO_2 samples. However, this does not mean that this is not the case, because the SiO_2 and LPCVD Si_3N_4 etch reaction could have stopped once the sacrificial layer had etched beyond the proximity etch distance as discussed earlier. The literature suggests that the SiO_2 and LPCVD Si_3N_4 reaction rates with fluorine are temperature dependent. Loewenstein [16] reported activation energies of 14.853 kJ/mol (3.55 kcal/mol) and 14.058 kJ/mol (3.36 kcal/mol) for LPCVD Si_3N_4 and SiO_2 respectively. Both reaction energies are positive. This implies an increased etch rate with increased temperature.

In summary, the data presented in this study and the literature suggests, that the selectivity of Si towards PECVD SiN, SiO_2 and LPCVD Si_3N_4 increases with decreasing temperature. However, the measurements also suggest, that significant selectivity improvements can only be expected at temperatures substantially below 0 °C. There are no vapour etch tools currently on the market that can operate in such a low-temperature regime.

C. Effect of Hydrogen on Selectivity

When hydrogen was added into the etch chamber it was, observed to have an impact on the etch selectivities of PECVD and LPCVD Si_3N_4. In particular, the PECVD SiN etch rate drops significantly. Assuming, that the fluorine radicals are causing the proximity etching effect it is reasonable to add hydrogen in order to form unreactive hydrogen fluoride HF according to;

$$H_2 + F \rightarrow HF + H \tag{2}$$

The hypothesis that the addition of hydrogen significantly reduces the number of reactive fluorine radicals, is supported by the decreasing polysilicon etch rates observed with increased hydrogen flows. However, the reaction is not completely halted for any of the materials investigated in this study. The reasons for this are unclear, and a detailed investigation is beyond the scope of this article. However, there are two possible explanations. Firstly, the formation of highly reactive hydrogen radicals as a product of the reaction in equation (2), might cause the continuous etching of these materials. A study into hydrogen plasma etching by Chang *et al.* [30] reported hydrogen radical etch rates of 15 Å/min for SiO_2 and LPCVD Si_3N_4 and 250 – 500 Å/min for silicon. These etch rates are roughly 10% of those reported here. However, the data is difficult to compare as it is unclear at which pressure their etch rate data was obtained. An alternative mechanism might be the formation of hydrogen fluoride in an excited state, as presented by Volynet *et al.* [21] and Jung *et al.* [22]. They found that the presence of excited hydrogen fluoride brings additional energy to the reaction site, enabling a selective etch reaction of LPCVD Si_3N_4 over SiO_2. Interestingly, even though different materials were etched, both their work and this study observed maximum etch rates after the addition of hydrogen.

In summary, the addition of hydrogen significantly improves the etch selectivity of LPCVD Si_3N_4 and PECVD SiN towards polysilicon. However, the data related to the impact of hydrogen on the selectivity of SiO_2 towards polysilicon showed no enhancement. This may be due to the fluorine radicals and hydrogen forming unreactive HF. However, the detailed mechanisms involved are yet unclear, and further investigations are required to understand the chemistry fully.

VI. Conclusion

In conclusion, this paper provides strong evidence supporting the hypothesis that the selectivity of various fluorine reactive materials to polysilicon reduces significantly if they are exposed to the etch reactions by-products in close proximity ($< 3\ \mu$m) to the sacrificial material during XeF_2 vapour etching. It is proposed that the fluorine radicals that form during the silicon etch, attack the LPCVD Si_3N_4, SiO_2, and PECVD SiN investigated in this study. For test structures used in this study, this resulted in selectivities as low as 6.3:1,

11.4 and 5:4 respectively. It should be remembered that these selectivities relate to the specific layout (“worst-case”) and architecture of test structures employed in this work. Their value is that any process enhancements that improve their selectivity can be confidently adopted for structures more typical of MEMS devices. With the proximity effect inhibiting the design and manufacturing possibilities of MEMS and NEMS two methods to improve the selectivity have been identified:

1) Reducing the process temperature by 15 °C improved the PECVD SiN selectivity from 5:4 to 7.4:4. However, significant improvements can only be expected when operating at low subzero degrees Celsius temperatures. Current commercial tools that operate in this temperature regime are not available, but should it be required, enhanced cooling systems offer the opportunity to realize this potential for selectivity improvement in the future.
2) Supplying hydrogen into the reaction chamber during etching yielded significant selectivity improvements. It is proposed that this improvement results from the fluorine radicals and the H_2 forming unreactive hydrogen fluoride molecules. This significantly reduces the etch rates of LPCVD Si_3N_4 and PECVD SiN. With the test structures at room temperature, the addition of hydrogen resulted in maximum selectivities of 38:1 and 12:1 for LPCVD Si_3N_4 and PECVD SiN respectively. A further advantage of hydrogen additions is that high polysilicon etch rates were maintained when using the hydrogen additions.

Clearly adding hydrogen to the XeF_2 vapour etch processes mitigates the proximity effect, and thereby creates new design and fabrication possibilities for MEMS and NEMS devices.

ACKNOWLEDGMENT

Markus Rondé thanks Norbert Radacsi, for his support while conducting this study. Furthermore, the authors thank memsstar Ltd for their helpful suggestions during the experimental design and results interpretation. The raw data underlying the finds reported in this work is available online from https://doi.org/10.7488/ds/2929.

REFERENCES

[1] J. R. Holt, R. C. Hefty, M. R. Tate, and S. T. Ceyer, “Comparison of the interactions of XeF_2 and F_2 with Si(100)(2 × 1),” *J. Phys. Chem. B*, vol. 106, no. 33, pp. 8399–8406, 2002.

[2] R. Maboudian, “Critical review: Adhesion in surface micromechanical structures,” *J. Vac. Sci. Technol. B, Microelectron. Nanometer Struct.*, vol. 15, no. 1, p. 1, Jan. 1997.

[3] U. Zaghloul, G. Papaioannou, B. Bhushan, F. Coccetti, P. Pons, and R. Plana, “On the reliability of electrostatic NEMS/MEMS devices: Review of present knowledge on the dielectric charging and stiction failure mechanisms and novel characterization methodologies,” *Microelectron. Rel.*, vol. 51, nos. 9–11, pp. 1810–1818, Sep. 2011.

[4] H. F. Winters and J. W. Coburn, “The etching of silicon with XeF_2 vapor,” *Appl. Phys. Lett.*, vol. 34, no. 1, pp. 70–73, 1979.

[5] F. I. Chang *et al.*, “Gas-phase silicon micromachining with xenon difluoride,” *Proc. SPIE*, vol. 2641, p. 117, Sep. 1995.

[6] V. M. Donnelly, “Review article: Reactions of fluorine atoms with silicon, revisited, again,” *J. Vac. Sci. Technol. A, Vac. Surf. Films*, vol. 35, no. 5, 2017, Art. no. 05C202.

[7] H. F. Winters and D. Haarer, “Influence of doping on the etching of Si(111),” *Phys. Rev. B, Condens. Matter*, vol. 36, no. 12, pp. 6613–6623, Oct. 1987.

[8] P. B. Chu *et al.*, “Controlled pulse-etching with xenon difluoride,” in *Proc. Int. Solid State Sens. Actuators Conf.*, Jun. 1997, pp. 665–668.

[9] J.-F. Veyan, M. D. Halls, S. Rangan, D. Aureau, X.-M. Yan, and Y. J. Chabal, “XeF_2-induced removal of SiO_2 near Si surfaces at 300 K: An unexpected proximity effect,” *J. Appl. Phys.*, vol. 108, no. 11, Dec. 2010, Art. no. 114914.

[10] M. Rondé, A. J. Walton, and J. G. Terry, “Test structure for measuring the selectivity in vapour etch processes,” in *Proc. IEEE 33rd Int. Conf. Microelectron. Test Struct. (ICMTS)*, Edinurgh, U.K., May 2020, pp. 1–5.

[11] M. Gorisse *et al.*, “Lateral field excitation of membrane-based aluminum nitride resonators,” in *Proc. Joint Conf. IEEE Int. Freq. Control Eur. Freq. Time Forum (FCS)*, May 2011, pp. 1–5.

[12] R. C. Hefty, J. R. Holt, M. R. Tate, and S. T. Ceyer, “Atom abstraction and gas phase dissociation in the interaction of XeF_2 with Si(100),” *J. Chem. Phys.*, vol. 129, no. 21, Dec. 2008, Art. no. 214701.

[13] R. C. Hefty, J. R. Holt, M. R. Tate, D. B. Gosalvez, M. F. Bertino, and S. T. Ceyer, “Dissociation of a product of a surface reaction in the gas phase: XeF_2 reaction with Si,” *Phys. Rev. Lett.*, vol. 92, no. 18, pp. 18–21, 2004.

[14] R. C. Hefty, J. R. Holt, M. R. Tate, and S. T. Ceyer, “Mechanism and dynamics of the reaction of XeF_2 with fluorinated Si(100): Possible role of gas phase dissociation of a surface reaction product in plasmaless etching,” *J. Chem. Phys.*, vol. 130, no. 16, Apr. 2009, Art. no. 164714.

[15] D. L. Flamm and V. M. Donnelly, “The design of plasma etchants,” *Plasma Chem. Plasma Process.*, vol. 1, no. 4, pp. 317–363, Dec. 1981.

[16] L. M. Loewenstein, “Temperature dependence of silicon nitride etching by atomic fluorine,” *J. Appl. Phys.*, vol. 65, no. 1, pp. 386–387, Jan. 1989.

[17] D. E. Ibbotson, J. A. Mucha, D. L. Flamm, and J. M. Cook, “Plasmaless dry etching of silicon with fluorine-containing compounds,” *J. Appl. Phys.*, vol. 56, no. 10, pp. 2939–2942, Nov. 1984.

[18] D. E. Ibbotson, D. L. Flamm, J. A. Mucha, and V. M. Donnelly, “Comparison of XeF_2 and F-atom reactions with Si and SiO_2,” *Appl. Phys. Lett.*, vol. 44, no. 12, pp. 1129–1131, Jun. 1984.

[19] M. J. M. Vugts, G. L. J. Verschueren, M. F. A. Eurlings, L. J. F. Hermans, and H. C. W. Beijerinck, “Si/XeF_2 etching: Temperature dependence,” *J. Vac. Sci. Technol. A, Vac. Surf. Films*, vol. 14, no. 5, pp. 2766–2774, 1996.

[20] B. E. E. Kastenmeier, P. J. Matsuo, and G. S. Oehrlein, “Highly selective etching of silicon nitride over silicon and silicon dioxide,” *J. Vac. Sci. Technol. A, Vac. Surf. Films*, vol. 17, no. 6, pp. 3179–3184, Nov. 1999.

[21] S. Rachidi *et al.*, “Isotropic dry etching of Si selectively to $Si_{0.7}Ge_{0.3}$ for CMOS sub-10 nm applications,” *J. Vac. Sci. Technol. A, Vac. Surf. Films*, vol. 38, no. 3, May 2020, Art. no. 033002.

[22] V. Volynets *et al.*, “Highly selective Si_3N_4/SiO_2 etching using an $NF_3/N_2/O_2/H_2$ remote plasma. I. Plasma source and critical fluxes,” *J. Vac. Sci. Technol. A, Vac. Surf. Films*, vol. 38, no. 2, 2020, Art. no. 023007.

[23] J.-E. Jung *et al.*, “Highly selective Si_3N_4/SiO_2 etching using an $NF_3/N_2/O_2/H_2$ remote plasma. II. Surface reaction mechanism,” *J. Vac. Sci. Technol. A, Vac. Surf. Films*, vol. 38, no. 2, 2020, Art. no. 023008.

[24] K. Sugano and O. Tabata, “Etching rate control of mask material for XeF_2 etching using UV exposure,” *Proc. SPIE*, vol. 4557, pp. 18–23, Sep. 2001.

[25] U. Streller, A. Krabbe, and N. Schwentner, “Selectivity in dry etching of Si(100) with XeF_2 and VUV light,” *Appl. Surf. Sci.*, vol. 106, pp. 341–346, Oct. 1996.

[26] E. Van de Ven, T. Shankoff, and R. Heinecke, “Gas etching of dielectrics and metals,” Standard Telecommun. Lab., Harlow, Essex, Tech. Rep., 1973. [Online]. Available: https://en.wikipedia.org/wiki/Standard_Telecommunication_Laboratories

[27] R. L. Maddox, “Applications of reactive plasma practical microelectronic processing systems,” *Solid State Technol.*, vol. 21, no. 4, p. 107, 1978.

[28] A. Jacob, “The versatile technique of RF plasma etching. III. Mechanistic considerations for selective etching,” *Solid State Technol.*, vol. 21, no. 4, pp. 95–98, 1978.

[29] B. S. Brunauer and P. H. Emmett, “Adsorption of gases in multimolecular layers,” *J. Amer. Chem. Soc.*, vol. 60, no. 2, pp. 309–319, 1938.

[30] R. P. H. Chang, C. C. Chang, and S. Darack, “Hydrogen plasma etching of semiconductors and their oxides,” *J. Vac. Sci. Technol.*, vol. 20, no. 1, pp. 45–50, 1982.

Appendix C: Second Peer Reviewed Journal Publication

Journal: IEEE Transactions on Semiconductor Manufacturing
Year: 2021
Title: Test Structure for Measuring the Selectivity in XeF_2 and HF Vapour Etch Processes
Authors: Markus Rondé, Anthony J. Walton, Jonathan G. Terry
Declaration: The study presented in this publication was designed, conducted and analysed by Markus Rondé. The text and figures were prepared by Markus Rondé. Jonathan Terry supervised the project and both he and Anthony Walton reviewed the manuscript and provided suggestions to improve it.

Test Structure for Measuring the Selectivity in XeF_2 and HF Vapour Etch Processes

Markus Rondé, Anthony J. Walton, Jonathan G. Terry

Abstract— **Etch selectivity between layers is an important parameter in the fabrication of microelectronics and microsystems. This is particularly true in the case of isotropic gas/vapour etching methods used to release free standing structures through the selective etching of sacrificial layers. Commonly used structural materials have been reported to be largely inert when exposed to a given vapour etchant, indicating high selectivity when measured against typical sacrificial layers. However, there is growing evidence that these structural layers are actually etched at an enhanced rate if they are located in the proximity of the sacrificial layer being removed. Hence, removal rates given in the literature, which have resulted from measurements of layers that have been etched in isolation, can no longer be trusted to characterize critical etch processes in device fabrication. In this paper, a test structure is reported that enables a far more appropriate determination of the etch selectivity between sacrificial and structural materials. The method is demonstrated with the two most common vapour etch processes. Firstly, the XeF_2 vapour etch of a polysilicon sacrificial layer located above a silicon nitride structural layer, and secondly, the HF vapour etch of silicon dioxide placed above a silicon nitride structural layer. Both test structure datasets are presented. The polysilicon and silicon nitride layers, etched with XeF_2 show a selectivity of 5:4. The silicon dioxide and silicon nitride layers etched with HF, show a selectivity of 6: 1 to 8: 1.**

Index Terms—**MEMS, NEMS, Vapour etching, test structure, XeF_2, Hydrogen fluoride**

I Introduction

Etching sacrificial layers to release free standing structures is a critical process step in the fabrication of micro and nano-electromechanical systems (MEMS/NEMS) Historically, sacrificial layers such as silicon or silicon dioxide were removed using wet etch processes However, the commercial advantages and novel scientific possibilities inherent with smaller sensors and actuators has fueled a trend towards miniaturization At the micro and nanoscale, the high surface-to-volume ratios may cause stiction resulting in the adherence of the released structures to the surface underlying the sacrificial layer Stiction [1] [2] results from surface tension during the drying of the liquid etchant [3] and can be avoided by the use of a gas/vapour phase etchant Vapour etching of silicon dioxide and silicon by hydrogen fluoride (HF) and xenon difluoride (XeF_2) respectively are now commonly used release processes in industry

Various test structures have been used to characterize vapour etch processes For instance, aperture test structures have been

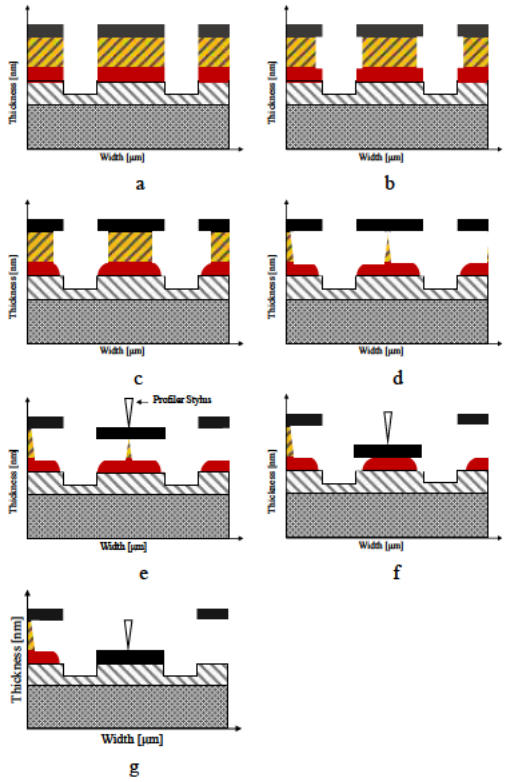

Fig 1 Shematic of the bridge array methodolgy (a) shows the test structure before etching (b)-(c) show the etch initiation on the sacrificial and structural material respectively (d)-(f) show the test structure with increasing etch time

Manuscript received xx xx xxxx; revised xx xx xxxx; accepted xx xx xxxx Date of publication xx xx xxxx; date of current version xx xx xxxx

Markus Rondé's work was supported by the EPSRC CDT in Sensing and Measurement EP/L016753/1 and the CENSIS Studentship Award programme

The authors are with the School of Engineering at the University of Edinburgh located at SMC, Kings Building, Alexander Crum Brown Road, Edinburgh, EH9 3FF, UK (e-mail: markus ronde@ed ac uk)

Color versions of one or more of the figures in this article are available online at https://ieeexplore ieee org Digital Object Identifier xxx

used to measure etch rates, trenching and loading [4][5][6][7] Sugano et al [8][9][10] used wagon wheel patterns to accurately measure etch undercuts and to investigate the aperture size effects, surface roughness' and etch rates in XeF_2 etching Finally, cantilever test structures have been used to demonstrate stiction free etching [11][12] and as proof of concept for novel vapour etch techniques [13]

To date, most vapour etch selectivity data has been obtained by blanket etching of wafers or chips Blanket layer etching does not reflect the reality of MEMS device manufacturing, because in most applications of sacrificial vapour phase etch processes, the structural layers of a device being fabricated are in close proximity to the sacrificial materials being removed It has been observed, that a structural material, which is not significantly affected when introduced to the vapour etch in isolation, can be severely attacked when in the proximity of a sacrificial material being etched [14][15] In this situation, determining the etch selectivity between the materials is non-trivial and requires a measurement method that can quantify the undercut etch rates of two materials on a single die when isotropically etched in close proximity to one another

Our previous work [16], presented a test structure specifically developed for this purpose along with experimental data for XeF_2 vapour etching This ICMTS Special Issue paper is an expansion of the conference paper It includes the original concept, methodology and experimental data and in addition, presents the test structure, fabrication methodology and experimental data for HF vapour etching This represents test structures and selectivity measurement methodologies for the two most common vapour etch techniques used in MEMS fabrication

For the XeF_2 experiment, the etch selectivity between a structural plasma enhanced chemical vapour deposited (PECVD) silicon nitride layer and a low pressure chemical vapour deposited (LPCVD) sacrificial polysilicon layer being processed in a commercial xenon difluoride vapour etch tool is determined Similarly for the HF experiment, the etch selectivities between a PECVD silicon dioxide sacrificial layer and a PECVD silicon nitride layer are measured after processing in a commercial HF vapour etch tool The following sections briefly explain the measurement method, elaborating on the layout and the design The interpretation of the resulting surface

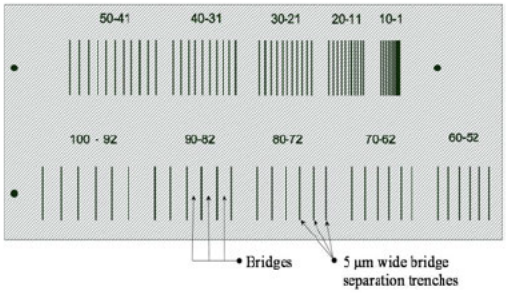

Fig 2 Design layout of the test structure showing the 5 x 300 µm trenches Each section is labelled with the bridge width The trenches are the dark lines and the separation gradually decrease by 1 µm at the top row and 2 µm at the bottom array

profile is then discussed with the presentation of evidence verifying the characterisation method Finally a review of the test structures' performance is given using a dataset obtained during experiments Special attention is given to the post-etch treatment of the HF test structure, as it was found to be important that residual stress in the copper capping layer was optimised for successful operation of the structure

II MEASUREMENT METHOD

The test procedure measures the mechanical displacement of an array of etch-released free-standing bridge structures The width of the bridge structures in the array is incrementally increased in a similar manner to [17] and [18], which uses cantilevers to measure etch rates Following an etch release process, a profilometer is scanned across the array of bridges and, if release has been achieved, the down force of the stylus vertically displaces the bridges, with the vertical displacement set by the thickness of etched material The width of the widest bridge structure that has been displaced by the thickness of the sacrificial layer is equal to twice the undercut distance This undercut distance and the etch time can then be used to determine the apparent etch rate The structural material is the layer below the sacrificial material and the etch rate of this second material can be obtained in a similar manner, from the

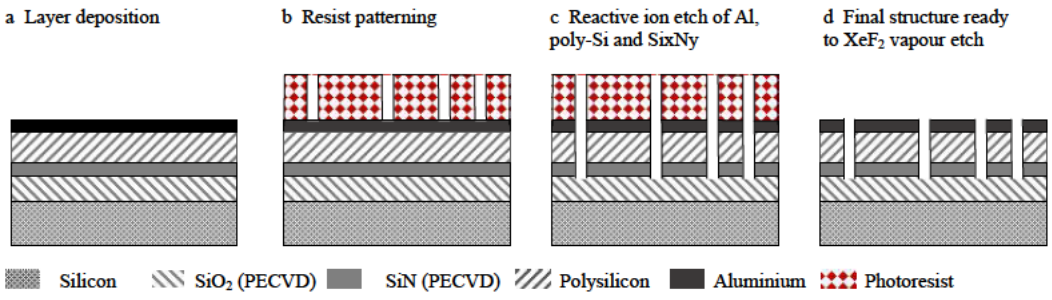

Fig 3 Schematic process flow of the fabrication of a XeF_2 vapour etch selectivity test structure

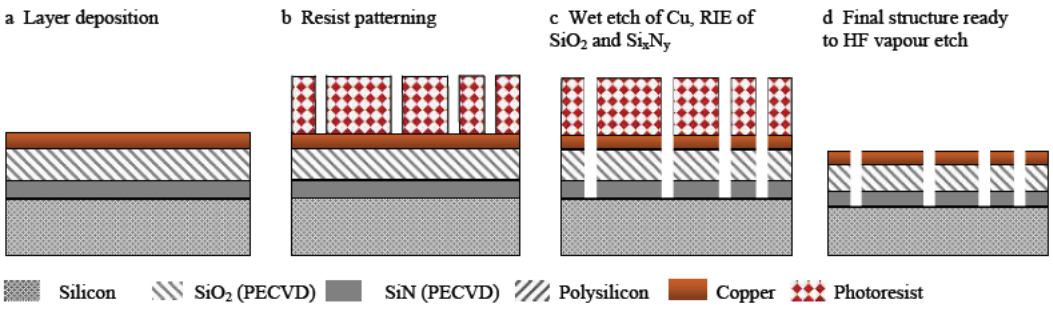

Fig 4 Schematic process flow of the fabrication of a HF vapour etch selectivity test structure

widest bridge that is displaced by the height of both the sacrificial and the structural layers Figure 1 shows a schematic cross-section of one of the bridges being gradually released and the stylus displacing the bridge during the measurement

III TEST STRUCTURE DESIGN

A. Layout

The test structure is formed of a stack of deposited thin films, comprising a structural layer, a sacrificial layer and finally a capping layer The XeF_2 structure reported here uses a PECVD silicon nitride structural layer in combination with a LPCVD polysilicon sacrificial layer These are capped by a layer of aluminium that is unaffected by the XeF_2 vapour etch The HF test structure also uses a PECVD silicon nitride structural layer However, in this case, a PECVD silicon dioxide sacrificial layer and a copper capping layer is used

In both cases, trenches are etched in the layer stack using a reactive ion etch, which defines the bridge structures and exposes the layer edges to the vapour etch process As part of the design the bridge width is incrementally reduced and the layout is shown in figure 2 For measurements of large undercuts the bridge width decreases from 100 to 52 µm in increments of 2 µm For smaller undercuts, narrower bridges are defined with widths from 50 to 2 µm in increments of 1 µm

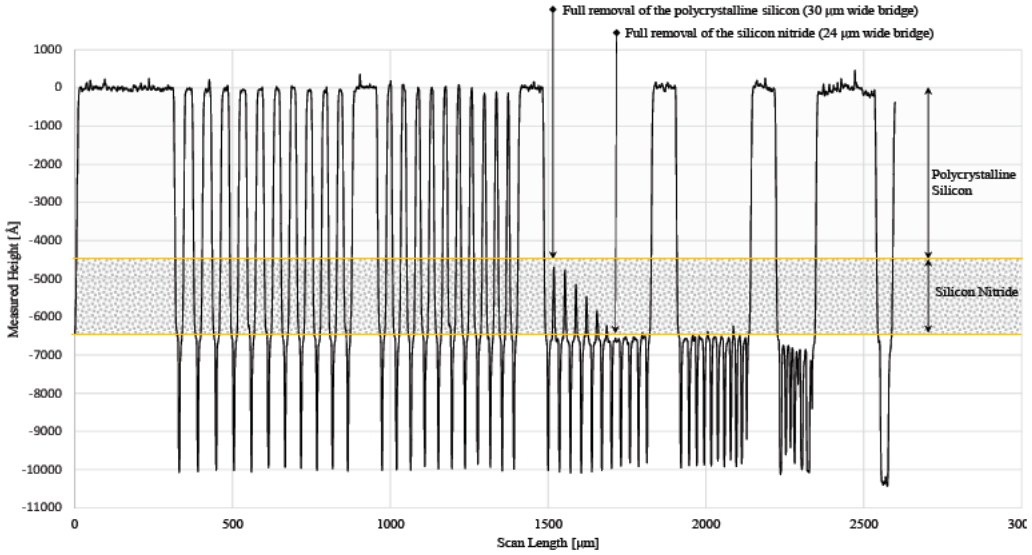

Fig 5 Surface profile retrieved after vapour etching the XeF_2 test structure The thicknesses of the polycrystalline silicon and silicon nitride layers are represented by the different underlyings of the graph

The bridge structure has a number of advantages over alternative architectures It is less prone to stiction issues during scanning, enabling a robust extraction of the 1D etch front propagation In addition, it gives less noisy deflection measurements compared with other designs such as the cantilever structures of [3] Finally each scan should have the format shown in figure 5 thereby confirming the correct operation of the test structure

For the initial investigation, bridges with lengths of 100 µm, 200 µm and 300 µm were employed The measured etch undercuts and selectivities were found to be independent of the bridge length However, the alignment of the shorter test structures for the automated profilometer measurement of multiple test structures becomes very time-consuming A bridge length of 300 µm was selected as it requires minimal wafer real estate for the test structure, while the layer thicknesses between 200-500 nm can withstand the vertical and horizontal displacement during measurement The 5 µm trench width between bridges enables the tip of the profilometer stylus to measure the full depth of the trenches and simplifies the photolithography

B. Layer Configuration

The test structure can be used to measure the selectivity of various materials in close proximity For example, figure 3 shows the fabrication process flow for a test structure used to determine the etch selectivity of polycrystalline silicon versus silicon nitride in XeF_2 vapour etching The structural layer is placed below the sacrificial layer, which allows the etch rates of the two materials to be determined with a single surface profilometry measurement

In this example, the 500 nm thick silicon dioxide etch stop layer and the 210 nm thick silicon nitride structural layer were deposited using plasma enhanced chemical vapour deposition (PECVD) at low and high frequencies respectively Silicon dioxide was selected as an etch stop because it is largely unaffected by the XeF_2 vapour etch process while remaining stable at high temperatures If the etchant used attacks silicon dioxide, a 50 nm thick platinum layer can be used as an alternative etch stop The 450 nm thick sacrificial layer of polycrystalline silicon and 350 nm thick capping layer of aluminum were deposited using LPCVD and sputter deposition respectively

Aluminum was employed as the capping layer, because it is not attacked by the XeF_2 vapour process, can be sputter deposited and reactive ion etched, while its mechanical properties prevent fracture of the bridges during the profilometer measurement Aluminum is not recommended as the first choice capping layer for hydrogen fluoride vapour etching, because it can fluorinate and the presence of the resulting particulates on the sample creates noise during the measurement Instead, we suggest using copper as the capping layer for the hydrogen fluoride test structures It is resistant to HF, does not fluorinate, and in contrast to polysilicon, the residual stress within the layers can be controlled by straightforward annealing processes The stress control method will be briefly elaborated on in a later section of this work

The remaining architecture of the HF test structure is very similar to the one for XeF_2 and is displayed in figure 4 A 500 nm thick PECVD silicon dioxide was used as a sacrificial layer along with a 250 nm PECVD silicon nitride structural layer An etch stop layer is not required for the HF test structure because hydrogen fluoride does not attack the underlying silicon wafer

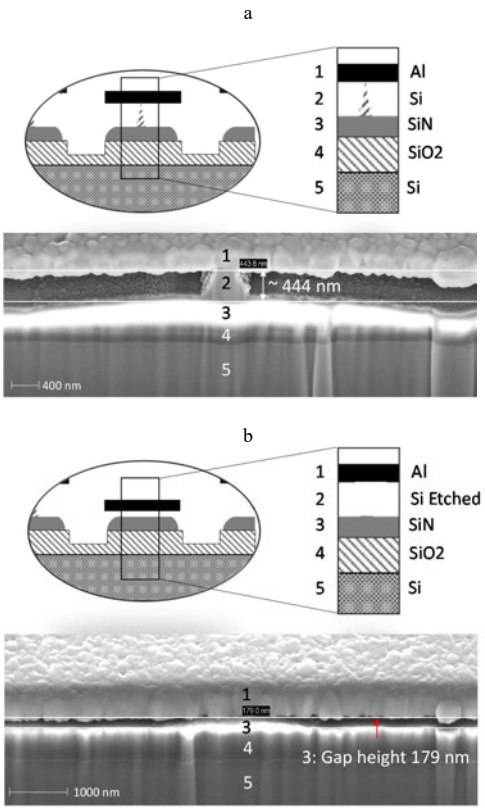

Fig 6 Scattering electron microscope (SEM) images of focus ion beam (FIB) cut crossesctions of a the centre of the 31 µm wide bridge The polycrystalline silicon pillar has not been fully removed yet and prevents deflection of the bridge during profiling b The polycrystalline silicon layer of the 28 µm wide bridge has been fully etched The bridge has deflected and is supported by the remaining silicon nitride

The patterning process is the same for both structures A contact mask aligner was used to transfer the pattern from a chromium photomask into a 3 µm thick layer of photoresist (SPR 220 – 3 0) which was subsequently developed for 1 minute in MF-26 In the case of the XeF_2 test structures, the trenches in the aluminum, polycrystalline silicon, and silicon nitride layer stack were reactive ion etched In the case of the HF test structures, the copper was wet etched, and the silicon dioxide and silicon nitride were reactive ion etched After the resist was removed, the wafer was diced into 90 chips with dimensions of 11 x 5 5 mm

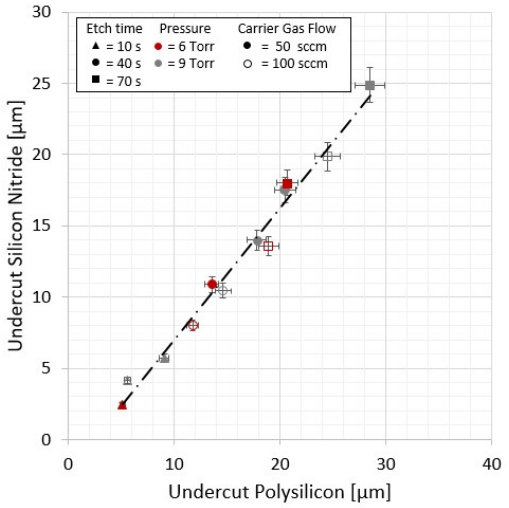

Fig 7 This example dataset presents the selectivity between polysilicon and PECVD silicon nitride It is based on 12 samples with the layer configuration and design presented in section III The etch parametes can be derived from the indivdual markers design The etchant was gassous XeF_2

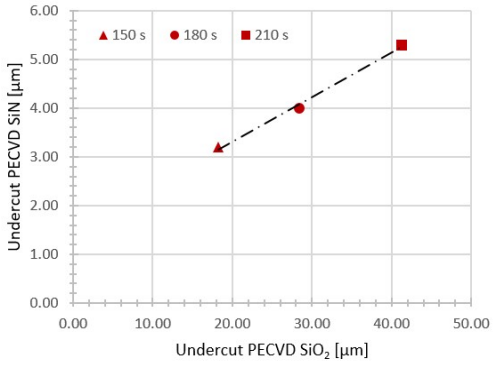

Fig 8 This example dataset presents the selectivity of PECVD SiO_2 over PECVD SiN It is based on three samples, that were etch at a pressure of 11 Torr at a temperature of 20°C The HF, H_2O and N_2 flows were 61, 95 and 9 sccm respectivley The etch time can be derived from the shape of the markers

IV INTERPRETING THE SURFACE PROFILE

After the test structures have been scanned by the profilometer the resulting surface profile is used to obtain the undercut for the sacrificial and the structural layer The measurement reading procedure is explained on the basis of test structures that were exposed to a xenon difluoride vapour for 40 seconds at a process pressure of 9 Torr, with a nitrogen carrier gas flow of 100 sccm, at a temperature of 30°C

The resulting surface profile is displayed in figure 5 For these particular process parameters, the 30 µm wide bridge was the widest one that has been vertically deflected by more than 450 nm (the thickness of the polysilicon) indicating the sacrificial material has been fully etched The resulting undercut is 15 µm with an apparent etch rate of 375 nm s^{-1} The 24 µm wide bridge has deflected by 650 nm (the combined thickness of the polysilicon and silicon nitride layers), indicating the structural layer of silicon nitride has also been fully etched with an apparent etch rate of 300 nm s^{-1} This suggests an etch selectivity between the polysilicon and silicon nitride layers of 5:4 Depending on the output format of the profilometer used, programming can be used to automatically extract the undercut data from the surface profile

V MEASUREMENT VERFICIATION

The test structure measurements were verified using two different methods for the XeF_2 etched samples As the physical mechanisms underlying both the selectivity measurement and verification methods are the same in each case, it was not necessary to repeat this for the HF test structures Firstly, five samples from a larger pool of chips, that were XeF_2 etched and measured during the process calibration, were randomly selected and the capping aluminum layer removed Energy-dispersive X-Ray spectroscopy (EDX) was used to determine if the silicon nitride was removed at the bridge width indicated by the surface profilometry In all cases, the EDX measurement agreed with the results of the surface profile Secondly, cross sectional SEM images of etched structures confirmed that the polycrystalline silicon and silicon nitride were removed under the bridge, indicated by the test structure

Figure 6a shows the 31 µm wide bridge being supported by a thin pillar of sacrificial polysilicon Figure 6b shows the 28 µm wide bridge of the same test structure In this case the sacrificial layer has been fully removed and the aluminum bridge is suspended above the silicon nitride layer

VI RESULT AND DISCUSSION

A. Experimental Result

A series of etch experiments was undertaken on a XeF_2 vapour etch tool, to characterize the performance of the test structures The tool operates in a continuous flow configuration, constantly supplying the xenon difluoride to the etch chamber It has the capability to control the processing pressure, chamber temperature and enabls additional supply gasses to be introduced into the etch chamber

The nitrogen carrier gas flows through a bubbler, introducing the xenon difluoride into the chamber The xenon difluoride concentration within the etch chamber is inversed proportional to the carrier gas flow An excerpt of a larger dataset is displayed in figure 7, with each of the 12 data points representing a sample They were etched at different process pressures, carrier gas flows and etch times at a constant temperature of 25°C Eight test structures were measured on each sample The average measurement and the etch parameters used are presented in figure 7 and the error bars indicate the standard deviation of each

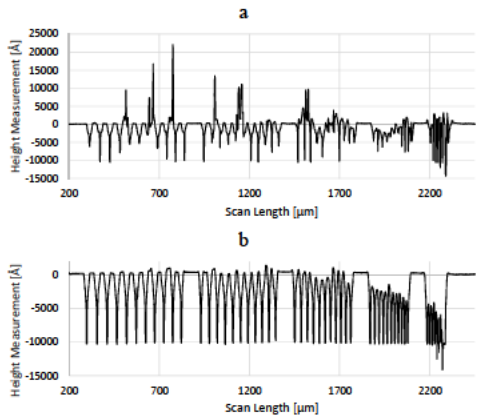

Fig 9 A comparison of the HF test structure's post etch surface profiles In (a) without heat treatment, and in (b) after annealing the etched test structure on a hotplate, set to 170°C for 60 seconds

dataset The data is consistent and shows a polycrystalline silicon to silicon nitride selectivity of 5:4 Furthermore, it shows

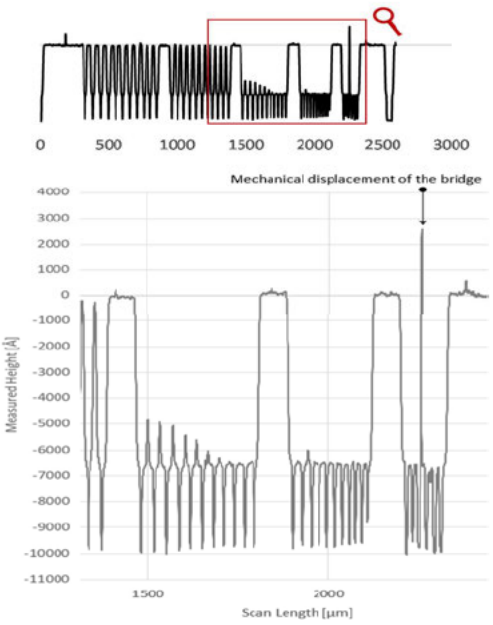

Fig 10 This surface profile was obtained from the same sample as figure 5's The signal is imprecise due to a horizontal displacement of a 8 µm wide bridge caused by a too high scan speed

that the selectivity is independent of the processing pressure, xenon difluoride concentration and etch time The reasons for this and methods to significantly improve the selectivity have been recently reported by the authors [15]

In addition to this, some preliminary data for an HF etch selectivity study is presented in figure 8 The dataset is less extensive than the one presented for XeF_2 processing, because in order to maintain comparable experimental etch conditions over a broader temperature and concentration range the process must operate at the vapour pressure of the gas mixture Hence, there is a single set of pressure, HF and H_2O flows for each set of processing temperature and HF gas concentration parameters

The data presented was obtained at a processing temperature of 20°C at an HF gas concentration of 37% However, it is important to take into account the processing time, because the memsstar Xeric HF etch system used in this study requires up to 40 seconds to stabilise the gas flows The dataset displayed in figure 8 suggests that the selectivity of PECVD silicon dioxide over PECVD silicon nitride increases over time from roughly 6:1 at an etch time of 150 seconds to 8:1 at an etch time of 210 seconds The reasons for this and methods to improve the HF etch selectivity are currently being investigated by the authors

B. Performance

A total of 56 chips with 8 test structures per chip, were vapour etched in a XeF_2 atmosphere at different conditions to characterize the resulting variance in the etch undercuts of the structures on each sample The maximum polysilicon and silicon nitride undercut standard deviations were 1 96 µm (mean 27 86 µm) and 2 2 µm (mean 28 5 µm) respectively The population standard deviations and the yield of successful measurements are displayed in table 1 The performance can be significantly improved by adopting the design and measurement considerations presented in the next section

TABLE I
PERFORMANCE OF XeF_2 TESTS STRUCTURE

	Polysilicon	SiN
Number of attempted measurements	448	448
Number of successful measurements	426	350
Successful measurements as %	95	75
Population Standard Deviation σ [µm]	0 4	0 37

C. Test Structure Measurement Consideration

The authors observed six modes that can cause a faulty or incomplete measurement Firstly, it is important to carefully define the etch time to prevent both over and under etching In this example, over-etching would occur once the 100 µm wide (widest) bridge is released, because in that case the maximum undercut cannot be determined Similarly, no measurement can be obtained, if twice the undercut is less than the width of the narrowest bridge Clearly, the test structure layout and the process to be evaluated are important considerations during the design process

Residual stress of the capping layer can result in faulty measurements because the bridges buckle and can not be displaced by the profiler stylus Such a profile is displayed in figure 9a This issue was observed for the copper capping layers during the development of the HF test structure, while the aluminium capping layer of the XeF_2 test structure was not affected Post vapour etch annealing of the HF test structures was experimentally investigated to resolve this issue

As suggested by the literature [19], a strong response of the residual stress was observed for the temperature range of 160 – 210 °C The optimum process, an example is displayed in figure 9b, was achieved when heating the sample to 170 °C for the duration of 60 seconds on a hotplate In this process, the stress within the layer moves from tensile to compressive Should the stress in the copper be non-optimal, then another successful approach is to scan the bridge array twice, first with a low downforce (< 3mg) to obtain the deflection of the narrow bridges and a second time with a large downforce (> 10 mg) to deflect the larger bridges

The three remaining measurement issues are caused by sub-optimal surface profiler settings Firstly, mechanical destruction of the bridges can occur if the downforce of the surface profiler's stylus is too high In consequence, the bridges are ripped from their anchoring, adhere to the stylus and contaminate the tool Secondly, the stylus bounces off the bridges if the downward force is too low This leads to a perturbed signal that resembles a positive bridge deflection up to 10 micrometres A downforce of 2 – 3 mg yielded the best results for the samples presented in this study

The measurement conditions identified in figure 10 result from a mechanical deflection of a narrow bridge caused by too high a scan speed This has only been observed on bridges that were narrower than 10 µm at scan speeds higher than 40 µm s^{-1} Hence robust measurements can be achived by reducing the scan speeds for samples were the accurate measurement of this segment of the test structure is essential

VII Conclusions

This paper and [16] have reported for the first time a bridge based test structure that can characterize the isotropic etch selectivity between two materials under realistic MEMS fabrication conditions The test structure is designed to be used in vapour etch processes but can also be adapted for wet etch release processes It can be employed to characterize a wide range of materials with the fabrication of the test structure being quick and straightforward

The measurement methodology has been demonstrated by HF and XeF_2 etching of example stacks of layer materials, which may not be those that would be used in a commercial process However, they provide an experimental dataset that clearly shows that these test structures deliver coherent measurement information The design can be employed in industrial MEMS fabrication processes, with the area required being small enough to be placed on production wafers

The test structure can be easily adapted to accommodate different dimensional requirements The measurements taken with this test structure are robust, because faulty measurements resulting from broken or contaminated bridges are evident from the profiler signal Individual test structure arrays can be manually measured within 15 seconds Large numbers of devices can be assessed by automating the process For instance, an automatic measurement algorithm was used on the Bruker Dektak XT profilometer to measure the test structures reported in this study Typically this can measure about 200 test structures within 2 hours

ACKNOWLEGEMENT

M R thanks Norbert Radacsi, for his support while conducting this study Furthermore, the authors thank memsstar Ltd for their helpful suggestions during the experimental design and results interpretation

Datashare

The data presented in this work is available online at https://doi org/10 7488/ds/2962

References

[1] R Maboudian and R T Howe, "Critical Review: Adhesion in surface micromechanical structures," *J. Vac. Sci. Technol. B Microelectron. Nanom. Struct.*, vol 15, no 1, pp 1-20, 1997, DOI: 10 1116/1 589247

[2] U Zaghloul, G Papaioannou, B Bhushan, F Coccetti, P Pons, and R Plana, "On the reliability of electrostatic NEMS/MEMS devices: Review of present knowledge on the dielectric charging and stiction failure mechanisms and novel characterization methodologies," *Microelectron. Reliab.*, vol 51, no 9–11, pp 1810–1818, 2011, DOI:10 1016/j microrel 2011 07 081

[3] N Tas, T Sonnenberg, H Jansen, R Legtenberg, and M Elwenspoek, "Stiction in surface micromachining," *J. Micromech. Microeng*, vol 6, pp 385–397, 1996

[4] P B Chu, *J.T Chen, R. Yeh, G.Lin, J.C.P. Huang, B.A. Warneke, K.S.J Pister* , "Controlled pulse-etching with xenon difluoride," *Int. Conf. Solid-State Sensors Actuators, Proc.*, vol 1, pp 665–668, 1997

[5] B Bahreyni and C Shafai, "Deep etching of silicon with XeF_2 gas," in *IEEE Canadian Conference on Electrical and Computer Engineering*, pp 460–464, 2002, DOI: 10 1109/CCECE 2002 1015269

[6] F I Chang, *R. Yeh, G. Lin, P.B.Chu, E.G. Hoffman, E.J.J. Kruglick, K.S.J. Pister*, "Gas-phase silicon micromachining with xenon difluoride," *Microelectron. Struct. Microelectromechanical Devices Opt. Process. Multimed. Appl.*, vol 2641, pp 117-128, 1995, DOI: 10 1117/12 220933

[7] L R Arana, N De Mas, R Schmidt, A J Franz, M A Schmidt, and K F Jensen, "Isotropic etching of silicon in fluorine gas for MEMS micromachining," *J. Micromechanics Microengineering*, vol 17, no 2, pp

384–392, 2007, DOI: 10 1088/0960-1317/17/2/026

[8] K Sugano and O Tabata, “Effects of aperture size and pressure on XeF_2 etching of silicon,” *Microsyst. Technol.*, vol 9, no 1–2, pp 11–16, 2003, DOI 10 1007/s00542-002-0195-5

[9] K Sugano and O Tabata, “Reduction in surface roughness and aperture size effect for XeF_2 etching of Si” *Proc. SPIE 4979 ,Micromaching Microfabr. Process Technol. VIII*, no January 2003, pp 62-69, 2003, DOI: 10 1117/12 473376

[10] K Sugano and O Tabata, “Etching Rate control of mask material for XeF_2 etching using uv exposure,” *Micromach. Microfabr. Process Technol. VII*, vol 4557, no September 2001, pp 18–23, 2001, DOI: 10 1117/12 442931

[11] K Shimaoka and J Sakata, “A New Full-Dry Processing Method for MEMS,” *R&D Rev. Toyota CRDL*, vol 37, no 3, pp 59–66, 2002

[12] J H Lee *et al.*, “Characterization of anhydrous HF gas-phase etching with CH_3OH for sacrificial oxide removal,” *Sensors Actuators, A Phys.*, vol 64, no 1, pp 27–32, 1998, DOI: 10 1016/S0924-4247(98)80054-X

[13] W I Jang, C A Choi, M L Lee, C H Jun, and Y T Kim, “Fabrication of MEMS devices by using anhydrous HF gas-phase etching with alcoholic vapor,” *IEEE J. Microelectromechanical Syst.*, no 12, pp 297-306, 2002, DOI: 10 1088/0960-1317/12/3/316

[14] J F Veyan, M D Halls, S Rangan, D Aureau, X M Yan, and Y J Chabal, “XeF_2-induced removal of SiO2near Si surfaces at 300 K: An unexpected proximity effect ,” *J. Appl. Phys.*, vol 108, no 11, pp 1-11, 2010, DOI: 10 1063/1 3517148

[15] M Rondé, A J Walton, and J G Terry, “Manipulating Etch Selectivities in XeF_2 Vapour Etching,” *IEEE J. Microelectromechanical Syst.*, no Accepted 05 12 2020, 2020

[16] M Rondé, A J Walton, and J G Terry, “Test Structure for Measuring the Selectivity in Vapour Etch Processes,” in *IEEE 33rd International Conference on Microelectronic Test Structures (ICMTS), Edinurgh, United Kingdom*, 2020, pp 1–5, 2020, DOI: 10 1109/ICMTS48187 2020 9107934

[17] A W Van Barel, Bert du Bois, Rita Van Hoof, Jef De Wachter, Ward De Ceuninck, “Apparent and steady-state etch rates in thin film etching and under-etching of microstructures: II Characterisation,” *J. Micromechanics Microengineering*, vol 20, no 5, pp 1-8, 2010, DOI: 10 1088/0960-1317/20/5/055034

[18] G Van Barel, L Mertens, W De Ceuninck, and A Witvrouw, “Apparent and steady-state etch rates in thin film etching and under-etching of microstructures: I Modelling,” *J. Micromechanics Microengineering*, vol 20, no 5, pp 1-6, 2010, DOI: 10 1088/0960-1317/20/5/055033

[19] R P Vinci, E M Zielinskie, and J Bravman, “Thermal strain and stress in copper thin films,” *Thin Solid Films*, vol 262, pp 142–153, 1995, DOI: 10 1016/0040-6090(95)05834-6

Appendix D: Process Recipes and Runsheets

This appendix includes the runsheets that list the process steps and parameters used during sample fabrication. Those runsheets refer to tool recipes. Those process recipes for thin film deposition and reactive ion etching are on the first and second page of this appendix. The following 7 documents are clustered in this appendix:

- Process recipes thin film deposition
- Process recipes thin film reactive ion etching
- Runsheet SiN-Reference
- Runsheet SiO2-Reference
- Runsheet SiN-PECVD
- Runsheet SiO2-PECVD
- Runsheet SiN-LPCVD
- Runsheet HF TS - SiO2: SiN
- Runsheet HF TS - SiO2: Si3N4
- Runsheet HF TS - SiO2-Ref
- Runsheet HF TS - SiN-Ref

Process Recipes Thin Film Deposition

Plasma Enhanced Chemical Vapour Deposition (PECVD)

Low frequency SiO2 (PECVD-SiO2)

Gas	Flow Rate [sccm]	RF Power	380 Khz	60W
N2	392	Platen Temperature	300°C	
SiH4	12	Showerhead Temperature	250°C	
N2O	1420	Pressure	550 mTorr	

Low Frequency SiN (PECVD SiN)

Gas	Flow Rate [sccm]	RF Power	380 Khz	60W
N2	1960	Platen Temperature	300°C	
SiH4	40	Showerhead Temperature	250°C	
NH3	20	Pressure	550 mTorr	

Furnace Deposition

Low Pressure Deposition of Si3N4 (LPCVD)

Gas	Flow Rate [sccm]	Temperature	800°C
NH3	10		
SiH2Cl2	15		

Ploysilicon Deposition

Gas	Flow Rate [sccm]	Temperature	620°C
SiH4	30		

Sputtering

OPT Copper Sputtering

Target	Copper	Power	1000W
		Voltage	474V
Gas	Flow Rate (sccm)		
Ar	50		

OPT Aluminium Sputtering

Target	Aluminium	Power	1000W

Process Recipes Thin Film Reactive Ion Etching

Reactive Ion Etching

JLS RIE 80 - Recipe 21 (Used to etch SiO2)

Gas	Flow (sccm)	RF Power	200W
CHF3	17.7	Bias Voltage	426V
Ar	20	Pressure	20 mTorr

JLS RIE 80 - Recipe 4 (Used to etch Si3N4 and PECVD SiN

Gas	Flow Rate (sccm)	RF Power	150W
CF4	60	Bias Voltage	304V
O2	4	Pressure	20 mTorr

THE UNIVERSITY of EDINBURGH
School of Engineering

The Scottish Microelectronics Centre,
Alexander Crum Brown Road,
The King's Buildings,
Edinburgh.
EH9 3FF

PROJECT DETAILS

Customer: Markus Rondé	**Project: SiN-REF**	**Batch No: 1**	**No. of Wafers 1**
Process flow:	**Wafer spec: 4" Si**	**Mask Set: mr-ts**	**Mask Set Rev: 1**

Layer Deposition

Step	Description	Equipment	Process Parameters	Results/Comments	Wfs Out	Date	Sign
1.	Deposition of Platinum	ANS	50nm	10nm Ti Adhesion + 50nm Pl		16/10/19	SR
2.	Deposition of SiN (Low Frequency)	PECVD	500 nm - Low Frequency SiN (time from logbook)	Average Thickness measured 5011A (Nanospec)		16/10/19	MR
3.	Deposit Al	OPT	350 nm Aluminium			16/10/19	MR

Patterning

Step	Description	Equipment	Process Parameters	Results/Comments	Wfs Out	Date	Sign
1.	Resist Deposition	Polo-Spinner	SPR 230-3.0 - 10s@700 , 60s@3000			16/10/19	MR
2.	Soft Bake	Hotplate	90s @ 115 C			16/10/19	MR
3.	Pattern	Karl Suss	25s Hard/contact			16/10/19	MR
4.	PEB	Hotplate	90s @ 115 C			16/10/19	MR
5.	Develop	Bowl	MF-26, 60s	Inspection Microscope – No problems detected		16/10/19	MR
6.	Dry etch	Al etcher	3sbd1 for 30 min	Inspection Microscope, aluminium fully etched		17/10/19	MR
7.	Dry Etch SiN	JLS	Recipe 4 for 10 minutes	Inspection – Nanospec- SiN etched		17/10/19	MR
8.	Wet strip resist	Solvent wet deck	½ hr in 1165 resist remover			17/10/19	MR
9.	Cleaning	Barrel Asher	30 min			17/10/19	MR
10	Dicing					18/10/19	EM

THE UNIVERSITY of EDINBURGH
School of Engineering

The Scottish Microelectronics Centre,
Alexander Crum Brown Road,
The King's Buildings,
Edinburgh.
EH9 3FF

PROJECT DETAILS

Customer: Markus Rondé	**Project: SiO2 -Ref**	**Batch No: 1**	**No. of Wafers 1**
Process flow:	**Wafer spec: 4" Si**	**Mask Set: MR-Ts**	**Mask Set Rev: 1**

Layer Deposition

Step	Description	Equipment	Process Parameters	Results/Comments	Wfs Out	Date	Sign
1.	Deposition of Platinum	ANS	50nm	10nm Ti adhesion + 50nm		16/10/19	MR
2.	Deposition of PECVD SiO2	PECVD	Low Frequency SiO2 (time from logbook)	Inspection Nanospec – Average 5014 A		16/10/19	MR
3.	Deposit Al	OPT	350 Aluminium			16/10/19	MR

Patterning

Step	Description	Equipment	Process Parameters	Results/Comments	Wfs Out	Date	Sign
1.	Resist Deposition	Polo-Spinner	SPR 230-3.0 - 10s@700 , 60s@3000			16/10/19	MR
2.	Soft Bake	Hotplate	90s @ 115 C			16/10/19	MR
3.	Pattern	Karl Suss	25s Hard/contact			16/10/19	MR
4.	PEB	Hotplate	90s @ 115 C			16/10/19	MR
5.	Develop	Bowl	MF-26, 60s	Inspection Microscope – No problems		16/10/19	MR
6.	Dry etch	Al etcher	3sbd1 for 30 min	Inspection Microscope – Aluminium etched		17/10/19	MR
7.	Dry Etch SiO2	JLS	Recipe 21 for 10min	Inspection Nanospec – SiO2 etched		17/10/19	MR
8.	Wet strip resist	Solvent wet deck	½ hr in 1165 resist remover			17/10/19	MR
9.	Cleaning	Barrel Asher	30 min			17/10/19	MR
10	Dicing					18/10/19	EM

THE UNIVERSITY of EDINBURGH
School of Engineering

The Scottish Microelectronics Centre,
Alexander Crum Brown Road,
The King's Buildings,
Edinburgh.
EH9 3FF

PROJECT DETAILS

Customer: Markus Rondé	**Project: SiN-PECVD**	**Batch No: 1**	**No. of Wafers 1**
Process flow:	**Wafer spec: 4" Si**	**Mask Set: MR-Ts**	**Mask Set Rev: 1**

Layer Deposition

Step	Description	Equipment	Process Parameters	Results/Comments	Wfs Out	Date	Sign
1.	Deposition of Platinum	ANS	50nm	10nm Ti Adhesion + 50nm Pl		11/12/19	MR
2.	Deposition of SiN	PECVD	Low-Frequency-SiN (Time from logbook)	Inspection Nanospec: average thickness 4500A		11/12/19	MR
3.	Deposition PolySi	Furance 4	1hr, 620 Ramp	4500-5000 A		11/12/19	MR
4.	Deposit Al	OPT	Aluminum Dep, 1hr	3500A		11/12/19	MR

Patterning

Step	Description	Equipment	Process Parameters	Results/Comments	Wfs Out	Date	Sign
1.	Resist Deposition	Polo-Spinner	10s@700 , 60s@3000	SPR 230-3.0		12/12/19	MR
2.	Soft Bake	Hotplate	90s @ 115 C			12/12/19	MR
3.	Pattern	Karl Suss	15s Hard/contact			12/12/19	MR
4.	PEB	Hotplate	90s @ 115 C			12/12/19	MR
5.	Develop	Wet deck	MF-26, 60s	Inspection Microscope: No problems		12/12/19	MR
6.	Dry etch Aluminium and Silicon	Al etcher	3sbd1 for 40 min	Inspection Microscope: Al+Si etched		12/12/19	MR
7.	Dry Etch SiN	JLS	Recipe 4 for 8 min	Inspection Nanospec: SiN removed		12/12/19	MR
8.	Wet strip resist	Solvent wet deck	1165, 10min @ 60C			12/12/19	MR
9.	Cleaning	Barrel Asher	10 min			12/12/19	MR
10	Dicing					13/12/19	EM

THE UNIVERSITY of EDINBURGH
School of Engineering

The Scottish Microelectronics Centre,
Alexander Crum Brown Road,
The King's Buildings,
Edinburgh.
EH9 3FF

PROJECT DETAILS

Customer: Markus Rondé	**Project: SiO2-PECVD**	**Batch No: 1**	**No. of Wafers 1**
Process flow:	**Wafer spec: 4" Si**	**Mask Set: MR-Ts**	**Mask Set Rev: 1**

Layer Deposition

Step	Description	Equipment	Process Parameters	Results/Comments	Wfs Out	Date	Sign
1.	Deposition of Platinum	ANS	50nm	10nm Ti Adhesion + 50nm Pl		11/12/19	MR
2.	Deposition of SiO2	PECVD	Low-Frequency-SiO2 (Time from logbook)	Inspection Nanospec: average thickness 5023A		11/12/19	MR
3.	Deposition PolySi	Furance 4	1hr, 620 Ramp	4500-5000 A		11/12/19	MR
4.	Deposit Al	OPT	Aluminum Dep, 1hr	3500A		11/12/19	MR

Patterning

Step	Description	Equipment	Process Parameters	Results/Comments	Wfs Out	Date	Sign
1.	Resist Deposition	Polo-Spinner	10s@700 , 60s@3000	SPR 230-3.0		12/12/19	MR
2.	Soft Bake	Hotplate	90s @ 115 C			12/12/19	MR
3.	Pattern	Karl Suss	15s Hard/contact			12/12/19	MR
4.	PEB	Hotplate	90s @ 115 C			12/12/19	MR
5.	Develop	Wet deck	MF-26, 60s	Inspection Microscope: No problems		12/12/19	MR
6.	Dry etch Aluminium and Silicon	Al etcher	3sbd1 for 40 min	Inspection Microscope: Al+Si etched		12/12/19	MR
7.	Dry Etch SiO2	JLS	Recipe 21 for 10 min	Inspection Nanospec: SiO2 removed		12/12/19	MR
8.	Wet strip resist	Solvent wet deck	1165, 10min @ 60C			12/12/19	MR
9.	Cleaning	Barrel Asher	10 min			12/12/19	MR
10	Dicing					13/12/19	EM

THE UNIVERSITY of EDINBURGH
School of Engineering

The Scottish Microelectronics Centre,
Alexander Crum Brown Road,
The King's Buildings,
Edinburgh.
EH9 3FF

PROJECT DETAILS

Customer: Markus Rondé	**Project: Si3N4-LPCVD**	**Batch No:**	**No. of Wafers 1**
Process flow:	**Wafer spec: 4" Si**	**Mask Set:**	**Mask Set Rev:**

Layer Deposition

Step	Description	Equipment	Process Parameters	Results/Comments	Wfs Out	Date	Sign
1.	Deposition of SiO2	PECVD	Low-Frequency-SiO2 (Time from logbook)	Inspection Nanospec: average thickness 5200A		12/12/19	MR
2.	Deposite Si3N4 (LPCVD)	Furnace 3	03:45:00, SiN Flat	Inspection nanospec: average thickness 4900A		12/12/19	MR
3.	Deposite PolySi	Furance 4	1hr, 620 Ramp	4500-5000 A		12/12/19	MR
4.	Deposit Al	OPT	Aluminum Dep, 1hr	3500A		12/12/19	MR

Patterning

Step	Description	Equipment	Process Parameters	Results/Comments	Wfs Out	Date	Sign
1.	Resist Deposition	Polo-Spinner	10s@700 , 60s@3000	SPR 230-3.0		12/12/19	MR
2.	Soft Bake	Hotplate	90s @ 115 C			12/12/19	MR
3.	Pattern	Karl Suss	15s Hard/contact			12/12/19	MR
4.	PEB	Hotplate	90s @ 115 C			12/12/19	MR
5.	Develop	Bowl	MF-26, 60s	Inspection Microscope: No problems		12/12/19	MR
6.	Dry etch Aluminium and Silicon	Al etcher	3sbd1 for 40 min	Inspection Microscope: Al+Si etched		12/12/19	MR
7.	Dry Etch SiN2	JLS	Recipe 4 for 8min	Inspection Nanospec: Si3N4 removed		12/12/19	MR
8.	Wet strip resist	Solvent wet deck	1165, 10min @ 60C			12/12/19	MR
9.	Cleaning	Barrel Asher	10 min			12/12/19	MR
10	Dicing					13/12/19	EM

THE UNIVERSITY of EDINBURGH
School of Engineering

The Scottish Microelectronics Centre,
Alexander Crum Brown Road,
The King's Buildings,
Edinburgh.
EH9 3FF

PROJECT DETAILS

Customer: Markus Rondé	**Project: HF-Cu-SiO2+SiN**	**Batch No:**	**No. of Wafers 1**
Process flow:	**Wafer spec: 4" Si**	**Mask Set:**	**Mask Set Rev:**

Layer Deposition

Step	Description	Equipment	Process Parameters	Results/Comments	Wfs Out	Date	Sign
1.	Deposit 250 nm PECVD SiN	PECVD	LF SiN	Target 250 nm			
2.	Measure			Result 263 nm			
3.	Deposit 500 nm SiO2	PECVD	LF-PECVD 00:07:30	Result 500 nm			
4.	Deposit 500 nm Cu	OPT	Ar Mill 3min + Dep 50 min	Result 500 nm			

Patterning

Step	Description	Equipment	Process Parameters	Results/Comments	Wfs Out	Date	Sign
1.	Resist Deposition	Polo-Spinner	10s@700 , 60s@3000	SPR 230-3.0			
2.	Soft Bake	Hotplate	90s @ 115 C				
3.	Pattern	Karl Suss	15s Hard/contact				
4.	PEB	Hotplate	90s @ 115 C				
5.	Develop	Bowl	MF-26, 60s				
6.	Wet etch Copper	Wet Deck	Copper etcher 70 seconds				
7.	Dry Etch SiO2	JLS	Recipe 21 for 30 min				
8.	Dry Etch SiN	JLS	Recipe 4 for 4 min				
9.	Develop	Ultra Sound bath	5 min in 1165 @ 65C + Ultrasound				
10	Dicing						

THE UNIVERSITY of EDINBURGH
School of Engineering

The Scottish Microelectronics Centre,
Alexander Crum Brown Road,
The King's Buildings,
Edinburgh.
EH9 3FF

PROJECT DETAILS

Customer: Markus Rondé	**Project: HF-TS: SiO2: Si3N4**	**Batch No:**	**No. of Wafers 1**
Process flow:	**Wafer spec: 4" Si**	**Mask Set:**	**Mask Set Rev:**

Layer Deposition

Step	Description	Equipment	Process Parameters	Results/Comments	Wfs Out	Date	Sign
1.	Deposit 250 nm Si3N4	Furnace	N2 Ramp	Target 250 nm			
2.	Measure	Nanospec		Result 215 nm			
3.	Deposit 500 nm SiO2	PECVD	LF-PECVD 7 min 30 S	Result 500 nm			
4.	Deposit 500 nm Cu	OPT	Ar Mill 3min + Dep 50 min	Result 500 nm			

Patterning

Step	Description	Equipment	Process Parameters	Results/Comments	Wfs Out	Date	Sign
1.	Resist Deposition	Polo-Spinner	10s@700 , 60s@3000	SPR 230-3.0			
2.	Soft Bake	Hotplate	90s @ 115 C				
3.	Pattern	Karl Suss	15s Hard/contact				
4.	PEB	Hotplate	90s @ 115 C				
5.	Develop	Bowl	MF-26, 60s				
6.	Wet etch Copper	Wet Deck	Copper etcher 70 seconds				
7.	Dry Etch SiO2	JLS	Recipe 21 for 30 min				
8.	Dry Etch Si3N4	JLS	Recipe 4 for 6 min				
9.	Develop	Ultra Sound bath	5 min in 1165 @ 65C + Ultrasound				
10	Dicing						

THE UNIVERSITY of EDINBURGH
School of Engineering

The Scottish Microelectronics Centre,
Alexander Crum Brown Road,
The King's Buildings,
Edinburgh.
EH9 3FF

PROJECT DETAILS

Customer: Markus Rondé	**Project: HF TS: SiO2 Ref**	**Batch No:**	**No. of Wafers 1**
Process flow:	**Wafer spec: 4" Si**	**Mask Set:**	**Mask Set Rev:**

Layer Deposition

Step	Description	Equipment	Process Parameters	Results/Comments	Wfs Out	Date	Sign
1.	Deposit 500 nm SiO2	PECVD	LF-PECVD 00:07:30	Result 500 nm			
2.	Deposit 500 nm Cu	OPT	Ar Mill 3min + Dep 50 min	Result 500 nm			

Patterning

Step	Description	Equipment	Process Parameters	Results/Comments	Wfs Out	Date	Sign
1.	Resist Deposition	Polo-Spinner	10s@700 , 60s@3000	SPR 230-3.0			
2.	Soft Bake	Hotplate	90s @ 115 C				
3.	Pattern	Karl Suss	15s Hard/contact				
4.	PEB	Hotplate	90s @ 115 C				
5.	Develop	Bowl	MF-26, 60s				
6.	Wet etch Copper	Wet Deck	Copper etcher 70 seconds				
7.	Dry Etch SiO2	JLS	Recipe 21 for 30 min				
8.	Develop	Ultra Sound bath	5 min in 1165 @ 65C + Ultrasound				
9.	Dicing						

THE UNIVERSITY of EDINBURGH
School of Engineering

The Scottish Microelectronics Centre,
Alexander Crum Brown Road,
The King's Buildings,
Edinburgh.
EH9 3FF

PROJECT DETAILS

Customer: Markus Rondé	**Project: HF TS: SiN-Ref**	**Batch No:**	**No. of Wafers 1**
Process flow:	**Wafer spec: 4" Si**	**Mask Set:**	**Mask Set Rev:**

Layer Deposition

Step	Description	Equipment	Process Parameters	Results/Comments	Wfs Out	Date	Sign
1.	Deposit 250 nm PECVD SiN	PECVD	LF SiN	Target 250 nm			
2.	Measure			Result 263 nm			

Patterning

Step	Description	Equipment	Process Parameters	Results/Comments	Wfs Out	Date	Sign
1.	Resist Deposition	Polo-Spinner	10s@700 , 60s@3000	SPR 230-3.0			
2.	Soft Bake	Hotplate	90s @ 115 C				
3.	Pattern	Karl Suss	15s Hard/contact				
4.	PEB	Hotplate	90s @ 115 C				
5.	Develop	Bowl	MF-26, 60s				
6.	Wet etch Copper	Wet Deck	Copper etcher 70 seconds				
7.	Dry Etch SiN	JLS	Recipe 4 for 4 min				
8.	Develop	Ultra Sound bath	5 min in 1165 @ 65C + Ultrasound				
9.	Dicing						